Introducing catechols into sequence-defined macromolecules to control adhesion to organic and inorganic surfaces

Inaugural dissertation

for the attainment of the title of doctor

in the Faculty of Mathematics and Natural Sciences

at the Heinrich-Heine-University Düsseldorf

presented by

Jan Lukas Ruben Fischer

from Cologne

Düsseldorf, Oktober 2020

From the Institute of Organic Chemistry and Macromolecular Chemistry at the Heinrich-Heine-University Düsseldorf

Published by permission of the

Faculty of Mathematics and Natural Sciences

Heinrich-Heine-University Düsseldorf

Supervisor: Prof. Dr. Laura Hartmann

Co-supervisor: Priv.-Doz. Dr. Klaus Schaper

Date of oral examination: 20.01.2021

I hereby declare that the thesis submitted is my own work without making use of impermissible aids, considering the “Rules on the Principles for Safeguarding Good Scientific Practice at Heinrich-Heine-University Düsseldorf”. All direct or indirect sources used are acknowledged in the bibliography as references. I further declare that I have not submitted this nor a similar thesis at any other examination board in order to obtain a degree.

Date and Place Lukas Fischer

Table of Contents

Abstract

Catechol moieties are mostly known for their important role in the unique ability of marine mussels to strongly stick to different surfaces in water and in presence of high salt concentrations. For this, mussels secrete a byssal thread that is made of different proteins that undergo surface contact, the so called mussel foot proteins (Mfps). These proteins consist of a high amount of the post translational modified amino acid L-DOPA, which presents a catechol moiety as side chain and is made responsible for their extraordinary adhesive properties. Catechols are not only interesting for their unique wet adhesive potential. Their chemical properties - the slow oxidation in basic conditions and subsequent reaction with nucleophiles like amines or thiols, also make them potential reactive components for use in eg. irreversible binding glycomimetic ligands. In nature, these biological macromolecules like proteins or glycoligands are synthesized with high control over sequence and positioning of functional side chains or interacting moieties.

Therefore, this work now introduces catechol moieties into a new class of biomimetic macromolecules, the so-called precision macromolecules. The working group of Prof. Hartmann recently developed a synthesis towards precision macromolecules, the solid phase polymer synthesis (SPPoS) for sequence-defined oligo(amidoamine)s. This synthesis is based on the Merrifield peptide synthesis and uses tailor made building blocks that present a free acid and an Fmoc protected amine, as well as a functional side chain. This thesis focused on developing new protocols on the basis of SPPoS to introduce catechol moieties into sequence-defined oligo(amidoamine)s and to synthesize biomimetic structures that investigate catechol binding to both, inorganic surfaces as well as proteins.

In the first part of this thesis, a new synthetic strategy was developed giving access to building blocks in a faster and more efficient way. By introducing a one-pot reaction for selective Fmoc and functional side chain introduction, a prior occurring rearrangement is bypassed, three synthetic steps could be removed and the yield was drastically increased. Using this improved synthesis, two new building blocks were synthesized: the methyl ether protected, catechol presenting building block CDS (Catechol-Diethylenetriamine-Succinic acid) and the trityl protected amine building block TrDS (Trityl-Diethylenetriamine-Succinic acid). For the CDS

building block, a selective cleavage of the methyl ether in presence of backbone aliphatic ether was developed by using trifluoromethanesulfonic acid and thioanisol for deprotection. With the building block TrDS, the synthesis of tertiary amine and primary amide structures was established by on resin deprotection of trityl and subsequent amide coupling with the desired functionality.

Applying the developed methods, two classes of catechol-functionalized precision macromolecules were synthesized. First, precision macromolecules were synthesized inspired by the adhesive properties of mussels combining catechols and cationic moieties. Although a third moiety is usually found in Mfps with surface contact, the primary amide side chain of asparagine, its influence on adhesive strength has not been investigated before and now was included in this study for the first time. Besides that, the influence of sequence was yet not considered in synthetic systems and was now realized for catechol-functionalized precision macromolecules.

In order to investigate the effects of precision macromolecule composition and monomer sequence on the adhesive properties, in collaboration with Alexander Strzelczyk and Jun.-Prof. Dr. Stephan Schmidt, all precision macromolecules were attached to so-called soft colloidal probes (PEG microgels) and evaluated for their adhesion against glass surfaces.

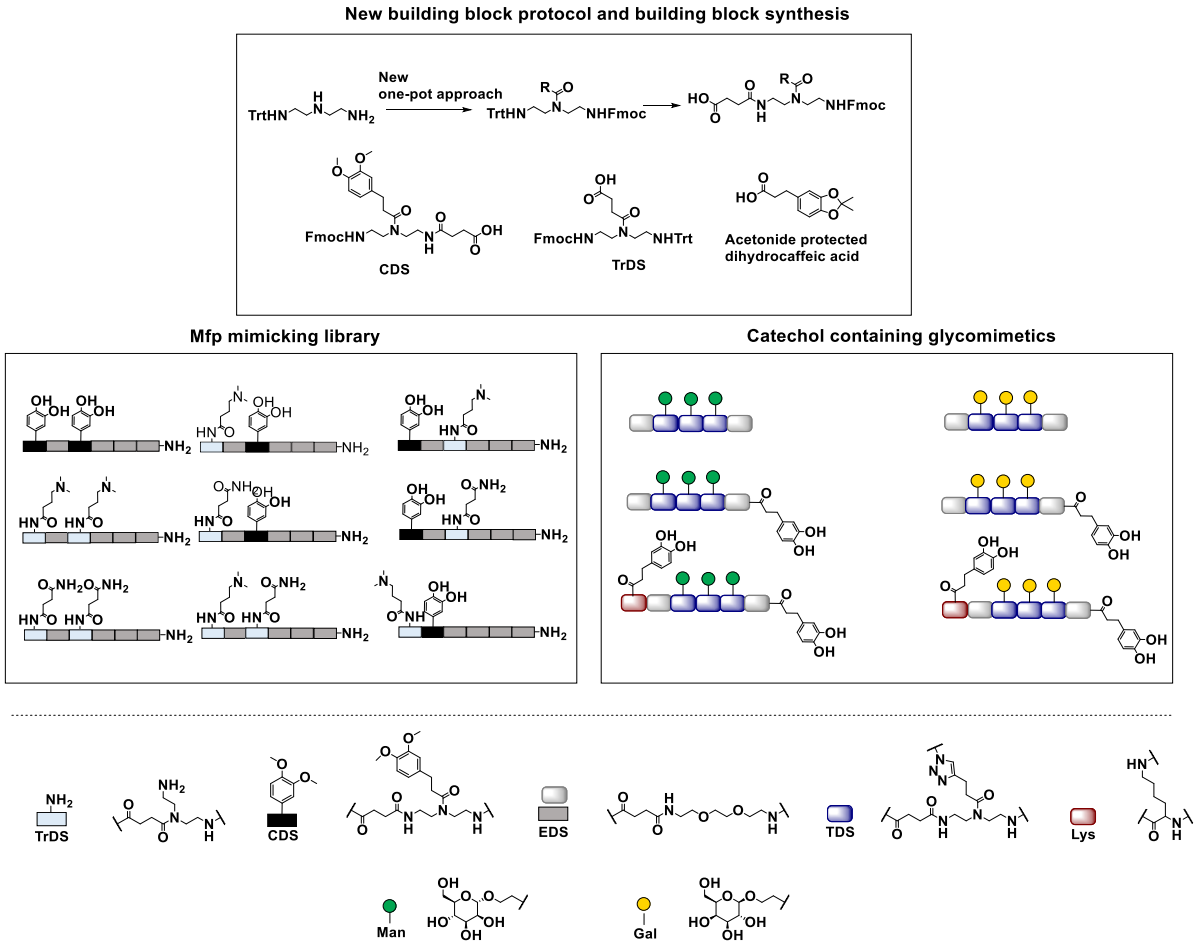

Figure 1: Schematic overview of projects described in this thesis.

It was found that the combination of catechol with either of the two other functional groups led to a synergistic effect and an increase of adhesion energy higher than the sum of its individual parts. For the tertiary amine this is already known and is explained with the potential of amines to break up the hydration layer of the surface to increase accessibility for the catechol. But for the first time, this work showed the significant contribution of the primary amide towards wet adhesion and its synergy with catechols. Furthermore, a strong influence of sequence and spacing of functional group presentation was shown. Both, decreasing the distance between catechol and tertiary amine and presenting the catechol in closer proximity to the surface in comparison to the primary amide led to a drastic increase of adhesion and loss of pH dependence. As a next step, this new knowledge could pave the way towards optimized biomimetic adhesives for eg. medical glues, as it shows optimal functional group composition and presentation as a blueprint for new polymers.

For a second class of catechol-functionalized sequence-defined oligo(amidoamine)s, catechols were introduced into precision glycomacromolecules to investigate their potential as reactive ligands. Glycomacromolecules are known to specifically bind bacterial adhesins and thereby block their adhesion, usually the first step of the infection process. However, this binding is highly reversible. In order to improve inhibitor effectivity, this could be combined with an additional covalent bond formation as was explored in this thesis by the introduction of catechol moieties. Together with Ricarda Steffens during her master thesis, the catechol moiety of dihydrocaffeic acid was acetonide protected and coupled to glycomacromolecules as assembled by previously established protocols of the Hartmann lab. Using turbidity and precipitation assays, it was shown, that combining catechols with the binding carbohydrate mannose improved the affinity towards ConA. The structures were also used in an adhesion-inhibiton assay with live *Escherichia coli* (*E. coli*), testing the relative inhibitory potential (RIP) for *E. coli* adhesion towards a mannan surface. For an incubation time of one hour, similar RIP values to prior tested structures were found, but increasing the incubation time to 24 hours led to an effective inhibition of bacterial adhesion, hinting towards an oxidation of catechol moieties and covalent binding over time. This covalent binding was also proven towards ConA by measuring MALDI-TOF and SDS-PAGE which showed additional mass peaks corresponding to ConA subunit and ligand. Here, the structure with one catechol on each side of the carbohydrate moieties acted as a staple to effectively block the binding site of ConA, proving the importance of catechol presentation. Importantly, in all assays no interaction was found for the catechol containing galactose oligomers, showing that the specificity of the carbohydrate unit is remained. This proof of concept builds the cornerstone of a new class of covalent lectin inhbitors that potentially could be used as glycomimetic therapeutics.

Overall, this work presents the successful establishment of methods for the sequence-defined introduction of catechols into synthetic macromolecules which significance was shown via two different applications, the synthesis of Mfp mimicking structures and glycomimetic structures. For both these applications, it was found that the position and presentation of catechol plays an integral role for final properties. This lays the foundation to further explore the potential of catechols in these fields, but also shows in general the importance of sequence-control in biomimetic polymers.

Kurzzusammenfassung

Katechole sind vor allem bekannt für ihre wichtige Rolle bei der einzigartigen Fähigkeit von Meeresmuscheln, sich im Wasser und in Gegenwart hoher Salzkonzentrationen stark an verschiedenen Oberflächen anhaften zu können. Dazu sekretieren die Muscheln einen Byssalfaden, der aus verschiedenen Proteinen besteht, die mit der Oberfläche in Kontakt kommen, den so genannten Muschelfußproteinen (Mfps). Diese Proteine bestehen zu einem hohen Anteil aus der posttranslational modifizierten Aminosäure L-DOPA, die als Seitenkette einen Katecholrest aufweist und für die außergewöhnlichen Hafteigenschaften verantwortlich gemacht wird. Katechole sind nicht nur wegen ihres einzigartigen Nassklebepotentials interessant. Ihre chemischen Eigenschaften - die langsame Oxidation unter basischen Bedingungen und die anschließende Reaktion mit Nukleophilen wie Aminen oder Thiolen - machen sie auch zu potentiell reaktiven Komponenten für den Einsatz z.B. in irreversibel bindenden glykomimetischen Liganden. In der Natur werden diese biologischen Makromoleküle wie Proteine oder Glykoliganden mit hoher Kontrolle über Sequenz und Positionierung funktioneller Seitenketten oder interagierender Einheiten synthetisiert.

Daher führt diese Arbeit nun Katecholeinheiten in eine neue Klasse von biomimetischen Makromolekülen ein, den so genannten Präzisionsmakromolekülen. Die Arbeitsgruppe von Prof. Hartmann hat kürzlich eine Synthese für Präzisionsmakromoleküle entwickelt, die Festphasen-Polymersynthese (SPPoS) für sequenzdefinierte Oligo(amidoamine). Diese Synthese basiert auf der Merrifield-Peptidsynthese und verwendet maßgeschneiderte Bausteine, die eine freie Säure und ein Fmoc-geschütztes Amin sowie eine funktionelle Seitenkette aufweisen. Diese Arbeit konzentrierte sich auf die Entwicklung neuer Protokolle auf der Basis von SPPoS zur Einführung von Katecholresten in sequenzdefinierte Oligo(amidoamine) zur Synthese biomimetischer Strukturen, die die Katecholbindung sowohl an anorganische Oberflächen als auch an Proteinen untersuchen.

Im ersten Teil dieser Arbeit wurde eine neue Synthesestrategie entwickelt, die einen schnelleren und effizienteren Zugang zu Bausteinen ermöglicht. Durch die Einführung einer Ein-Topf-Reaktion für die selektive Einführung von Fmoc und funktioneller Seitenkette wird eine vorher stattfindende Umlagerung umgangen, drei synthetische Schritte konnten gespart und die Ausbeute drastisch erhöht werden. Mit Hilfe dieser verbesserten Synthese konnten

zwei neue Bausteine synthetisiert werden: der Methylether-geschützte, Katechol präsentierende Baustein CDS (Catechol-Diethylentriamin-Bernsteinsäure) und der Trityl-geschützte Amin-Baustein TrDS (Trityl-Diethylentriamin-Bernsteinsäure). Für den CDS-Baustein wurde eine selektive Spaltung des Methylethers in Gegenwart von aliphatischem Rückgratether unter Verwendung von Trifluormethansulfonsäure und Thioanisol zur Entschützung entwickelt. Mit dem Baustein TrDS wurde die Synthese von tertiären Amin- und primären Amidstrukturen durch Entfernung der Trityl-Gruppe am Harz und anschließende Amidkupplung mit der gewünschten Funktionalität etabliert.

Unter Anwendung der entwickelten Methoden wurden zwei Klassen von Katechol-funktionalisierten Präzisionsmakromolekülen synthetisiert. Zunächst wurden Präzisionsmakromoleküle synthetisiert, die durch die adhäsiven Eigenschaften von Muscheln inspiriert wurden und Katechole und kationische Anteile kombinieren. Obwohl ein dritter Anteil gewöhnlich in Mfps mit Oberflächenkontakt zu finden ist, das primäre Amid der Seitenkette von Asparagin, wurde dessen Einfluss auf die Haftfestigkeit bisher nicht untersucht und nun erstmals in dieser Studie einbezogen. Darüber hinaus wurde der Einfluss der Sequenz bei synthetischen Systemen noch nicht berücksichtigt und nun für Katechol-funktionalisierte Präzisionsmakromoleküle realisiert.

Um die Auswirkungen von Zusammensetzung und Monomersequenz auf die Hafteigenschaften zu untersuchen, wurden in Zusammenarbeit mit Alexander Strzelczyk und Jun.-Prof. Dr. Stephan Schmidt alle Präzisionsmakromoleküle an sogenannten weichen kolloidalen Sonden (PEG-Mikrogele) angebracht und auf ihre Haftung an Glasoberflächen untersucht.

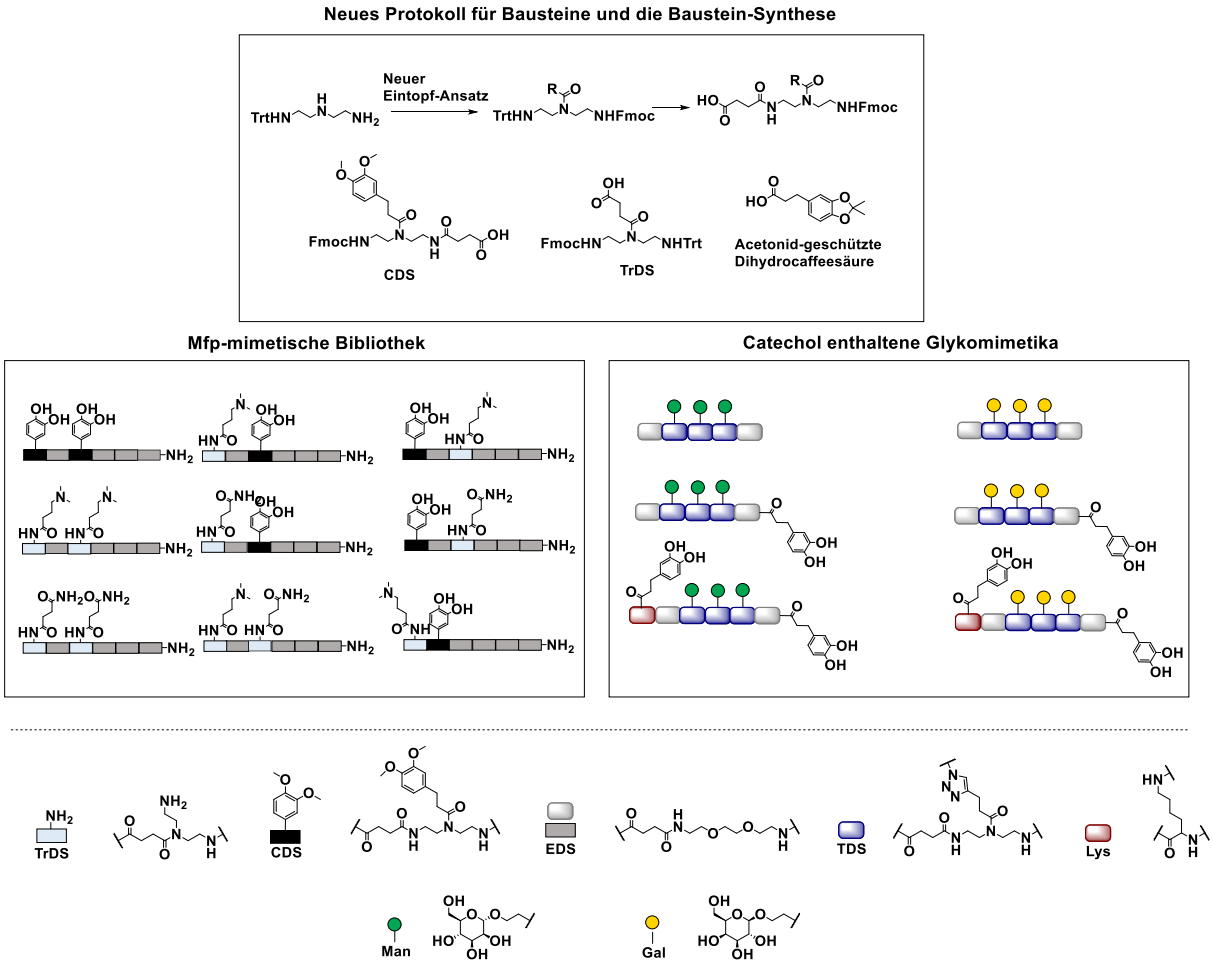

Abbildung 1: Schematischer Überblick über die Projekte die in dieser Arbeit präsentiert werden.

Es wurde festgestellt, dass die Kombination von Katechol mit einer der beiden anderen funktionellen Gruppen zu einem synergistischen Effekt und einer Erhöhung der Adhäsionsenergie führte, die höher war als die Summe seiner Einzelteile. Für das tertiäre Amin ist dies bereits bekannt und wird mit dem Potential der Amine erklärt, die Hydratationsschicht der Oberfläche aufzubrechen, um die Zugänglichkeit für das Katechol zu erhöhen. Allerdings wurde in dieser Arbeit zum ersten Mal der signifikante Beitrag des primären Amids zur Nasshaftung und seine Synergie mit den Katecholen gezeigt. Darüber hinaus wurde ein starker Einfluss der Reihenfolge und des Abstands der Darstellung der funktionellen Gruppen gezeigt. Sowohl die Verringerung des Abstands zwischen Katechol und tertiärem Amin als auch die Präsentation des Katechols in größerer Nähe zur Oberfläche im Vergleich zum primären Amid führten zu einem drastischen Anstieg der Adhäsion und einem Verlust der pH-Abhängigkeit. In einem nächsten Schritt könnte dieses neue Wissen den Weg zu optimierten biomimetischen Klebstoffen für z.B. medizinische Klebstoffe ebnen, da es eine

optimale Zusammensetzung und Präsentation der funktionellen Gruppen als Blaupause für neue Polymere zeigt.

Für eine zweite Klasse von Katechol-funktionalisierten, sequenzdefinierten Oligo(amidoamine)n wurden Katechole in Präzisionsglykomakromoleküle eingebracht, um ihr Potenzial als reaktive Liganden zu untersuchen. Es ist bekannt, dass Glykomakromoleküle bakterielle Adhäsine spezifisch binden und dadurch ihre Adhäsion blockieren, was normalerweise der erste Schritt des Infektionsprozesses ist. Diese Bindung ist jedoch in hohem Maße reversibel. Um die Wirksamkeit des Inhibitors zu verbessern, könnte dies mit einer zusätzlichen kovalenten Bindungsbildung kombiniert werden, wie in dieser Arbeit durch die Einführung von Katecholresten untersucht wurde. Zusammen mit Ricarda Steffens während ihrer Masterarbeit wurde der Katecholanteil der Dihydrocaffeesäure Acetonid-geschützt und an Glykomakromoleküle gekoppelt, die nach zuvor etablierten Protokollen des Hartmann-Labors zusammengestellt wurden. Mit Hilfe von Trübungs- und Fällungstests konnte gezeigt werden, dass die Kombination von Katecholen mit dem bindenden Kohlenhydrat Mannose die Affinität zu ConA verbesserte. Die Strukturen wurden auch in einem Adhäsions-Inhibitions-Assay mit lebenden *Escherichia coli* (*E. coli*) verwendet, bei dem das relative Inhibitionspotential (RIP) für die Adhäsion von *E. coli* gegenüber einer Mannan-Oberfläche getestet wurde. Bei einer Inkubationszeit von einer Stunde ergaben sich ähnliche RIP-Werte wie bei zuvor getesteten Strukturen, aber die Erhöhung der Inkubationszeit auf 24 Stunden führte zu einer wirksamen Hemmung der Bakterienadhäsion, was auf eine Oxidation der Katecholreste und eine kovalente Bindung im Laufe der Zeit hindeutet. Diese kovalente Bindung wurde auch gegenüber ConA nachgewiesen, indem MALDI-TOF und SDS-PAGE gemessen wurden, die zusätzliche Massenpeaks zeigten, die der ConA-Untereinheit und dem Liganden entsprachen. Hier wirkte die Struktur mit einem Katechol auf jeder Seite der Kohlenhydrateinheiten als Klammer, um die Bindungsstelle von ConA wirksam zu blockieren, was die Bedeutung der Katecholpräsentation bewies. Wichtig ist, dass in allen Assays keine Wechselwirkung für die katecholhaltigen Galaktose-Oligomere gefunden wurde, was zeigt, dass die Spezifität der Kohlenhydrateinheit erhalten bleibt. Dieser Proof-of-Concept bildet den Grundstein für eine neue Klasse von kovalenten Lektininhibitoren, die potenziell als glykomimetische Therapeutika eingesetzt werden könnten.

Insgesamt stellt diese Arbeit die erfolgreiche Etablierung von Methoden zur sequenz-definierten Einführung von Katecholen in synthetische Makromoleküle vor, deren Bedeutung durch zwei verschiedene Anwendungen, die Synthese von Mfp-imitierenden Strukturen und glykomimetischen Strukturen, gezeigt wurde. Für beide Anwendungen wurde festgestellt, dass die Position und Präsentation von Katechol eine wesentliche Rolle für die endgültigen Eigenschaften spielt. Dies bildet die Grundlage für die weitere Erforschung des Potentials von Katecholen in diesen Bereichen, zeigt aber auch allgemein die Bedeutung der Sequenzkontrolle in biomimetischen Polymeren.

List of Publications

Publications included in this thesis

Fischer, L., Strzelczyk, A., Wedler, N., Kropf, C., Schmidt, S., & Hartmann, L. (2020). Sequence-defined positioning of amine and amide residues to control catechol driven wet adhesion. *Chemical Science.*

Fischer, L., Steffens, R., Paul, T., & Hartmann, L. (2020). Catechol-functionalized sequence-defined glycomacromolecules as covalent inhibitors of bacterial adhesion. *Polymer Chemistry*.

Patents included in this thesis

Application DE 102019208832.5 “Polymere für die Behandlung von Oberflächen”.

Publications not included in this thesis

Shamout, F., Fischer, L., Snyder, N. L., & Hartmann, L. (2020). Recovery, Purification, and Reusability of Building Blocks for Solid Phase Synthesis. *Macromolecular Rapid Communications*, *41*(2), 1900473.

1. Introduction

1.1 Adhesive properties of marine mussels

The term marine mussel is commonly used for members of the family Mytilidae, bivalve molluscs which live on the shores, exposed to harsh conditions like tidal waves. To live in these conditions, members of this family attach strongly to surfaces via their byssal threads, which are formed by secreted filaments made of several different compartments.[1] The achieved adhesion is remarkably strong, especially for the presence of water and high ion concentrations, both conditions that form thin layers on surfaces inhibiting surface contact. Furthermore, marine mussels are capable of adhering to almost all surfaces, natural and man-made.[2] For example, the accumulation of mussels on the bottom of ships results in an increase of up to 30% of fuel consumption.[3] Because of this, a lot of effort is put into developing anti-fouling surface coatings. The unique adhesion of the byssal threads also makes them an interesting target for the development of biomimetic adhesives. Properties like the wide range of accepted surfaces and tolerance of water and high salt concentrations let to the investigation of the underlying mechanisms of adhesion.

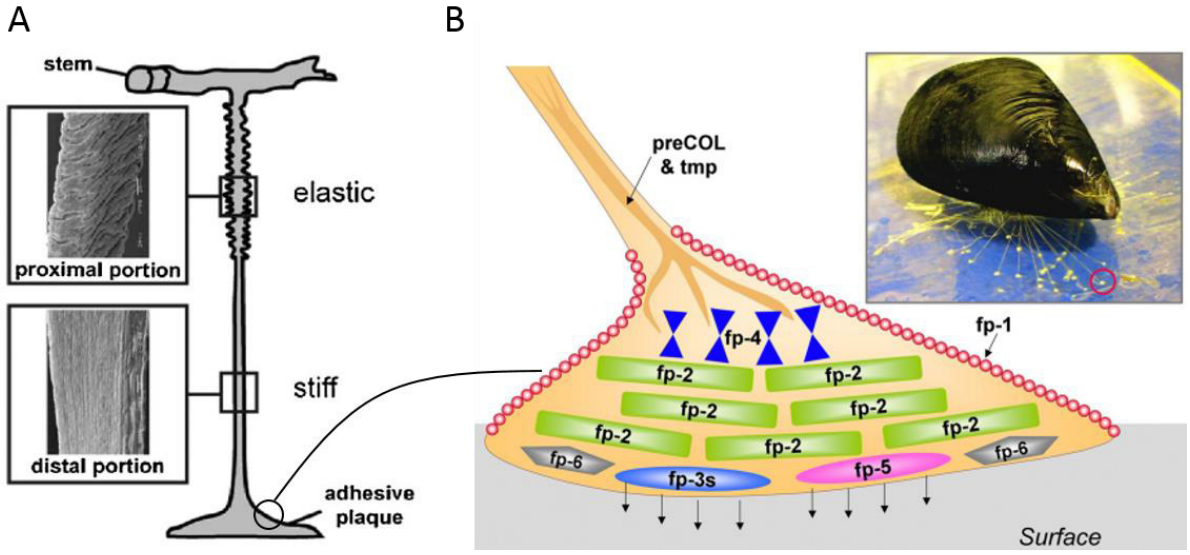

Figure 1: A) The secreted byssal thread used for surface anchoring; B) Schematic presentation of proteins found in the adhesive plaque (reprinted with permission).[4,5]

The byssal threads that are anchoring the mussel to the surface consist entirely of proteins and can be divided in different functional parts (Figure 1 A).[6] Nearest to the mussel, the

proximal portion has mechanical properties similar to rubber with 200% elasticity. The second, distant portion of the byssal thread, forms a rigid structure with a Young´s modulus of 500 MPa.[7] The distant portions ends in the adhesive plague, the part with surface contact and responsible for anchoring.

The adhesive plaque itself is made out of so called mussel foot proteins (Mfps) that are either structural proteins forming the plaque or adhesive proteins with surface contact, with in total six different proteins identified so far.[8] As shown in Figure 1 B, the main structural protein is Mfp-2 which crosslinks with itself via cations like Ca^{2+} and Fe^{3+} and is responsible for the structural integrity.[9] In direct surface contact Mfp-3, Mfp-5 and Mfp-6 can be found.[10] Regarding the investigation of the mechanism of adhesion, these proteins are the target of interest. The analysis of the amino acid sequence for these proteins reveals certain abundantly found amino acids e.g. cationic residues and a high amount of L-DOPA (Figure 2 A).[11,12] Here, L-DOPA is especially interesting, as it is synthesized posttranslational from tyrosine which indicates a special role for the adhesive properties.[13]

Mfp-3 is the most polymorphic of the Mfps, with a mass of 5 to 7.5 kDa and up to 35 different found variations.[14] Characteristically for Mfp-3 is the conversion of tyrosine to L-DOPA and arginine to 4-hydroxyarginine. Generally, the variants of Mfp-3 can be divided into two forms, Mfp-3 fast moving (Mfp-3f) and Mfp-3 slow moving (Mfp-3s), named after their electrophoretic clustering.[15] Mfp-3f is L-DOPA rich (~20%) and highly positively charged (~25%) while the Mfp-3s variant has a lower amount of DOPA (<10%) and cationic residues (<10%).[14] The positive charges for both variants are introduced by either arginine or lysine, although the most frequently found variants pre dominantly display arginine.[16] The only other abundantly found functional amino acid is asparagine with a content of up to 18%, which indicates that the primary amide functionality plays an important role for the properties of Mfp-3 and adds primary amides to the potential adhesive groups (Figure 2 B).[17] Surprisingly, the contribution of asparagine or primary amides was not studied so far.

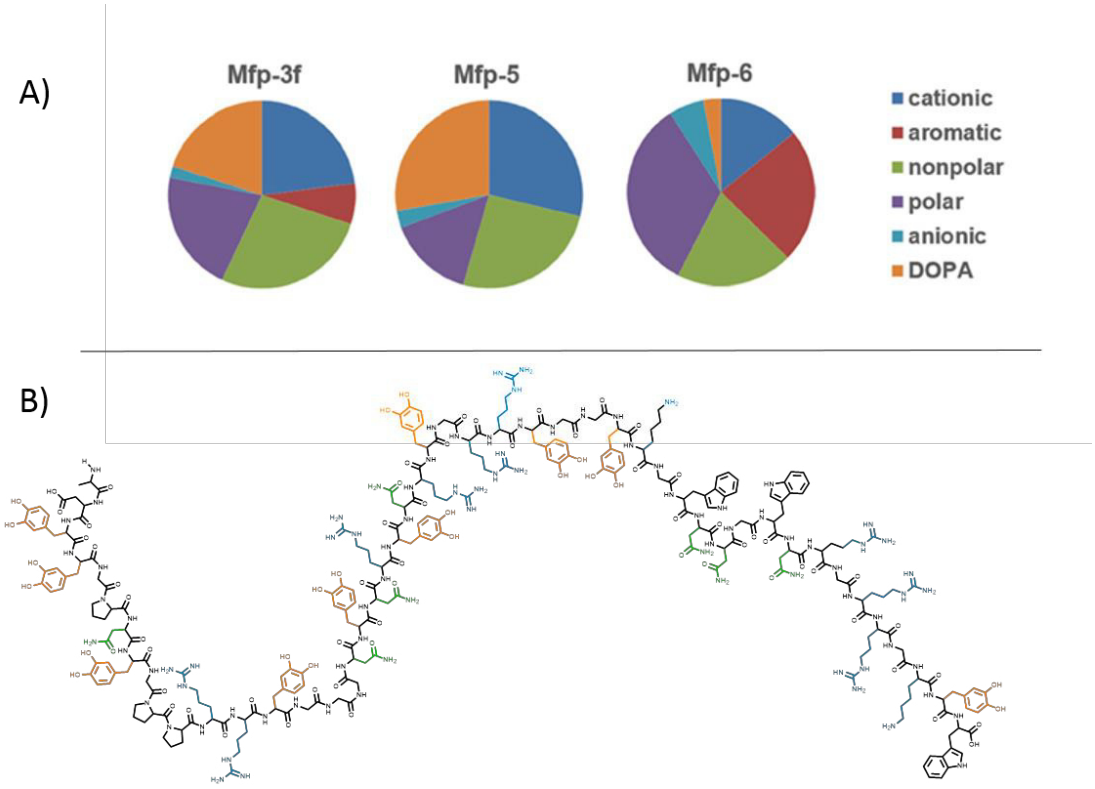

Figure 2: A) Amino acid composition of mussel foot proteins with surface contact (reprinted with permission); B) Primary structure of an Mfp-3f variant with catechols (orange), primary amides (green) and cationic residues (blue) colour marked. The arginine groups displayed here are in reality randomly 4-hydroxylated (40-80%).[4,16,18]

In contrast to the highly variable Mfp-3, mussel foot protein 5 (Mfp-5) is the least polymorphic protein in the adhesive plaque with a mass of 8.9 kDa and a conserved sequence of 99 amino acids of which 28 are L-DOPA.[19] Beside the high amount of L-DOPA, Mfp-5 also has a high density of positively charged amino acids (28%). Here, most positive charges are introduced by lysine. As an additional post-translational modification the phosphorylation of serine can be found with approximately 5%, which is known to be a modification with the ability to bind to calcareous minerals.[20]

Mfp-6 is the third protein with surface contact and while it has a similar amino acid composition as the other two, namely a high amount of cationic residues (16%) and tyrosine (20%), Mfp-6 has a low degree of post-translational modification resulting in only 3% L-DOPA.[8] Unique about Mfp-6 is the abundance of cysteine (11%) with only a small amount of these in disulfide bonds. The presented free thiols fulfil two different functions. First, they can cure the secreted proteins by crosslinking with oxidized catechol, which is shown by the presence

of 5-*S*-cysteinyl-Dopa in the plaque.[8] The second function also involves oxidized catechol, as the free thiols can control the equilibrium of catechol and benzoquinone in other plaque proteins by oxidation of two thiols to a disulfide bond and simultaneous reduction of benzoquinone.[21] This, in addition to the low L-DOPA amount, means that Mfp-6 most likely does not directly contribute to adhesion but acts as a cofactor.

In summary, so far it was shown that Mfp-3 and Mfp-5 are the main reason for the extraordinary surface adhesion of marine mussel byssal threads. As Mfp-3 is a highly polymorphic protein, it likely is responsible for the adaption to different surfaces and chemical environments and Mfp-6 functions as curing agent and antioxidant. These properties of marine mussels sparked a lot of research towards materials mimicking the wet adhesion. On the basis of the chemical composition of the mussel foot proteins, investigations into the underlying mechanism were widely conducted.

1.1.1 Mechanism of adhesion and the role of L-DOPA

Mussel foot proteins found in the adhesive plaque of marine mussels are made responsible for the extraordinary wet adhesion to different surfaces. The two proteins with surface contact, Mfp-3 and Mfp-5, have a high degree of post-translation modifications. Most of these modifications are hydroxylations that can be found on different amino acids like arginine, proline, lysine or tyrosine.[22] Normally, most of these function as a point of further modification or crosslinking, and to increase overall hydrophilicity. However, in the case of the conversion of tyrosine to L-DOPA, the additional hydroxyl group results in the formation of a catechol moiety, which has distinct chemical properties.[23]

One of the main chemical features of the catechol group is the oxidation to benzoquinones, which they undergo in the presence of oxygen and basic pH levels.[24] This two-electron, two-proton oxidation is reversible and results in benzoquinones that can react in a Michael-addition like reaction with nucleophiles or an additional catechol moiety (Figure 3 A).[25] Through this, the amino acid L-DOPA can covalently crosslink proteins in the adhesive plaque, which is thought to be one pathway, besides coordinative crosslinking, for plaque curing.[26] In fact, analysis of mussel foot proteins turned out to be difficult since the plaque is almost completely insoluble which was circumvented by limiting the oxidation during the curing

process.[27] On the other hand, oxidation of L-DOPA results in the loss of a lot of possible surface interactions (Figure 3 B). This is the reason that the redox state of L-DOPA needs to be controlled to find an efficient equilibrium between cohesion and adhesion.[21] This is, as already stated, controlled by Mfp-6 by reducing dopaquinone to Dopa through forming a disulfide bond with two cysteine residues.

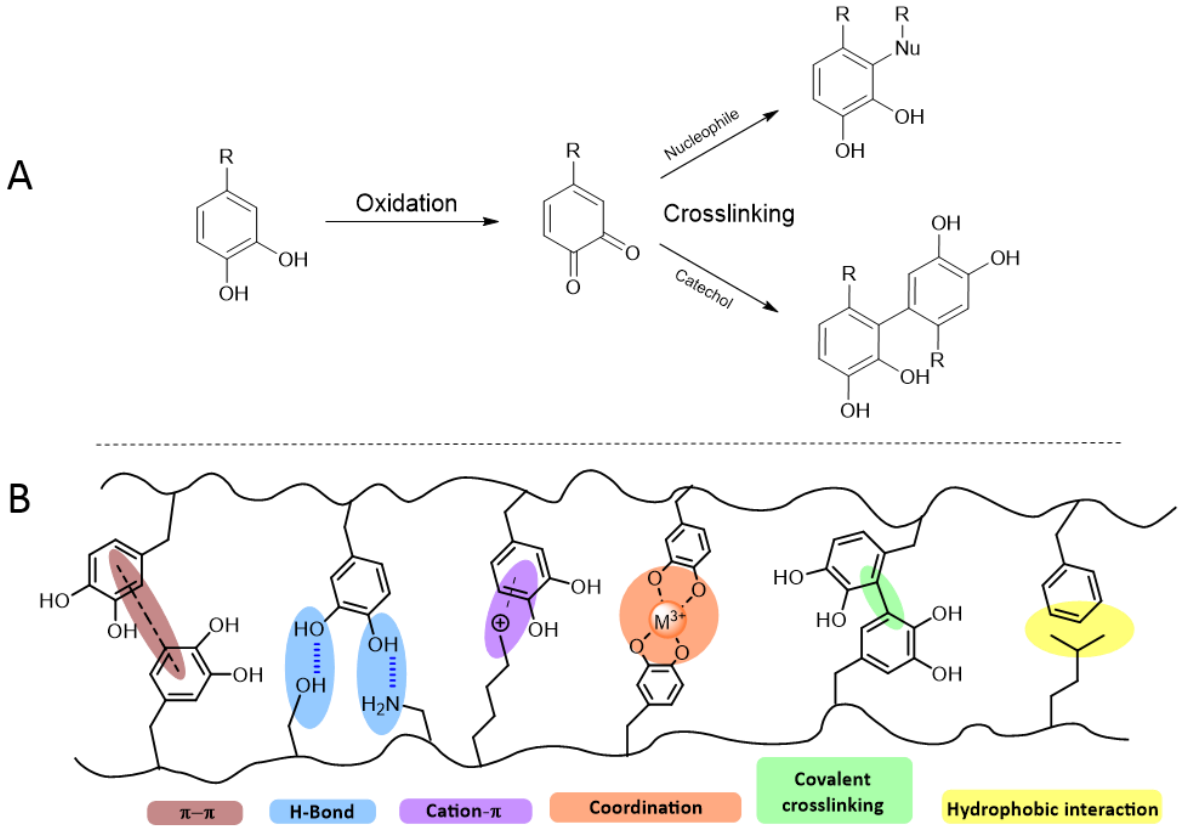

Figure 3: A) Possible reaction pathways after oxidation of catechol; B) The different molecular interactions the catechol moiety can participate in.

Besides offering a point for crosslinking, L-DOPA is made responsible for the strong interaction of the adhesive plaque with different surfaces in aqueous media. As shown in Figure 3 B, catechol moieties can participate in a lot of different intermolecular forces that can explain the adhesion to organic as well as inorganic surfaces.[28] Inorganic surfaces mainly consist of metals and oxides and the catechol group can interact with both through its hydroxyl groups.[29] Metal ions but also metal surfaces can be strongly complexed via the oxygen atoms, an effect that is pH dependant. At pH 2 the catechol moiety forms H-bonds with the surface while coordinating to the metal component starting at pH 5.[29] For organic surfaces there are even more possible interactions. Again, the hydroxyl groups can undergo H-bonds but in

contrast to inorganic surfaces, the phenyl part plays an increasing role by participating in π-π and cation-π interactions as well as in hydrophobic interactions.[30] Overall, the catechol moiety performs two functions, it crosslinks the different mussel foot proteins resulting in cohesion and undergoes interaction with a variety of surface groups for adhesion.

This extraordinary strong adhesion was also shown by adhesion measurements with isolated mussel foot proteins. For example, a Mfp-3f variant was isolated and its adhesion against Mica and TiO_2 surfaces at different pH values was measured by Israelachvili et al.[31] Here, a pH dependence was shown, with strongest adhesion at pH 3 and lower adhesion at pH 5.5 and pH 7. This is mainly explained with an increase in deprotonated form of catechol with higher pH which limits its ability to interact in H-bonds. It was also observed, like prior explained, that the binding shifts towards coordination with higher pH values. Another factor in pH dependant adhesion is the increasing oxidation rate of catechols at higher pH values resulting in lower adhesion values for Mfp-3 over time.[32] The negative effects of oxidation could be prevented by mixing Mfp-3 and Mfp-6 in surface force apparatus measurements, which shows the reductive potential of the cysteine rich Mfp-6.[33]

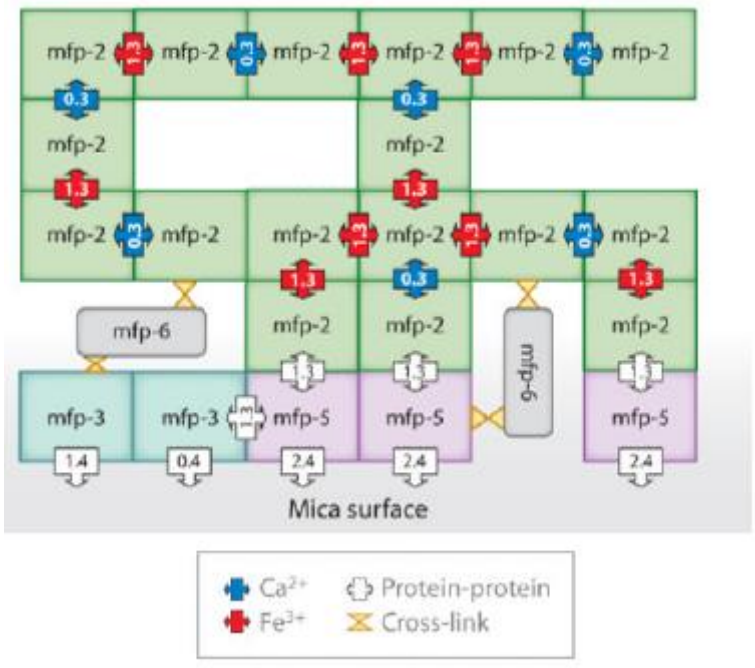

Figure 4: Interactions between mussel foot proteins in the adhesive plaque (reprinted with permission).[4,17]

In another study the comparison between Mfp-1 and Mfp-3 showed which different functions the proteins fulfil.[13] The protein with surface contact, Mfp-3, was capable of glueing two mica surfaces together while Mfp-1 did not mediate surface contact. Similar results were found for another protein, Mfp-2, which was unable to bridge between two mica surfaces.[9] The difference here was, that by adding Fe^{3+}, Mfp-2 was able to reversible crosslink with itself to successfully glue two mica surfaces to each other. More importantly, it was observed that in presence of Fe^{3+}, the protein adheres strongly to Mfp-5 and that the surface interaction of Mfp-2 can effectively be displaced by Mfp-3. In summary this proves the prior stated composition of the abyssal plaque, with Mfp-3 and Mfp-5 responsible for surface adhesion and Mfp-2 resulting in effective crosslinking and structural integrity of the byssus while Mfp-6 is controlling the redox equilibrium of L-DOPA (Figure 4).

The investigation of mussel foot proteins in adhesion measurements showed the basic functions of catechol and the interplay between proteins in the adhesive plaque, but the complexity of the proteins makes it difficult to resolve the structure-property relationship in detail. To better understand the mechanism and potential of mussel inspired wet adhesion a lot of different materials and polymers were synthesized. The catechol moiety can hereby be introduced in two different ways, as part of the polymer chain itself or as a side chain. For example as part of the first polymer class, Messersmith et al. synthesized a polymer from dopamine by polymerization in basic aqueous media.[34] During this reaction dopaquinone is formed and reacts with the primary amine via Schiff base formation or Michael type addition with subsequent polymerization resulting in a crosslinked network. Although forming an effective coating for a variety of surfaces, this type of polymerization offers little insights into the adhesive mechanisms. For mechanistic studies, the use of vinyl monomers is better suited. These can be easily generated by the reaction of dopamine with acrylic or methacrylic acid chloride. Usually, the catechol moiety is protected, e.g. by borax, by conversion with acetone or by more stable variants like the methyl ether.[23]

Using this synthetic approach, a lot of structures where synthesized to investigate the underlying mechanisms of wet adhesion and the following questions could already be answered:

1) Why is the L-DOPA amount fixed at around 20% and how important is the catechol moiety for wet adhesion?

2) Which role do the other functional groups in mussel foot proteins play?

North et al. investigated the first question by synthesizing poly(catechol-styrene) copolymers with varying catechol content between 0% and 40%.[35] Measuring the lap shear strength on aluminium substrates revealed highest adhesion for 22% catechol content. Similar results were received by Li et al. with vinylpyrrolidine based polymers containing catechol.[36] Lap shear testing on glass substrates showed highest adhesion for 16% catechol. These results are in line with the L-DOPA amount found in mussel foot proteins and show that there are diminishing returns with increasing amounts. A reason for this could be an equilibrium between adhesive and cohesive interaction, meaning with higher content catechols are more likely to be in direct proximity to each other and can interact via H-bonds and π-π stacking resulting in lower surface accessibility.[37] On the other hand, the catechol moiety seems to be essential in its entirety for adhesion. Hou et al. synthesized two different alginate hydrogels, one with tyramine and one with dopamine.[38] Lap shear tests showed a 10-fold increase in adhesion for the catechol hydrogel versus the phenol hydrogel, although both functionalities can take part in similar interactions.

To tackle the second question, Narkar et al. synthesized hydrogels from dopamine methacrylate with either an anionic or cationic co-monomer.[39] These structures were tested in a Johnson-Kendall-Roberts mechanics assay against quartz and amine functionalized glass. Overall, anionic and cationic groups increased catechol driven adhesion against both surfaces, although adhesion for cationic hydrogels was more pH dependant. Similar results were achieved by Maier et al. for the combination of catechol and cationic residues, but they were also able to gather further insights into the mechanism.[40]

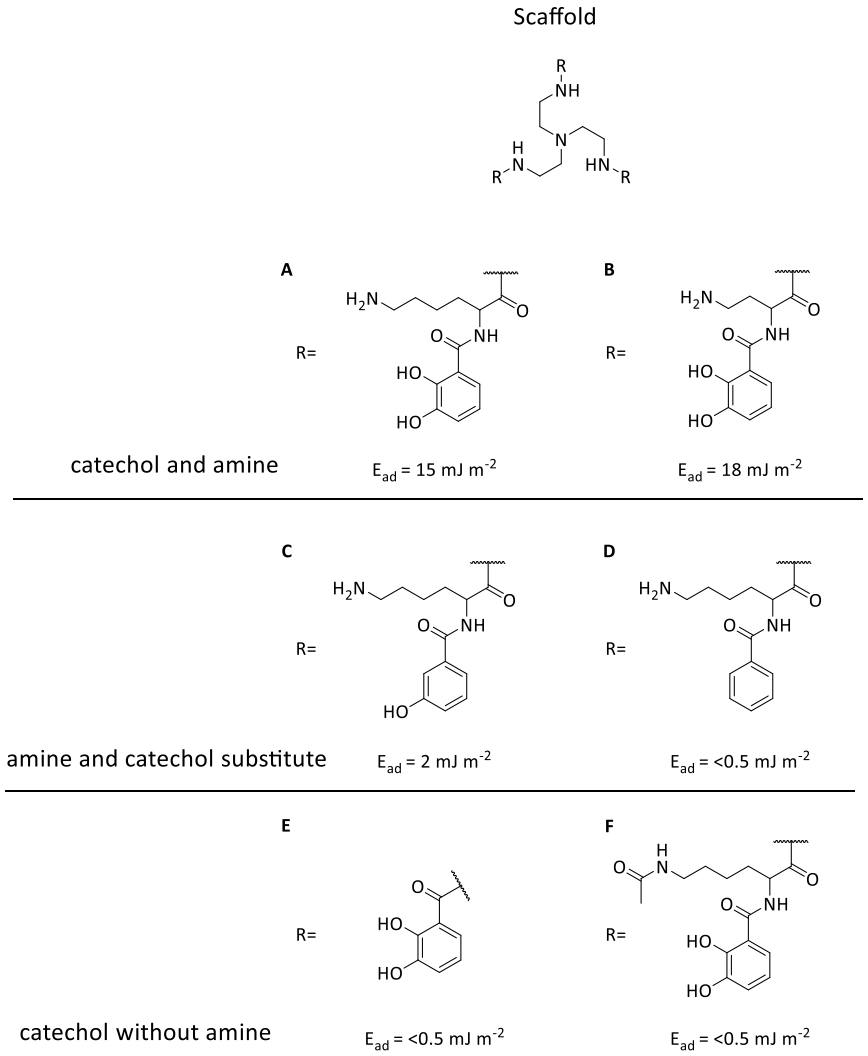

Figure 5: Synthesized structures by Maier et al. to investigate a synergy between catechol and cationic residues with corresponding adhesion energies stated.[40]

They synthesized different siderophores presenting catechols and lysines with variants replacing catechol with phenol and lysine with its acetylated form (Figure 5). With these systems, they could show that there is a strong synergy between lysine and catechol resulting in high adhesion values, an effect that was not observed for the structurally similar phenol moiety or in absence of the amine. It was also shown via film thickness measurements, that the lysine can displace the hydration layer on the surface which enables binding of the catechol. Another factor that increases adhesion was found by Wang et al.[41] By synthesizing different copolymers presenting catechols and alkyl chains of varying length, they could show that longer alkyl chains resulted in higher adhesion values for a wide range of substrates. This means that the potential to form hydrophobic interactions is another important parameter to tune wet adhesion.

In summary, key aspects of the mechanisms behind mussel inspired wet adhesion could already be resolved. Similar to the amount of L-DOPA found in Mfps, synthetic polymers exhibit highest adhesion at around 20% catechol groups, likely due to an interplay between adhesion and cohesion. The replacement of catechols with the similar phenol moiety resulted in significantly lower adhesion, showing the reason for the posttranslational conversion of tyrosine to L-DOPA. Furthermore, a reason for the incorporation of high amounts of cationic residues and tryptophan were found. Cationic charges are able to break up the hydration layer on the target surface, the main barrier for wet adhesion. Besides that, the introduction of hydrophobic interactions can increase adhesion, which shows the importance of the aromatic part of L-DOPA. Nevertheless, two factors regarding the adhesive potential of Mfps have so far not been investigated. Mussel foot proteins also exhibit a high amount of primary amide residues, a group yet not considered as adhesive functionality. Also cationic, primary amide residues and L-DOPA are all presented in close proximity, which raises the questions regarding the influence of position and distance between the functional groups, something that was probably yet not investigated due to the limitations of classical, disperse polymers.

1.1.2 Applications of biomimetic adhesives

A wide range of mussel foot protein inspired polymers were already synthesized that have potential use in several applications. The wet adhesion to surfaces under difficult conditions makes these biomimetic polymers interesting targets for biomedical glues.[10] There are great challenges for effective biomedical glues, two surfaces need to be adhered together in the presence of body fluids and the glue needs to be non-toxic and non-immunogenic. For a working biomedical glue, you need a liquid polymer mixture that can be applied with accuracy and that cures after administration in seconds.[42] Here, the catechol can possibly function as both adhesive and cohesive unit. For example Lee et al. synthesized PEG polymers that were modified with L-DOPA.[43] The PEG part functions as biocompatible filler and the DOPA is responsible for adhesion and crosslinking. These polymers formed hydrogels under oxidative conditions with curing times as low as 30 seconds. A wide range of PEG based glues were already synthesized, differing in architecture, molecular weight and amount of catechol end groups to control curing and degradation time.[44,45] Taking it one step further, Brubaker et al.

managed to transplant extraheptic islets into mice using a catechol-PEG hydrogel with observed biocompatibility of the adhesive even after one year.[46]

Besides the PEG based polymers, chitosan-catechol conjugates are promising candidates for medical use.[47] Chitosan is a natural occurring polysaccharide which presents free amine groups and is biocompatible and non-toxic.[48] It can be functionalized via amide bonding with hydrocaffeic acid to generate water soluble adhesives that present catechol and primary amine groups.[49] These conjugates can also crosslink via the catechol groups into hydrogels that exhibit high adhesion towards tissues.[50] These can be used as wound sealings, Ryu et al. created chitosan-catechol/pluronic polymers that were injected into haemorrhaging sites to effectively stop bleeding.[51] Furthermore, these materials offer potential use as drug delivery systems since the chitosan part is biodegradable. Qiao et al. managed to synthesize a hydrogel via ion coordination driven catechol crosslinking that incorporates doxorubicin to achieve kidney-specific drug delivery via transmembrane transport and pH sensitive release.[52] Another possible application is the use as biosensors, since catechols can take part in electrochemical reactions they can be used to identify redox-active bacterial metabolites for *in situ* monitoring.[53]

The use of catechols in hydrogels also offers the possibility to generate self-healing materials. For this the ability of catechols to complex ions or boronates is used. For example, catechol polymers can be cross-linked via metal ions to a hydrogel that can seal cuts after rupturing.[54] A similar effect can be achieved using boronate as complexing agent.[55] This mechanism can also be used to generate a smart adhesive that reacts to pH value.[56] By introducing catechols and phenylboronic acids into one polymer, strong surface adhesion can be achieved at low pH values. Elevated pH leads to interaction between boronic acid and catechols, inhibiting surface interaction.

Another application for catechol containing polymers is the use as surface coating. The catechol moiety can take two functions here, either used as surface anchor or as presented adhesive group for sticky coatings. Most effort has been spent on creating anti-fouling coatings using catechols for surface anchoring in combination with a second, anti-fouling part. The main class of polymers here are PEG based and can be e.g. single chains with catechol end group-functionalization or multi-arm polymers.[57,58] These polymers result in significant reduction in binding of proteins, bacteria and cells to coated surfaces. Some were already

deployed with success as protective coatings for stents and tested in mice model with significantly reduced bacterial load for coated versus uncoated implants.[59] Although PEG has good anti-fouling properties, a high degree of swelling and a lack of biodegradability limits its medical use.[60] Modern variants exploit peptoids, zwitterionic polymers or biopolymers as anti-fouling alternatives.[10]

1.2 The role of lectins in nature

There are several natural macromolecules that control biological functions in all living organisms, namely nucleic acids, proteins, lipids and carbohydrates. Long only famous for their function as energy source or as structural polymers, carbohydrates came into the focus of research over the past few decades for their diverse biological functions.[61] Carbohydrates can be found on the surfaces of nearly all cells, were they are presented as either glycolipids or glycoproteins and make up to 10% of the plasma membrane as the so called glycocalyx (Figure 6).[62]

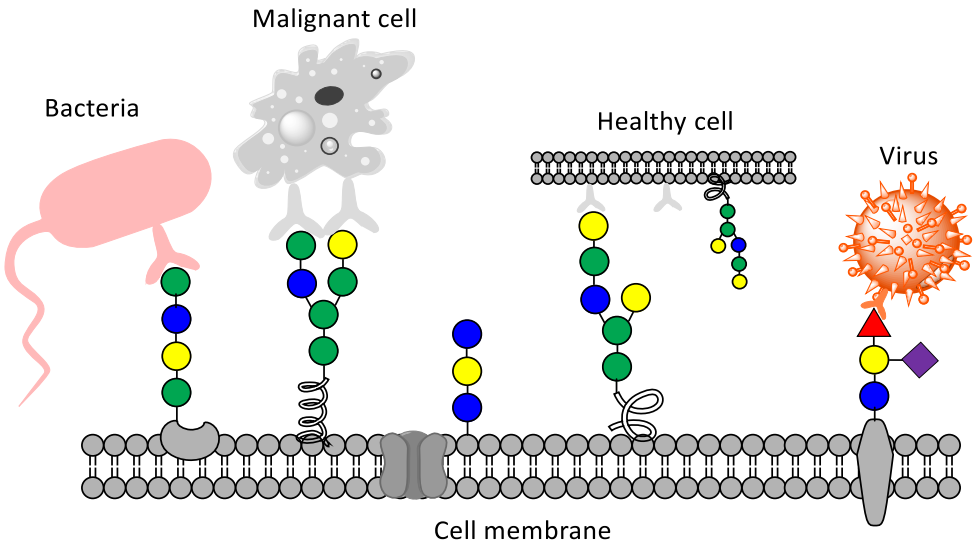

Figure 6: Schematic presentation of a cell, its glycocalyx and possible interactions.

The carbohydrates presented on cells act as ligands for certain carbohydrate binding proteins, called lectins, and take part in processes like cell-cell communication and pathogen recognition.[63] These processes need a certain specificity and affinity, which is achieved through a complex, multivalent glycosylation pattern on proteins and lipids.[64] The chemical nature of saccharides enables crosslinking at several positions, and in combination with the

use of a wide array of different monosaccharides, diverse structures can be build. In humans, the glycocalyx is mainly formed by ten different building blocks, monosaccharides, of which the most common ones are shown in Figure 7.[65]

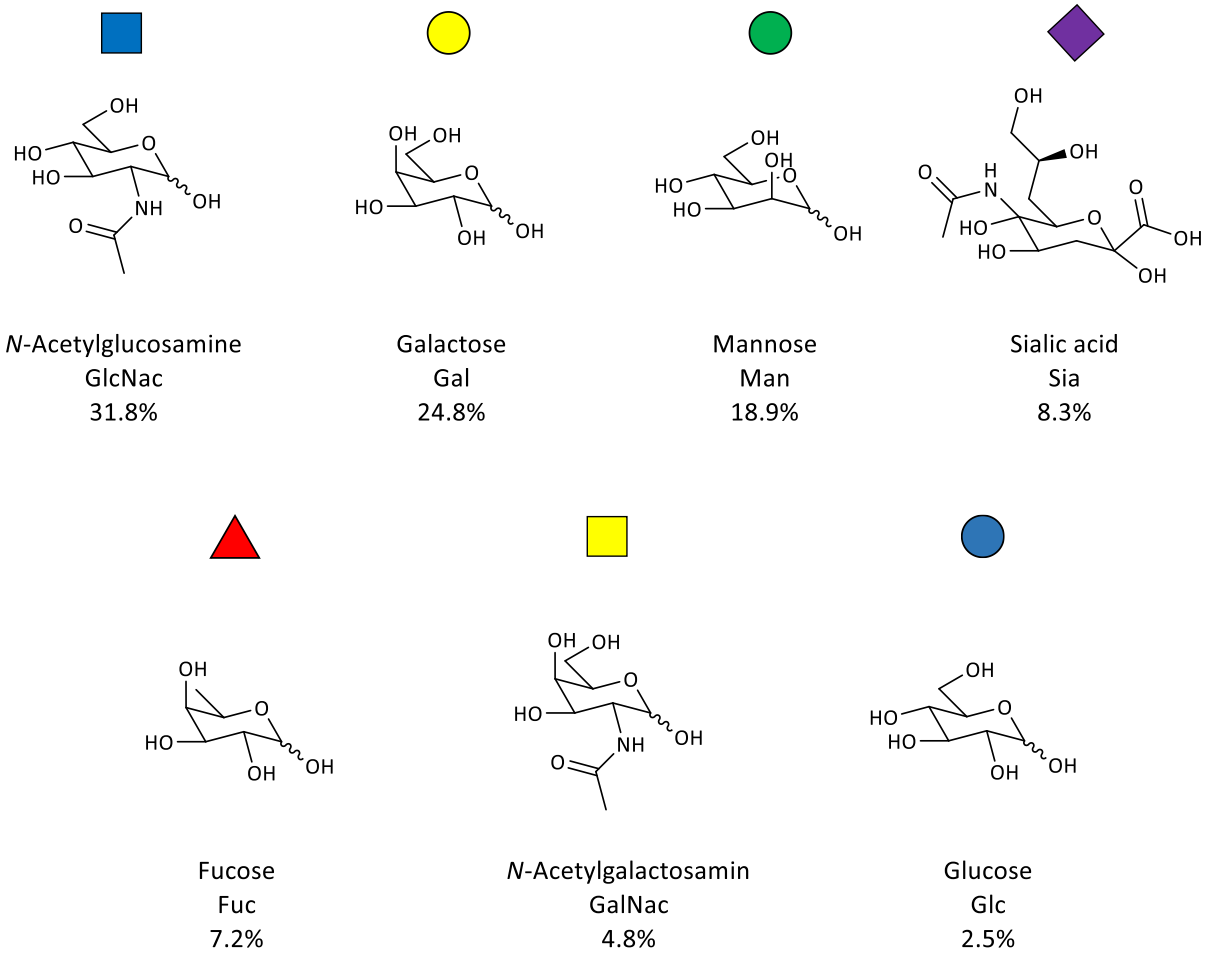

Figure 7: Shown are the most common carbohydrates found on human cells with their name, abbreviation, percentage of presentation and symbol from the Consortium of Funtional Glycomics.[65]

Lectins selectively bind to one or more of these monosaccharides via their carbohydrate binding domain (CBD) with relatively low binding energy for a receptor-ligand interaction.[66] The weak affinity of a single carbohydrate and the arising problem of specificity with only ten available binding moieties is circumvented by displaying branched, multivalent oligo – and polysaccharides that present multiple carbohydrates with a certain geometry resulting in high ligand-receptor specificity and high binding affinity.[67] Here, the binding affinity for multivalent systems is bigger than the sum of binding energies that would be achieved with the single carbohydrates.

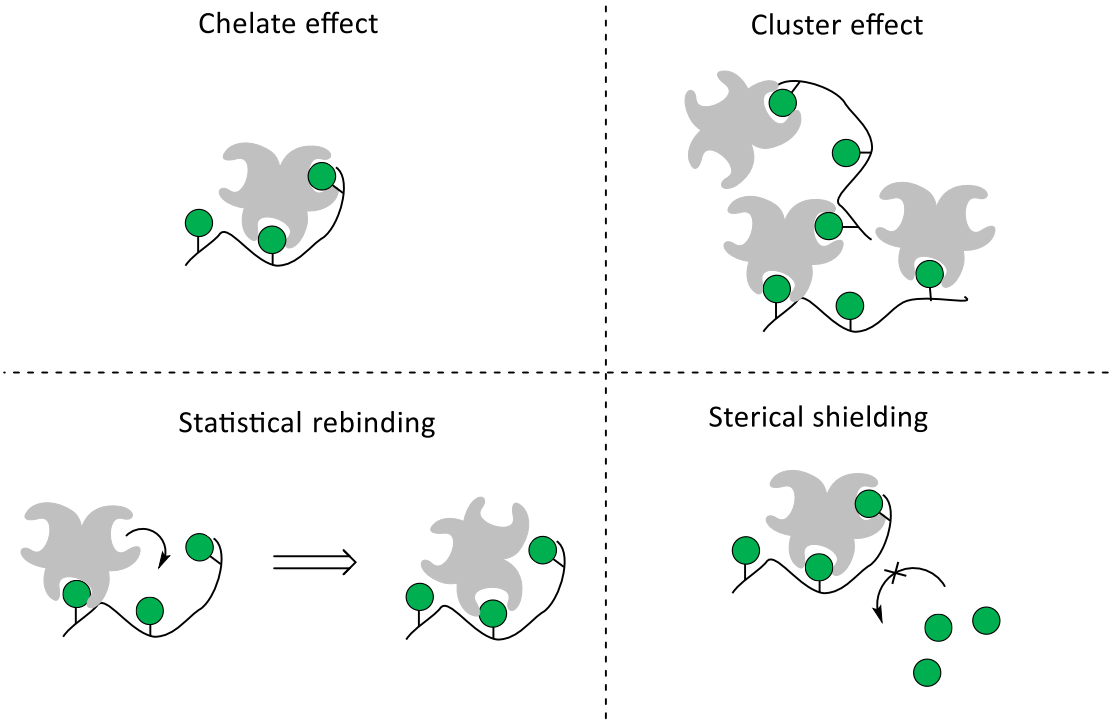

Figure 8: Schematic overview of multivalency effects that can occur for the interaction of multivalent ligands with lectin receptors (according to Kiessling et al.).[68]

This increase is the result of several multivalency effects, namely chelate effect, clustering effect, statistical rebinding and sterical shielding (Figure 8).[66,69] The chelate effect plays a role for lectins with multiple binding sites or lectins that form multimeric structures. Here, a multivalent carbohydrate ligand can bind simultaneous to more than one binding site, potentiating the affinity of its components. A similar mechanism is involved in the clustering effect, where multiple lectins are brought together with a multivalent ligand to increase the overall binding affinity, an effect of especial importance for membrane bound lectins, as the resulting contact can initiate signal transduction.[68] On the other hand, statistical rebinding describes the effect, that a ligand that presents multiple carbohydrates can easily replace a leaving binding moiety in the CBD with one in close proximity, basically locally increasing the concentration of ligands. The last effect, sterical shielding, is not directly connected to the binding event, but stems from the fact that oligo – and polysaccharides are large macromolecules that occupy space around the CBD after a binding event. These macromolecules then can effectively block the access to the CBD to inhibit competition with other ligands. Besides these effects, many lectins also ultilize non-binding regions of ligands and offer secondary binding domains, further increasing affinity and specificity.[70,71]

All these mentioned effects are utilized by lectins to fulfil a wide range of physiological functions in microorganisms, plants and animals. The research into lectins and their interactions was kick-started with the first isolation of a pure lectin, Concanavalin A (ConA), which was extracted from the Jack Bean in 1919 by Sumner and was the basis for the characterization of the fundamental mechanism of lectin interaction.[72,73] Since then, countless lectins were identified, isolated and in detail investigated to resolve their role in physiological functions and as a potential target for a new generation of therapeutics.

1.2.1 Lectins as therapeutical targets

Numerous functions in the human body are regulated by lectins and their interaction with carbohydrates. Lectins are key parts of important and elemental physiological functions and as that offer a valuable target for the development of therapeutics. For example, there are two general parts of the immune system, the innate and the acquired immunity. The acquired immunity is highly adaptive and only found in higher vertebrates and the innate immunity is evolutionary universal and initially was thought to be mainly characterized by unspecific phagocytosis.[74] But contrary to that initial belief, the innate immune system presents high specificity and can distinguish between pathogens and self. This is achieved through recognition of pathogen-associated molecular patterns (PAMPs) by different classes of receptors.[75] One of these classes are lectins, and the main representative is the mannan-binding lectin (MBL) which is a highly oligomeric protein with up to 700 kDa and belongs to the collectins, a group of collagenous calcium dependant defensive lectins.[76] It was shown that MBL binds to yeasts, bacteria, viruses and even parasites by recognizing mannose or GlcNac presenting oligosaccharides on their cell surface which results in the activation of the complement system and subsequent activation of phagocytes that digest the marked pathogen.[77] Problems in the biosynthesis of MBL or genetic mutations can result in a significant reduced immune system and general vulnerability to infections.

Similar processes, but in a reverse relationship, play a crucial role in human infections with pathogens like bacteria and viruses. These pathogens use lectins like adhesins and toxins that bind to surface carbohydrates of targeted cells and initiate or mediate infection pathways. The carbohydrate pattern presented on cells varies for different animals, cell types, tissues

and development stages.[78] Thus, microbes can use lectins to specialize on certain targets and circumvent defence mechanisms.[79]

One example for this is the bacterium *Pseudomonas aeruginosa* (*P. aeruginosa*) which is responsible for acute and chronic cystic fibrosis, pneumonia and infection of open wounds and is a problematic candidate for treatment as antibiotic resistances are increasing.[80] As for other pathogenic microorganisms, a crucial step for infection is the adhesion to host cells which is often mediated by surface glycoconjugates via selective bacterial receptor binding.[81] For *P. aeruginosa*, it was shown that glycoconjugates on epithelial and endothelial cells are recognized.[82] For this, two receptors were identified that take part in this process, the galactose binding LecA and the fucose binding LecB, both soluble lectins that are found in the cytoplasm as well as in the outer membrane.[83] It was shown that mutants without LecA or LecB have reduced adhesion to A549 lung cells and overall lower infectious potential.[84] Besides mediating the initial adhesion process, both lectins also take part in later stages of the infection as virulence factors. LecA has a cytotoxic effect on epithelial cells and LecB is involved in protease IV activity which is responsible for tissue damage.[85] As both are part of the initial adhesion step and later acting as virulence factors, targeting LecA and LecB to inhibit their interactions could be a promising tool to control *P. aeruginosa* infections. One potential way to deactivate these two lectins and the processes they take part in is to offer ligands with higher affinity than the natural occurring ligands on the targeted cells. In fact, nature already uses this approach to prevent enteric diseases in newborn by blocking the adhesion of pathogenic bacteria to the duodenual epithelium with oligosaccharides secreted in human milk.[86] This also applies to *P. aeruginosa* as fucosylated human milk oligosaccharides were found that specifically inhibit LecB. Following this approach, a lot of work was done on the synthesis of biomimetic structures to find more potent inhibitors for both LecA and LecB. More effective inhibitors can either be generated by altering the carbohydrate moiety and its interactions in the CBD or by synthesizing multivalent ligands.

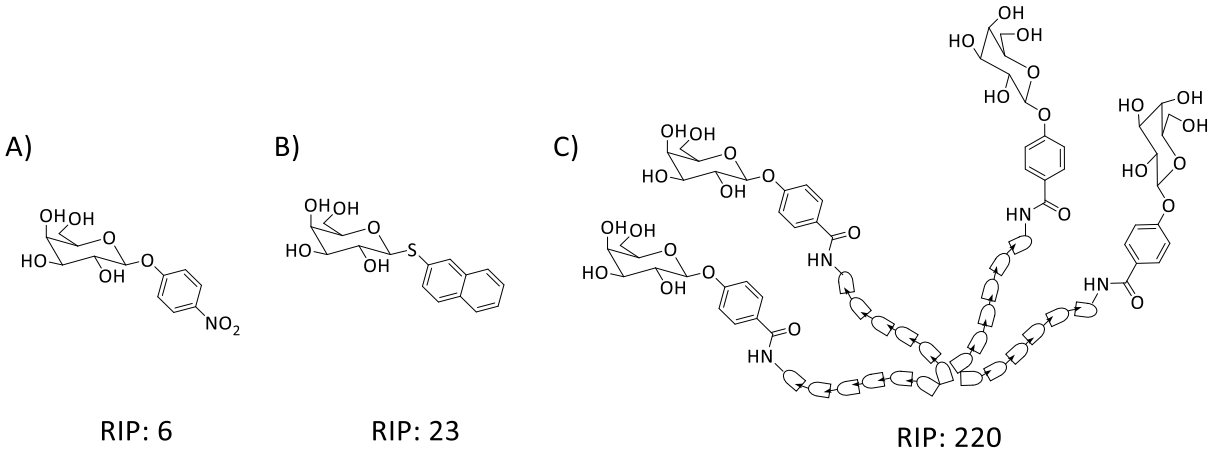

Figure 9: Exemplary inhibitors of LecA with their relative inhibitory potential (RIP).

First studies on LecA ligands were conducted by Garber et al. with substituted galactose derivates where hydrophobic and thiogalactoside variants showed higher inhibition of LecA than galactose itself.[87] This was later also shown and quantified in ITC measurements with *p*-nitrophenyl-β-galactoside, which showed a K_D value of 14 µM in comparison to 87 µM for galactose, which means it has a 6 times higher relative inhibitory potential per carbohydrate unit (RIP) (Figure 9 A).[88] They could also show, that the increase in affinity can be attributed to a hydrophobic environment in the entrance of the carbohydrate binding domain, enabling additional interactions. In continuation of this work, Rodrigue et al. synthesized aromatic thioglycosides that were even more potent, as shown in a competition-inhibition assay with LecA where the best structure was found to be 23 times more effective than α-methyl-galactose (Figure 9 B).[89] At some point, the optimization of single carbohydrate moieties is limited and the way to further advance the development is to mimic the multivalent presentation of carbohydrates in natural ligands. Kadam et al. managed to synthesize peptide dendrimers that present four galactose units with different linkages. Their best binder achieved a K_D value of 0.1 µM in ITC measurements, which is 220 times as effective per galactose unit as isolated galactose (Figure 9 C).[88] This drastic multiplication of affinity can be attributed to the above described multivalency effects.

Another pathogen that uses a lectin-carbohydrate interactions as crucial adhesion step during infection is *Escherichia coli* (*E. coli*), which is responsible for over 85% of acute cystitis cases.[90] *E. coli* can have proteinogenic, hair-like pili on the cell surface with which they can attach to mannose presenting tissue, eg. in the bladder, a process which is necessary for successful infection.[91] After attachment, the pili also mediate contact between bacteria cells to form

biofilms, which is a state in which bacteria are better protected against host defence mechanisms and antibiotics.[92] The key protein in these processes is located at the tip of type 1 pili and is a mannose binding lectin called FimH and prime target for potential treatment of cystitis. It was already shown that FimH based vaccination can drastically reduce colonization of bladder mucosa by *E. coli*, showing how crucial the lectin interaction is for adhesion.[93] Another established standard treatment is the dietary uptake of high amounts of mannose during urinary tract infections to disrupt the FimH interaction with tissue through competitive inhibition.[94] Following this approach, it is of high interest to develop more potent ligands for FimH that can inhibit its interaction with mannose presenting tissue. The findings for FimH are similar to the ones presented for LecA, as the introduction of hydrophobic moieties drastically increases affinity. The *p*-nitrophenyl variant of mannose has a RIP of 70 in comparison to the methyl variant as shown by Sharon.[95] Sperling et al. managed to optimize monovalent mannose ligands by introducing squaric acid ethylesters to increase the RIP to 7000 and Nagahori et al. even further increased the inhibitory potential to over 10000 by presenting multiple mannose on dendrimers, again utilizing multivalency effects. Indeed, today there are numerous studies on synthetic carbohydrate-based ligands targeting FimH.[96] One reason is that there are several well established assays to quantify the FimH-ligand interaction, and competition-inhibition assays on live bacteria can be done cheap and easily in high throughput. One of these assays was introduced by the working group of Lindhorst and is based on fluorescence marked *E.coli* (Figure 10).[97]

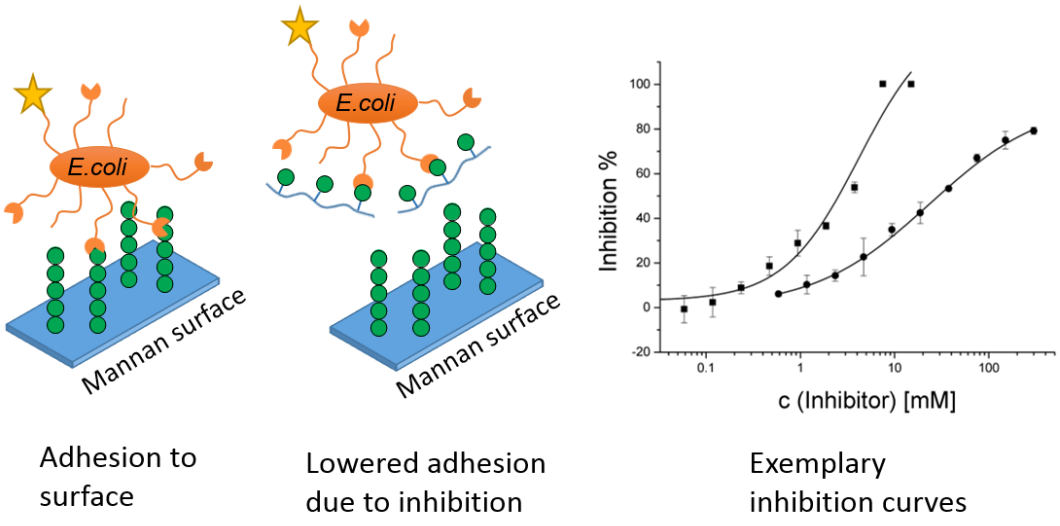

Figure 10: Schematic illustration of the adhesion-inhibition assay introduced by the working group of Lindhorst and an exemplary inhibition curve.[97]

For this assay, multiwell plates are coated with mannan, a linear mannose polymer, and the binding of *E. coli* to mannan is measured in presence of varying concentrations of inhibitor to calculate an IC_{50} value. By also using α-methyl mannose on every plate, relative inhibitory potentials (RIPs) can be calculated to compare results between different plates and experiments.

These are only two examples of lectins of pathogenic microorganisms, as there are a wide range of bacteria and viruses that use lectins to similar effect.[78] Furthermore, these interactions also play part in other diseases such as tumorigenesis. There are many factors that result in a healthy cell to become a malignant and metastatic cell. A variety of environmental factors, genetic changes and prepositions can influence these developments and as a result most cancerous cells and tumours are unique regarding their cellular markers.[98] Nevertheless, nearly all malignant cells present a changed glycosylation pattern compared to healthy cells which can be attributed to different glycosyltransferase activities and results in specific glycoconjugate presentation by which malignant cells can be distinguished from normal cells.[99-102] These variations result in so called tumour associated carbohydrate antigens like the Thomson-nouveau or Thomson-Friedenreich antigen and are most of the time characterized either by the presentation of sialic acids or by branched N-linked *N*-acetylgalactosamines.[103-105] These unique patterns offer potential use in cancer therapy and diagnostics, as there are already carbohydrate based vaccinations in development and glycosylation patterns can be used as a marker to identify patients with e.g. pancreatic cancer.[106,107] Another approach that could make use of these patterns is targeted drug delivery by attaching cytotoxic drugs to lectins that target cancerous cells and release the drug only after accumulation.[108]

Not only the glycosylation changes when cells become cancerous, but certain lectins become overexpressed and take part in crucial steps in tumorigenesis. For example, galectins are overexpressed in different cancer types and are associated with preventing apoptosis, a programmed cell death that would kill malignant cells, as well as increasing resistance against cisplatin, one of the most common chemotherapeutics.[109-111] Galectins are a family of 15 so far identified lectins that bind to galactoside moieties and can be divided in several structural subgroups but all have a conserved carbohydrate binding domain.[112] One of the better investigated tumor-associated galectins is Gal-3, which is a chimeric protein that self-

aggregates to oligomers and was shown to play a role in tumor metastasis, as it mediates the adhesion to fibronectin which is crucial for migration of cancerous cells.[113,114] Gal-3, and galectins in general, only fulfil their role when binding to specific ligands, which means that again a potential therapeutic approach is blocking the CBD with highly affine inhibitors. For this different classes of inhibitors are already being investigated, for example aldoximes which introduce hydrophobic moieties at the anomeric center and can reach K_D values of 330 µM, aromatic substituted LacNAc derivatives with K_D values as low as 1.3 µM or lactose functionalized dendrimers that achieved nanomolar IC_{50} values in inhibition studies, showing promising results to eventually develop carbohydrate based, targeted chemotherapeutics.[115-117]

As shown, lectins fulfil important and positive functions in human physiology, but are also used by pathogens in infection pathways and can turn malignant in cancerous cells. As a result, lectins can be used as a potential therapeutic target, as the inhibition of their carbohydrate-ligand interaction can also inhibit their pathogenic processes. There are several promising, highly specialized glycomimetics already synthesized and investigated and in general multivalent systems are so far shown to be the most efficient candidates. Most of the synthetic tools towards multivalent structures are limited due to their dispersity, in comparison natural ligands have very defined structures and architectures increasing specificity and affinity. In addition, even high affinity ligands only inhibit the target lectin reversibly, resulting in clearance from the receptor over time. One possible, next generation approach would be to include reactive groups into sequence-defined, multivalent ligands to covalently and irreversibly inhibit lectin binding sites.

1.3 Solid phase polymer synthesis

As prior stated, macromolecules play important roles in biological functions in all living organisms. Most of these structures such as DNA, proteins or the carbohydrates in the glycocalyx are monodisperse polymers with complete control over sequence and architecture, which is essential for their function. The already described examples of mussel inspired wet adhesion and carbohydrate ligand-lectin interactions are mainly investigated with either small molecules, or polymers that show some degree of dispersity, limiting the degree to which their underlying mechanisms can be investigated.[118] Because of this, it is of

high interest to develop and use methods to achieve full sequence-control in macromolecules.

One possible way to achieve this goal, is using solid phase based synthesis as developed by Merrifield.[119] The core principle of this kind of synthetic strategy is to use building blocks (e.g. amino acids) that present a free acid and a protected amine group (Figure 11). These structures are coupled to a functionalized resin and subsequently the amine function is deprotected. The next building block is then added via amide coupling and in an iterative approach of deprotection and coupling, sequence-defined structures can be built. Besides the complete control over the sequence, advantages of solid phase based synthesis are easy separation of product from the reaction solution and the modular set-up, which makes the introduction of a wide range of functionalities possible.[120]

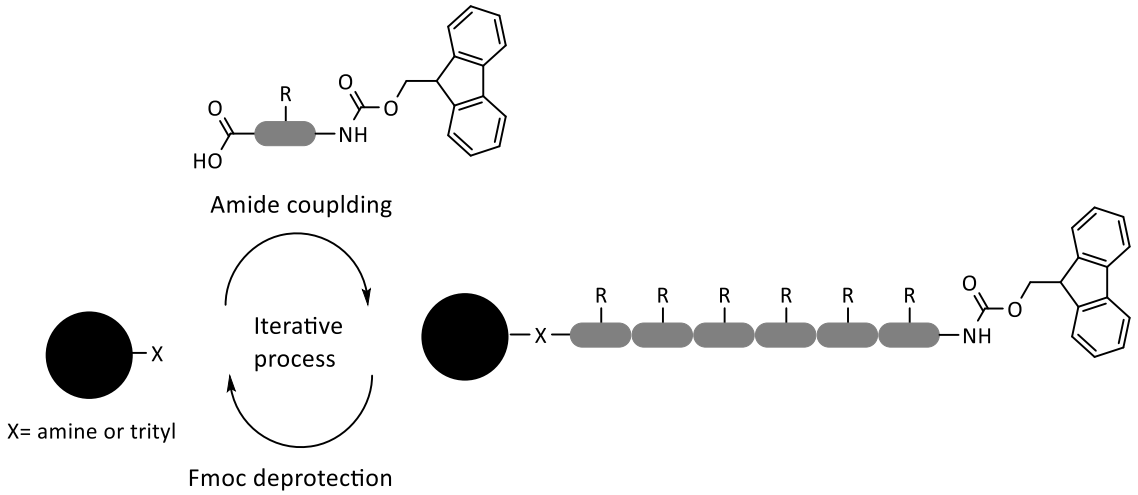

Figure 11: Schematic reaction cycle of solid phase based synthesis.

An example for this is the solid phase polymer synthesis (SPPoS) developed by the working group of Prof. Hartmann, which yields sequence-defined oligo(amidoamine)s.[121] This synthesis is based on the Fmoc peptide synthesis and uses similar linker, protection groups and reagents (Figure 12). The starting point for this synthesis is the resin, which consists of porous beads made from an unsoluble, cross-linked polymer that present a functional group. Most resins are made of an copolymer of styrene and divinylbenzene and modern resins, like the TentaGel® resin, are additionally grafted with PEG chains to optimize swelling and surface interaction behaviour.[122] As point of attachment for building blocks, different linker can be chosen that come with different initial coupling and final cleavage conditions. One of the first

resins, the Merrifield resin, used a simple chloromethyl group directly at the polymer as linkage which was cleaved after peptide assembly by hydrofluoric acid.[123] Today, most commonly used linkers are 2-chloro tritylchloride which releases a free acid under mild acidic conditions (1% trifluoroacetic acid), and the rink amide linker which releases a primary amide and needs high amounts of acid (up to 95% trifluoroacetic acid).[124] As side chain, and orthogonal amine protection to Fmoc, the Boc, Alloc or trityl group can be used (see Figure 12).[125] Fmoc itself is cleaved by piperdine, which acts as a base for deprotection as well as scavenger for the forming vinyl species.

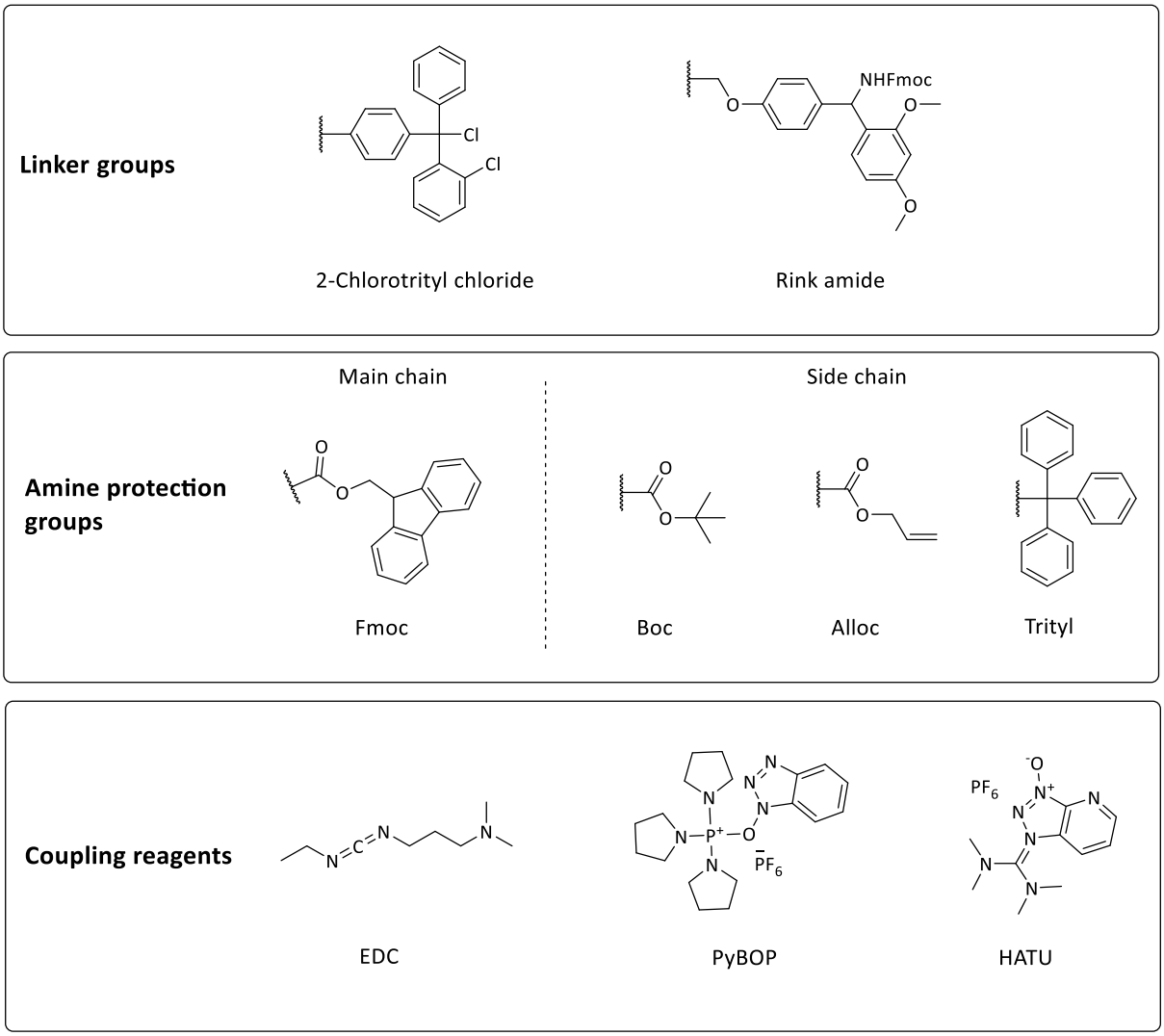

Figure 12: Overview of resin linker, orthogonal amine protection groups and coupling reagents commonly used for SPPoS.

For the amide bond coupling for main chain elongation, different activation reagents can be used. They all activate the acid moiety via the formation of an active ester which afterwards

reacts with the free amine on solid support.[126] One of the classic strategies is using carbodiimides like EDC, which in a first step forms an intermediate with the deprotonated acid to subsequent react with a suitable alcohol to the active ester and an urea side product. Main disadvantage is an occurring acyl transfer to an unreactive species and overall lower coupling efficiency in comparison to other common reagents.[127] The newer generation of coupling reagents combines the moiety for acid activation and the alcohol for active ester formation into one molecule. These reagents can be divided into two classes, the phosphonium salts like PyBOP and the uronium salts like HATU. Both classes initiate the coupling by reacting with the acid to release the nucleophilic hydroxyl benzotriazole (HOBt), which then reacts with the formed intermediate to generate the active ester. This reaction is driven by the formation of a thermodynamically favourable side product, phosphoramide for phosphonium based and tetramethylurea for uronium based reagents.

Basically any structure with a free acid and Fmoc protected amine can be used to create polymers on solid support using the described methods. For the already mentioned SPPoS, Hartmann et al. developed special building blocks to create sequence-defined oligo(amidoamine)s with a variety of functionalities and architectures (Figure 13).

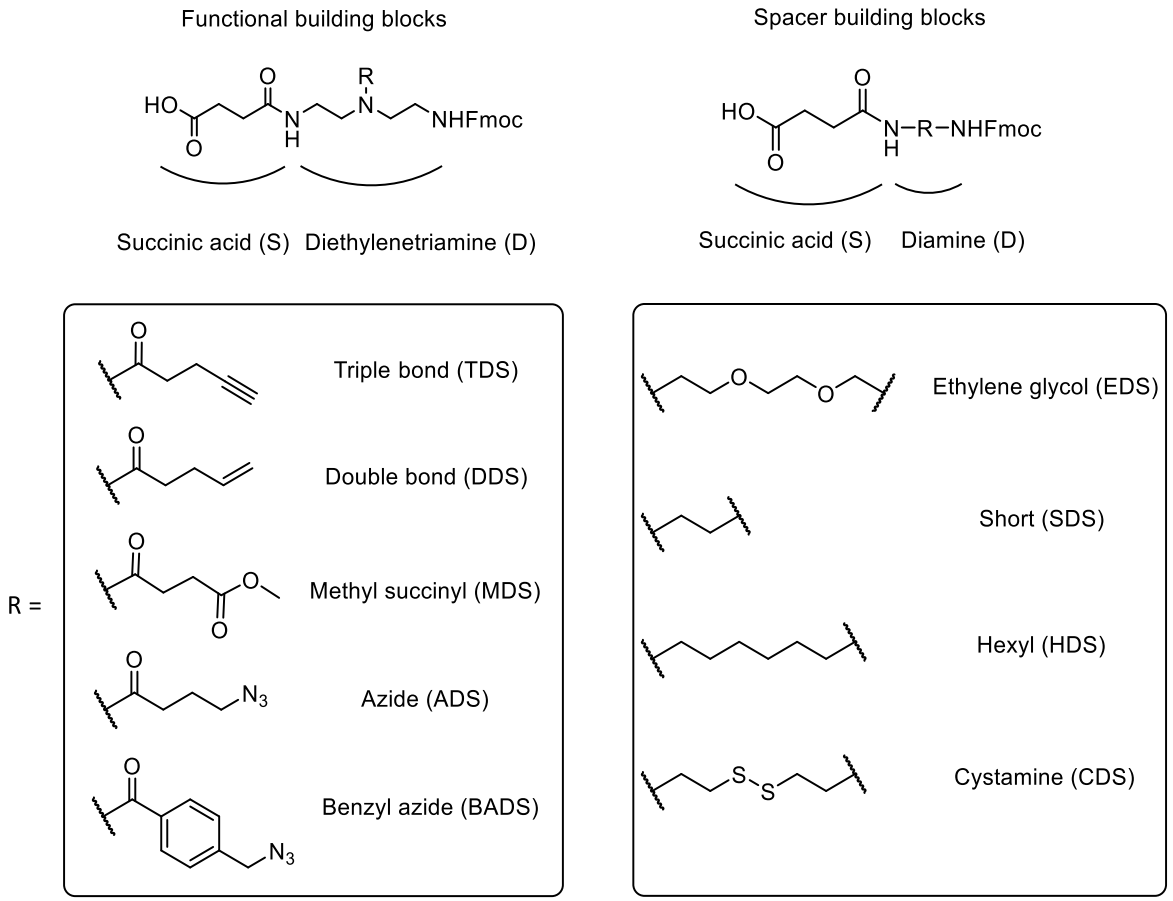

Figure 13: Overview of the two different classes of building blocks, functional building blocks (eg. TDS[121], DDS[128], MDS[129], ADS[130], BADS[131]) and spacer building blocks (eg. EDS[121], SDS[128], HDS[132], CDS[132]).

The basis for these specialized structures are functional building blocks that are synthesized from diethylenetriamine.[128] By introducing a succinic acid on one primary amine and Fmoc on the other one, solid phase synthesis compatible building blocks are created. Using the left over secondary amine, additional functionalities can be introduced. Following this synthesis, a diverse library of building blocks was developed (Figure 13). The most frequently used functionality is the alkyne moiety, which is mainly used for attachment of azide functionalized carbohydrates via copper-catalysed azide-alkyne cycloaddition (CuAAC).[121] To control the length of the macromolecule, the spacing between functional groups and the overall physicochemical properties of the backbone, several spacer building blocks were introduced that utilize either an ethylene glycol unit or alkyl chains of varying length.[133]

This SPPoS was already utilized to synthesize various glycomimetics that differ in carbohydrate presentation, architecture and hydrophobicity or with additional secondary

binding motifs. Because of its unique kit of building blocks, this synthesis is interesting in general for its potential to generate sequence-defined biomimetic macromolecules.

2. Aims and Outlines

The catechol moiety is a functional group with unique chemical properties. It can undergo a variety of molecular interactions with all kind of surfaces or other molecules in solution. Furthermore, catechols can oxidize to a benzoquinone form, an electrophile which can react for example with amines or crosslink to other catechol units. This moiety is part of a wide range of biological structures and signalling molecules but is foremost famous for its part in the outstanding wet adhesion of mussel foot proteins. To transfer these properties to synthetic systems could pave the way to new adhesives for the medical field or efficient and environmentally friendly coating strategies. Strong molecular interactions are not only important for adhesion but also in ligand-receptor binding. The introduction of catechols into natural ligands could increase their affinity and even open the possibility of covalent binding through catechol oxidation. One possible application for this is the inhibition of bacterial or viral adhesion to host cells through catechol presenting glycomimetics.

The natural structures in both these examples are synthesized in a defined, monodisperse manner with control over sequence and length. Because of this, the aim of this work is to investigate the presentation of catechols in biomimicking macromolecules. It is anticipated that the sequence and positioning of these moieties has a direct influence on adhesive strength and ligand-receptor interaction. However, there is only limited access to methods for the synthesis of sequence-defined macromolecules. For this, the working group of Prof. Hartmann developed sequence-defined oligo(amidoamine)s that are based on tailor-made building blocks presenting a free carboxylic acid and a protected amine. These building blocks are assembled on solid support via sequential deprotection and coupling protocols. By using functional building blocks presenting reactive side-chains, the assembled scaffolds can be further modified to create macromolecules with control over length, sequence and functionality.

Overall, the goal of this thesis is to develop new methods for the sequence-defined presentation of catechols in macromolecules via solid phase synthesis. These methods will be used to synthesize Mfp mimicking structures and to investigate the mechanism of catechol

driven wet adhesion. In a subsequent project, new catechol presenting glycomimetics will be synthesized for the inhibition of bacterial adhesion.

In the first part of this thesis, a new route towards functional building blocks will be developed. The goal is to reduce the number of overall steps to decrease time required for synthesis and increase the overall yield. With the new protocol, building blocks for the introduction of catechols, tertiary amines and primary amides for solid phase synthesis will be developed. Furthermore, the use of these building blocks for successful synthesis of catechol containing macromolecules will be demonstrated.

In the second part, the newly developed synthetic strategy will be used to synthesize a library of Mfp mimicking oligomers via solid phase synthesis. These structures will be characterized in detail and deployed in assays for adhesion measurement to shine a light on the underlying mechanisms of adhesion regarding controlled presentation of functional groups. As assay the so called SCP-RICM assay will be used. For this, PEG microgels will be functionalized with the synthesized oligomers and the adhesion will be measured against a glass surface at different conditions.

As a third and final step, catechol containing sequence-defined oligomers will be used to synthesize glycomimetics for covalent lectin inhibition. Here, the solid phase synthesis will be used to present carbohydrates and catechols on one scaffold and to investigate the influence of catechol presentation on inhibition potential and covalent binding capability. Therefore, a library of mannose and galactose presenting structures will be synthesized and their lectin binding will be quantified via turbidity and precipitations assays. Furthermore, their ability to inhibit bacterial adhesion will be measured and the covalent binding will be investigated via MALDI-TOF and SDS-PAGE.

3. Results and Discussion

3.1 Synthesis of mussel foot protein mimicking oligo(amidoamine)s

This first chapter of the thesis will describe the development of the synthesis of biomimetic, mussel foot protein like oligo(amidoamine)s via solid phase polymer synthesis (SPPoS). The goal was to establish a synthesis towards structures that present catechols, tertiary amines and primary amides in any combination with control over position and spacing. For this, a new synthesis route towards functional, solid phase compatible building blocks was introduced that reduced the overall steps and increased the yield, as well as prevents any form of rearrangement that was observed for the original synthetic route. This new protocol was used to synthesize two different building blocks, a methyl ether protected catechol building block and a building block that presents a trityl protected amine for further functionalization on solid support. It was shown that both building blocks can be used for solid phase synthesis applying Fmoc-based peptide chemistry. Furthermore, the deprotection of the methyl ether group was established on an exemplary, catechol containing oligomer and the deprotection of the trityl group and subsequent functionalization with tertiary amine or primary amide, respectively, was introduced.

3.1.1 Towards a new route for functional building blocks

For SPPoS, two different kinds of monomeric units are used, functional and spacer building blocks. A prerequisite for the use in SPPoS is the incorporation of a free carboxylic acid and an Fmoc protected amine as well as sufficient solubility in suitable solvents like DMF or NMP. In addition to this, their synthesis needs to be suitable in large scale, as high excess of building blocks is needed to achieve full conversion in each coupling step. For both kinds of building blocks, Hartmann et al. developed protocols that can be easily altered for the introduction of new moieties, either in functional or spacer units.[121] The spacer building blocks can be synthesized in three steps with high yield, but the synthesis of functional building blocks is more challenging. The route is comprised of seven steps and starts with diethylenetriamine as precursor (Figure 14).

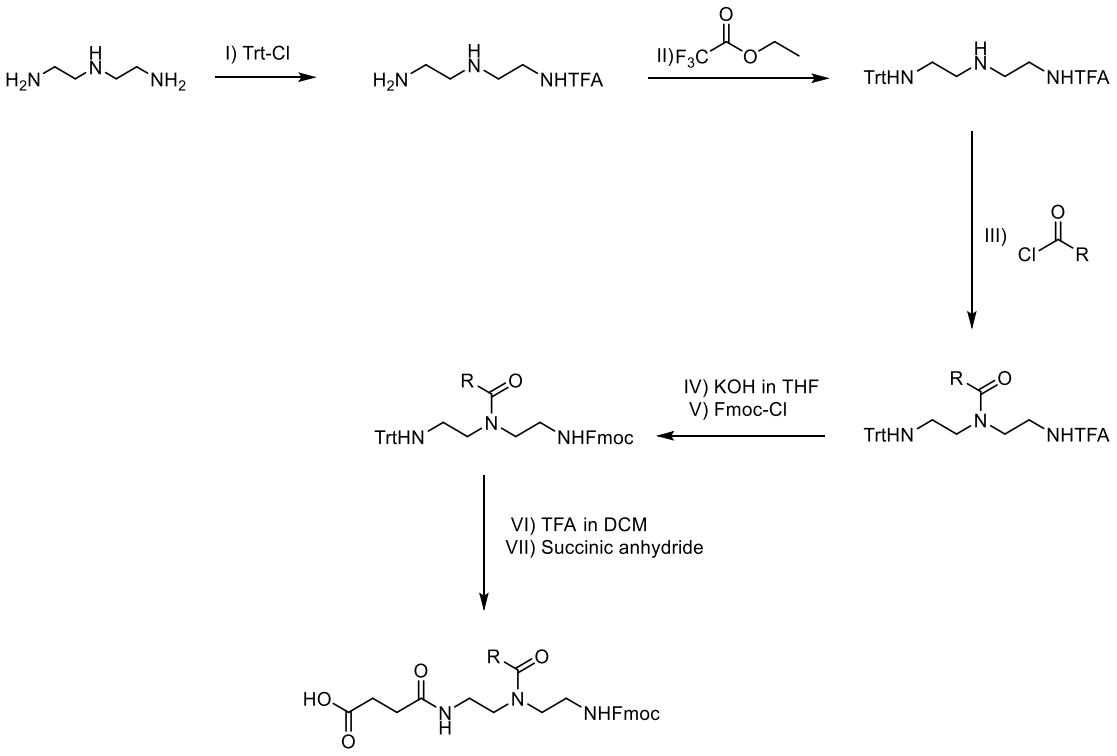

Figure 14: Established synthesis route towards functional building blocks for SPPoS.

In a first step, one primary amine is selectively protected with trityl by using low equivalents of reagent. The second primary amine is then converted using trifluoroacetic acid ethyl ester which only reacts with primary amines. The desired functional handle is introduced as a side chain at the secondary amine by using an acid chloride for amide formation. The next steps remove the temporary protection groups and introduce the final moieties. First, the TFA group is removed in basic conditions and Fmoc is coupled to the building block. In the end, the trityl group is removed with trifluoroacetic acid (TFA) and the carboxylic acid is incorporated through succinic anhydride. This lengthy synthesis results in a time and material consuming synthesis with low overall yield, usually between 20 and 30%. This is due to several factors. First, there are two temporary protection groups introduced to enable the asymmetric functionalization of diethylenetriamine, adding unnecessary steps. Besides that, a lot of product is lost due to frequently occurring purification steps, the intermediates after step II and III are crystallized. Furthermore, during the basic deprotection of the TFA protection group (Step IV), a rearrangement can occur where the functional side chain shifts to the deprotected primary amine. For this reason, the reaction needs to be tightly controlled and stopped after a certain amount of time to limit the formation of rearrangement side-product. Not only does this decrease the overall yield, but it also means that the synthesis for

any new building block needs to be optimized in regards to the kinetic of the mentioned rearrangement.

Because of these limitations, the goal was to develop an optimized synthesis route that reduces the reactions steps, increases yields and removes the possibility of any rearrangement. The first idea to achieve these goals was to eliminate the use of any temporary protection groups. This means, that either succinic acid or Fmoc needs to be selectively coupled to one of the primary amines (Figure 15)

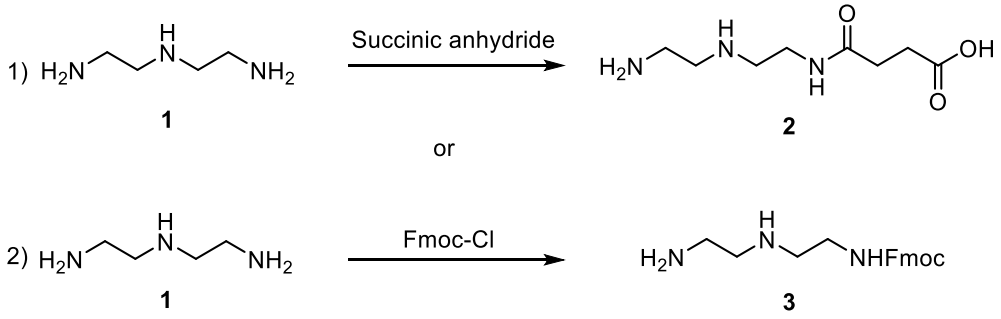

Figure 15: Reactions for direct introduction of final moieties; 1) 0.25 eq. succinic anhydride in DCM for 2 h; 2) 0.25 eq. Fmoc-Cl in DCM for 2 h.

Both reactions were done similar to the original protocol, as 0.25 equivalents of reagent were used to ensure only one primary amine is functionalized. The first reaction showed conversion via TLC, but the hydrophilic product could not be separated from the residual diethylenetriamine. For the second reaction, conversion again took place as shown via TLC, but the wanted product could not be isolated. After work up, a rubbery, insoluble white solid remained. This residue likely stems from the decomposition of the Fmoc moiety by the residual amine functionalities during work up, which could potentially polymerize, explaining the insolubility.

As a result, the initial protection with the temporary trityl group was hold onto, and the next approach was to replace the TFA protection step with the introduction of Fmoc or succinic acid (Figure 16).

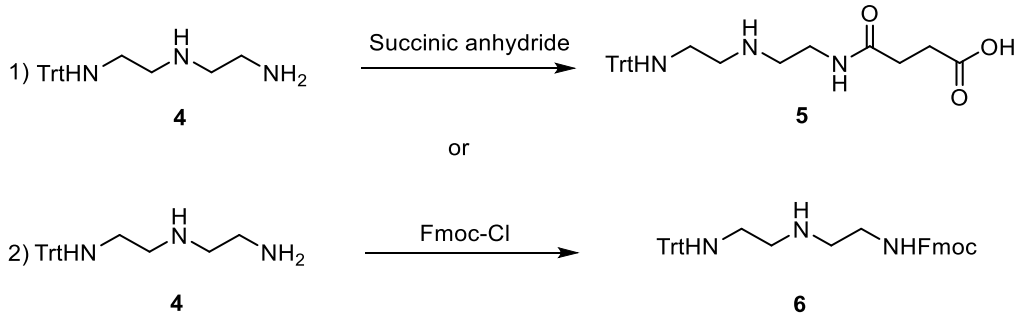

Figure 16: Reactions for introducing the final moieties as second step; 1) 1 eq. succinic anhydride, 3 eq. triethylamine in DCM for 2 h; 2) 1 eq. Fmoc-Cl, 3eq. triethylamine in THF for 2 h.

For both reactions, exactly one equivalent was used to completely convert the primary amine. This time, a product could be isolated for the first reaction, but the reaction was not selective for the primary amine, as two products with approximately a 1:1 ratio and the same mass could be identified via LC-MS, likely corresponding to functionalized primary and secondary amine. Similar results were observed for the protection with Fmoc-Cl by measuring LC-MS from the reaction solution, rendering both of these reactions not suitable for a new synthetic protocol. These results were expected for the first reaction, as succinic anhydride is a highly reactive and small residue that is likely to also react with the steric hindered secondary amine. However, for the introduction of Fmoc, it was anticipated that the bulky group should discriminate between the accessible primary amine and the hindered secondary amine in proximity to the trityl group. A reason could be, that the reagent, Fmoc-Cl, is too reactive and readily reacts with any nucleophile. To test this hypothesis and to possibly achieve selective conversion of the primary amine, as alternative reagent Fmoc-OSu was used as it is bulkier and less reactive than Fmoc-Cl.

*Table 1: Results for the conversion of structure **4** with Fmoc-OSu in comparison to Fmoc-Cl, as determined by RP-HPLC after 3 h.*

Reagent	Temperature [°C]	Addition Time [h]	Secondary amine [%]
Fmoc-OSu	-78	2	0.5
Fmoc-OSu	-78	0	0.4
Fmoc-OSu	0	2	1
Fmoc-OSu	0	0	1
Fmoc-OSu	20	1	1.1
Fmoc-Cl	20	0	50

With this reagent, intermediate **4** was converted by different temperatures and different time over which the reagent was slowly added to the reaction solution. By measuring LC-MS of the reaction solution after 3 hours, the amount of reacted secondary amine was determined (Table 1). A correlation was found between temperature and amount of secondary amine functionalized: lower temperature led to a lower amount of secondary amide formed, which means that the selectivity is kinetically driven. Although even the highest amount of 1.1% is negligible, -78°C were chosen as temperature for further reactions to prevent increasing side reaction due to less efficient heat exchange for larger scales.

With these results the first milestone towards an optimised and shorter synthetic route was achieved. Unfortunately the product **6** could not be isolated, probably again due to a cleavage of the Fmoc group by the secondary amine. As an alternative, the direct conversion of the secondary amine in a one-pot approach was tested (Figure 17).

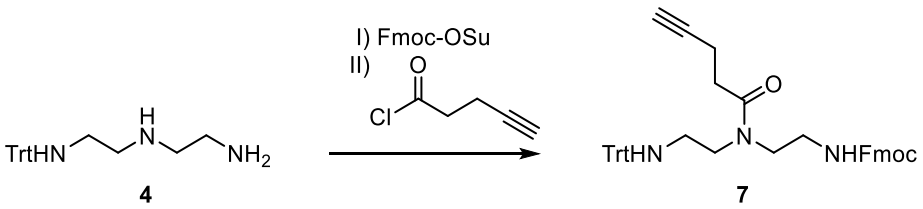

*Figure 17: One-pot reaction for introducing Fmoc and side chain into TDS intermediate **7**; I) 1 eq. Fmoc-Osu, 3 eq. triethylamine in THF at -78°C for 2 h; II) 1.3 eq. acid chloride overnight.*

As reagent for the side chain, pentynoic acid chloride was chosen, as this is the side chain of the well-established TDS (Triple bond-Diethylenetriamine-Succinic acid) building block. After addition of Fmoc-OSu and full conversion as determined by TLC, the acid chloride was directly added to the reaction solution. Here, the product could be successfully isolated, establishing a one-pot synthesis that selectively protects the primary amine with the final Fmoc moiety and then directly introduces the final side chain in one reaction step. To prove that indeed the primary amine was functionalized in this reaction and to show feasibility of the new synthetic route, the last two steps towards the final product were performed with intermediate **7** (Figure 18).

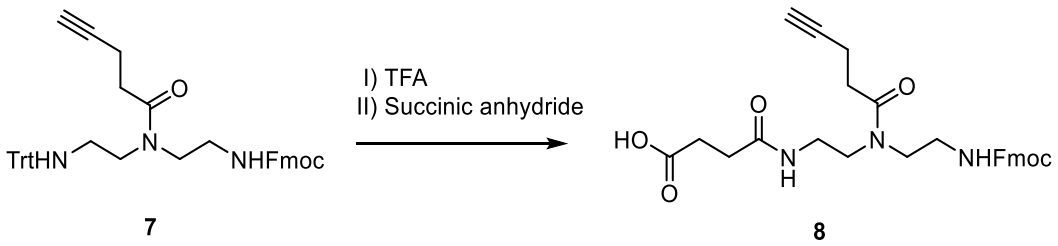

*Figure 18: Final steps towards building block TDS (**8**); I) 10% TFA in DCM for 1 h and subsequent precipitation; II) 1.3 eq. succinic anhydride, 3 eq. triethylamine in DCM for 2 h*

After cleavage of the TFA protection group and addition of succinic anhydride, TDS (**8**) was isolated as final product with a yield of 55%, doubling the usual yield of the previously established protocol.[121] To prove successful synthesis, LC-MS measurements with TDS from the previous and new route were performed. In addition, these were compared to the product of the previous synthetic route where rearrangement occurred (Figure 19).

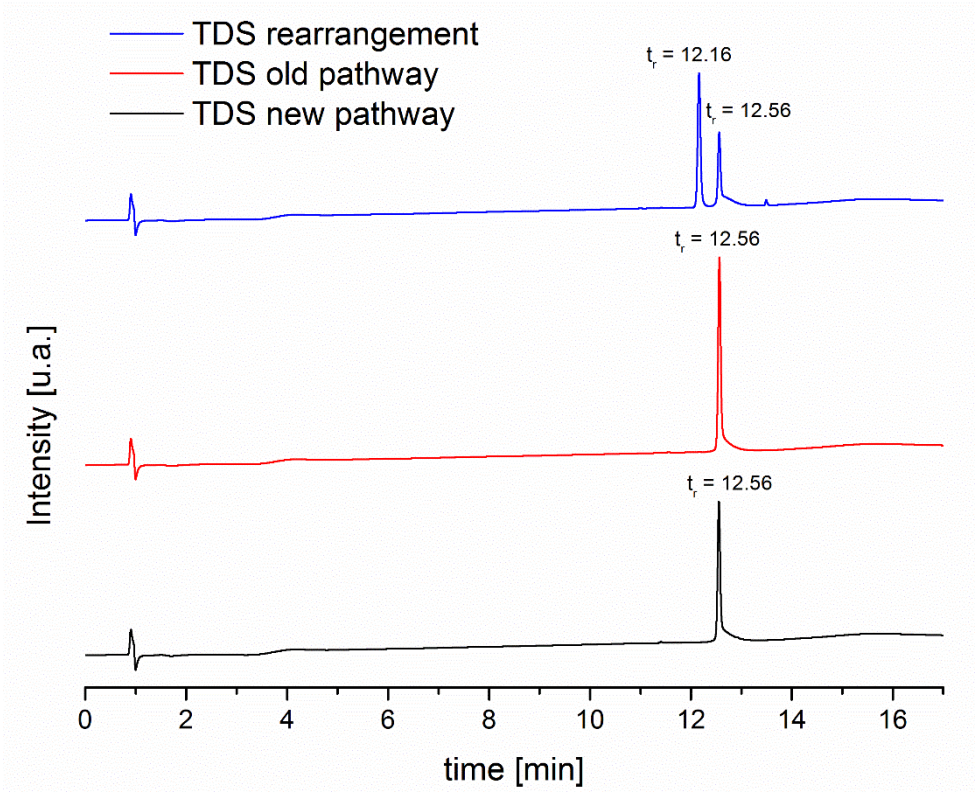

Figure 18: RP-HPLC measurement of TDS received by the new route (black), the previous route (red) and from a batch where rearrangement occurred (blue). Gradient from 100% A (95/5 H_20/MeCN, 0.1% formic acid) to 50% B (95/5 MeCN/H_2O, 0.1% formic acid) over 17 min at 25°C.

The comparison between the black and red graph clearly shows, that the new synthetic approach yielded the same product as the old method. The blue graph shows the product

mixture for a synthesis batch were rearrangement occurred, which happens when the mentioned TFA cleavage is terminated too late. This shows one of the disadvantages of the old synthetic route but also shows that the functionalization of secondary versus primary amine can be distinguished via HPLC, proving that the introduction of Fmoc was selective towards the primary amine.

In summary, a new synthetic route was established that utilizes a one-pot reaction to selectively introduce two final moieties (Figure 19). With this, the use of one temporary protection group can be circumvented, reducing the overall steps from seven to four, increasing the yield from 20-30% to over 50% for the established building block TDS and reducing the overall material usage. Furthermore, no rearrangement can occur with this method making the introduction of new building blocks easier and faster.

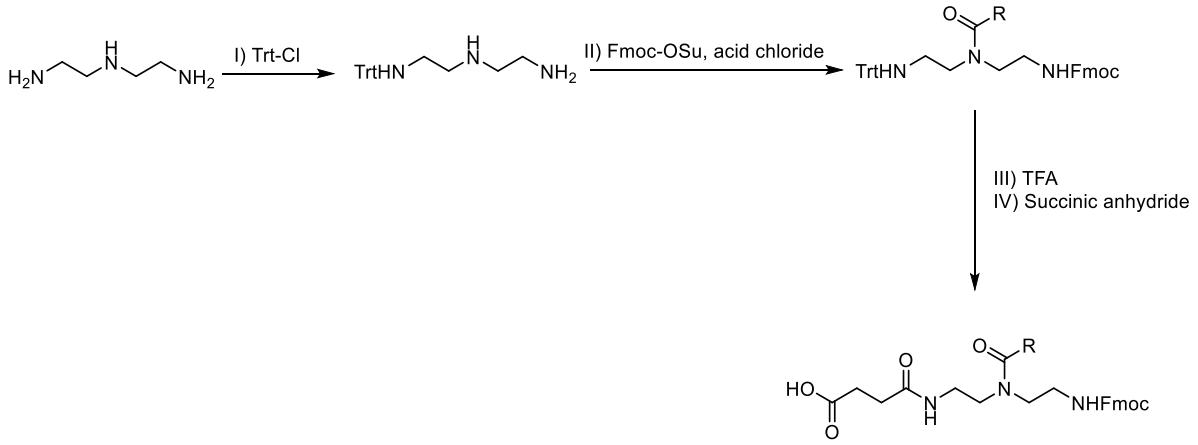

Figure 19: Overview of the newly introduced synthetic route towards functional building blocks.

3.1.2 Introduction of the catechol moiety

In this subchapter, the synthesis of catechol presenting oligo(amidoamine)s via SPPoS as basis for biomimetic, adhesive structures will be presented. There are two approaches to synthesize functional oligomers on solid support (Figure 20). The first one is using a building block with a reactive group that can be functionalized with the desired moiety after assembly on the scaffold. An example for this is the alkyne presenting building block TDS, that is regularly used in combination with various azido-functionalized sugars.

The advantage of this approach is that one building block can be synthesized in large scale and then be used for multiple structures. The biggest disadvantage is that this approach is

limited when different moieties on one scaffold are wanted as additional functionalization steps are needed. For this, the second approach is more suited, where a new building block is synthesized directly presenting the wanted functionality.

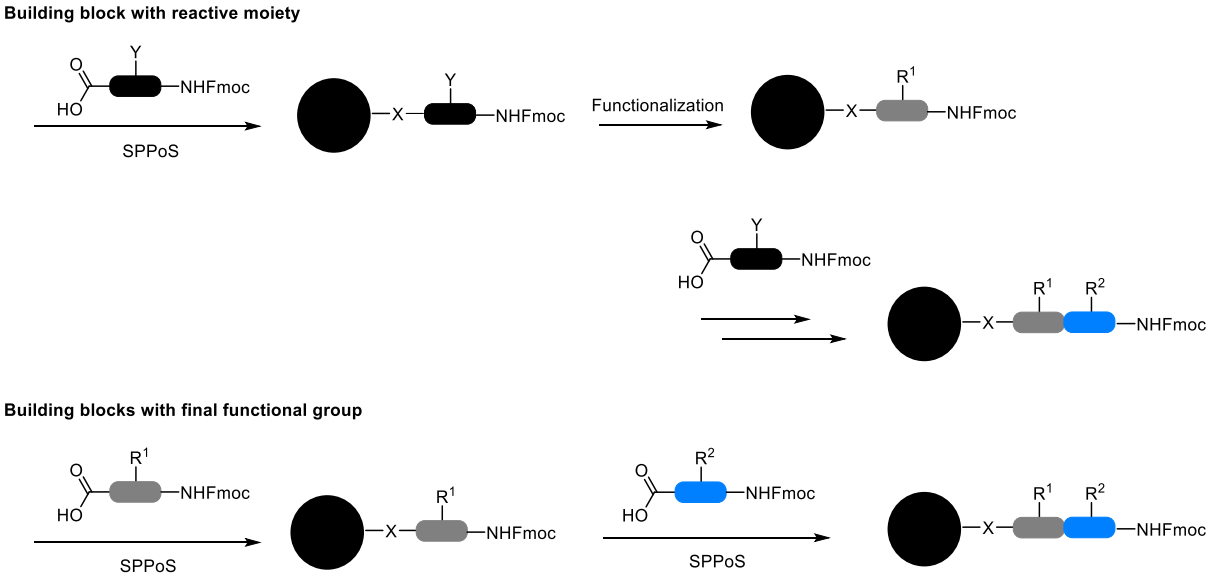

Figure 20: Different approaches for building block design for use in SPPoS.

As the goal was to combine catechols with tertiary amines and primary amides, a new building block was introduced. For this, the new synthetic route described before was used. Using this route, the wanted functionality, in this case the catechol, is exposed to high amounts of acid during trityl deprotection of the building block synthesis as well as final cleavage from solid support. Furthermore, the amide couplings during building block and solid phase synthesis as well as the Fmoc deprotection are accompanied by high concentrations of bases. As the catechol moiety is highly reactive and readily oxidizes, a protection strategy needed to be used that can withstand repetitive acidic and basic conditions. Although there are several protection groups available for catechols, only the stable formation of an ether bond at both hydroxyl groups can withstand the aforementioned conditioned. For this, a precursor is commercially available that was directly used in the building block synthesis, 3-(3,4-dimethoxyphenyl)propionic acid. With this, a new building block called CDS (**9**) (Catechol-Diethylenetriamine-Succinic acid) presenting a protected catechol moiety was successfully synthesized with a yield of 60% and a purity of 98% as determined by RP-HPLC (Figure 21 A, see SI 3.2 for full analysis).

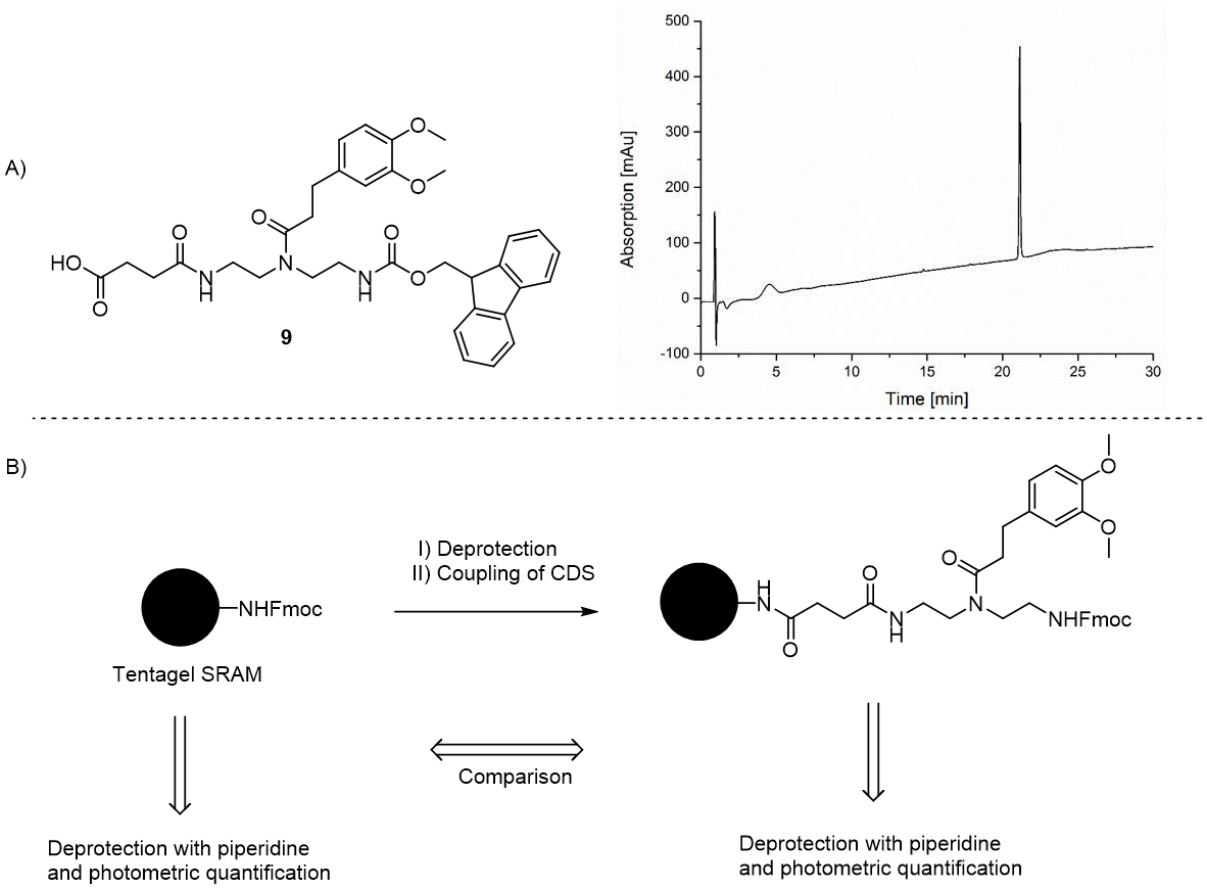

Figure 21: A) Structure and RP-HPLC of the new building block CDS. Gradient from 100% A (95/5 H20/MeCN, 0.1% formic acid) to 100% B (95/5 MeCN/H2O, 0.1% formic acid) over 30 min at 25°C; B) Schematic overview of coupling efficiency measurement.

As first step to deploy a new building block, the coupling efficiency on solid support was measured. For this, the loading of a resin, here TentaGel® SRAM, was tested by photometric quantification of the amount of Fmoc that was cleaved, which represents the amount of functional groups on the resin. This was then compared to the amount of Fmoc that was cleaved after CDS was coupled to the solid phase (Figure 20 B). In this case, the new building block CDS achieved a coupling efficiency of 98% using standard coupling protocol (see SI 3.2), which is sufficient for use in SPPoS. The next step was to use the building block in the synthesis of an oligomer, and the goal was to show that multiple catechol moieties can be incorporated in one scaffold and then to use this structure to optimize the deprotection of the catechol (Figure 22).

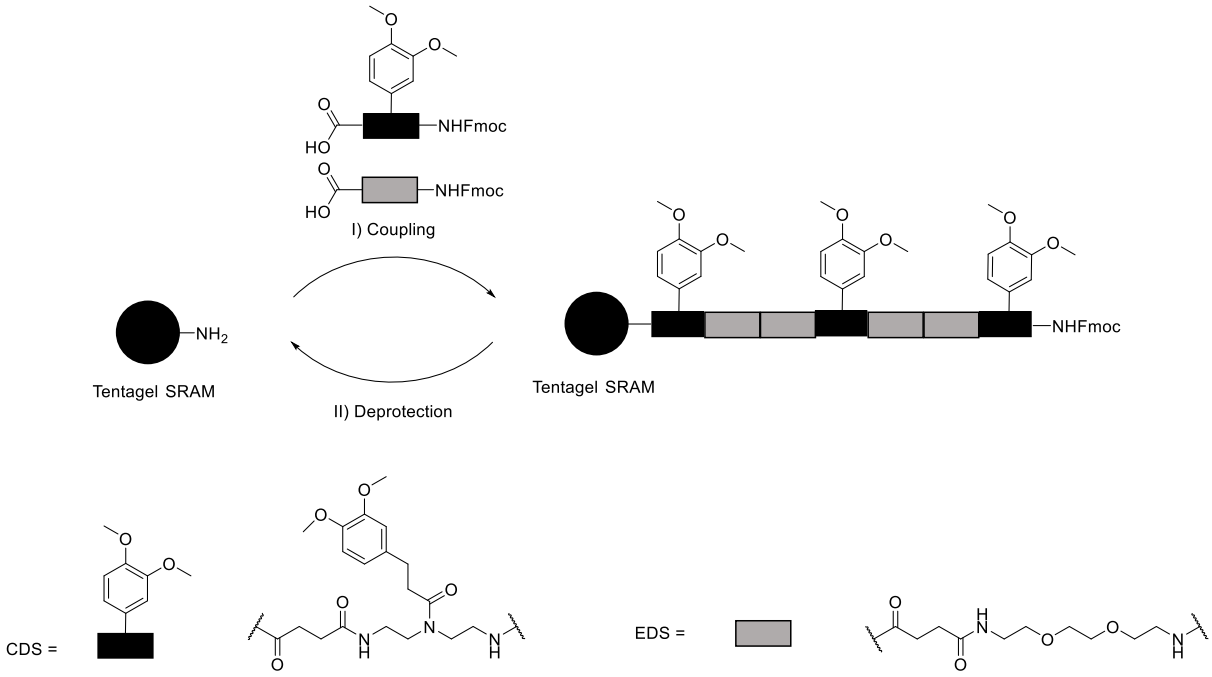

Figure 22: Reaction scheme of solid phase polymer synthesis utilizing new building block CDS; I) 5 eq. building block, 5 eq. PyBOP, 10 eq. DIPEA for 1 h, wash 10x with DMF; II) 25% piperidine in DMF for 30 min, was 10x with DMF.

A test oligomer was synthesized using the standard SPPoS protocol (see SI 3.2) with the functional building block CDS and spacer building block EDS (Ethylene glycol-Diamine-Succinic acid). EDS incorporates an ethylene glycol unit into the backbone to increase water solubility and control spacing between functional groups, which is important for the later following final structures and their application. After assembly of the scaffold on solid support, the terminal Fmoc group was removed and the amine was deactivated with acetic anhydride. Afterwards the structure was cleaved from the resin with 95% TFA and precipitated in diethyl ether to yield the protected oligomer **10** after freeze drying.

The final step towards catechol presenting oligo(amidoamine)s was to develop a suitable deprotection strategy (Figure 23). Requirements for this were full conversion towards free catechol, a low amount of side products and stability of the scaffold.

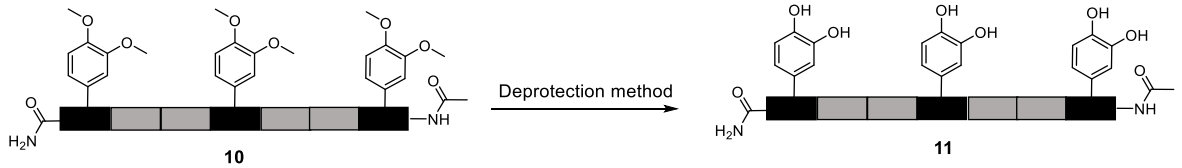

*Figure 23: Deprotection of oligomer **10**.*

Of special consideration was that the building block EDS introduces an ethylene glycol unit into the backbone, an aliphatic ether that potentially could get cleaved by the same conditions as the methyl ether. Furthermore, stability of the forming free catechol needs to be considered, excluding any deprotection method with basic conditions. Several of the standard ether cleavage conditions[134] were tested and evaluated by LC-MS to measure the overall conversion and amount of formed side product (Table 2).

*Table 2: Optimisation of the deprotection as determined by conversion of oligomer **10** by RR-HPLC measurement.*

Reagent	Eq. per catechol	Reaction time [h]	Solvent	Highest conversion [%]	Stability of the backbone
BBr_3	1-10	1-24	DCM	100	No
$AlCl_3$	2-40	24	DCM	0	Yes
$AlCl_3$ + Dodecanthiol	2-40	24	DCM	0	Yes
$InBr_3$	2-40	24	Ethanol	Partial	Yes
LiBr	2-40	24	Ethanol	0	Yes

Since deprotection methods involving basic conditions were excluded, several lewis acids were deployed. Boron tribromide, a very strong lewis acid and one of the most frequently used ether cleavage reagents, did in fact deprotect the catechol moieties to full conversion, but unfortunately it also cleaved the ether bonds in the backbone which could not be circumvented by low equivalents or short reaction times. The methyl ether groups are in direct proximity to an aromatic system and therefore less stable then the aliphatic ether groups of the backbone, so the idea was to use less strong lewis acids to potentially differentiate between both ether groups. Following this idea, aluminium chloride, indium bromide and lithium bromide were used in different concentrations and with different reaction times, and in the case of aluminium chloride in presence of an additional scavenger, dodecanthiol. Alumium chloride and lithium bromide both showed no conversion for catechol and backbone at all concentrations, and indium bromide selectively cleaved only on methyl ether group per catechol moiety. As next approach, a so called “push-pull” method published by Kiso et al. was used.[135] This protocol uses the superacid trifluoromethanesulfonic acid (TFMSA) to protonate an ether, which opens any alkyl rest to a nucleophilic attack of a

scavenger, in this case thioanisol. This method had potential to be selective towards the methyl ether in presence of an aliphatic ether backbone, because the sterically demanding scavenger thioanisol needs access to the ether bond, which is limited in the backbone. First tests using this protocol in TFA as solvent were promising, as a high conversion was observed with low amounts of backbone cleavage. This reaction was optimized in regards to concentration of reagents and reaction time to yield a final protocol of 16 eq. TFMSA and 8 eq. thioanisol per protected catechol moiety in TFA for 16 hours. With this protocol, structure **10** was successfully deprotected to almost full conversion with only limited cleavage of the EDS backbone (Figure 24).

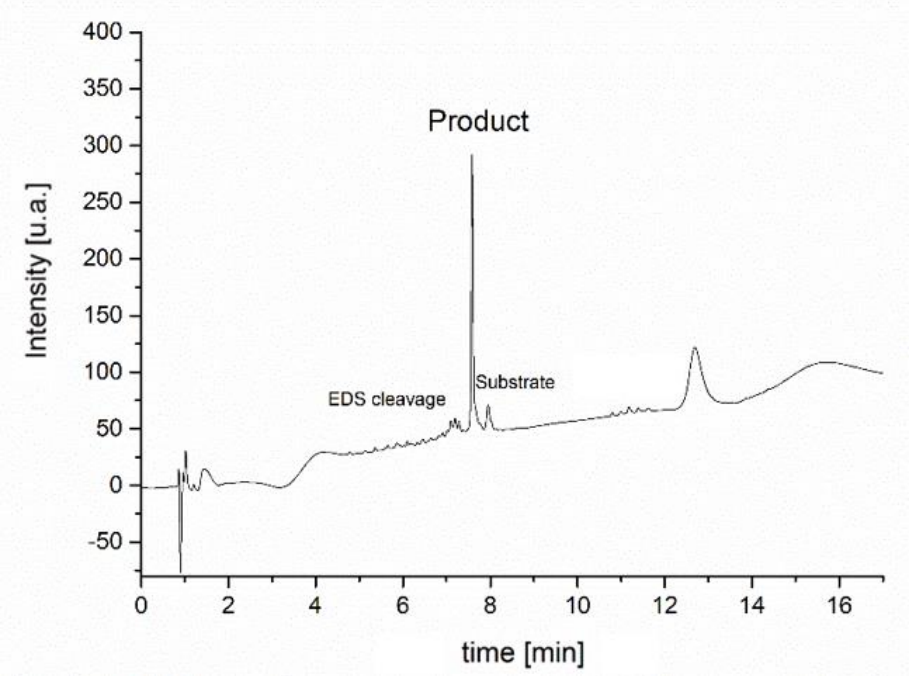

*Figure 24: RP-HPLC of the catechol deprotection towards product **11**. Gradient from 100% A (95/5 H20/MeCN, 0.1% formic acid) to 50% B (95/5 MeCN/H2O, 0.1% formic acid) over 17 min at 25°C*

Thus, a method to synthesize catechol presenting oligo(amidoamine)s was successfully developed. On the basis of the above presented new synthesis route, the building block CDS was introduced and successfully employed in solid phase synthesis towards a multivalent test structure. Furthermore the methyl protected catechol could be deprotected in solution following an optimized protocol utilizing the acid TFMSA and scavenger thioanisol.

3.1.3 Introduction of tertiary amine and primary amide

Adhesive mussel foot proteins are prominent for their high amount of L-DOPA, a catechol presenting amino acid. Although this moiety is the main focus of research into mussel inspired wet adhesives, there are other functionalities with high concentration in Mfps, namely cationic residues and primary amides. This part of the thesis aimed at developing a synthesis route towards oligo(amidoamine)s that can incorporate tertiary amines and primary amides simultaneously, as well as the newly introduced catechol building block CDS. This also could have been achieved through the incorporation of commercial amino acids, for example asparagine and lysine, although the later would present a primary amine. There are mainly two problems with using amino acids for these kinds of structures. First, they strongly interact with biological systems e.g. they are immunogenic and susceptible to proteases which would limit their application as medical glues or even in washing detergents. The second problem is that amino acids are small and only contribute a short part to the backbone, making it difficult to synthesize larger macromolecules that only present a few, specific side groups and are still soluble in water. Similar to the introduction of the catechol, the idea was to synthesize two different building blocks with a tertiary amine respectively primary amide side chain for easy combination of all functionalities. The design for the tertiary amine building block was based on the established spacer building blocks, as a diamine intermediate (**12**) presenting a tertiary amine is commercially available (Figure 25).

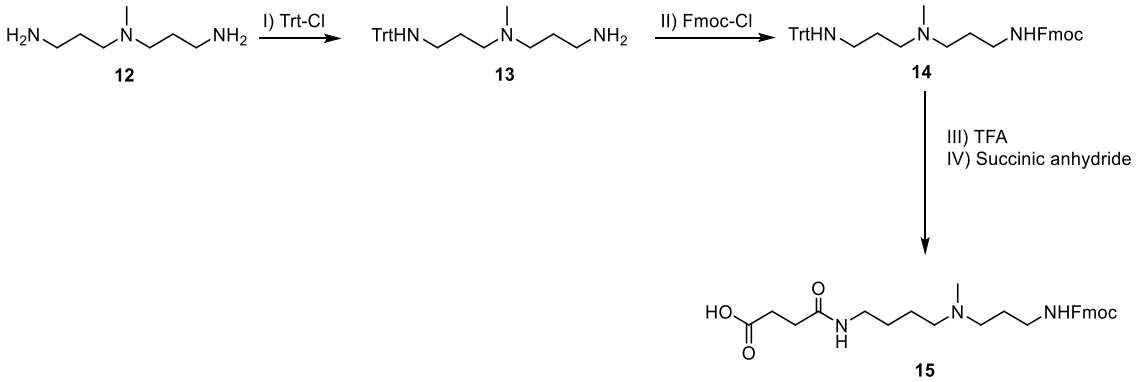

*Figure 25: Synthesis scheme of tertiary amine building block **15;** I) 0.25 eq. Trt-Cl in DCM; II) 1.3 eq. Fmoc-Cl, 3 eq. triethylamine in DCM; III) 10% TFA in DCM for 1 h, subsequent precipitation; IV) 1.3 eq. succinic anhydride, 3 eq. triethylamine in DCM for 2 h.*

In the first step, one of the primary amines was selectively protected with low equivalents of trityl chloride. The second primary amine was then converted using Fmoc chloride and in a subsequent step the trityl group was removed via TFA. The desired terminal acid group was introduced through conversion with succinic anhydride. All steps to the final product were done without additional purification steps, because of the potential of the basic tertiary amine to cleave the Fmoc group. Because of this, the successful synthesis was followed via TLC, showing full conversion for all steps. The cleavage of the Fmoc group by the tertiary amine was tried to be prevented for the final product by working up the last reaction with a 20% aqueous citric acid solution, before dissolving the raw product in acetone for recrystallization. Unfortunately, no product could be isolated as overnight a rubbery white solid precipitated that was not soluble in any solvent and could not be characterized. This can be presumably attributed to the cleavage of the Fmoc group and polymerization of the cleavage product, as was also observed during the development of the new building block synthesis.

For the introduction of the primary amide, the new protocol for functional building blocks was utilized. Using the trityl intermediate **4**, the primary amide was introduced using the acid chloride of succinamic acid (Figure 26).

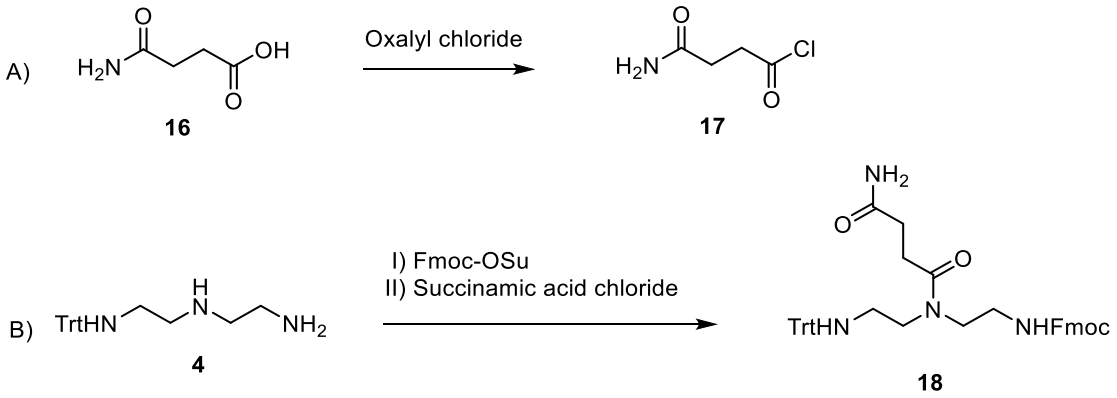

*Figure 26: Introduction of the primary amide residue into a functional building block intermediate; A) 1.5 eq. oxalyl chloride, 5 eq. DMF in DCM for 1 h; B) I: 1 eq. Fmoc-OSu, 3 eq. triethylamine in THF at -78°C for 2 h, II: 1.5 eq. Succinamic acid chloride (**17**) overnight.*

The succinamic acid chloride **17** was synthesized by reaction of the acid with oxalyl chloride, the standard protocol used for various other building blocks, including CDS.[136] The acid chloride was not further purified but directly used in the reaction to the building block

intermediate **18**. This reaction was controlled by TLC and full conversion was observed, although multiple product spots formed. After work-up, the desired product (**18**) was unfortunately not isolated. An explanation could be the nucleophilic character of the primary amide, which potentially could react with the acid chloride to several side products.

To combat the possible side products formed by the primary amide, the succinamic acid (**16**) could be selectively protected at the primary amide, but possible solid phase compatible protection groups, e.g. the trityl group, are not stable in the following steps in the building block synthesis, and vice versa. Adding to this the synthetic problems for the proposed tertiary amine building block made the approach of synthesizing a building block that can be functionalized with both moieties after assembly of the backbone the better alternative (see Figure 20). For this, structures are needed that present the wanted functional group with a second functionality that can be used for coupling to the backbone. For both the tertiary amine and the primary amide, an acid is commercially available that could be used for amide coupling to a free amine presented on an assembled scaffold (Figure 27 A). As a result, a protected amine presenting building block is needed, and the protection group needs to be stable towards the bases during coupling and deprotection. Furthermore, the cleavage condition for the protection group cannot cleave the solid phase linker. There are different protection groups available for amines that would fit these limitations, for example the Alloc group which is base and acid stable and is cleaved by palladium catalysis, or weakly acidic labile groups like Boc or trityl.[134] The trityl group is especially interesting, since this group is used as a temporary protection group in the functional building block synthesis. When introducing the succinic acid at the secondary amine now, the trityl group can stay in the structure to give a protected amine functional building block (Figure 27 B).

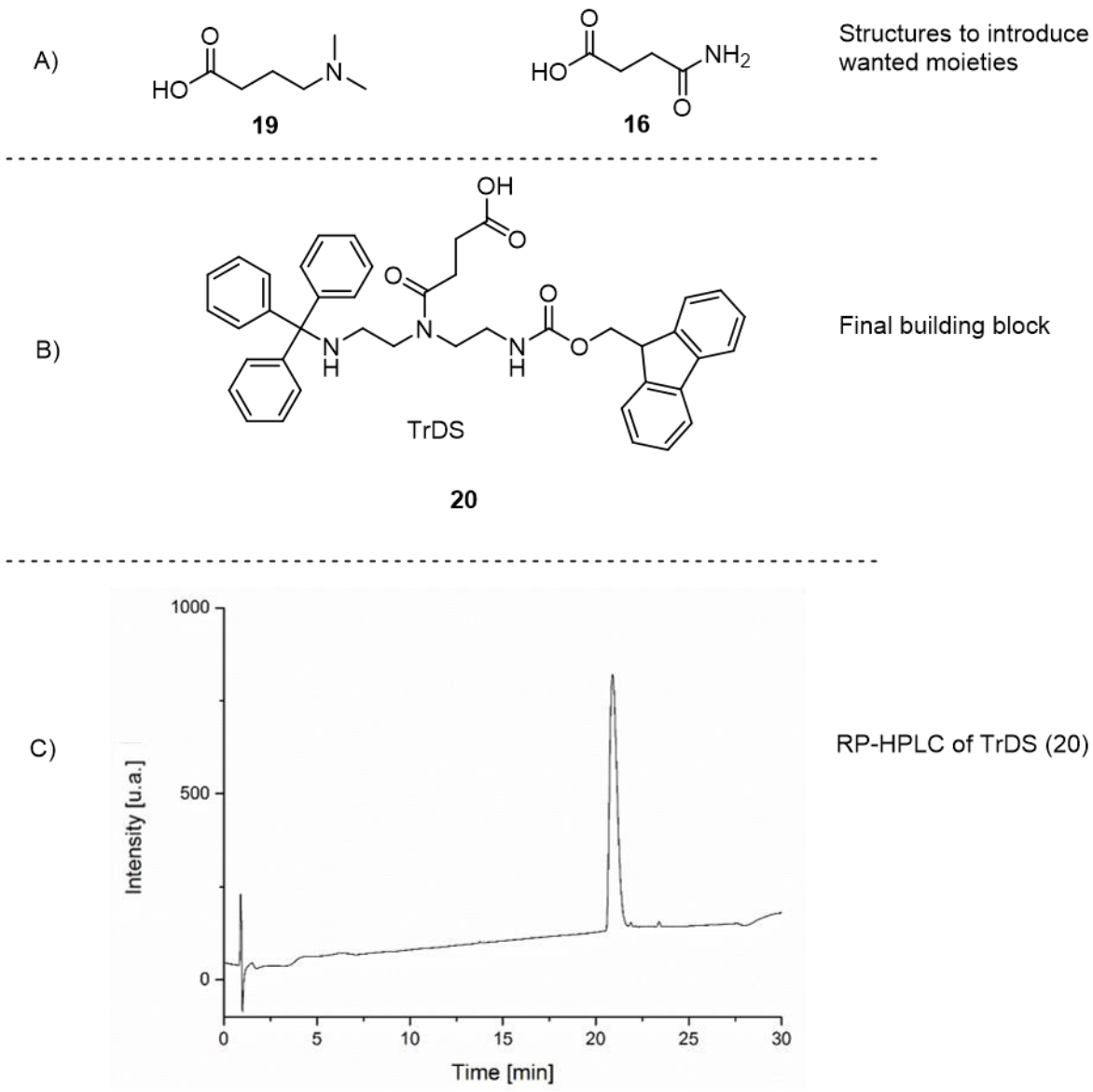

*Figure 27: Overview of structures to introduce functional groups via amide formation; A) Acids presenting tertiary amine (**19**) and primary amide (**16**) that could be used for amide formation on solid support; B) New building block TrDS (**20**) to introduce a protected primary amine into a scaffold on solid support; C) RP-HPLC of the new building block TrDS (**20**). Gradient from 100% A (95/5 H20/MeCN, 0.1% formic acid) to 100% B (95/5 MeCN/H2O, 0.1% formic acid) over 30 min at 25°C.*

This building block, called TrDS (Trityl-Diethylenediamine-Succinic acid) (**20**), was synthesized via the first two steps of the newly developed building block synthesis, by using succinic anhydride as reagent for the functional side chain (see Figure 19). TrDS was synthesized with a purity of 99% as determined by RP-HPLC and a yield of 60% (see Figure 27). In comparison to other functional building blocks, the acid functionality is placed at the secondary amine and the trityl protected primary amine acts as the functional side chain. As a result, TrDS has

a shorter backbone than other functional building blocks. As mentioned before, the first step to use a new building block in SPPoS is to determine the coupling efficiency, which was measured as 99% for TrDS. The idea was to use TrDS to assemble a scaffold that can be functionalized on solid support with either tertiary amines or primary amides. This is based on investigations done by Palladino et al.[137], that showed that the trityl group can be effectively cleaved by low concentrations of HCl in trifluoroethanol, a condition not affecting the acid labile rink amide linker. After deprotection of the side chain primary amine, the desired functionalities were supposed to be introduced via the typical amide coupling protocol used during scaffold assembly of the SPPoS. This idea was shown to be successful and was directly used to synthesize the final structures presented in chapter 3.2. As an example, the synthesis of one of the final oligomers, the combination of catechol and tertiary amine, is shown in Figure 28. Here, the complete scaffold was assembled on solid support, the trityl group removed by treatment with 0.1M HCl in trifluoroethanol and the tertiary amine introduced via standard amide coupling. After this, the standard SPPoS protocols for Fmoc removal and cleavage from solid support were applied (for details see SI 3.2).

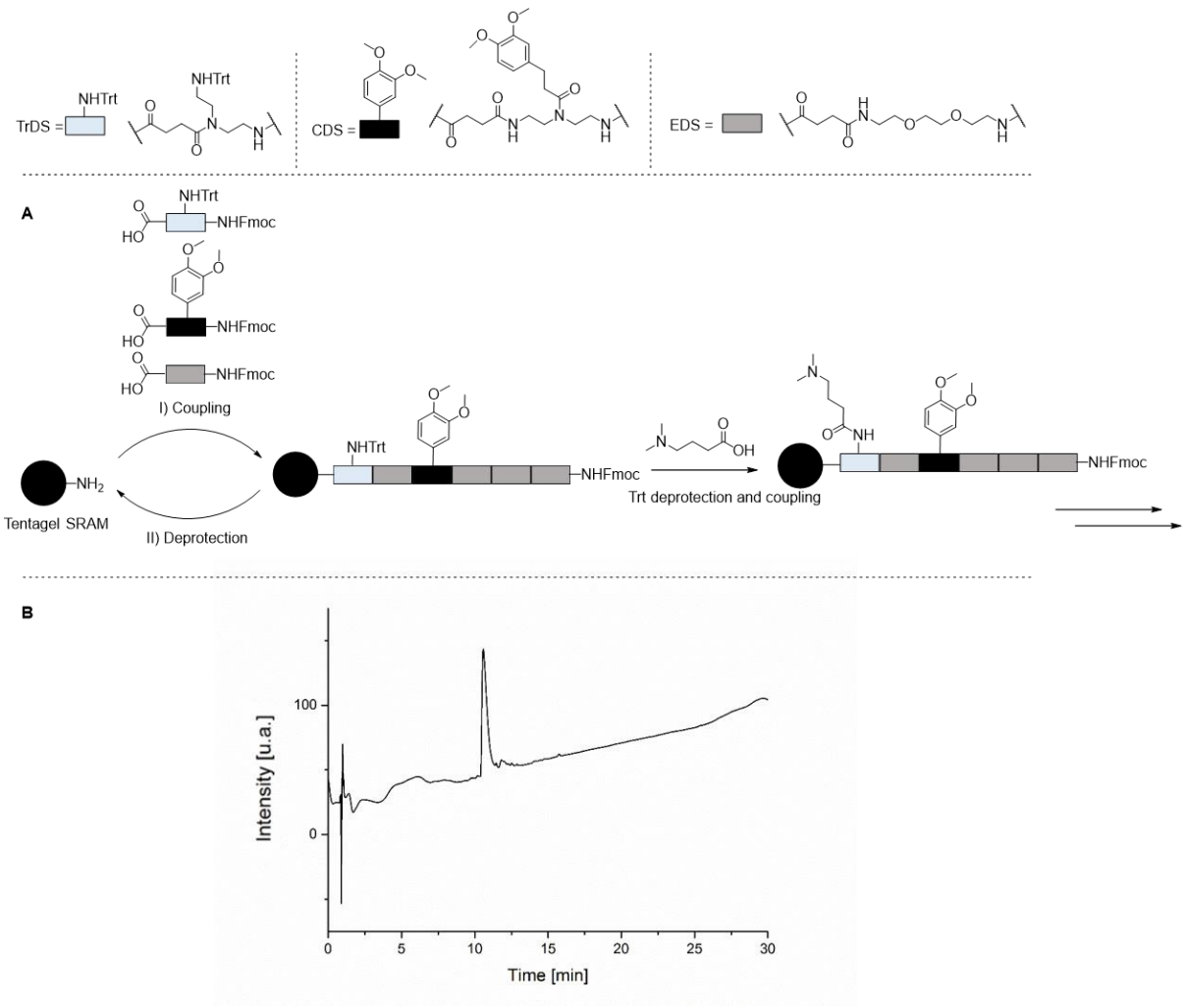

*Figure 28: A) Synthesis of an oligomer on solid support presenting a catechol and tertiary amine unit using the new building blocks TrDS (**20**) and CDS (**9**); B) RP-HPLC of the oligomer after Fmoc removal and cleavage from solid support. Gradient from 100% A (95/5 H20/MeCN, 0.1% formic acid) to 100% B (95/5 MeCN/H2O, 0.1% formic acid) over 30 min at 25°C.*

All in all, a new route towards functional building blocks was introduced, reducing the overall number of synthetic steps. By using a one-pot approach that selectively introduces two final moieties in one step, the material use was drastically decreased and the yield was doubled. The suitability of the new route was shown by synthesizing the established building block TDS, increasing the yield from around 25% to over 50%. Furthermore, this route eliminates the possibility of a rearrangement, making it easier to introduce new moieties. The optimized protocol was used to synthesize two new building blocks, CDS with a catechol moiety and TrDS with a trityl protected amine. The first building block was used to develop the synthesis of catechol containing oligo(amidoamine)s after methyl ether deprotection using TFMSA and thioanisol. The second building block, TrDS, can be used for further functionalization of a

scaffold on solid support with any structure with a free acid via amide coupling. This was used to introduce tertiary amines and primary amides into oligomers, which can be combined with CDS to obtain a wide variety of Mfp mimicking structures with control over sequence and composition.

The following two chapters will show two applications of the synthetic methods to introduce catechols into macromolecules. Chapter 3.2 will present the published work on catechol-containing sequence-defined macromolecules and their use to establish structure-function relations for the combination of different functional groups (catechol, amine and amide) as well as their position and spacing and towards adhesive properties. Chapter 3.3 will present the published work on sequence-defined catechol presenting glycomimetics and their potential to inhibit bacterial adhesion and to covalently bind to lectin receptors as well as the influence of catechol presentation.

3.2 Sequence-defined positioning of amine and amide residues to control catechol driven wet adhesion.

Authors: **L.Fischer[1]**, A.K. Strzelczyk[1], N. Wedler, C. Kropf, S. Schmidt and L. Hartmann

Journal: Chemical Science

DOI: 10.1039/D0SC03457F

Impact Factor: 9.346 (2019)

[1]: Contributed equally.

Own contributions:

Introduction of a new synthetic route towards functional building blocks. Development and optimization of two new functional building blocks presenting a catechol moiety and a trityl protected primary amine. Development and optimization of a method for selective deprotection of ether protected catechol groups in solution. Development and optimization of a method to introduce primary amide and tertiary amine residues via the trityl protected primary amine building block on solid support. Synthesis and purification of all shown structures presenting catechols, tertiary amines and primary amides. Characterization of all compounds via RP-HPLC, ^{1}H-NMR, ^{13}C-NMR, and HR-ESI. Collaborative evaluation and interpretation of the adhesion measurements as well as collaborative visualization of the results. Collaborative writing of the manuscript.

Chemical Science

ROYAL SOCIETY OF CHEMISTRY

EDGE ARTICLE

View Article Online
View Journal

Cite this: DOI: 10.1039/d0sc03457f

All publication charges for this article have been paid for by the Royal Society of Chemistry

Sequence-defined positioning of amine and amide residues to control catechol driven wet adhesion†

Lukas Fischer,‡[a] Alexander K. Strzelczyk,‡[a] Nils Wedler,[b] Christian Kropf,[b] Stephan Schmidt*[a] and Laura Hartmann *[a]

Received 22nd June 2020
Accepted 28th August 2020

DOI: 10.1039/d0sc03457f

rsc.li/chemical-science

Catechol and amine residues, both abundantly present in mussel adhesion proteins, are known to act cooperatively by displacing hydration barriers before binding to mineral surfaces. In spite of synthetic efforts toward mussel-inspired adhesives, the effect of positioning of the involved functional groups along a polymer chain is not well understood. By using sequence-defined oligomers grafted to soft hydrogel particles as adhesion probes, we study the effect of catechol–amine spacing, as well as positioning relative to the oligomer terminus. We demonstrate that the catechol–amine spacing has a significant effect on adhesion, while shifting their position has a small effect. Notably, combinations of non-charged amides and catechols can achieve similar cooperative effects on adhesion when compared to amine and catechol residues. Thus, these findings provide a blueprint for the design of next generation mussel-inspired adhesives.

Introduction

Marine organisms such as mussels, barnacles, or sandcastle worms are prime examples of biological wet adhesion. They exhibit strong attachments to inorganic and organic surfaces in aqueous medium, even in the presence of high salt concentrations.[1,2] In aqueous environment, the adhesion is inhibited by both water and hydrated salt ions through the formation of thin layers preventing the direct contact between adhesive groups at the material surfaces.[3,4] Mussels in particular have evolved adhesive proteins (mussel foot proteins, Mfps) that circumvent this problem by displacing the hydration layers and then bridging to the surface *via* strong bonding primarily through L-3,4-dihydroxyphenylalanine (DOPA) groups.[5–7] Recent findings state that the high amount of DOPA in proximity to cationic amino acids is responsible for these unique properties.[8–10] This synergistic effect between DOPA and primary amines is due to dispatching the hydration layer of the surface *via* charged amines allowing the catechol residues to bind to the surface. Such synergy between catechol (DOPA) and charged groups could be confirmed using synthetic polymers combining anionic and cationic residues.[11–13] Inspired by the adhesive properties of the Mfps, a wide range of polymers with high DOPA content were synthesized toward advanced adhesives and surface coatings.[1,6,14–23] However, sequence effects like the spacing of the charged groups and catechol residues were given little attention for the design of such mussel-inspired synthetic adhesives.

The adhesive proteins of mussels contain a large amount of DOPA and amine residues, *e.g.* Mfp-5 carries 30 mol% DOPA and 28 mol% amines, which are usually in close proximity.[23] However, another class of residue typically represented at higher than 10 mol% (in Mfp-2, Mfp-3, Mfp-4, and Mfp-6) is asparagine carrying a primary amide.[24–27] Asparagine as a "helix-breaker" residue is believed to increase the flexibility of the Mfps improving the accessibility of the adhesive DOPA groups. Intriguingly, for Mfp-3 the amide side chains are predominantly found in direct proximity to amine and DOPA residues.[27] The function of Mfp-3 as a primer for strong underwater adhesion has been shown by direct adhesion measurements *via* atomic force microscopy or the surface force apparatus,[7,28] but the role of amide side chains on adhesion has not been studied so far. Therefore, in this study we present the synthesis of sequence-defined oligo(amidoamine)s carrying selected combinations of catechol, tertiary amine and primary amide residues, similar to the arrangement of arginine, DOPA and amine residues found in Mfp-3 and study their adhesion energies on glass surfaces.

Results and discussion

Synthesis of sequence defined oligomers

As a cationic residue a tertiary amine was chosen to prevent crosslinking with the catechols particularly at higher pH. In addition, choosing this non-natural cationic residue instead of

[a]Institut für Organische und Makromolekulare Chemie, Heinrich-Heine-Universität Düsseldorf, Universitätsstr. 1, 40225 Düsseldorf, Germany. E-mail: stephan.schmidt@hhu.de; laura.hartmann@hhu.de

[b]Laundry & Home Care, Henkel AG & Co. KGaA, Henkelstr. 67, 40589 Düsseldorf, Germany

† Electronic supplementary information (ESI) available: Materials and methods, chemical analysis. See DOI: 10.1039/d0sc03457f

‡ LF and AKS contributed equally to this work.

primary amines might provide additional indication that the catechol–amine synergy is due to the removal of the hydration layer by the charge effect and not due to additional hydrogen bonding by the amines. Along these lines, as a non-natural spacer building block between the catechol, amine and amide residues we use a short ethylene glycol chain (EDS block) to show the feasibility of transferring the catechol driven adhesion mechanism to synthetic polymers. The oligomer synthesis was adapted from an already established method using tailor-made building blocks for solid phase assembly to generate the sequence-defined structures.[29,30] Similar to solid phase peptide synthesis, the building blocks carry both, a carboxy and an Fmoc protected primary amine group, that allow step-wise chain growth on an amine functionalized resin. Here two new building blocks were synthesized, one carrying a protected catechol moiety and one carrying an orthogonal protected primary amine, to later introduce the tertiary amine and primary amide *via* amide coupling on solid support (Fig. 1).

A major challenge in the solid phase synthesis of sequence-defined polymers is the access to tailor-made building blocks in sufficient quantity and purity, ideally in a time and cost-efficient manner. Here, an advanced method providing the required building blocks was developed streamlining the previous approach to a straightforward 3-step route with greatly improved atom economy and higher yields.[29,31–34] In the first step, one of the two primary amines of diethylenetriamine was protected using trityl chloride. Afterward, the second primary amine was selectively converted using Fmoc-OSu in THF at −78 °C, with subsequent addition of an activated acid which carries the desired side chain functionality. The last step includes the cleavage of the trityl group and reaction with succinic anhydride. With this new protocol two different building blocks were synthesized. The first building block TrDS (**1**) offers a trityl protected amine, orthogonal to the Fmoc protection group, for further functionalization during solid phase synthesis. The second novel building block CDS (**2**) was developed to introduce a methyl ether protected catechol moiety in the side chain using the acyl chloride of 3-(3,4-dimethoxyphenyl)propionic acid. This protecting strategy ensured stability during acidic conditions of the building block synthesis as well as basic conditions during solid phase synthesis. Together with the previously introduced building blocks EDS, TrDS, and CDS, solid phase supported synthesis following previously reported coupling conditions was applied (Fig. 2). The oligomer scaffold was assembled by step-wise amide coupling and subsequent Fmoc deprotection of the terminal amine. For the introduction of side chains presenting a tertiary amine or primary amide groups, the TrDS building block was used: after full synthesis of the backbone, the trityl group of TrDS was cleaved using 0.15 M HCl in trifluorethanol, a condition resulting in full release of the trityl group while maintaining stability of the acid labile solid support.[35] Next, the desired side chain functionalities were introduced by coupling the corresponding carboxylic acid using PyBOP as a coupling reagent. After cleavage of the oligomer from the solid phase, the catechol moieties were deprotected using trifluormethanesulfonic acid and thioanisole in trifluoracetic acid following a procedure previously introduced by Kiso *et al.*[36] Full deprotection and successful isolation of the desired oligomer

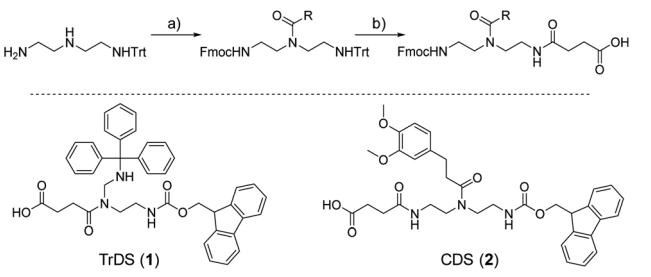

Fig. 1 New synthesis route towards functional building blocks; (a) Fmoc-OSu, 3 eq. triethylamine in THF at −78 °C followed by 1 eq. activated acid; (b) 10 eq. TFA in DCM followed by precipitation and 1 eq. succinic anhydride, 3 eq. triethylamine in DCM.

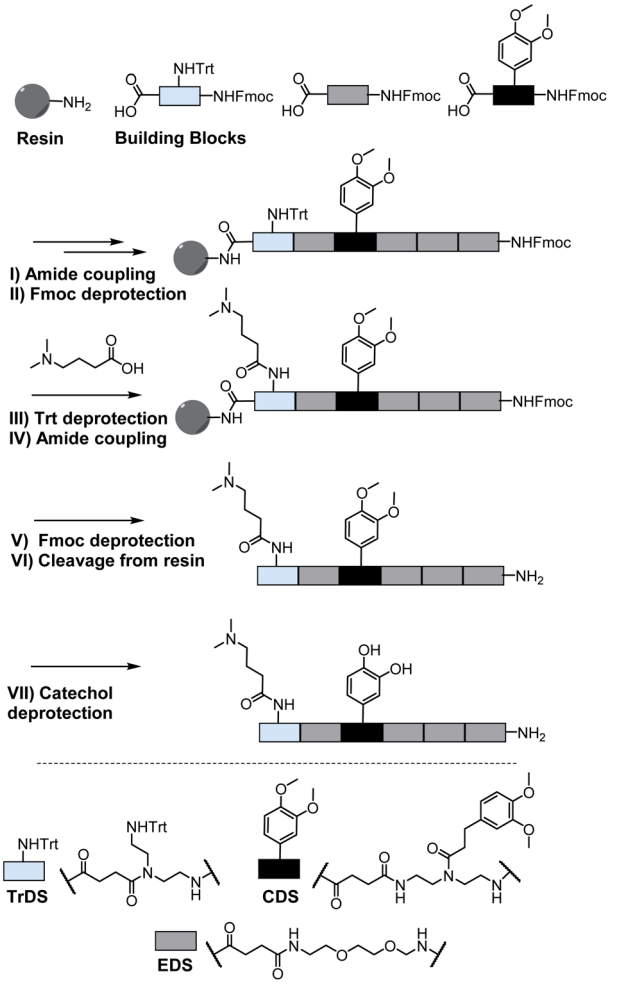

Fig. 2 Exemplary scheme for solid phase synthesis of an oligomer using a rink amide resin; (I) 5 eq. building block, 5 eq. PyBOP, 10 eq. DIPEA in DMF; (II + V) 20% piperidine in DMF; (III) 0.15 M HCl in trifluoroethanol; (IV) 10 eq. acid, 10 eq. PyBOP, 20 eq. DIPEA; (VI) 95% TFA, 2.5% DCM and 2.5% triisopropylsilane; (VII) 16 eq. trifluoromethanesulfonic acid, 8 eq. thioanisole in TFA.

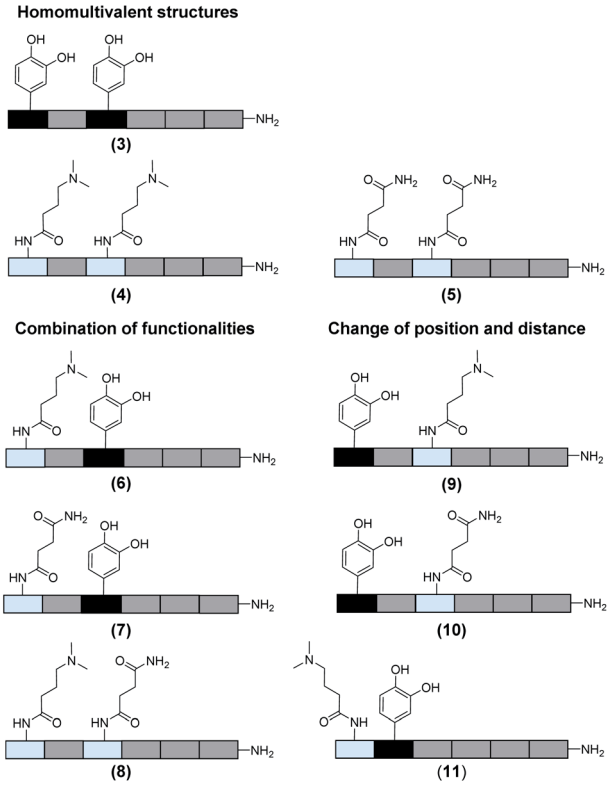

Fig. 3 Overview of the oligomers.

structures were confirmed by ^{1}H-NMR, ^{13}C-NMR and HR-ESI MS (see ESI S4†).

In total 9 different oligomers were synthesized (Fig. 3). All structures carry a terminal amine group for later coupling onto microgels and use in adhesion studies. In order to study combination and positioning effects of the different functional groups on adhesion, various sets of oligomers were synthesized. As homofunctional structures, the oligomers **3–5** each carry two identical functional groups, either catechol, tertiary amine, or primary amide both in position 1 and 3. Oligomers **6**, **7** and **8** combine two of the functional groups to form the three possible combinations. Oligomers **9** and **10** change the position of catechol and amine or amide, to investigate the influence of the order of functional groups. In addition, oligomer **11** reduces the spacing between amine and catechol. All oligomers have a length of six building blocks with the EDS building blocks serving as spacers between the functional building blocks keeping the overall size of all oligomers the same. Importantly, for all catechol bearing structures, oxidation in water was not observed within several days (see ESI S8†). Therefore, we assume that in the course of the following adhesion studies, catechol–quinone transitions did not take place.

SCP preparation and adhesion measurements

For the adhesion measurements, soft microgels (soft colloidal probes, SCPs) based on poly(ethylene glycol) (PEG) were functionalized with the sequence-defined oligomers (**3–11**) and allowed to settle and bind to glass surfaces.[37] The glass surfaces were used here as a model for inorganic silica-based materials. To prepare the SCPs, microdroplets of poly(ethylene glycol diacrylamide) were formed *via* liquid–liquid phase separation in a concentrated sodium sulphate solution followed by UV crosslinking (Fig. 4).[38] The oligomers were introduced by grafting of crotonic acid under UV irradiation in presence of benzophenone followed by the repeated coupling of the oligomers *via* carbodiimide chemistry. The degree of oligomer functionalization in the PEG network was determined in two steps *via* titration with toluidine blue, a crotonic acid binding dye.[37] First, the amount of crotonic acid was determined before coupling the oligomers. Second, the residual, unreacted crotonic acid residues were titrated after the oligomer coupling step. The coupling efficiency was larger than 90%, and the oligomer functionalization degrees were determined as ~86 μmol per gram PEG (see ESI S5†). Hence, 13.5–14.2 wt% of the PEG-SCPs are oligomers. Using the SCP elastic moduli as an estimate for the specific volume in of PEG in water,[39] the PEG swelling degree can be calculated giving an oligomer concentration of 11 mmol l^{-1} in the SCP scaffold.[37]

Upon adhesion, the SCPs mechanically deform and form distinct contact areas with the glass surface. To quantify the SCP-adhesion energies (W_{adh}) on glass, the contact radii (a) were measured by micro-interferometry (Fig. 5) and evaluated by the Johnson–Kendall–Roberts (JKR) model of adhesion:[40–42]

$$a^3 = \frac{9\pi R^2 W_{adh}(1-\nu^2)}{2E} \quad (1)$$

where W_{adh} is the adhesion energy, E is the elastic modulus of the SCPs, and ν the Poisson ratio. The adhesion energies were read from the plots of the contact area a and the SCP radius R (Fig. 5). The SCP method allows detecting adhesion energies with high precision and has been broadly applied, *e.g.* to study biomolecular interactions,[42,43] hydrophobic forces,[44] and analytes in the solute by very sensitive competitive binding assays.[41,45]

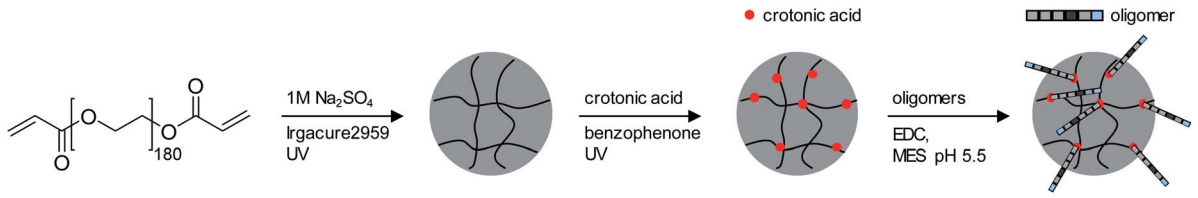

Fig. 4 Synthesis of PEG based SCPs. (1) liquid–liquid phase separation of PEG macromonomers in 1 M $NaSO_4$ followed by UV crosslinking; (2) photochemical grafting of crotonic acid using benzophenone; (3) coupling of oligomers by carbodiimide chemistry.

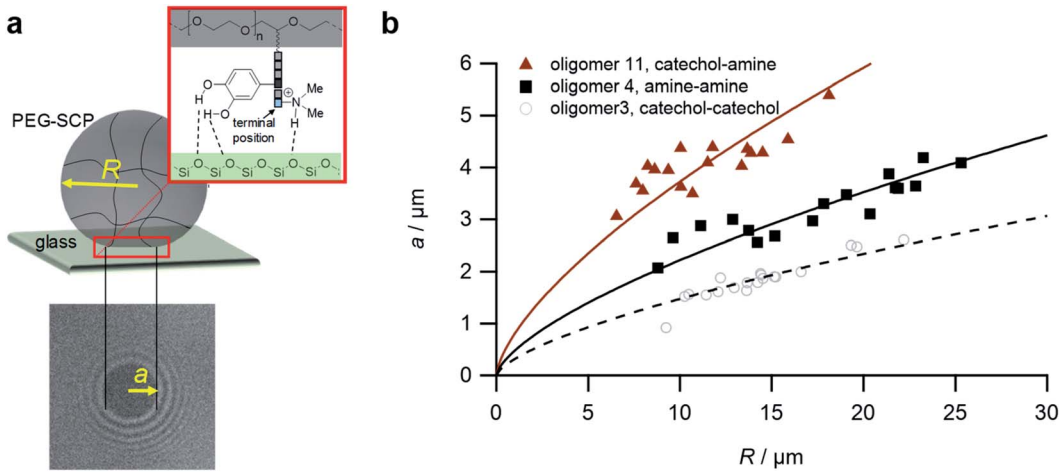

Fig. 5 The SCP adhesion assay. (a) Schematic representation of an oligomer-functionalized SCP adhering to a glass slide. The reflection interference contrast microscopy image (bottom) shows a typical contact area (dark area in the center) and newton rings providing the geometry of the SCP, *i.e.* the parameters *a* and *R*. (b) Typical JKR plots and fits (lines) according to eqn (1) depicting the oligomers **3** (empty circles), **4** (squares) and **11** (triangles).

To control the solute conditions, the SCP-adhesion assay was conducted in 0.1 M sodium chloride and between pH 3–8 (Fig. 6). The pH controls the glass surface charge by protonation/deprotonation of the silanol groups, which broadly affects the adhesion. At low pH the surface is able to donate hydrogen bonds to the ethylene glycol groups at the PEG and EDS backbone, whereas almost complete deprotonation is expected at pH 7,[46] rendering the surface unable to donate hydrogen bonds. In addition, the hydration barrier is stronger for charged surfaces at high pH.[47] This explains the observed overall decreasing adhesion energies with increasing pH for all oligomers (Fig. 6b). The measurements confirmed the synergistic effect between cationic amines and catechols since the catechol/amine (**6**, **9** and **11**) combinations always achieve higher adhesion when compared to catechol/catechol (**3**). This shows that the catechol/amine synergy also works with tertiary amines instead of the natural primary amines supporting the hypothesis that it is the charge-induced displacement of the hydration layer that increases catechol binding. With the sequence-controlled oligomers we could additionally show the effect of catechol/amine spacing. In case where the catechol and amine residues are in close vicinity (**11**), the adhesion energy is drastically amplified compared to the oligomers with an additional EDS spacer between catechol and amine (**6** and **9**). In addition, the adhesion was affected by changing the position of the catechol and amine residues (**6** and **9**). When the amine is

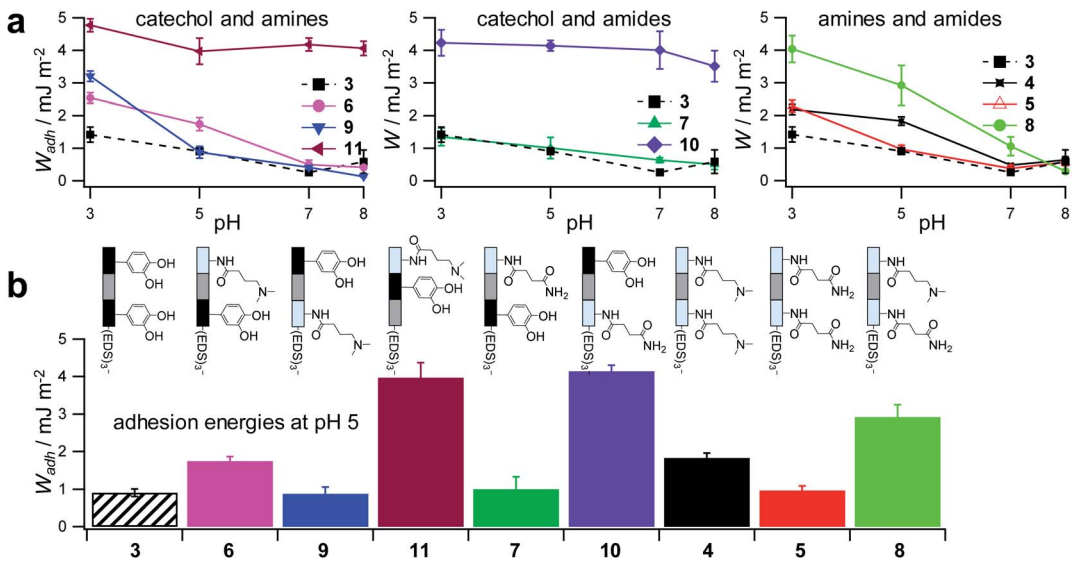

Fig. 6 Adhesion energies measured for oligomer-functionalized SCPs (a) measurements against a glass surface in 0.1 M sodium chloride solution from pH 3 to pH 8. (b) Adhesion energies mimicking the pH during protein secretion in initial mussel adhesion.[2] Oligomer concentration normalized adhesion energy values are very similar to non-normalized values (ESI S9†).

located at the terminating position (the free chain end not attached to the SCP) (**6**), the decrease in adhesion between pH 3 and pH 5 is not as strong when compared to the oligomer with the catechol at the terminating position (**9**). This could be due to the increased ionic interactions between the terminal amine and the partially deprotonated surface at pH 5 compensating the loss of silanol hydrogen bonding at elevated pH. Comparison with structures that do not contain catechol but combinations of amines and primary amide side chains confirm this trend (**4**, **5** and **8**). The amides can interact with the silica groups at the surface *via* hydrogen bonding but when cationic amines are included (**8**) the adhesion appears to be stronger at elevated pH on the anionic glass surface due to additional ionic bonding. Overall, these results agree with earlier studies on the synergistic adhesion effects of amine and catechol residues,[8,9] but for the first time show that their positioning and spacing is of key importance to maximize such synergy. Along these lines, *via* dynamic single molecule adhesion measurements Li *et al.*[10] found that reversing the amine catechol positioning affects the adhesion, which they attributed to a different load distribution within the molecules upon pull-off.

Surprisingly, the combination of amide and catechol residues showed an even larger dependence on the residue positioning. In case the catechol is the terminating group (**10**), the adhesion energy is significantly stronger when compared to placing the amide at the chain end (**7**). The adhesion is even stronger when compared to amine/catechol combinations with similar spacing (**6** and **9**). This suggests that there are additional interactions amplifying the catechol-mediated adhesion with the glass surface, similar to the amine/catechol synergism. For amide/catechol combinations this could be in part due to the ionic resonance structure of the primary amide (25–30% ionic character)[48] helping to displace the surface hydration layer on the glass surface. In addition, we hypothesize that there is an intricate balance between intra- and intermolecular hydrogen bond interactions. Intramolecular hydrogen bonding of the functional side chains would reduce their interaction with the surface and thus the overall adhesion. It seems that the introduction of primary amide side chains shifts this balance toward promoting adhesion. We have observed previously for sequence-controlled oligomers mimicking biopolymers that indeed the positioning of residues and the resulting variations in the conformation of the molecule play a key role for their intermolecular interactions *e.g.* when targeting protein receptors.[49] We cannot conclude yet on the mechanisms of increasing catechol-mediated adhesion when introducing primary amide side chains but when looking back at the natural role model, Mfp-3, DOPA moieties are indeed very often accompanied by neighbouring asparagine building blocks. Thus the effect we observe here is likely to take place also in the natural mussel adhesives. The spacing of the functional residues in the natural Mfps can be much shorter, usually one to four amino acids apart, compared to the spacing in the oligomers, which is equivalent to a spacing of about seven amino acids. Nevertheless, we could still detect a synergy between the functional groups, perhaps due to the coiling of the flexible backbone resulting in shorter effective spacings. This indicates that the synergy of the functional groups could be transferred to structurally different synthetic polymers.

Conclusions

Taken together, combining catechols and amines on a scaffold promotes wet adhesion in accordance with the literature.[8–10] Intriguingly, the spacing of these residues on the polymer chain strongly affects adhesion to negatively charged silica surfaces. Charged moieties and catechols should be very close to maximize adhesion, which is also in accordance with their positioning in the mussel adhesion proteins. Notably also non-natural charged residues such as the tertiary amines used here are capable of increasing the catechol binding due to the displacement of hydration layers and condensed ions. In addition, introducing other functional groups present in the natural sequences such as primary amides may also have synergistic effects on adhesion as they showed increased adhesion in comparison to the amine/catechol combinations in this study. Further studies will be required to reveal the molecular mechanisms behind a potential synergy between amides and catechols and the effect of polymer conformation on catechol driven adhesion. Although details of the potential mechanism remain unknown, this shows that there is still much to be learned and much to be gained by controlling the positioning of interacting residues in bio-inspired sequence-controlled polymers.

Conflicts of interest

The authors filed a patent application DE 102019208832.5 “Polymere für die Behandlung von Oberflächen”.

Acknowledgements

The authors acknowledge funding by Henkel AG & Co. KGaA.

Notes and references

1 A. H. Hofman, I. A. van Hees, J. Yang and M. Kamperman, *Adv. Mater.*, 2018, **30**, e1704640.
2 J. H. Waite, *J. Exp. Biol.*, 2017, **220**, 517–530.
3 J. Israelachvili and H. Wennerström, *Nature*, 1996, **379**, 219–225.
4 Y. Li, C. Liang, L. Gao, S. Y. Li, Y. Z. Zhang, J. Zhang and Y. Cao, *Mater. Chem. Front.*, 2017, **1**, 2664–2668.
5 M. Yu, J. Hwang and T. J. Deming, *J. Am. Chem. Soc.*, 1999, **121**, 5825–5826.
6 B. P. Lee, P. B. Messersmith, J. N. Israelachvili and J. H. Waite, *Annu. Rev. Mater. Res.*, 2011, **41**, 99–132.
7 H. Lee, N. F. Scherer and P. B. Messersmith, *Proc. Natl. Acad. Sci. U. S. A.*, 2006, **103**, 12999–13003.
8 G. P. Maier, M. V. Rapp, J. H. Waite, J. N. Israelachvili and A. Butler, *Science*, 2015, **349**, 628–632.
9 M. V. Rapp, G. P. Maier, H. A. Dobbs, N. J. Higdon, J. H. Waite, A. Butler and J. N. Israelachvili, *J. Am. Chem. Soc.*, 2016, **138**, 9013–9016.

10 Y. Li, T. Wang, L. Xia, L. Wang, M. Qin, Y. Li, W. Wang and Y. Cao, *J. Mater. Chem. B*, 2017, **5**, 4416–4420.
11 A. R. Narkar, J. D. Kelley, R. Pinnaratip and B. P. Lee, *Biomacromolecules*, 2018, **19**, 1416–1424.
12 Q. Zhao, D. W. Lee, B. K. Ahn, S. Seo, Y. Kaufman, J. N. Israelachvili and J. H. Waite, *Nat. Mater.*, 2016, **15**, 407–412.
13 B. K. Ahn, S. Das, R. Linstadt, Y. Kaufman, N. R. Martinez-Rodriguez, R. Mirshafian, E. Kesselman, Y. Talmon, B. H. Lipshutz, J. N. Israelachvili and J. H. Waite, *Nat. Commun.*, 2015, **6**, 8663.
14 J. H. Ryu, P. B. Messersmith and H. Lee, *ACS Appl. Mater. Interfaces*, 2018, **10**, 7523–7540.
15 Q. Zhang, G. Nurumbetov, A. Simula, C. Y. Zhu, M. X. Li, P. Wilson, K. Kempe, B. Yang, L. Tao and D. M. Haddleton, *Polym. Chem.*, 2016, **7**, 7002–7010.
16 H. Lee, S. M. Dellatore, W. M. Miller and P. B. Messersmith, *Science*, 2007, **318**, 426–430.
17 Q. Ye, F. Zhou and W. M. Liu, *Chem. Soc. Rev.*, 2011, **40**, 4244–4258.
18 S. Moulay, *Polym. Rev.*, 2014, **54**, 436–513.
19 E. Faure, C. Falentin-Daudre, C. Jerome, J. Lyskawa, D. Fournier, P. Woisel and C. Detrembleur, *Prog. Polym. Sci.*, 2013, **38**, 236–270.
20 J. Yang, J. Keijsers, M. van Heek, A. Stuiver, M. A. C. Stuart and M. Kamperman, *Polym. Chem.*, 2015, **6**, 3121–3130.
21 N. Patil, C. Jerome and C. Detrembleur, *Prog. Polym. Sci.*, 2018, **82**, 34–91.
22 N. L. Venkatareddy, P. Wilke, N. Ernst, J. Horsch, M. Weber, A. Dallmann and H. G. Boerner, *Adv. Mater. Interfaces*, 2019, **6**, 1900501.
23 Q. Wei, K. Achazi, H. Liebe, A. Schulz, P. L. M. Noeske, I. Grunwald and R. Haag, *Angew. Chem., Int. Ed.*, 2014, **53**, 11650–11655.
24 H. Zhao and J. H. Waite, *Biochemistry*, 2006, **45**, 14223–14231.
25 H. Zhao and J. H. Waite, *J. Biol. Chem.*, 2006, **281**, 26150–26158.
26 L. M. Rzepecki, K. M. Hansen and J. H. Waite, *Biol. Bull.*, 1992, **183**, 123–137.
27 V. V. Papov, T. V. Diamond, K. Biemann and J. H. Waite, *J. Biol. Chem.*, 1995, **270**, 20183–20192.
28 Q. Lin, D. Gourdon, C. Sun, N. Holten-Andersen, T. H. Anderson, J. H. Waite and J. N. Israelachvili, *Proc. Natl. Acad. Sci. U. S. A.*, 2007, **104**, 3782–3786.
29 D. Ponader, F. Wojcik, F. Beceren-Braun, J. Dernedde and L. Hartmann, *Biomacromolecules*, 2012, **13**, 1845–1852.
30 D. Ponader, P. Maffre, J. Aretz, D. Pussak, N. M. Ninnemann, S. Schmidt, P. H. Seeberger, C. Rademacher, G. U. Nienhaus and L. Hartmann, *J. Am. Chem. Soc.*, 2014, **136**, 2008–2016.
31 K. S. Bucher, P. B. Konietzny, N. L. Snyder and L. Hartmann, *Chem.–Eur. J.*, 2019, **25**, 1–10.
32 M. Baier, M. Giesler and L. Hartmann, *Chem.–Eur. J.*, 2018, **24**, 1619–1630.
33 F. Wojcik, A. G. O'Brien, S. Gotze, P. H. Seeberger and L. Hartmann, *Chem.–Eur. J.*, 2013, **19**, 3090–3098.
34 T. Freichel, S. Eierhoff, N. L. Snyder and L. Hartmann, *J. Org. Chem.*, 2017, **82**, 9400–9409.
35 P. Palladino and D. A. Stetsenko, *Org. Lett.*, 2012, **14**, 6346–6349.
36 Y. Kiso, K. Ukawa, S. Nakamura, K. Ito and T. Akita, *Chem. Pharm. Bull.*, 1980, **28**, 673–676.
37 H. Q. Wang, F. Jacobi, J. Waschke, L. Hartmann, H. Lowen and S. Schmidt, *Adv. Funct. Mater.*, 2017, **27**, 1702040.
38 D. Pussak, M. Behra, S. Schmidt and L. Hartmann, *Soft Matter*, 2012, **8**, 1664–1672.
39 G. Hild, R. Okasha, M. Macret and Y. Gnanou, *Macromol. Chem. Phys.*, 1986, **187**, 2271–2288.
40 K. L. Johnson, K. Kendall and A. D. Roberts, *Proc. R. Soc. London, Ser. A*, 1971, **324**, 301–313.
41 D. Pussak, D. Ponader, S. Mosca, S. V. Ruiz, L. Hartmann and S. Schmidt, *Angew. Chem., Int. Ed.*, 2013, **52**, 6084–6087.
42 F. Jacobi, A. Camaleño de la Calle, S. Boden, A. Grafmüller, L. Hartmann and S. Schmidt, *Biomacromolecules*, 2018, **19**, 3479–3488.
43 V. T. Moy, Y. K. Jiao, T. Hillmann, H. Lehmann and T. Sano, *Biophys. J.*, 1999, **76**, 1632–1638.
44 J. Erath, S. Schmidt and A. Fery, *Soft Matter*, 2010, **6**, 1432–1437.
45 D. Rettke, J. Döring, S. Martin, T. Venus, I. Estrela-Lopis, S. Schmidt, K. Ostermann and T. Pompe, *Biosens. Bioelectron.*, 2020, **165**, 112262.
46 K. Leung, I. M. B. Nielsen and L. J. Criscenti, *J. Am. Chem. Soc.*, 2009, **131**, 18358–18365.
47 J. N. Israelachvili, in *Intermolecular and Surface Forces*, ed. J. N. Israelachvili, Academic Press, San Diego, 3rd edn, 2011, pp. 577–616, DOI: 10.1016/B978-0-12-375182-9.10021-1.
48 C. R. Kemnitz and M. J. Loewen, *J. Am. Chem. Soc.*, 2007, **129**, 2521–2528.
49 K. S. Bucher, H. Yan, R. Creutznacher, K. Ruoff, A. Mallagaray, A. Grafmuller, J. S. Dirks, T. Kilic, S. Weickert, A. Rubailo, M. Drescher, S. Schmidt, G. Hansman, T. Peters, C. Uetrecht and L. Hartmann, *Biomacromolecules*, 2018, **19**, 3714–3724.

Supporting Information

Sequence-defined positioning of amine and amide residues to control catechol driven wet adhesion.

Lukas Fischer,[†a] Alexander K. Strzelczyk, [†a] Nils Wedler,[b] Christian Kropf,[b] Stephan Schmidt[*a] and Laura Hartmann*[a]

[a.] *Institut für Organische und Makromolekulare Chemie, Heinrich-Heine-Universität Düsseldorf, Universitätsstr. 1, 40225 Düsseldorf, Germany.*
[b.] *Laundry & Home Care, Henkel AG & Co. KGaA, Henkelstr. 67, 40589 Düsseldorf, Germany.*

Contents

Supporting Information

S1 Materials and methods

Materials

Triisopropylsilane (TIPS) (98%), triethylsilane (99%) and 4-(dimethylamino)butyric acid hydrochloride (98%) were purchased from Sigma-Aldrich. Diisopropylethylamine (DIPEA) (≥99%) was purchased from Carl Roth. Dimethylformamide (DMF) (99.8%, for peptide synthesis), piperidine (99%), triphenylmethyl chloride (Trt-Cl) (98%) and succinic anhydride (99%) were purchased from Acros Organics. Dichloromethane (DCM) (99.99%), sodium chloride (99.98%), tetrahydrofuran (THF) (analytical reagent grade), ethyl acetate (analytical reagent grade) and sodium hydrogen carbonate (analytical reagent grade) were purchased from Fisher Scientific. Triethylamine (pure) was purchased from AppliChem. Trifluoroacetic acid (TFA) (99%) and (benzotriazol-1-yloxy)tripyrrolidinophosphonium hexafluorophosphate (PyBOP) (98%) were purchased from Fluorochem. Succinamic acid (97%) and Thioanisol (99%) were purchased from Alfa Aesar. 3-(3,4-Dimethoxyphenyl)propionic acid (99%) was purchased from BLD Pharmatech Ltd. Fmoc-Osu (99%), trifluoromethanesulfonic acid (98%) and trifluoroethanol (99%) were purchased from Carbolution. Diethyl ether (contains BHT as inhibitor, >99%) was purchased from Honeywell. Tentagel® S RAM resin was purchased from Rapp Polymere. Sodium sulfate (99.5%) was purchased from fisher chemicals. Polyethylene glycol diacrylate (PEG(8000)-DiAc) was purchased from Alfa Aesar. Irgacure 2959 (98%) and crotonic acid (98%) were purchased from Sigma-Aldrich. Benzophenone (99%) was purchased from Acros Organics. 1-Ethyl-3-(3-dimethylaminopropyl)carbodiimid-hydrochlorid (EDC HCl) (≥99%) was purchased from Carl Roth. Water was purified with a Milli-Q system (Millipore) obtaining a final resistivity of 18 MΩcm.

Oligomer synthesis

All oligomers were synthesized using the building blocks EDS, TrDS and CDS as previously described.[1] The oligomers were assembled via iterative deprotection and amide coupling on a Tentagel® S RAM resin. For deprotection, the resin was treated with 20% piperidine in DMF (2x 15 min) and washed with DMF (10x). For the coupling step, the building block (5 eq.) and PyBOP (5 eq.) were dissolved in DMF and DIPEA (10 eq.) was added. The resin was treated with the coupling solution for 1 hr with subsequent DMF washing (10x). After assembly of the full sequence, the trityl groups were cleaved by treating the resin with 0.1 M HCl in trifluorethanol (2x1.5 h). Then the resin was washed with DMF (5x) and the free amines were deprotonated with 20% DIPEA in DMF for 10 minutes. For introducing the side chains, the resin was treated for 1 hr with a solution of solution of either succinamic acid or 4-(dimethylamino)butyric acid (5 eq.), PyBOP (5 eq.) and DIPEA (10 eq.) in DMF and washing in DMF (10x) afterward. The structures were cleaved from solid support with a solution of TFA/TIPS (95/5), precipitated in diethyl ether and the precipitate was lyophilized. All oligomers with a protected catechol moiety were deprotected by treatment with 16 eq. trifluoromethanesulfonic acid and 8 eq. thioanisole per methyl ether in TFA for 16 h. Afterward the

reaction solution was precipitated in diethyl ether and the deprotected oligomers were lyophilized. The chemical analysis of the building block and oligomers are shown in the supporting information S1-S4)

Soft colloidal probe (SCP) synthesis

A dispersion of poly(ethylene glycol diacrylamide) (PEGdAAm, 50 mg, 6.3 µmol, Mn = 8000 Da) microdroplets was prepared by phase separation in 10 mL 1M sodium sulfate solution under vigorous agitation.[2] Irgacure 2959 (2.1 mg, 5.4 µmol) was added and the dispersion was photopolymerized under UV light for 90 s (Heraeus HiLite Power curing unit (Heraeus Kulzer, Germany). The diameter of received microgels was between 10-40 µm. After centrifugation/washing, crotonic acid was grafted onto the SCPs by exchange of water with ethanol, addition of benzophenone (250 mg, 1.4 mmol) and crotonic acid (1.5 g, 17.7 mmol) flushing with nitrogen for 60 s followed by UV irradiation for 1080 s.[3] The particles were washed with ethanol and water to remove all reactants. In the final step, the oligomers with unprotected amine end groups were coupled to crotonic acid on the SCPs in 0.1 M MES buffer pH 5.5 containing 32.5 mM (1-ethyl-3-[3-dimethylaminopropyl]carbodiimide hydrochloride), and 0.225 mM oligomers followed by washing with water. The carbodiimide coupling was repeated to maximize the functionalization degree for all oligomers (supporting information S5).

SCP characterization

AFM force-indentation measurements with a NanoWizard 2 system (JPK instruments AG, Berlin, Germany) was performed to determine the elastic moduli of the SCPs. As AFM probe a silica particle with a diameter of 4.6 µm was adhered with epoxy glue onto a tipless, non-coated cantilever (spring constant 0.32 N/m; CSC12, NanoAndMore GmbH). Several force curves were recorded for different SCPs and analyzed with an appropriate contact model developed by Glaubitz et al. (supporting information S6). The degree of oligomer functionalization in the SCP network was determined by titrating crotonic acid residues with toluidine blue O (TBO). 1.0 mL of a dispersion containing crotonic acid functionalized SCPs were dried by first exchanging the water by ethanol in the continuous phase and then treating in a vacuum oven at 50°C until constant weight. After the dry mass was determined, 1.0 mL of 312.5 µM TBO solution at pH10 was added and shaken in the dark for 12 hrs. Next, 0.3 mL of the TBO solution supernatant of the was diluted with 1.7 mL water at pH 10 and the absorbance at 633 nm was detected and compared to the TBO reference (no infusion of SCPs) to calculate the degree of crotonic acid functionalization. Comparing the amount of SCP crotonic acid functionalization before and after the oligomer coupling gave the oligomer functionalization degree (supporting information S5).

S2 Instrumentation

Nuclear Magnetic Resonance Spectroscopy (NMR)

^{1}H-NMR and ^{13}C NMR were recorded on a Bruker Avance III 300, a Bruker Avance DRX-500 or a Bruker Avance III 600. Chemical shifts were reported as delta (δ) in parts per million (ppm) and

coupling constants as *J* in Hertz (Hz). Multiplicities are stated as following: s = singlet, d = doublet, t = triplet, q = quartet, m = multiplet.

High Resolution – Mass Spectrometry (HR-MS)

HR-MS measurements were conducted on a Bruker UHR-QTOF maxis 4G with a direct inlet via syringe pump, an ESI source and a quadrupole Time of Flight (QTOF) analyzer. Samples were dissolved in water with a concentration of 1 mg/mL.

Reversed Phase – High Pressure Liquid Chromatography (RP-HPLC)

RP-HPLC was performed with an Agilent 1260 Infinity instrument coupled to a variable wavelength detector (VWD) set to 214 nm. As a column a Poroshell 120 EC-C18 1.8 µM (3.0x50 mm, 2.5 µm) reversed phase column was used. The mobile phase A consisted of 95/5 H_2O/MeCN with 0.1% formic acid and mobile phase B consisted of 95/5 MeCN/H_2O with 0.1% formic acid. The flowrate for all measurements was 0.4 mL/min.

Preparative Reversed Phase – High Pressure Liquid Chromatography (Prep-RP-HPLC)

Prep-RP-HPLC was conducted on an Agilent 1260 Infinity instrument coupled to a variable wavelength detector (VWD) set to 214 nm. As a column a CAPCELL PAL C18 (20mml.D. x 250 mm, 5 µm) reversed phase column was used. The mobile phase A consisted of H_2O with 0.1% formic acid and mobile phase B consisted of MeCN with 0.1% formic acid. All samples were purified with a flowrate of 10 ml/min and a gradient of 100% A to 50% A over 15 min. Fractions were collected by an automated collector and were then lyophilized.

Freeze Dryer

Lyophilization of the final structures was conducted on an Alpha 1-4 LD plus instrument from Martin Christ Freeze Dryers GmbH. The lyophilization was done at a pressure of 0.1 mbar.

Supporting Information

S3 Building Block Synthesis and Chemical Analysis

The building block EDS was synthesized according to literature.[4]

Synthesis Route for Functional Building Blocks

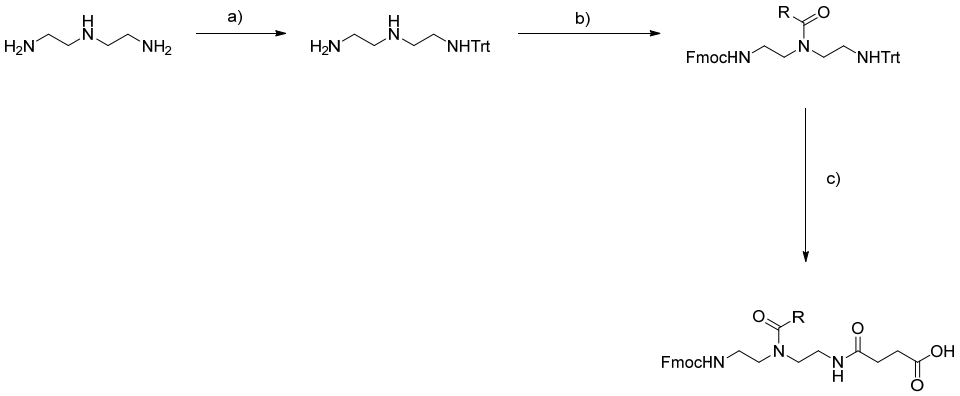

Figure S1. Overview of building block synthesis route: a) 0.25 eq. trityl chloride in DCM; b) 1 eq. Fmoc-OSu, 3 eq. triethylamine in THF at -78°C for 2 h followed by 1 eq. activated acid; c) 10 eq. TFA in DCM for 1 h followed by precipitation and 1 eq. succinic anhydride, 3 eq. triethylamine in DCM for 2 h.

Functional building blocks were synthesized with the new synthesis route shown in Figure S1.

a) To a solution of diethylenetriamine in DCM a solution of trityl chloride (0.25 eq.) in DCM was added over 1 h at 0°C. The reaction was stirred for 16 h at room temperature and afterwards extracted with a saturated $NaHCO_3$ solution (3x). The organic phase was dried with $MgSO_4$ and the solvent was evaporated under reduced pressure to give the crude product as a brown oil.

b) The crude product of a) was dissolved in THF and triethylamine (3 eq.) and a solution of Fmoc-OSu (1 eq.) in THF was added over 2 h at -78°C. Afterwards the activated acid (1 eq.) in THF was added and the reaction was stirred for 16 h at room temperature. The reaction mixture was extracted with a saturated NaCl solution (3x) and the organic phase was dried with $MgSO_4$ and the solvent was evaporated under reduced pressure to give the crude product as a brown foam.

c) The crude product of b) was dissolved in DCM and triethylsilane (10 eq.) and 10 vol-% TFA were added. The reaction was stirred at room temperature for 1 h. Afterwards the solvent was evaporated under reduced pressure and the product was precipitated in diethyl ether. The precipitate was dissolved in DCM and triethylamine (3 eq.) and succinic anhydride (1 eq.) were added. The reaction was stirred for 2 h at room temperature and afterwards extracted with a citric acid solution (3x). The organic phase was dried with $MgSO_4$ and the solvent was evaporated under reduced pressure to give the crude product as a brown foam.

4-((2-((((9H-fluoren-9-yl)methoxy)carbonyl)amino)ethyl)(2-(tritylamino)ethyl)amino)-4-oxobutanoic acid (TrDS) (**1**)

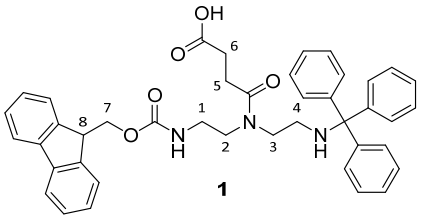

TrDS (**1**) was synthesized following the synthesis route in Figure S1 (step a and b). The crude product was recrystallized in DCM and diethyl ether (1:1) to give a white powder with a yield of 24 g (72%).

^{1}H-NMR (600 MHz, DMSO-d_6, 80°C) δ [ppm]: 7.86 (d, J = 7.6 Hz, 2H, Fmoc-H), 7.67 (d, J = 7.4 Hz, 2H, Fmoc-H), 7.45-7.35 (m, 8H, Fmoc-H, Trt-H), 7.32 (t, J = 7.6 Hz, 2H, Fmoc-H), 7.29 (t, J = 7.7 Hz, 6H, Trt-H), 7.19 (t, J = 7.3 Hz, 3H, Trt-H), 4.44-4.29 (m, 2H, H-7), 4.25-4.20 (m, 1H, H-8), 3.30-2.55 (m, 8H, H-1,H-2,H-3,H-4), 2.50-2.20 (m, 4H, H-5,H-6).

^{13}C-NMR (126 MHz, $CDCl_3$+DMSO-d_6) δ [ppm]: 174.25, 172.26, 156.26, 156.13, 145.16, 143.47, 140.65, 128.05, 127.94, 127.43, 127.15, 126.56, 125.92, 124.70, 124.61, 119.40, 119.38, 70.43, 65.73, 65.21, 53.20, 48.47, 46.73, 45.95, 45.35, 42.00, 38.79, 31.00, 29.24, 29.10, 28.67, 27.67, 27.36, 24.93, 22.08, 14.81, 13.66.

HR-ESI-MS: calculated mass for $C_{42}H_{42}N_3O_5$ $[M+H]^+$ 668.3119, found 668.3119.

RP-HPLC (gradient from 0% to 100% eluent B over 30 min at 25°C): t_r=20.9 min, relative purity 98%.

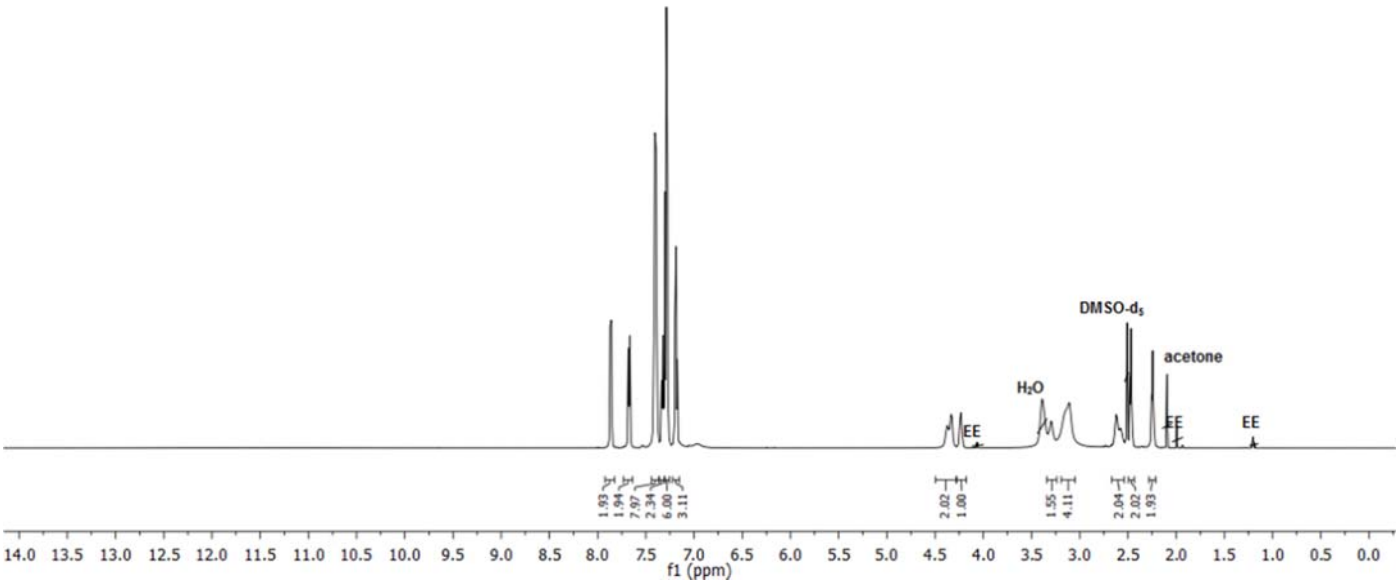

Figure S2. ^{1}H-NMR spectrum of compound **1** (600 MHz, DMSO-d_6, 80°C).

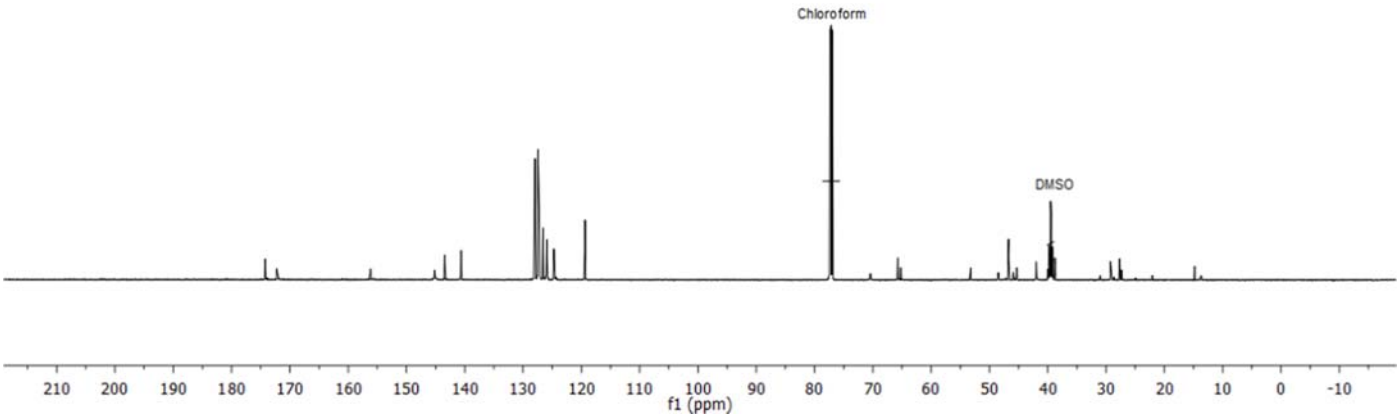

Figure S3. ^{13}C-NMR spectrum of compound **1** (126 MHz, $CDCl_3$+DMSO-d_6).

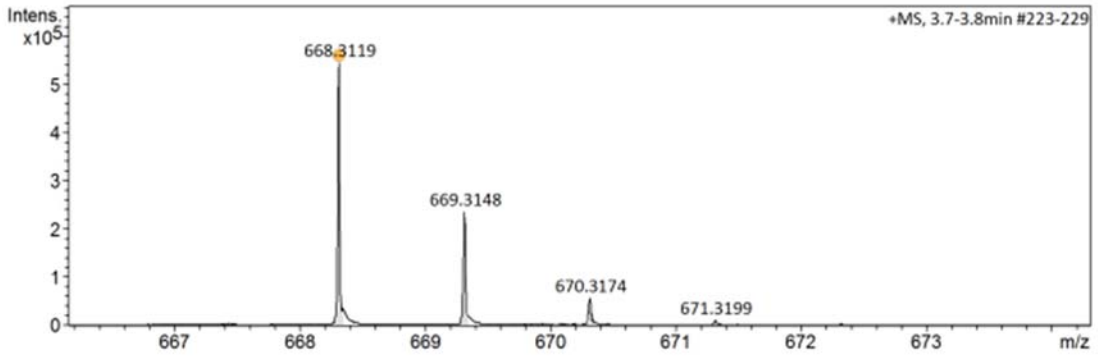

Figure S4. HR-ESI (ESI$^+$ Q-TOF) of compound **1**.

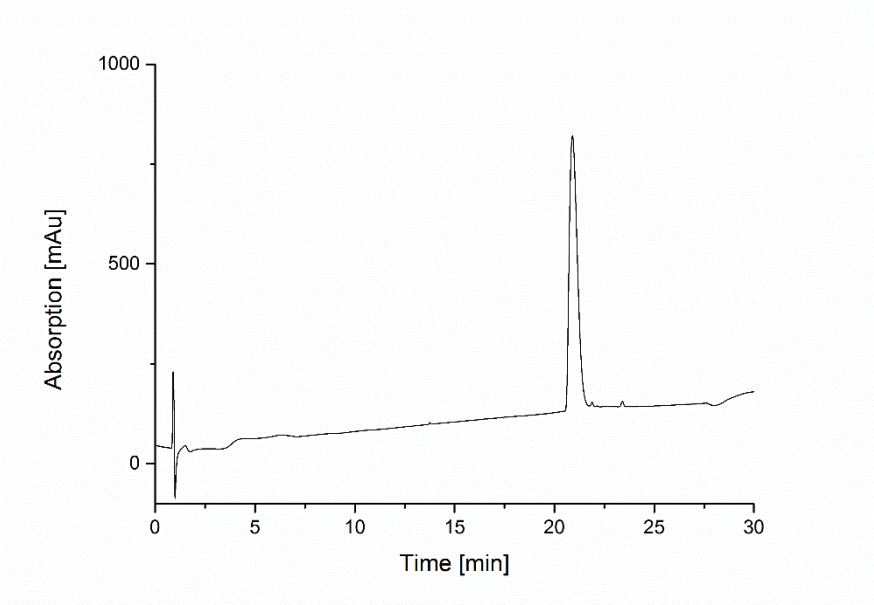

Figure S5. RP-HPLC chromatogram of compound **1** (gradient from 0% to 100% eluent B over 30 min at 25°C).

7-(3-(3,4-dimethoxyphenyl)propanoyl)-1-(9H-fluoren-9-yl)-3,11-dioxo-2-oxa-4,7,10-triazatetradecan-14-oic acid (CDS) (**2**)

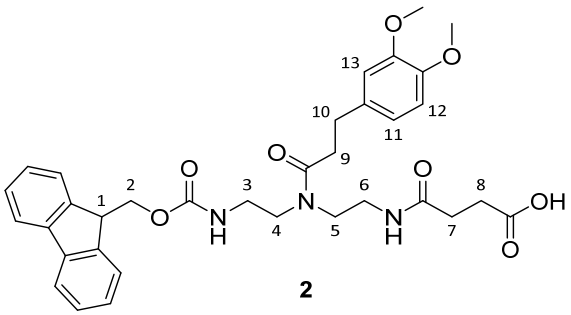

2

CDS (**2**) was synthesized following the synthesis route in Figure S1. The crude product was recrystallized in acetone and DCM (1:1) to give a white powder with a yield of 17 g (60%).

^{1}H-NMR (600 MHz, DMSO-d_6) δ [ppm]: 8.1 (m, NH), 7.9 (m, NH), 7.88 (d, J = 7.7 Hz, 2H, Fmoc-H), 7.68 (d, J = 7.4 Hz, 1H, Fmoc-H), 7.64 (d, J = 7.5 Hz, 1H. Fmoc-H), 7.47 (m, NH), 7.41 (t, J = 7.5 Hz, 2H, Fmoc-H), 7.36-7.29 (m, 2H, Fmoc-H,NH), 6.83-6.60 (m, 3H, H-11, H-12, H-13), 4.28 (dd, J = 17.4, 7.0 Hz, 2H, H-2), 4.21 (t, J = 7.0 Hz, 0.5H, H-1), 4.16 (t, J = 7.0 Hz, 0.5H, H-1), 3.75-3.63 (m, 6H, H-14), 3.29 (m, 4H, H-4, H-5), 3.19-3.07 (m, 4H, H-3, H-6), 2.75-2.69 (m, 2H, H-9), 2.60-2.55 (m, 2H, H-10), 2.45-2.38 (m, 2H, H-7), 2.35-2.27 (m, 2H, H-8).

^{13}C-NMR (126 MHz, DMSO-d_6) δ [ppm]: 174.25, 172.26, 156.26, 156.13, 145.16, 143.47, 140.65, 128.05, 127.94, 127.43, 127.15, 126.56, 125.92, 124.70, 124.61, 119.40, 119.38, 70.43, 65.73, 65.21,

53.20, 48.47, 46.73, 45.95, 45.35, 42.00, 38.79, 31.00, 29.24, 29.10, 28.67, 27.67, 27.36, 24.93, 22.08, 14.81, 13.66.

HR-ESI-MS: calculated mass for $C_{34}H_{40}N_3O_8$ $[M+H]^+$ 618.2810, found 618.2807.

RP-HPLC (gradient from 0% to 100% eluent B over 30 min at 25°C):t_r=21.1 min, purity 99%.

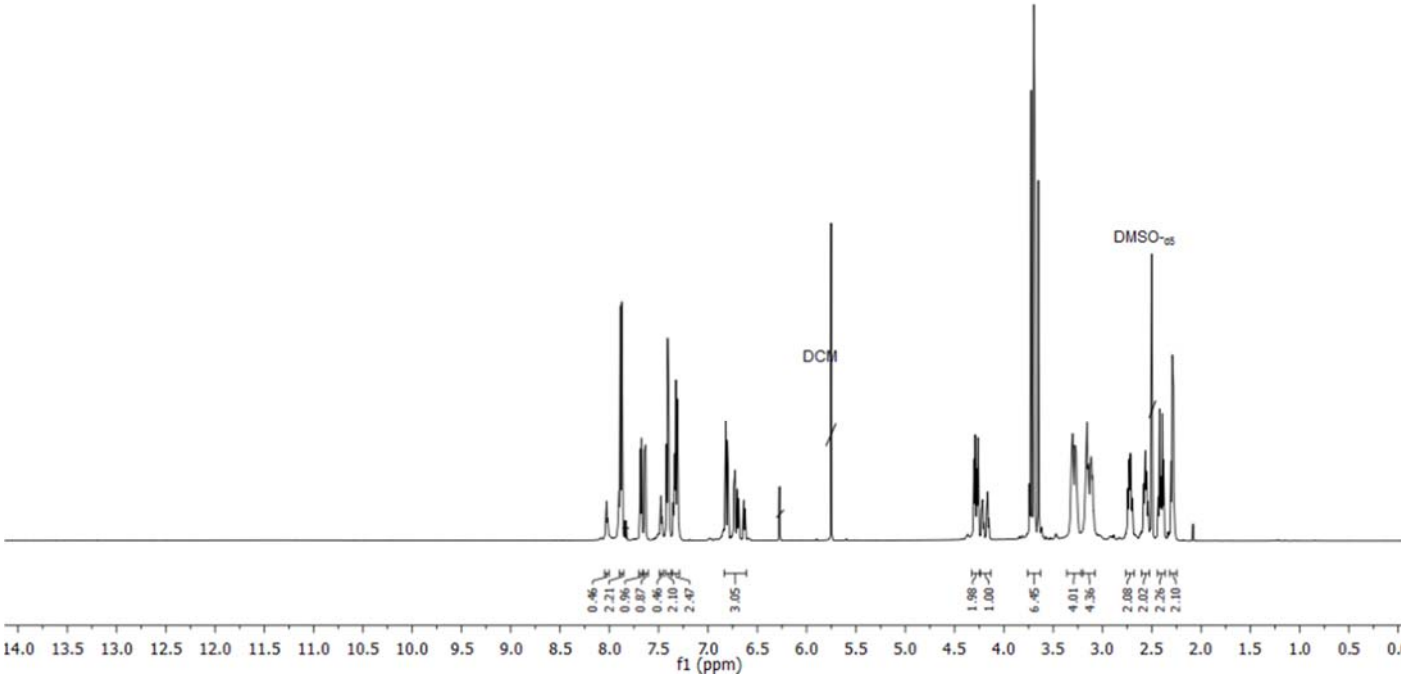

Figure S6. ^{1}H-NMR spectrum of compound **2** (600 MHz, DMSO-d_6).

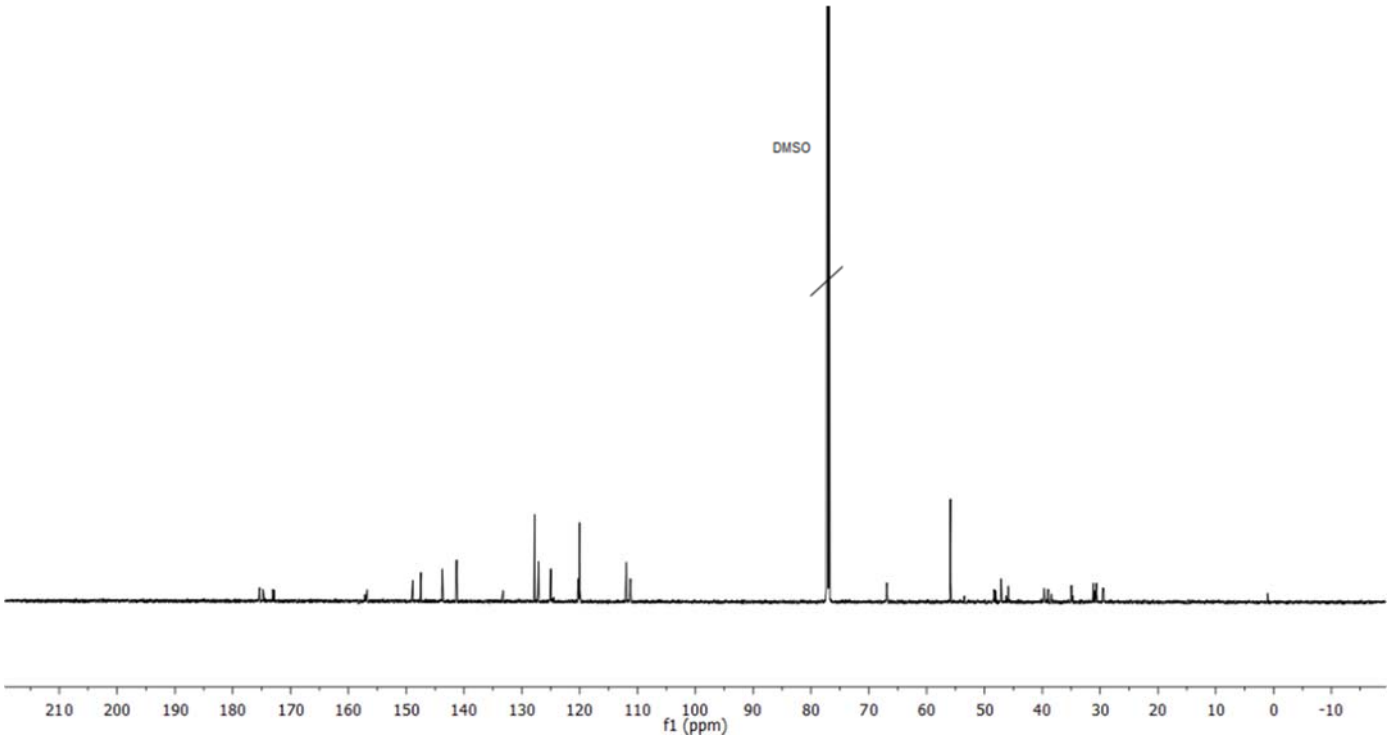

Figure S7. ^{13}C-NMR spectrum of compound **2** (126 MHz, DMSO-d_6).

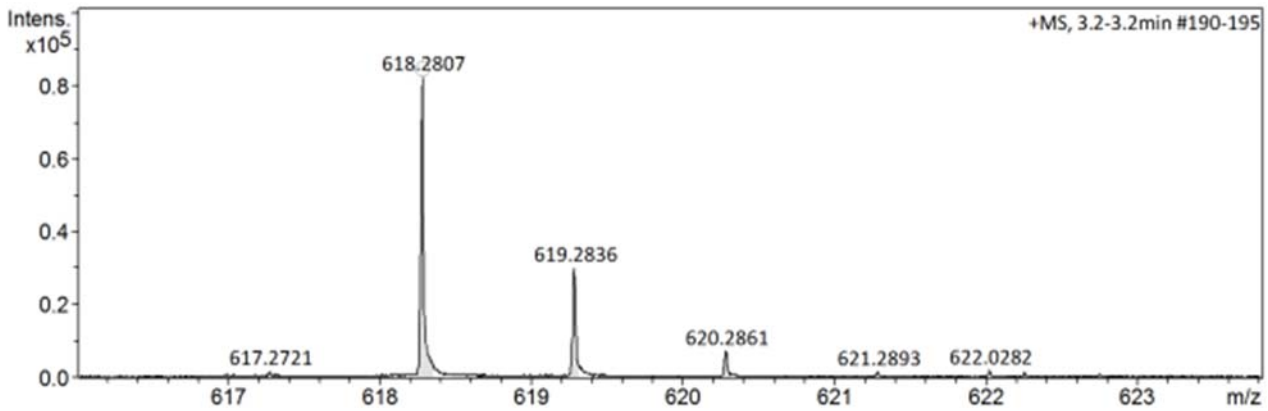

Figure S8. HR-ESI (ESI$^+$ Q-TOF) of compound **2**.

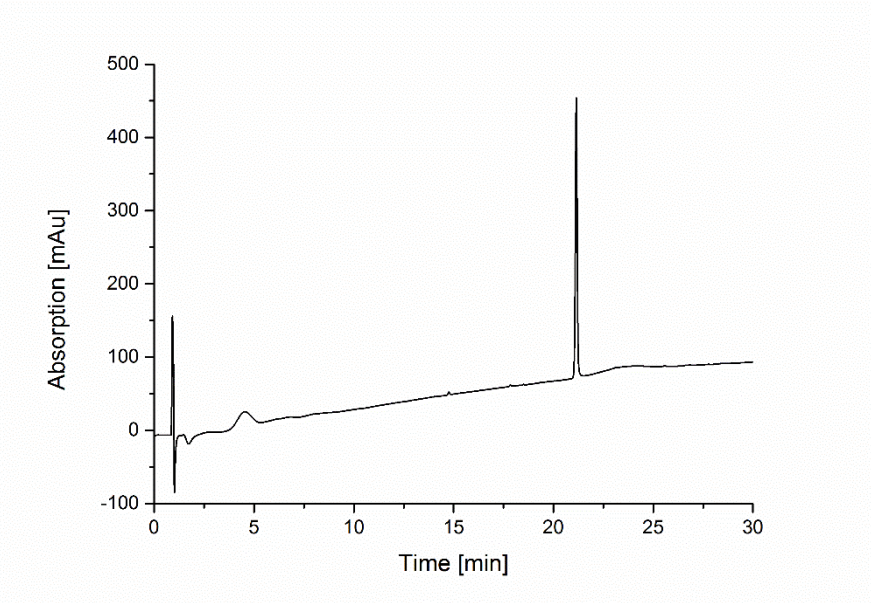

Figure S9. RP-HPLC chromatogram of compound **2** (gradient from 0% to 100% eluent B over 30 min at 25°C).

S4 Oligomer Synthesis and Chemical Analysis

All oligomers were synthesized on solid support according to literature[1] using the building blocks EDS, TrDS and CDS.

On Resin Deprotection Of Trityl

The resin was treated with 0.1 M HCl in trifluorethanol (2x1.5 h). Afterwards the resin was washed with DMF (5x) and the free amines were deprotonated with 20% DIPEA in DMF for 10 minutes.

Side Chain Coupling

After trityl deprotection the resin was treated for 1 h with a solution of 5 eq. acid, 5 eq. PyBOP and 10 eq. DIPEA in DMF. Afterwards the resin was washed with DMF (10x).

Deprotection Of Catechols

All oligomers with a protected catechol moiety were deprotected in solution. For this they were treated with 16 eq. trifluoromethanesulfonic acid and 8 eq. thioanisole per methyl ether in TFA for 16 h. Afterwards the reaction solution was precipitated in diethyl ether and the deprotected oligomers were freeze dried.

Oligomer Chemical Analysis

(**3**) *protected*

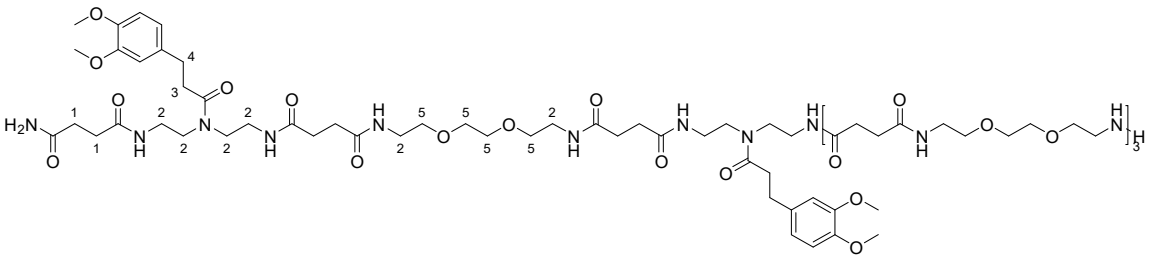

Compound **3 protected** was obtained with a yield of 64% after cleavage from solid support and lyophilization. .

^{1}H-NMR (600 MHz, D_2O) δ [ppm]: 6.90 (m, 4H, $H_{Aromatic}$), 6.79 (d, J = 8.3 Hz, 2H, $H_{Aromatic}$), 6.75 (d, J = 8.0 Hz, 2H, $H_{Aromatic}$), 3.80 (s, 6H, OCH_3), 3.78 (s, 6H, OCH_3) 3.74-3.54 (m, 32H, H-5), 3.40-3.17 (m, 32H, H-2), 2.82 (m, 4H, H-4), 2.64 (m, 4H, H-3), 2.51-2.36 (m, 24H, H-1).

^{13}C-NMR (126 MHz, D_2O) δ [ppm]: 178.36, 178.23, 176.63, 175.73, 175.68, 175.64, 175.59, 175.55, 175.53, 175.51, 175.49, 175.38, 175.36, 149.04, 147.63, 134.91, 121.82, 113.12, 112.81, 70.55, 70.42, 69.82, 67.36, 56.61, 56.56, 48.05, 45.86, 45.77, 40.09, 39.89, 39.82, 38.29, 37.99, 35.20, 35.14, 31.97, 31.93, 31.90, 31.84, 31.76, 31.70, 31.67, 31.58, 31.17, 31.03.

HR-ESI-MS: calculated mass for $C_{78}H_{132}N_{15}O_{26}$ $[M+3H]^{3+}$ 564.9817, found 564.9825.

RP-HPLC (gradient from 0% to 50% eluent B over 30 min at 25°C):t_r=14.0 min, purity 92%.

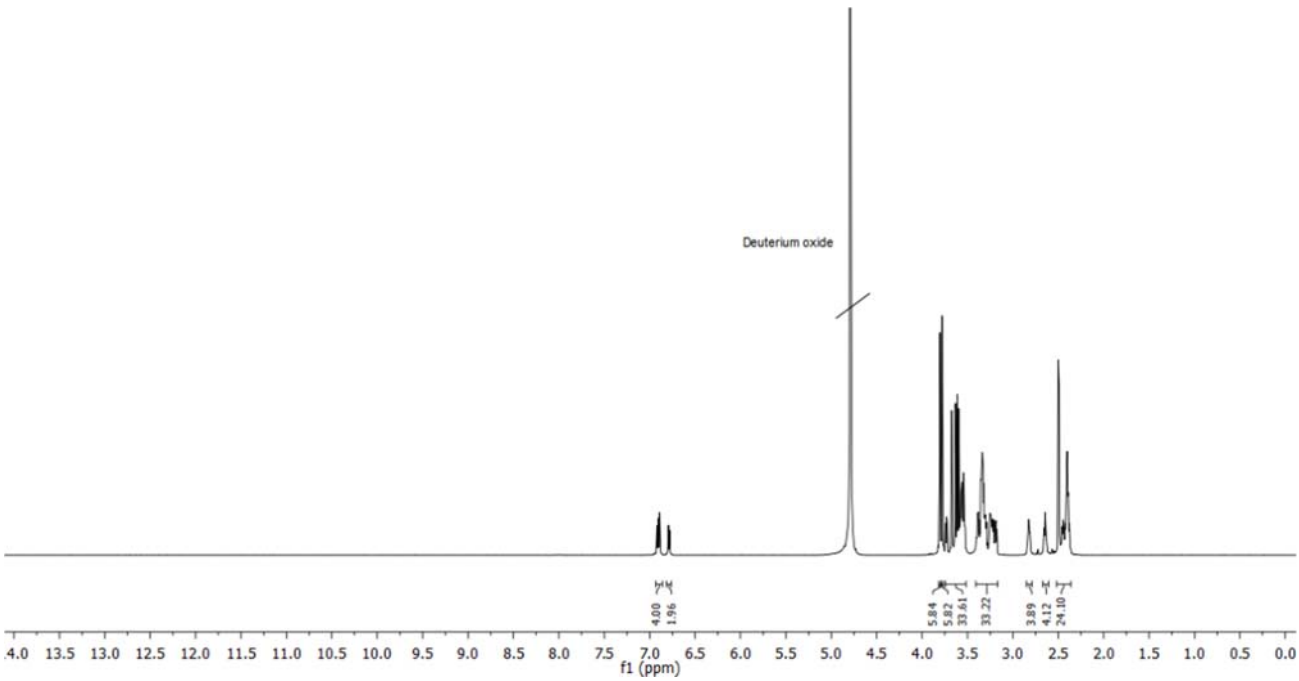

Figure S10. ^{1}H-NMR spectrum of oligomer **3** protected (600 MHz, D_2O).

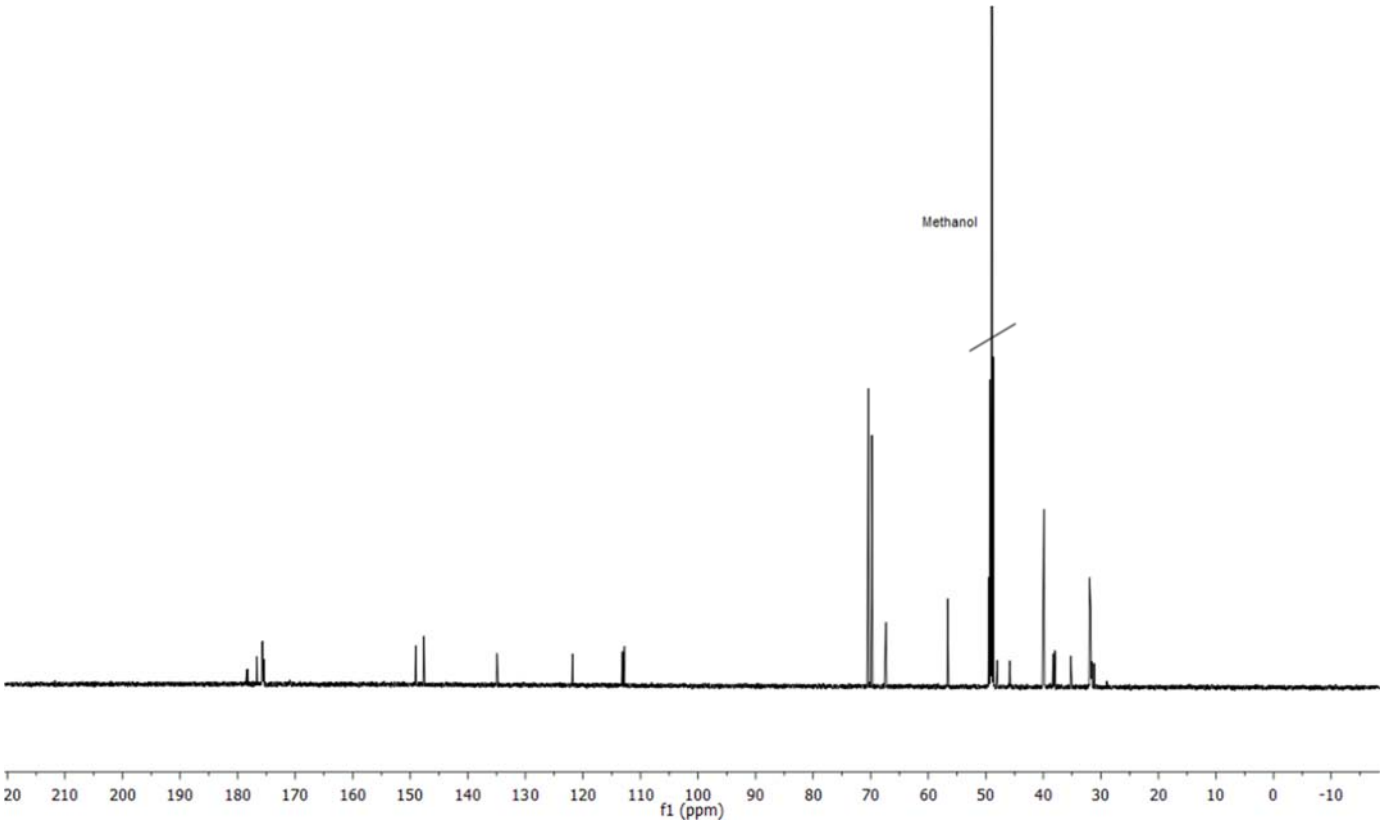

Figure S11. ^{13}C-NMR spectrum of oligomer **3** protected (126 MHz, D_2O).

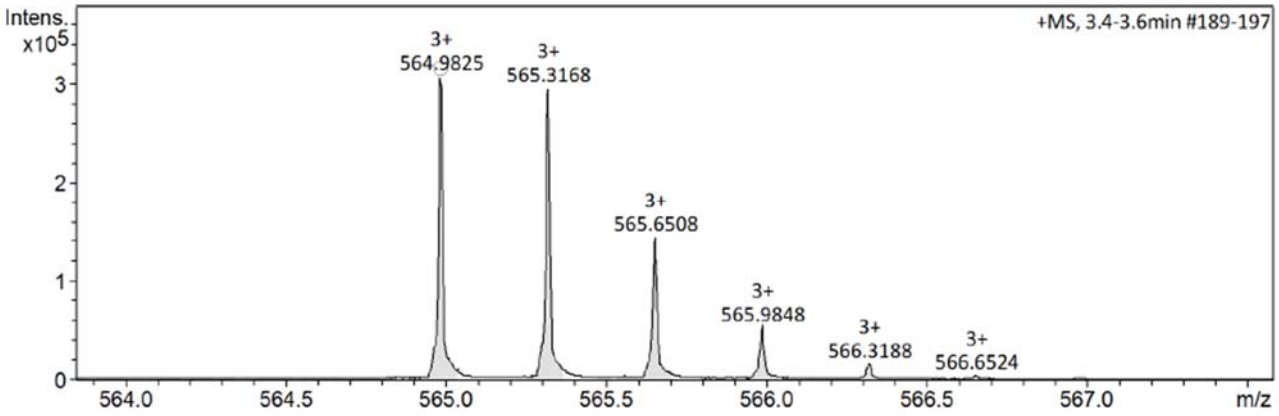

Figure S12. HR-ESI (ESI$^+$ Q-TOF) of oligomer **3** protected.

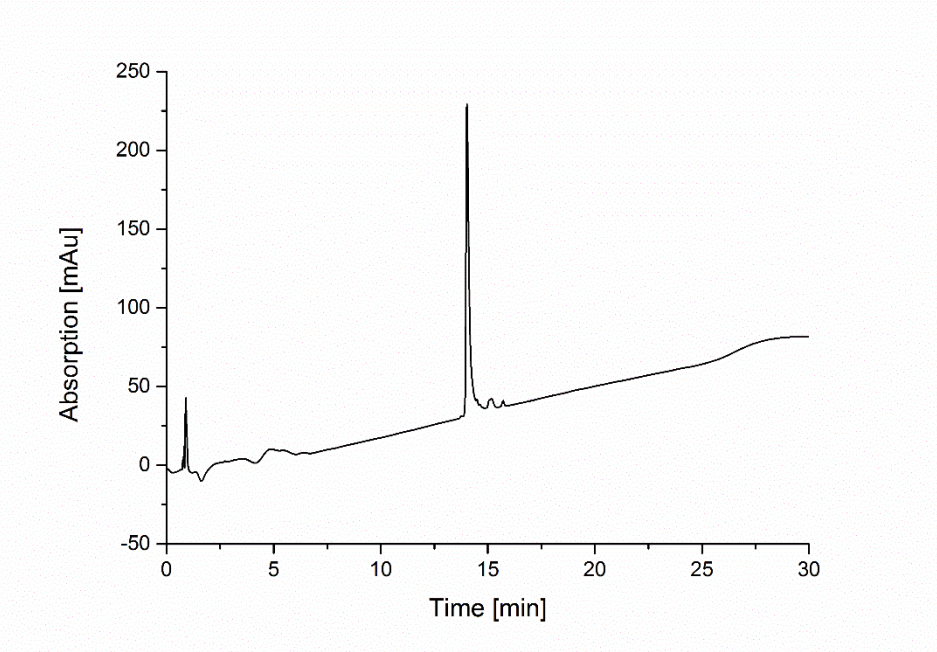

Figure S13. RP-HPLC chromatogram of compound **3** protected (gradient from 0% to 50% eluent B over 30 min at 25°C).

(**3**)

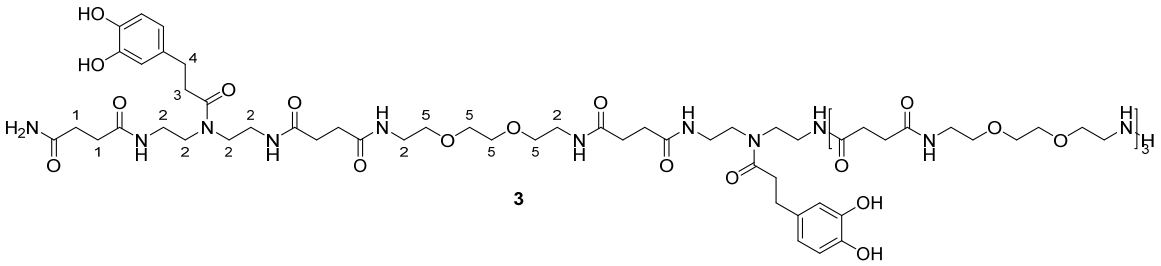

3

Compound **3** was obtained with a yield of 32% after deprotection, purification by preparative RP-HPLC and lyophilization.

^{1}H-NMR (500 MHz, D_2O) δ [ppm]: 8.32 (s, NH), 6.91 (dd, J = 8.0 Hz, 1.8 Hz, 2H, $H_{Aromatic}$), 6.85 (s, 2H, $H_{Aromatic}$), 6.75 (d, J = 8.0 Hz, 2H, $H_{Aromatic}$), 3.86-3.64 (m, 32H, H-5), 3.52-3.27 (m, 32H, H-2), 2.85 (m, 4H, H-4), 2.71 (m, 4H, H-3), 2.62-2.48 (m, 24H, H-1).

^{13}C-NMR (126 MHz, D_2O) δ [ppm]: 176.46, 176.39, 176.37, 175.40, 175.37, 175.29, 175.20, 175.09, 144.54, 144.48, 142.86, 134.10, 134.07, 121.17, 121.13, 118.92, 116.82, 116.78, 116.70, 70.12, 69.97, 69.37, 66.90, 45.41, 45.33, 39.67, 39.47, 39.40, 37.88, 37.62, 34.79, 31.61, 31.57, 31.53, 31.48, 31.42, 31.38, 31.23, 30.96, 30.79, 30.69.

HR-ESI-MS: calculated mass for $C_{78}H_{132}N_{15}O_{26}$ $[M+3H]^{3+}$ 564.9817, found 564.9825.

RP-HPLC (gradient from 0% to 50% eluent B over 30 min at 25°C):t_r=12.3 min, purity 93%.

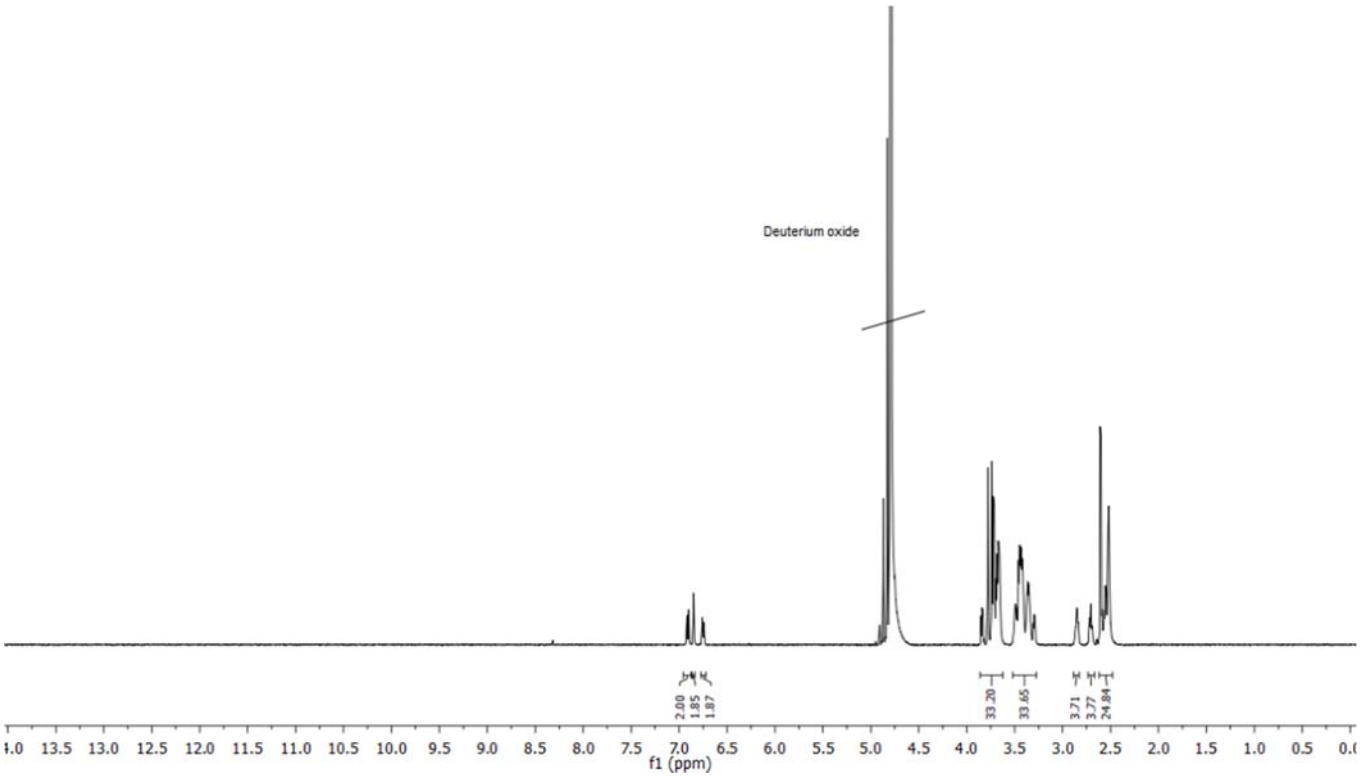

Figure S14. ^{1}H-NMR spectrum of compound **3** (500 MHz, D_2O).

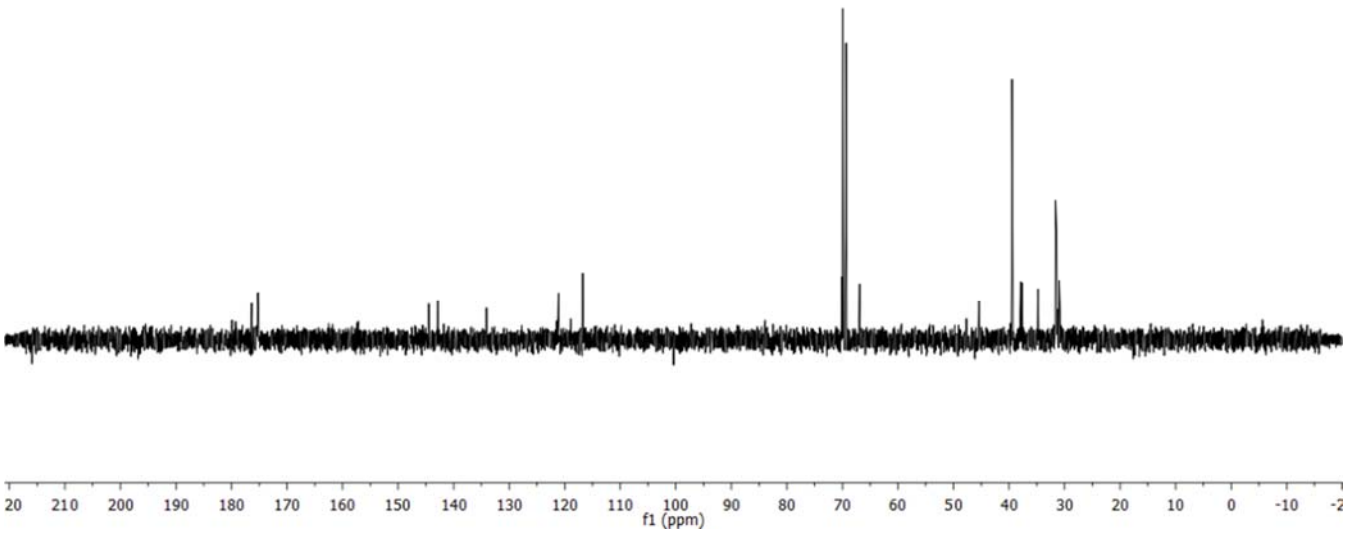

Figure S15. ^{13}C-NMR spectrum of compound **3** (126 MHz, D_2O).

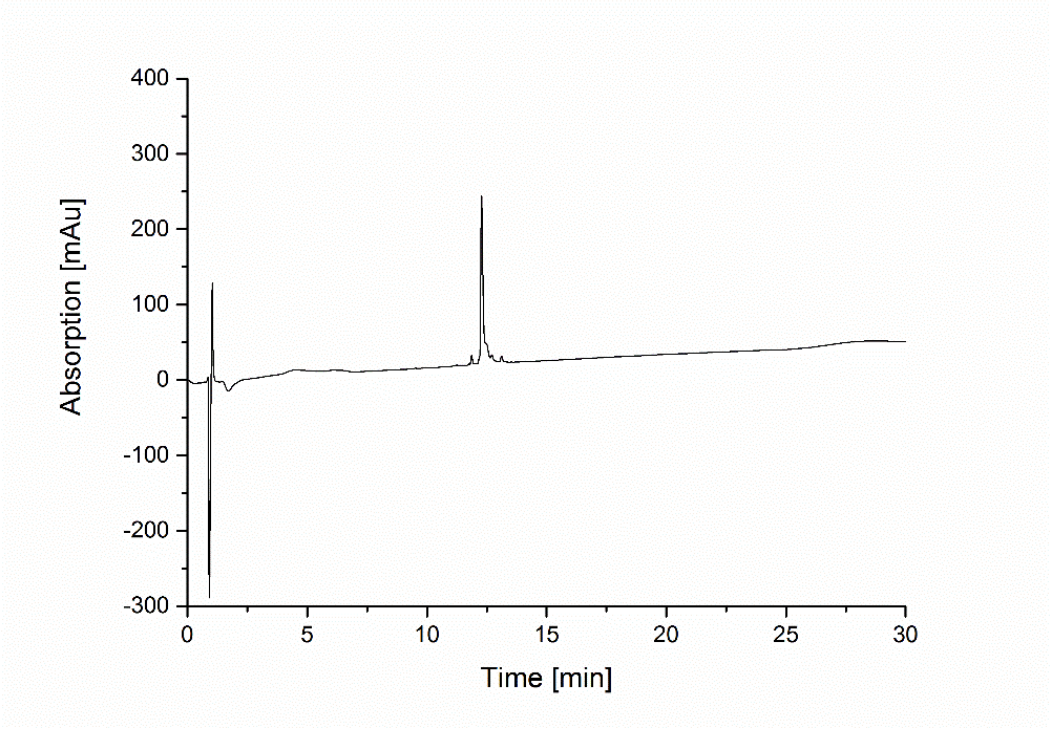

Figure S16. RP-HPLC chromatogram of compound **3** (gradient from 0% to 50% eluent B over 30 min at 25°C).

(**4**)

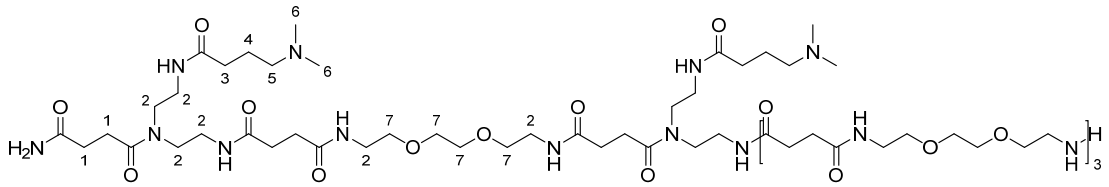

4

Compound **4** was obtained with a yield of 45% after purification by preparative RP-HPLC and lyophilization.^{1}H-NMR (500 MHz, D_2O) δ [ppm]: 8.47 (s, NH), 3.79-3.58 (m, 32H, H-7), 3.57-3.28 (m, 32H, H-2), 3.25-3.10 (m, 4H, H-5), 2.89 (s, 12H, H-6), 2.80 (m, 2H, H-8), 2.69 (m, 4H, H-3), 2.60-2.30 (m, 24H, H-1), 2.98 (m, 4H, 4-H).

^{13}C-NMR (126 MHz, D_2O) δ [ppm]: 175.85, 175.79, 175.65, 175.60, 175.56, 171.71, 70.42, 69.81, 57.96, 43.63, 39.87, 37.90, 31.98, 31.91, 31.84, 21.01, 20.98.

HR-ESI-MS: calculated mass for $C_{68}H_{130}N_{17}O_{22}$ $[M+3H]^{3+}$ 512.3187, found 512.3183.

RP-HPLC (gradient from 0% to 50% eluent B over 30 min at 25°C):t_r=7.1 min, purity 99%.

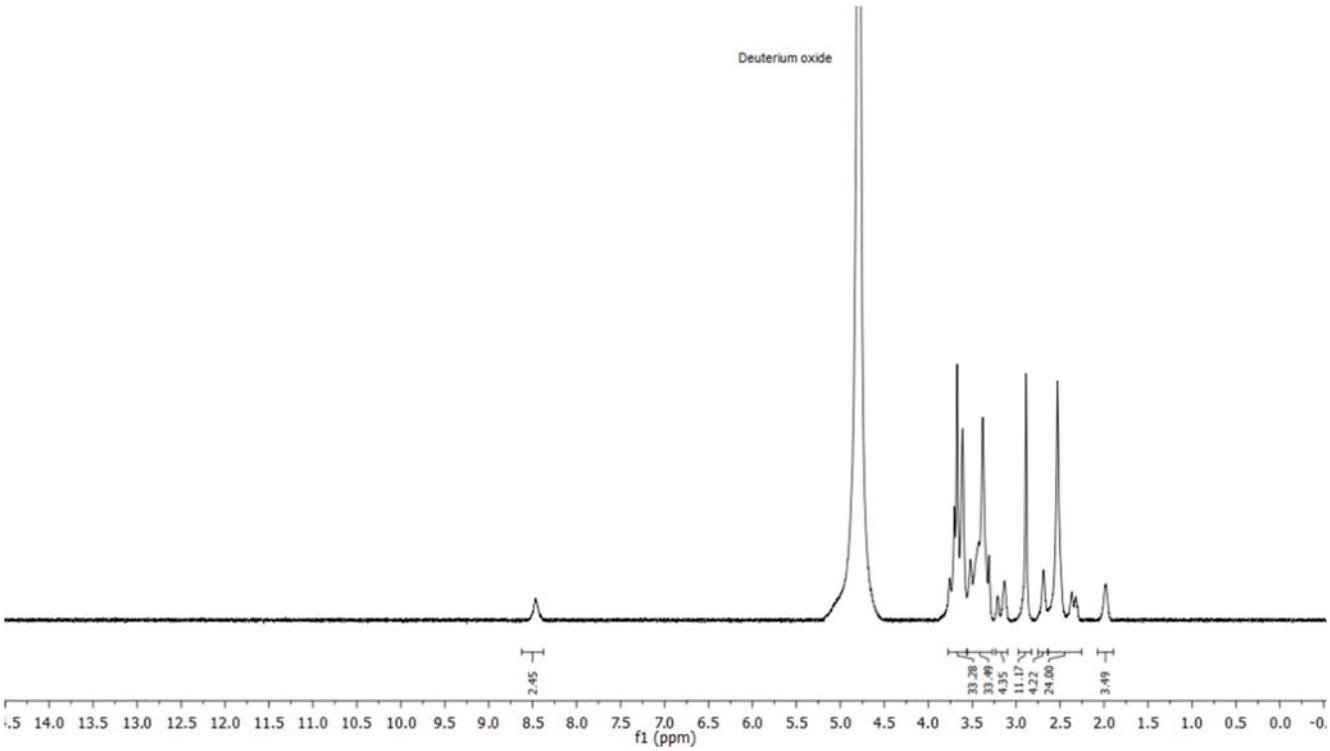

Figure S17. ^{1}H-NMR spectrum of compound **4** (500 MHz, D_2O).

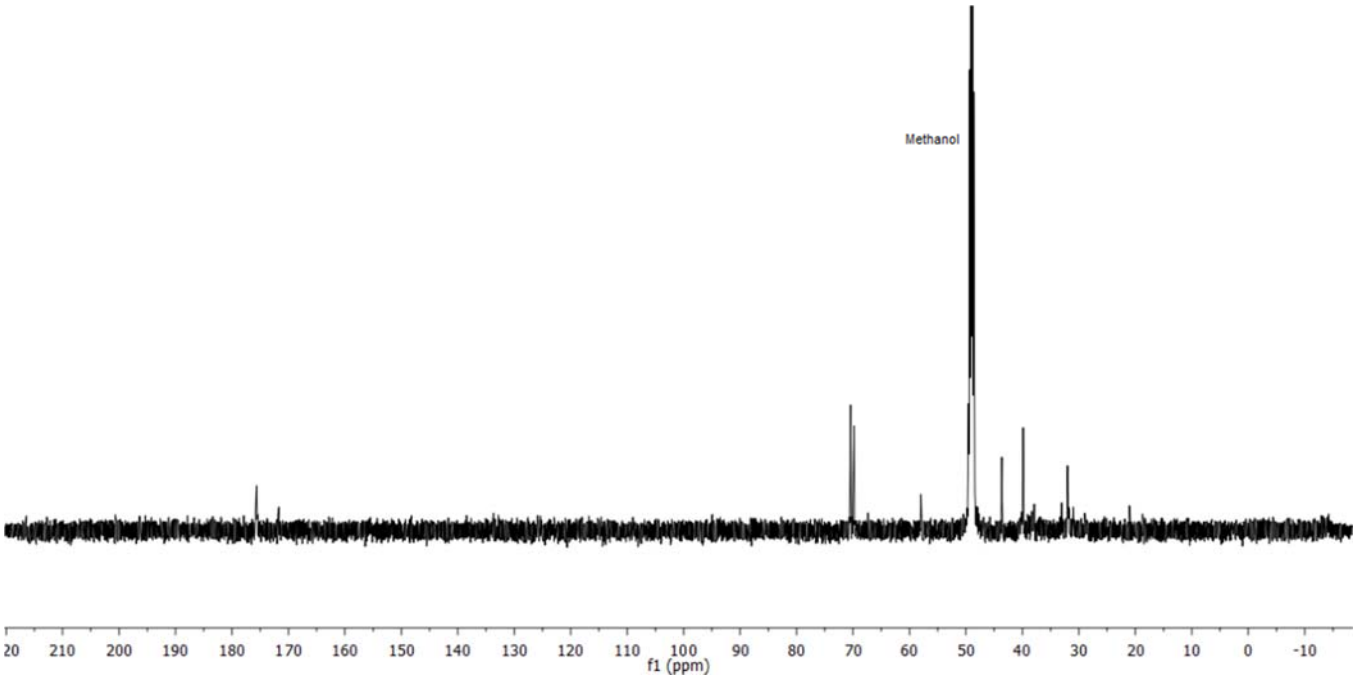

Figure S18. ^{13}C-NMR spectrum of compound **4** (126 MHz, D_2O).

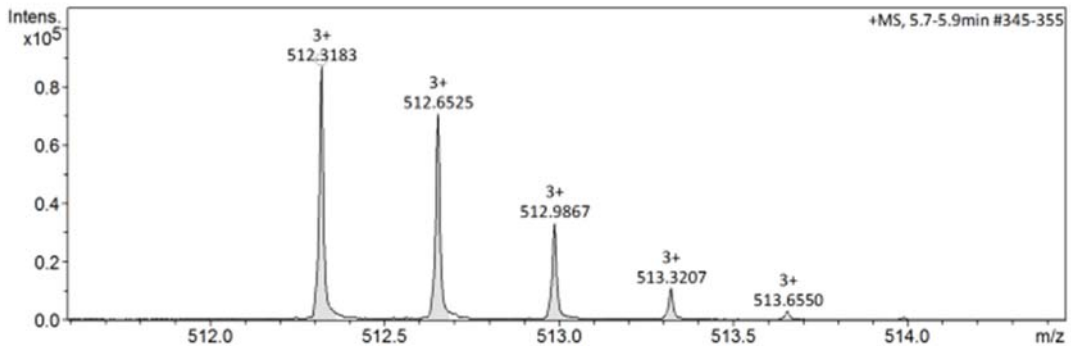

Figure S19. HR-ESI (ESI$^+$ Q-TOF) of compound **4**.

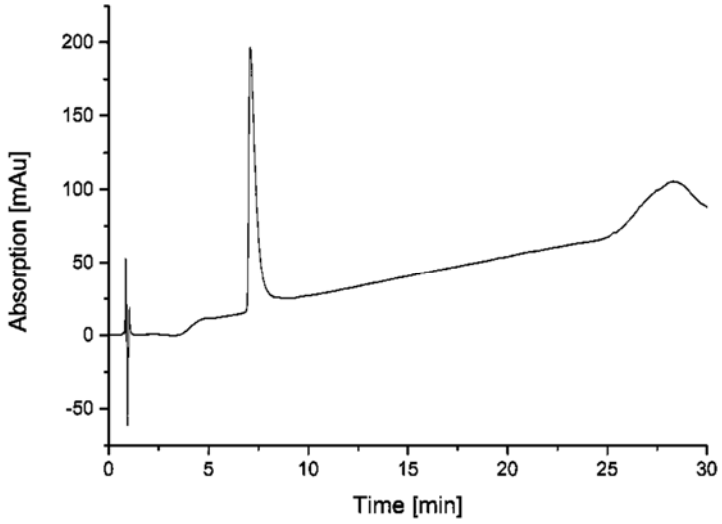

Figure S20. RP-HPLC chromatogram of compound **4** (gradient from 0% to 50% eluent B over 30 min at 25°C).

(**5**)

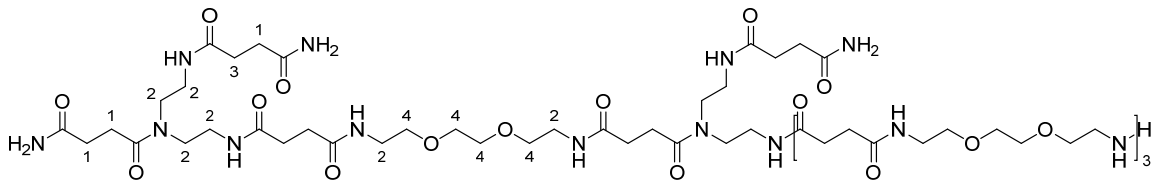

5

Compound **5** was obtained with a yield of 35% after purification by preparative RP-HPLC and lyophilization.

^{1}H-NMR (500 MHz, D_2O) δ [ppm]: 8.49 (s, NH), 3.80-3.59 (m, 32H, H-4), 3.57-3.20 (m, 32H, H-2), 2.71 (m, 4H, H-3) 2.60-2.46 (m, 28H, H-1).

^{13}C-NMR (126 MHz, D_2O) δ [ppm]: 175.73, 175.66, 175.63, 175.58, 175.53, 175.50, 175.47, 108.36, 108.21, 100.86, 70.54, 70.40, 69.80, 39.87, 39.80, 32.00, 31.95, 31.91, 31.87, 31.83, 31.79, 31.70, 31.67, 31.64, 28.94, 28.68.

HR-ESI-MS: calculated mass for $C_{64}H_{118}N_{17}O_{24}$ $[M+3H]^{3+}$ 502.9506, found 502.9499.

RP-HPLC (gradient from 0% to 50% eluent B over 30 min at 25°C):t_r=8.3 min, purity 94%.

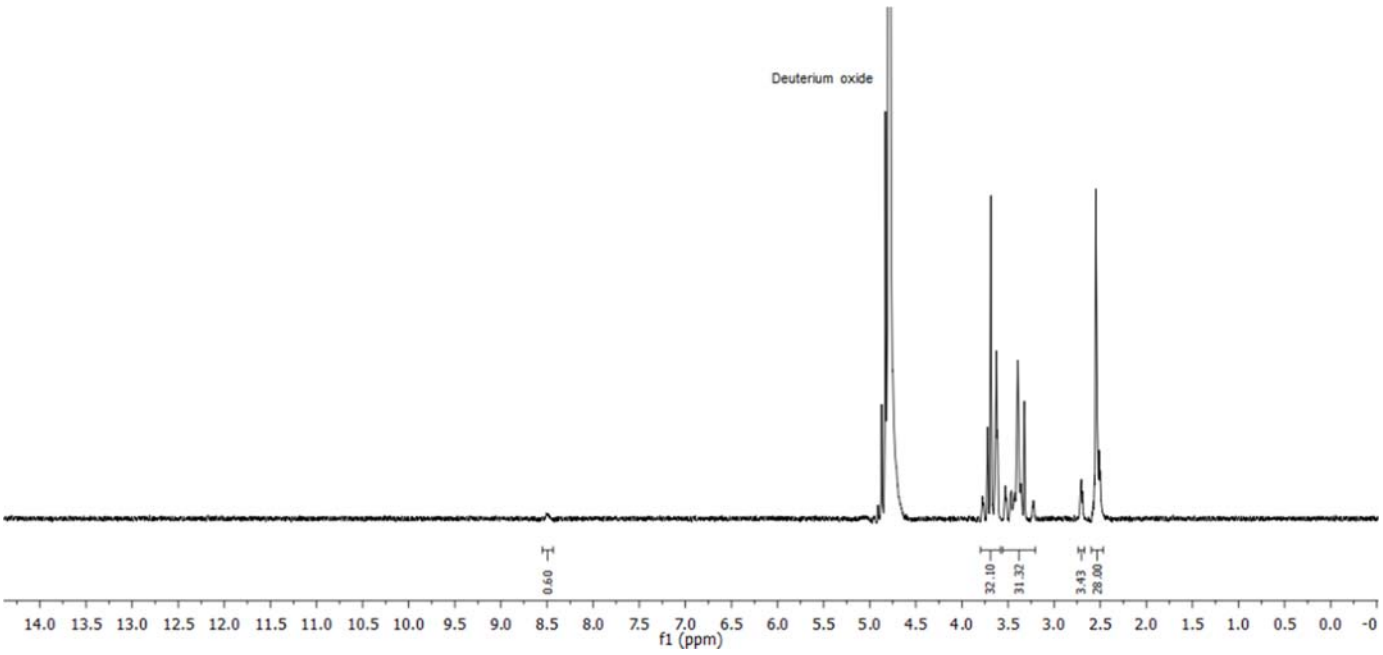

Figure S21. ^{1}H-NMR spectrum of compound **5** (500 MHz, D_2O).

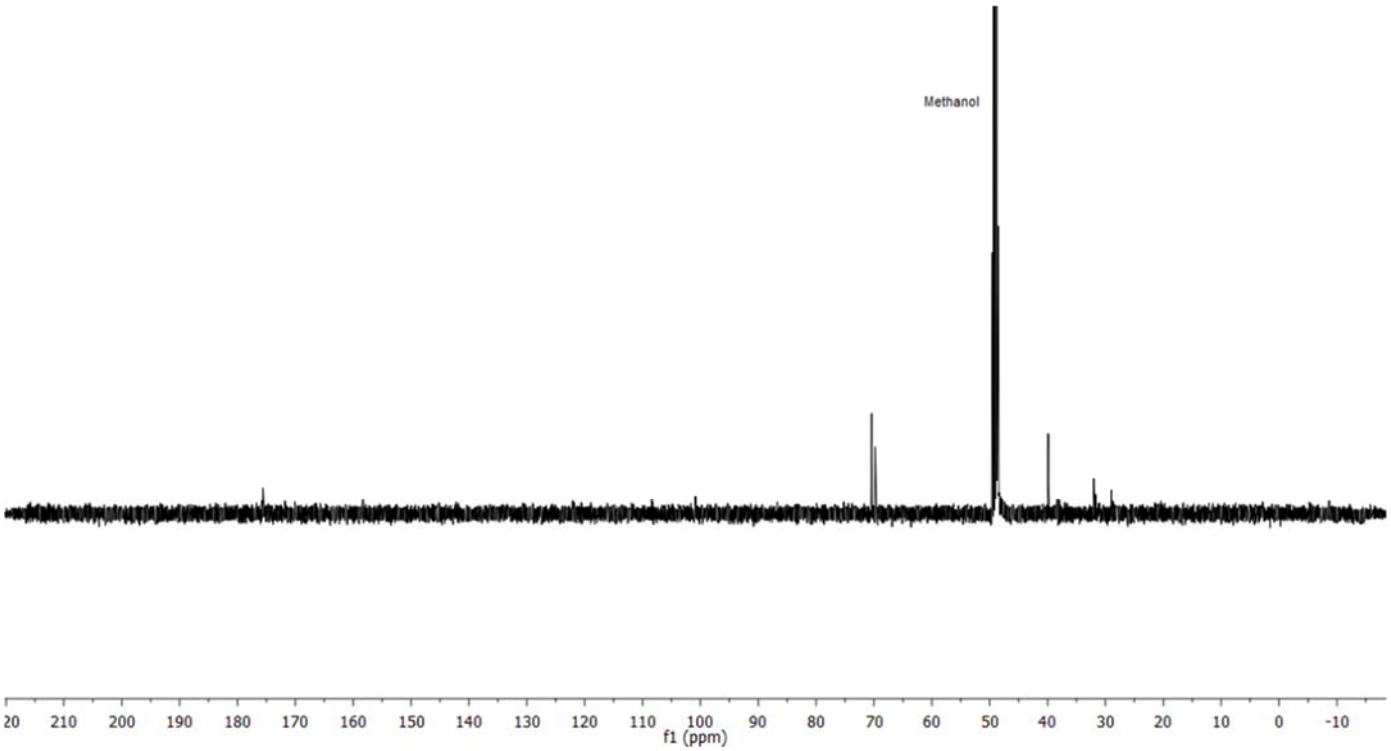

Figure S22. ^{13}C-NMR spectrum of compound **5** (126 MHz, D_2O).

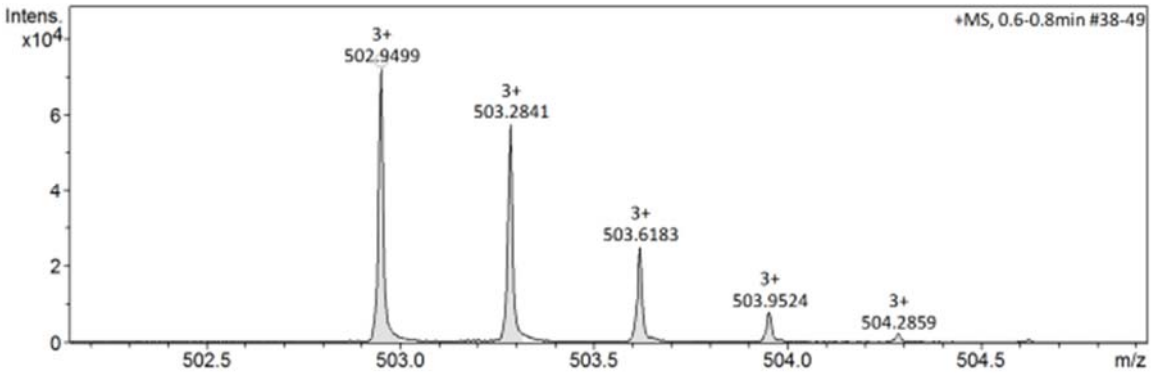

Figure S23. HR-ESI (ESI$^+$ Q-TOF) of compound **5**.

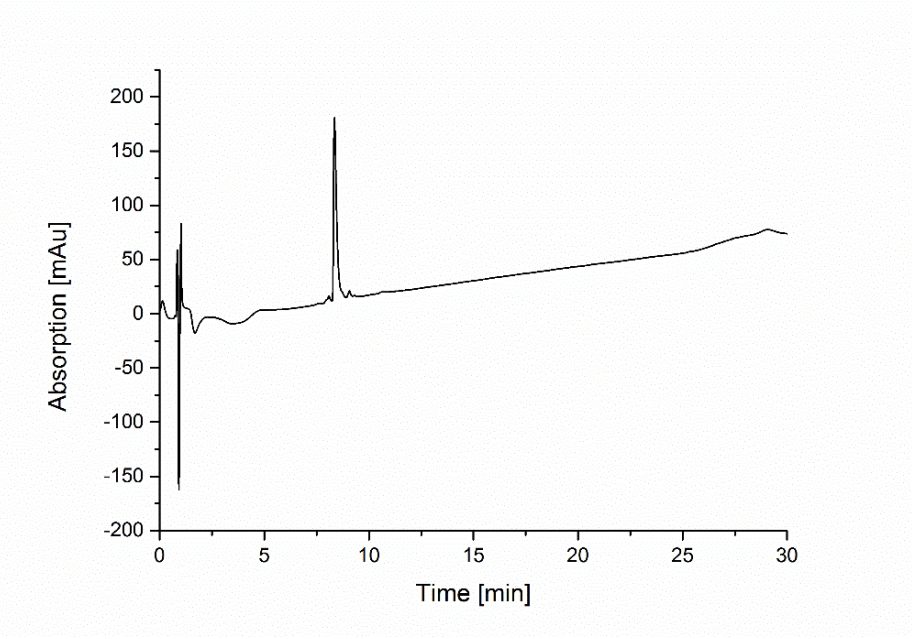

Figure S24. RP-HPLC chromatogram of compound **5** (gradient from 0% to 50% eluent B over 30 min at 25°C).

(**6**) *protected*

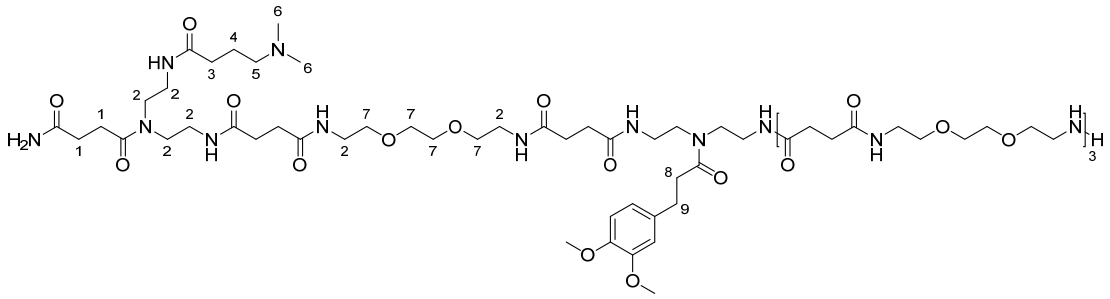

Compound **6** protected was obtained with a yield of 72% after cleavage from solid support and lyophilization.

^{1}H-NMR (500 MHz, D_2O) δ [ppm]: 6.92 (m, 2H, $H_{Aromatic}$), 6.81 (m, 1H, $H_{Aromatic}$), 3.81 (s, 3H, OCH_3), 3.79 (s, 3H, OCH_3), 3.74-3.51 (m, 32H, H-7), 3.50-3.15 (m, 32H, H-2), 3.09 (m, 2H, H-5), 2.85 (m, 8H, 6-H, 9-H), 2.64 (m, 4H, 3-H, 8-H), 2.53-2.25 (m, 24H, 1-H), 1.94 (m, 2H, 4-H).

^{13}C-NMR (126 MHz, D_2O) δ [ppm]: 178.60, 176.60, 175.81, 175.67, 175.61, 175.58, 175.50, 175.46, 175.35, 149.15, 147.73, 134.99, 130.73, 121.84, 120.71, 118.39, 116.08, 115.65, 113.76, 113.33, 113.05, 70.55, 70.39, 69.78, 67.29, 66.81, 57.95, 56.75, 56.67, 48.06, 47.95, 47.77, 45.91, 45.81, 43.62, 40.09, 39.87, 39.25, 39.07, 38.91, 38.31, 38.17, 38.00, 37.90, 35.17, 33.02, 32.90, 31.99, 31.86, 31.75, 31.62, 30.96, 28.94, 28.85, 20.99, 20.94, 15.04.

HR-ESI-MS: calculated mass for $C_{73}H_{131}N_{16}O_{24}$ $[M+3H]^{3+}$ 538.6502, found 538.6499.

RP-HPLC (gradient from 0% to 50% eluent B over 30 min at 25°C):t_r=10.6 min, purity 87%.

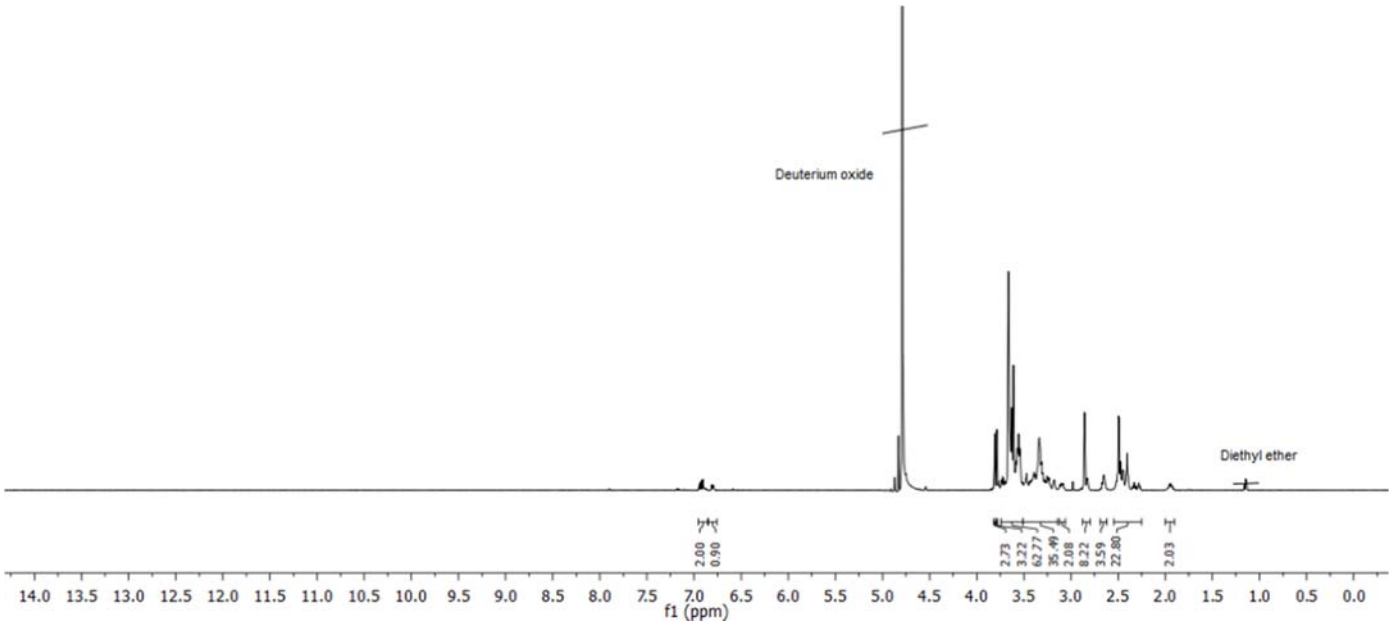

Figure S25. ^{1}H-NMR spectrum of compound **6** protected (500 MHz, D_2O).

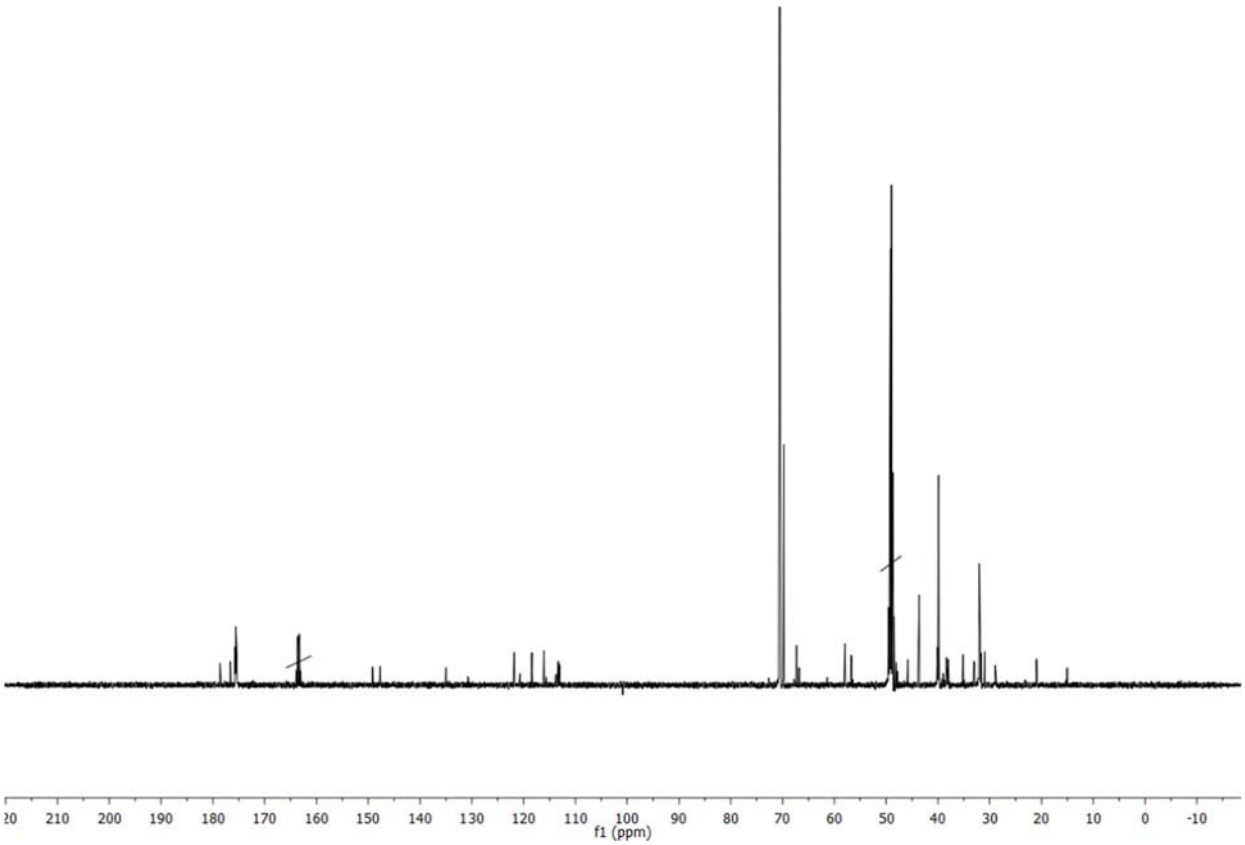

Figure S26. ^{13}C-NMR spectrum of compound **6** protected (126 MHz, D_2O).

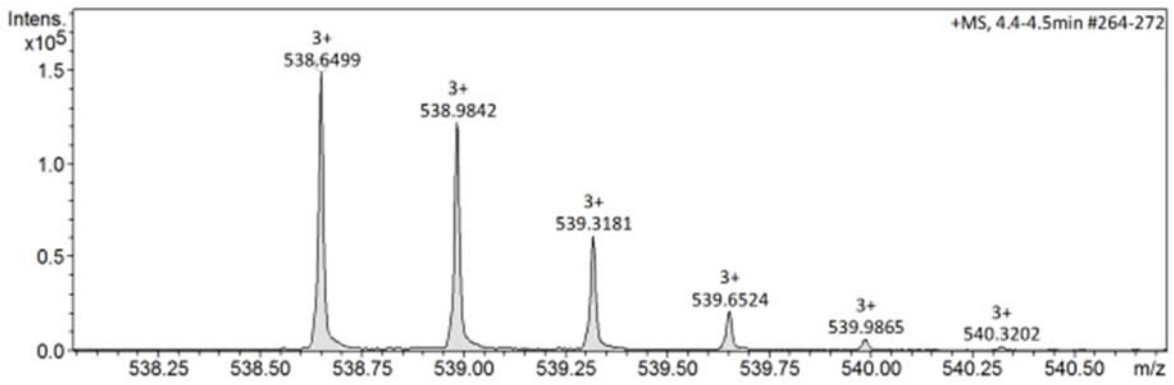

Figure S27. HR-ESI (ESI$^+$ Q-TOF) of compound **6** protected.

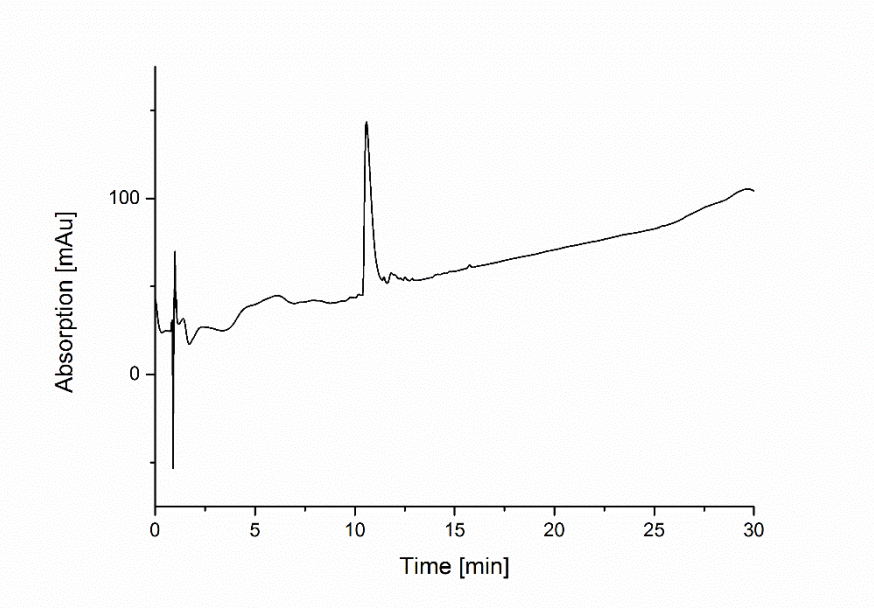

Figure S28. RP-HPLC chromatogram of compound **6** protected (gradient from 0% to 50% eluent B over 30 min at 25°C).

(**6**)

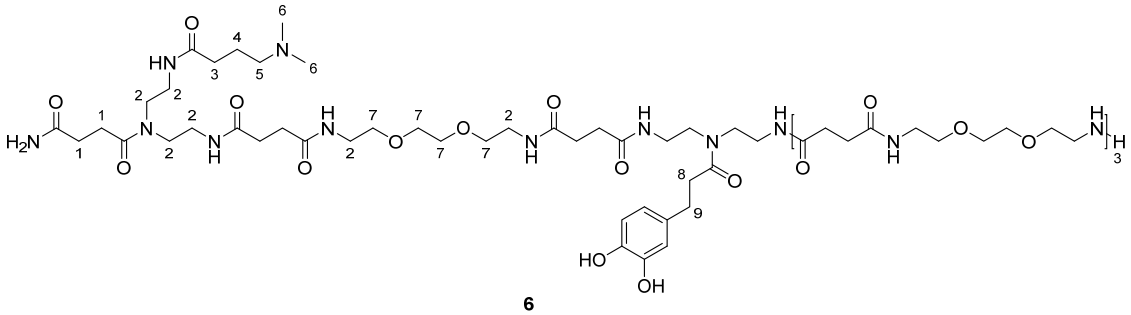

6

Compound **6** was obtained with a yield of 26% after deprotection, purification by preparative RP-HPLC and lyophilization.

^{1}H-NMR (500 MHz, D_2O) δ [ppm]: 6.84 (d, J = 8.0 Hz, 1H, $H_{Aromatic}$), 6.78 (s, 1H, $H_{Aromatic}$), 6.69 (d, J = 7.5 Hz1H, $H_{Aromatic}$), 3.77-3.55 (m, 32H, H-7), 3.53-3.20 (m, 32H, H-2), 3.12 (m, 2H, H-5), 2.88 (m,

6H, H-6,), 2.78 (t, J = 7.3 Hz, 2H, H-9), 2.68 (t, J = 6.7 Hz, 2H, H-3), 2.64 (t, J = 7.3 Hz, 2H, H-8), 2.56-2.30 (m, 24H, H-1), 1.97 (m, 2H, H-4).

^{13}C-NMR (126 MHz, D_2O) δ [ppm]: 180.71, 178.76, 177.92, 177.82, 177.77, 177.72, 177.69, 177.64, 177.62, 177.59, 177.48, 123.52, 119.08, 72.47, 72.34, 71.74, 69.30, 59.83, 50.01, 49.88, 49.68, 47.79, 47.71, 47.64, 45.58, 42.00, 41.82, 41.76, 40.18, 40.06, 39.92, 39.82, 39.80, 37.20, 34.98, 34.85, 33.93, 33.89, 33.86, 33.79, 33.73, 33.68, 33.36, 32.88, 30.90, 30.81, 23.00, 22.94.

HR-ESI-MS: calculated mass for $C_{71}H_{127}N_{16}O_{24}$ $[M+3H]^{3+}$ 529.3064, found 529.3067.

RP-HPLC (gradient from 0% to 50% eluent B over 30 min at 25°C):t_r=8.3 min, purity 97%.

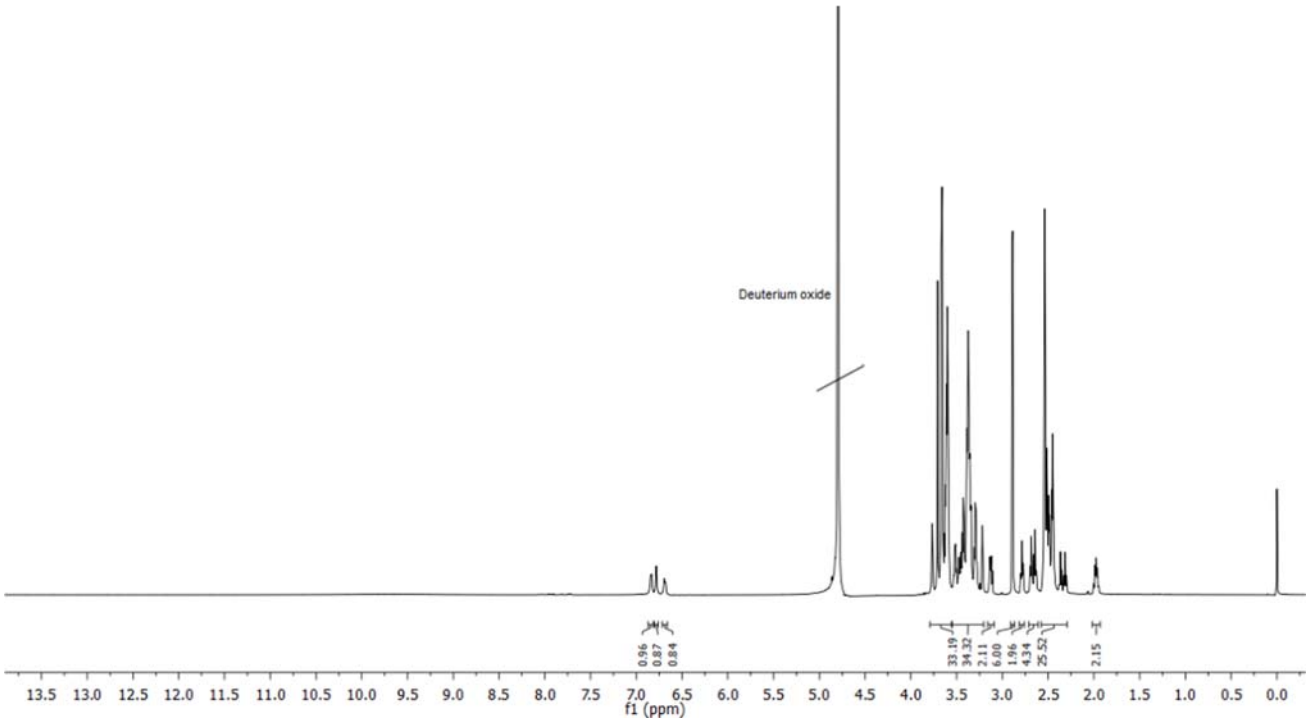

Figure S29. ^{1}H-NMR spectrum of compound **6** (600 MHz, D_2O).

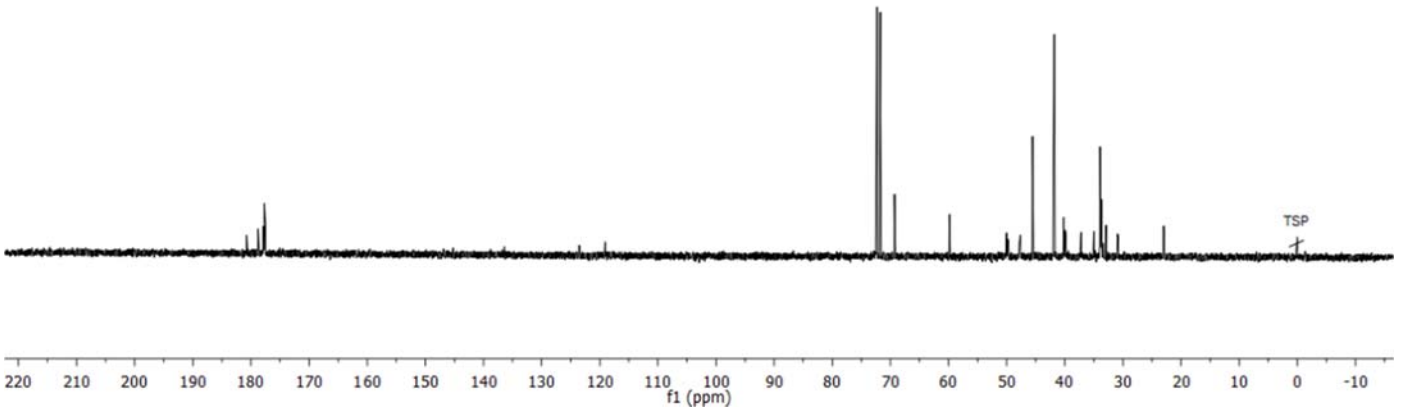

Figure S30. ^{13}C-NMR spectrum of compound **6** (126 MHz, D_2O).

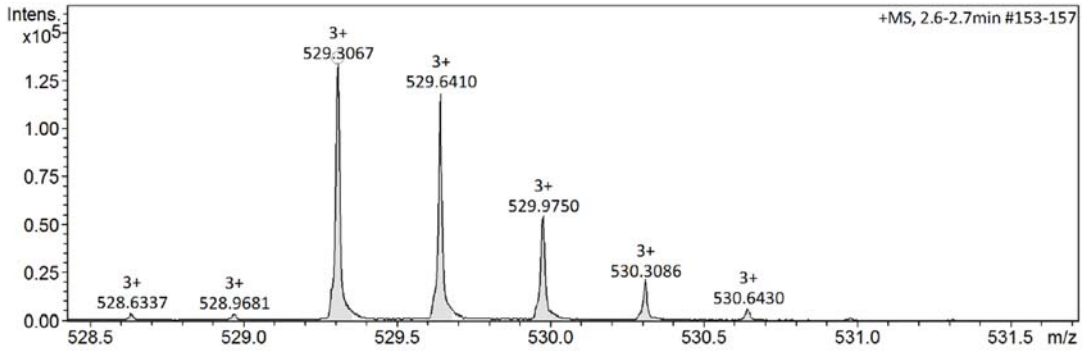

Figure S31. HR-ESI (ESI$^+$ Q-TOF) of compound **6**.

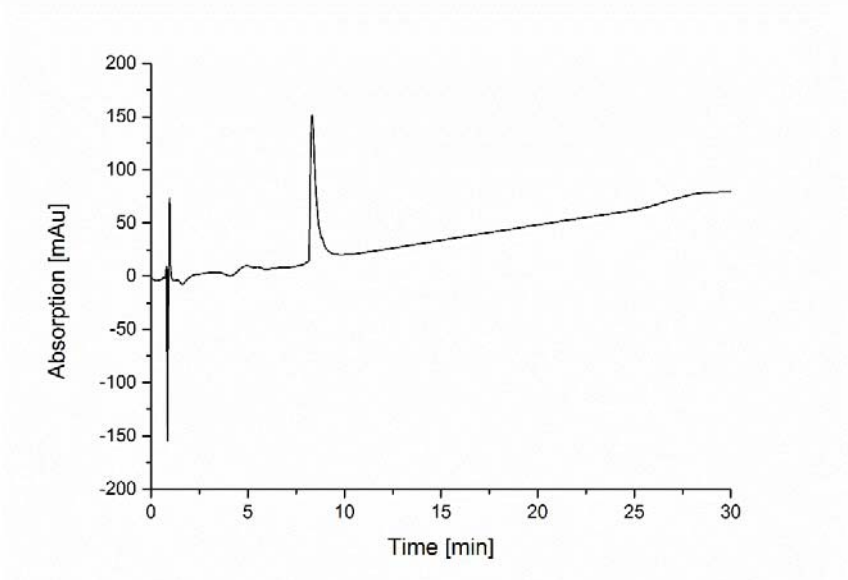

Figure S32. RP-HPLC chromatogram of compound **6** (gradient from 0% to 50% eluent B over 30 min at 25°C).

(7) *protected*

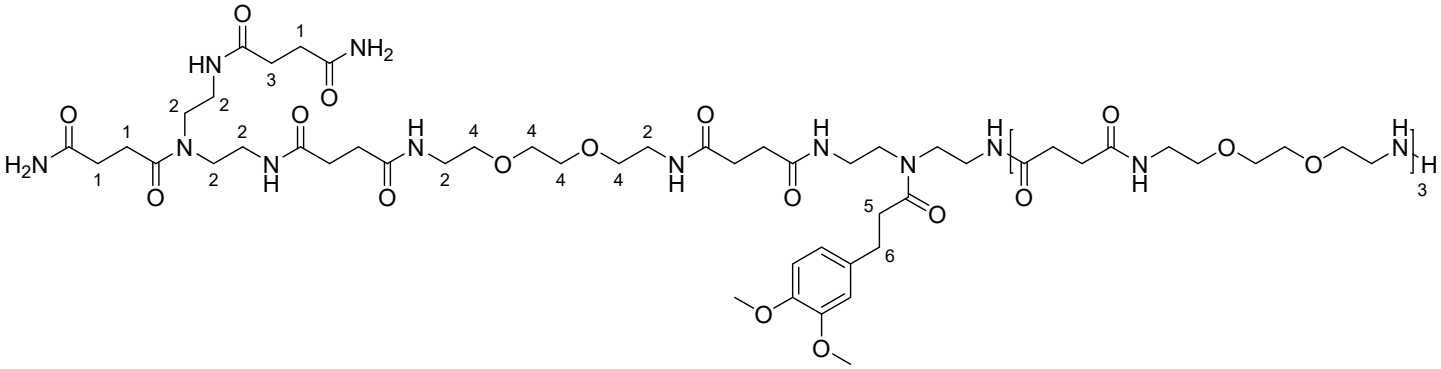

7 protected was obtained with a yield of 52% after cleavage from solid support and lyophilization.

^{1}H-NMR (500 MHz, D_2O) δ [ppm]: 8.49 (s, NH), 6.98 (d, J = 8.2 Hz, 1H, $H_{Aromatic}$), 6.95 (d, J = 2.0 Hz, 1H, $H_{Aromatic}$), 6.85 (d, J = 8.2 Hz, 2.0 Hz, 1H, $H_{Aromatic}$), 3.85 (s, 3H, OCH_3), 3.83 (s, 3H, OCH_3) 3.77-3.49 (m, 32H, H-4), 3.47-3.20 (m, 32H, H-2), 2.87 (t, J = 7.3 Hz, 2H, H-6), 2.69 (m, 4H, H-3, H-5), 2.62-2.45 (m, 26H, H-1).

^{13}C-NMR (126 MHz, D_2O) δ [ppm]: 178.64, 176.60, 175.67, 175.65, 175.59, 175.56, 175.52, 175.49, 175.45, 175.33, 171.61, 149.16, 147.75, 134.99, 121.84, 113.29, 113.00, 70.57, 70.43, 69.82, 67.33, 56.72, 56.65, 48.07, 46.06, 45.81, 40.11, 39.88, 39.82, 38.31, 38.00, 37.94, 35.21, 31.99, 31.96, 31.92, 31.86, 31.80, 31.74, 31.71, 31.66, 31.24, 31.14, 31.01, 28.93.

HR-ESI-MS: calculated mass for $C_{71}H_{125}N_{16}O_{25}$ $[M+3H]^{3+}$ 533.9662, found 533.9665.

RP-HPLC (gradient from 0% to 50% eluent B over 30 min at 25°C):t_r=10.7 min, purity 97%.

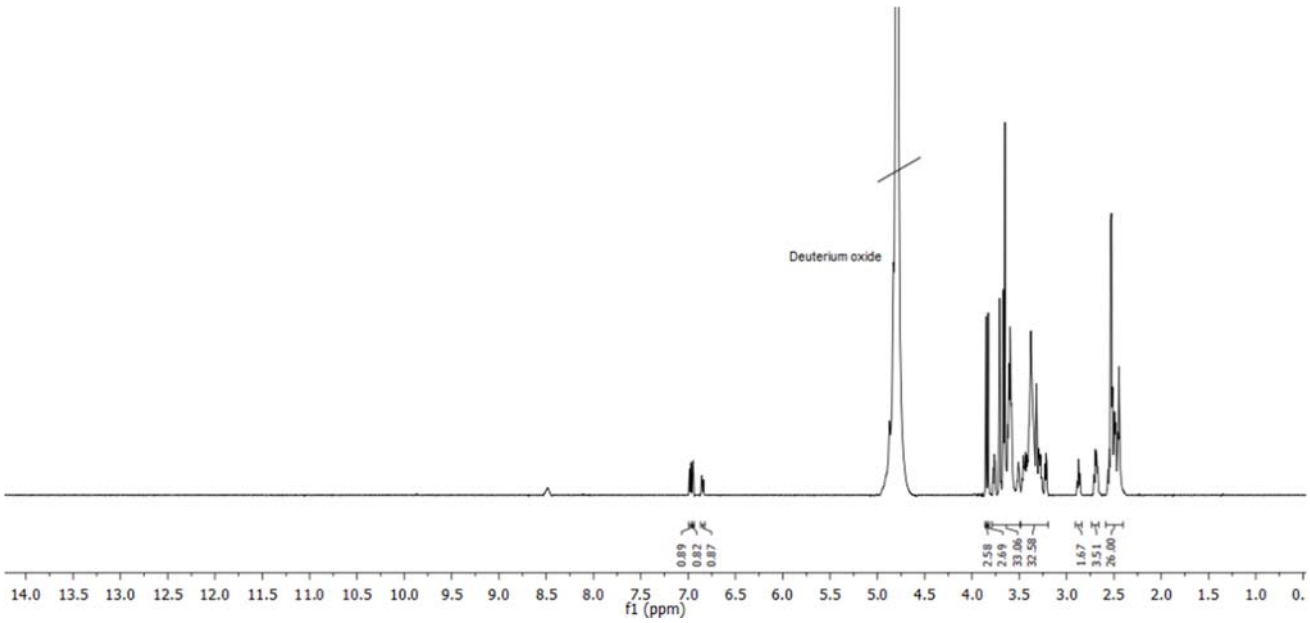

Figure S33. ^{1}H-NMR spectrum of compound **7** protected (600 MHz, D_2O).

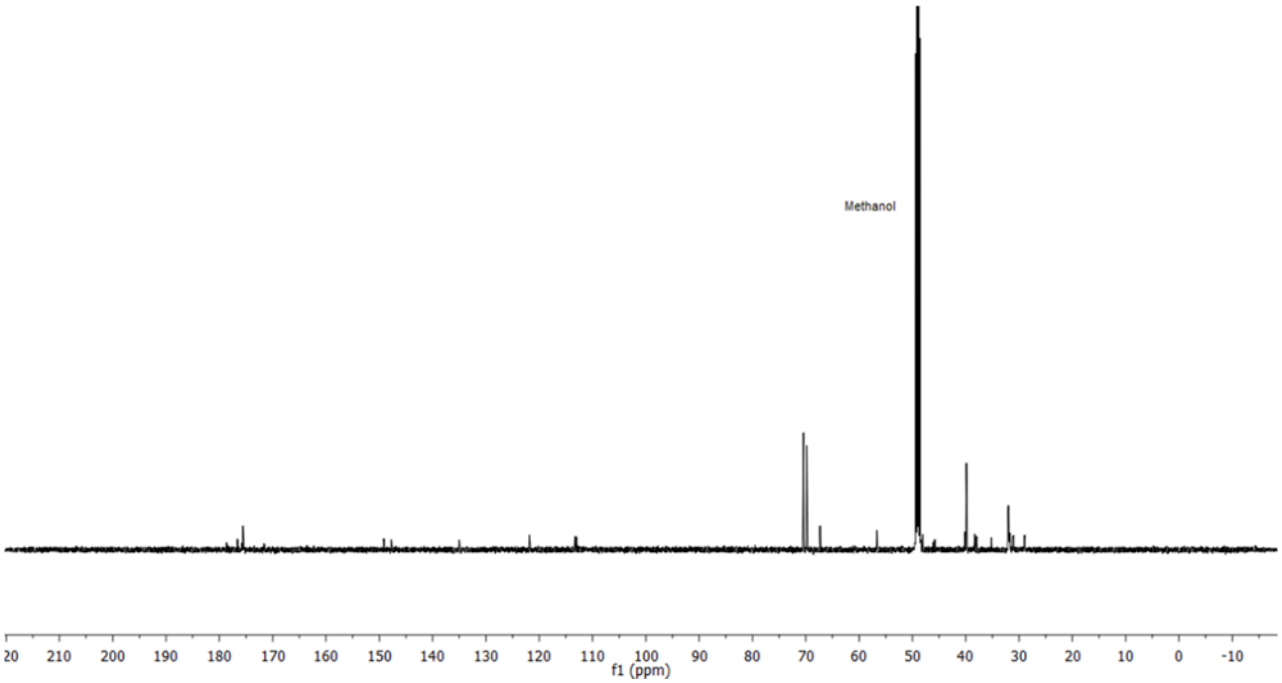

Figure S34. ^{13}C-NMR spectrum of compound **7** protected (126 MHz, D_2O).

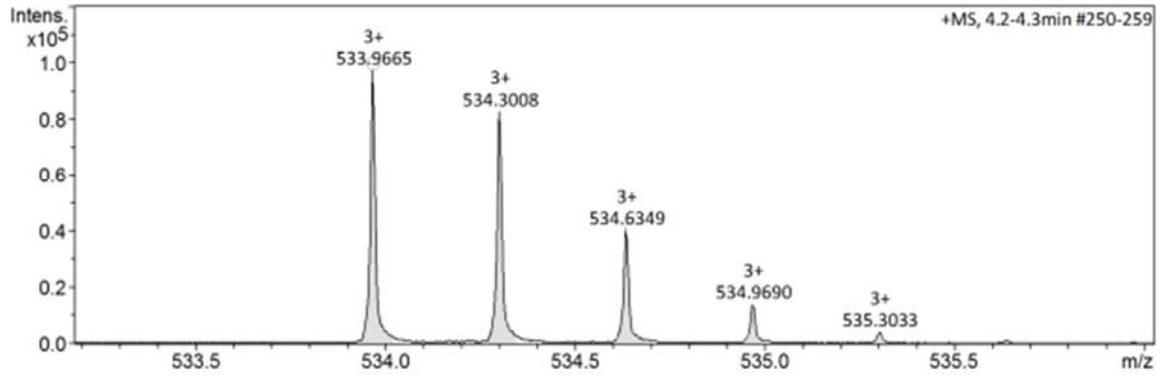

Figure S35. HR-ESI (ESI$^+$ Q-TOF) of compound **7** protected.

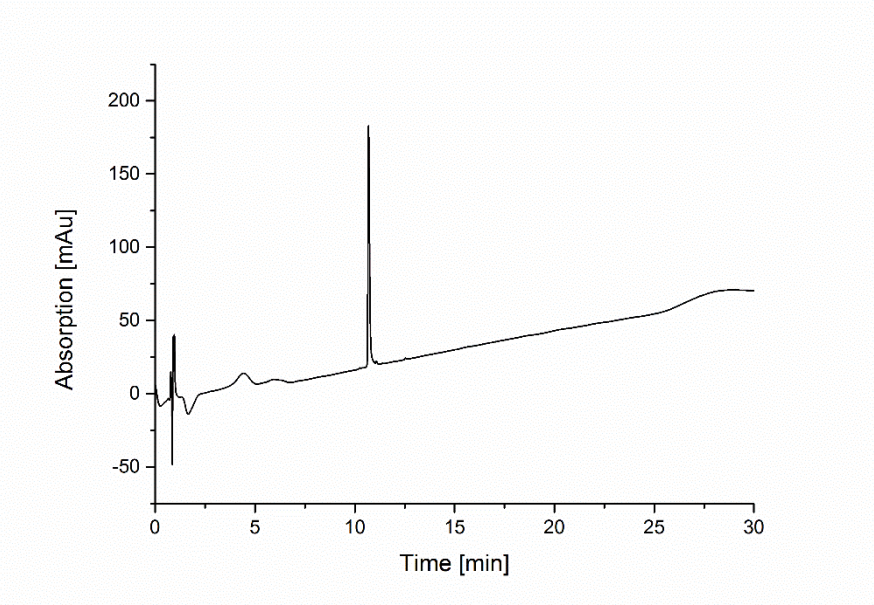

Figure S36. RP-HPLC chromatogram of compound **7** protected (gradient from 0% to 50% eluent B over 30 min at 25°C).

(**7**)

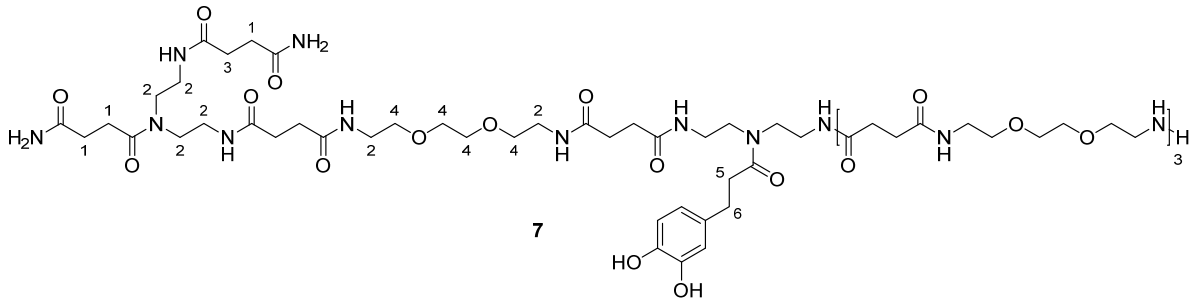

7

Compound **7** was obtained with a yield of 24% after deprotection, purification by preparative RP-HPLC and lyophilization.

^{1}H-NMR (500 MHz, D_2O) δ [ppm]: 8.45 (s, NH), 6.83 (d, J = 8.0 Hz, 1H, $H_{Aromatic}$), 6.77 (d, J = 2.1 Hz, 1H, $H_{Aromatic}$), 6.68 (dd, J = 8.0 Hz, 2.1 Hz, 1H, $H_{Aromatic}$), 3.78-3.56 (m, 32H, H-5), 3.51-3.20 (m, 32H, H-2), 2.79 (t, J = 7.0 Hz, 2H, H-4), 2.66 (m, 4H, H-3, H-6), 2.54-2.43 (m, 26H, H-1).

^{13}C-NMR (126 MHz, D_2O) δ [ppm]: 178.50, 175.91, 175.88, 175.81, 175.74, 175.66, 175.64, 171.96, 171.93, 144.91, 134.45, 117.15, 70.41, 69.81, 67.37, 39.88, 39.81, 38.25, 37.91, 35.23, 31.98, 31.94, 31.91, 31.85, 31.82, 31.76, 31.75, 31.70, 31.61, 31.60, 29.00.

HR-ESI-MS: calculated mass for $C_{69}H_{121}N_{16}O_{25}$ $[M+3H]^{3+}$ 524.6224, found 524.6221.

RP-HPLC (gradient from 0% to 50% eluent B over 30 min at 25°C):t_r=6.5 min, purity 85%.

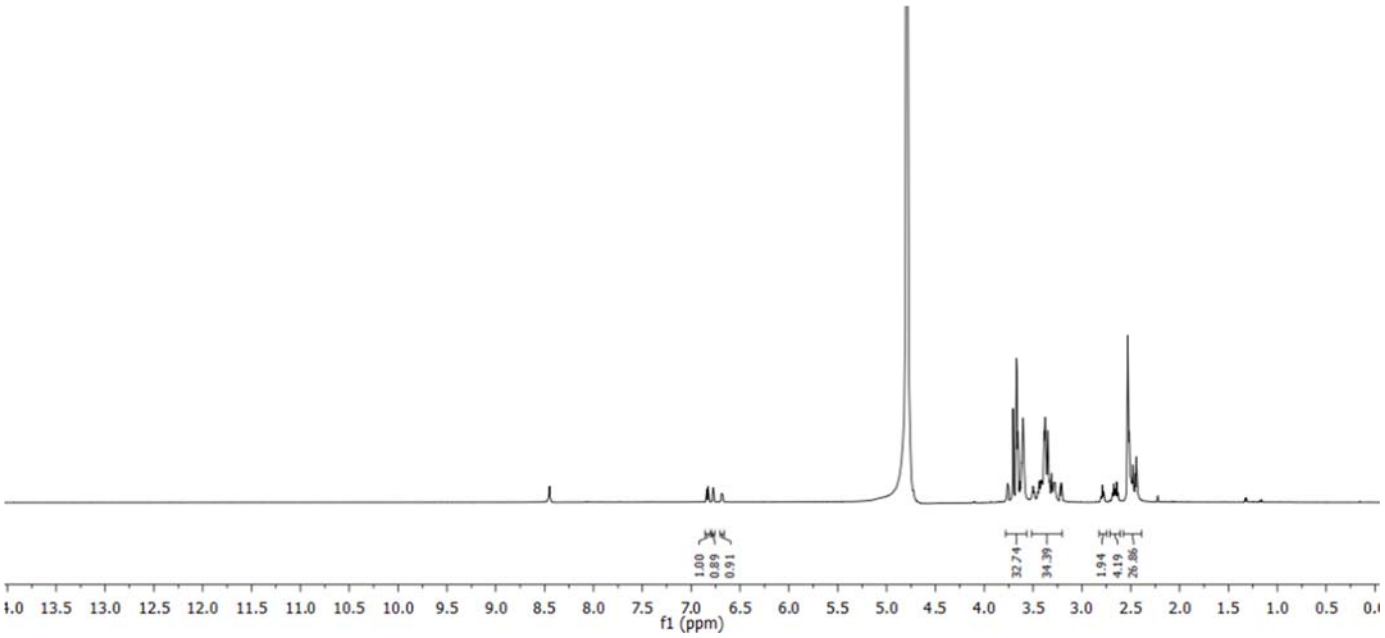

Figure S37. ^{1}H-NMR spectrum of compound **7** (600 MHz, D_2O).

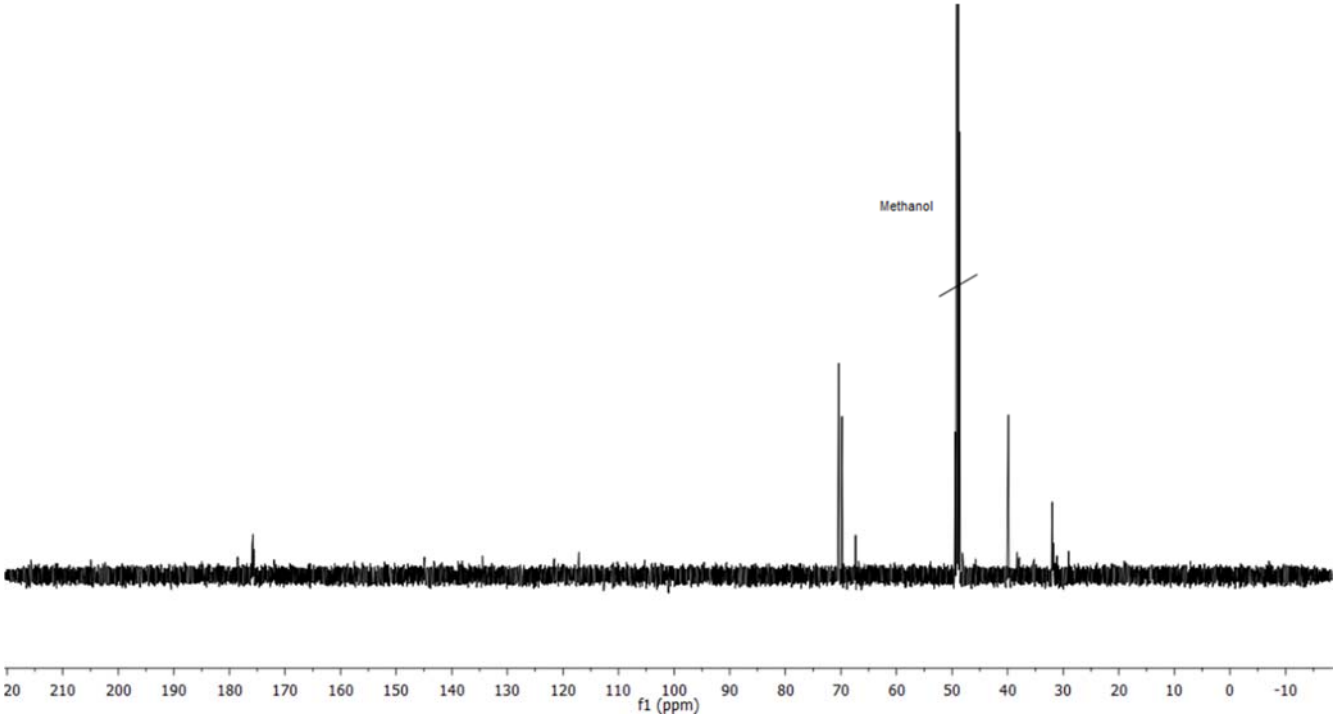

Figure S38. ^{13}C-NMR spectrum of compound **7** (126 MHz, D_2O).

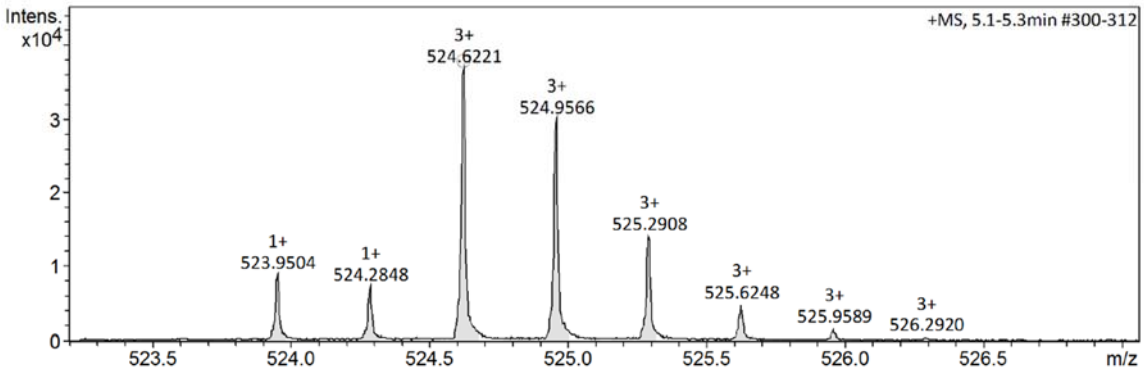

Figure S39. HR-ESI (ESI^+ Q-TOF) of compound **7**.

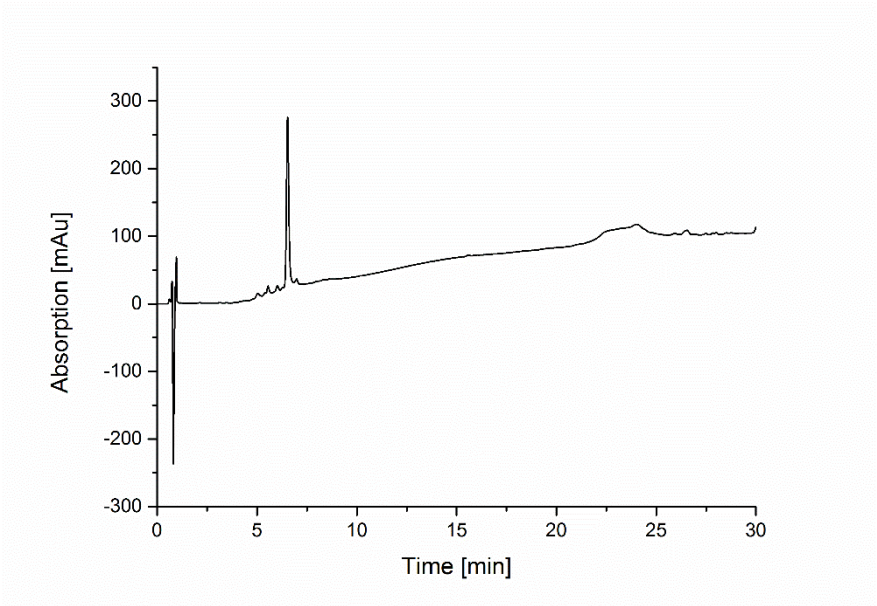

Figure S40. RP-HPLC chromatogram of compound **7** (gradient from 0% to 50% eluent B over 30 min at 25°C).

(**8**)

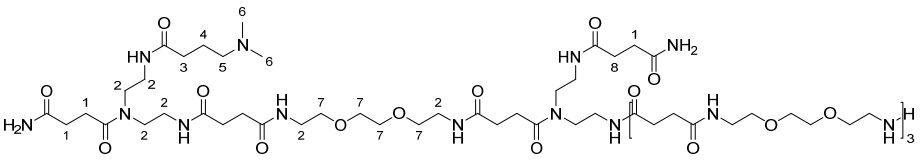

8

Compound **8** was obtained with a yield of 34% after purification by preparative RP-HPLC and lyophilization.

^{1}H-NMR (600 MHz, D_2O) δ [ppm]: 8.48 (s, NH), 3.75-3.56 (m, 32H, H-7), 3.52-3.17 (m, 32H, H-2, Methanol), 3.11 (m, 2H, H-5) 2.86 (m, 6H, H-6), 2.67 (m, 4H, H-3, H-8), 2.55-2.27 (m, 26H, H-1), 1.95 (m, 2H, H-4).

^{13}C-NMR (126 MHz, D_2O) δ [ppm]: 70.58, 70.47, 70.45, 69.89, 69.86, 69.85, 43.63, 40.11, 39.90, 31.99, 31.91, 31.88, 31.84, 31.82, 31.78, 31.63.

HR-ESI-MS: calculated mass for $C_{66}H_{124}N_{17}O_{23}$ $[M+3H]^{3+}$ 507.6347, found 507.6356.

RP-HPLC (gradient from 0% to 50% eluent B over 30 min at 25°C):t_r=1.2 min, purity 91%.

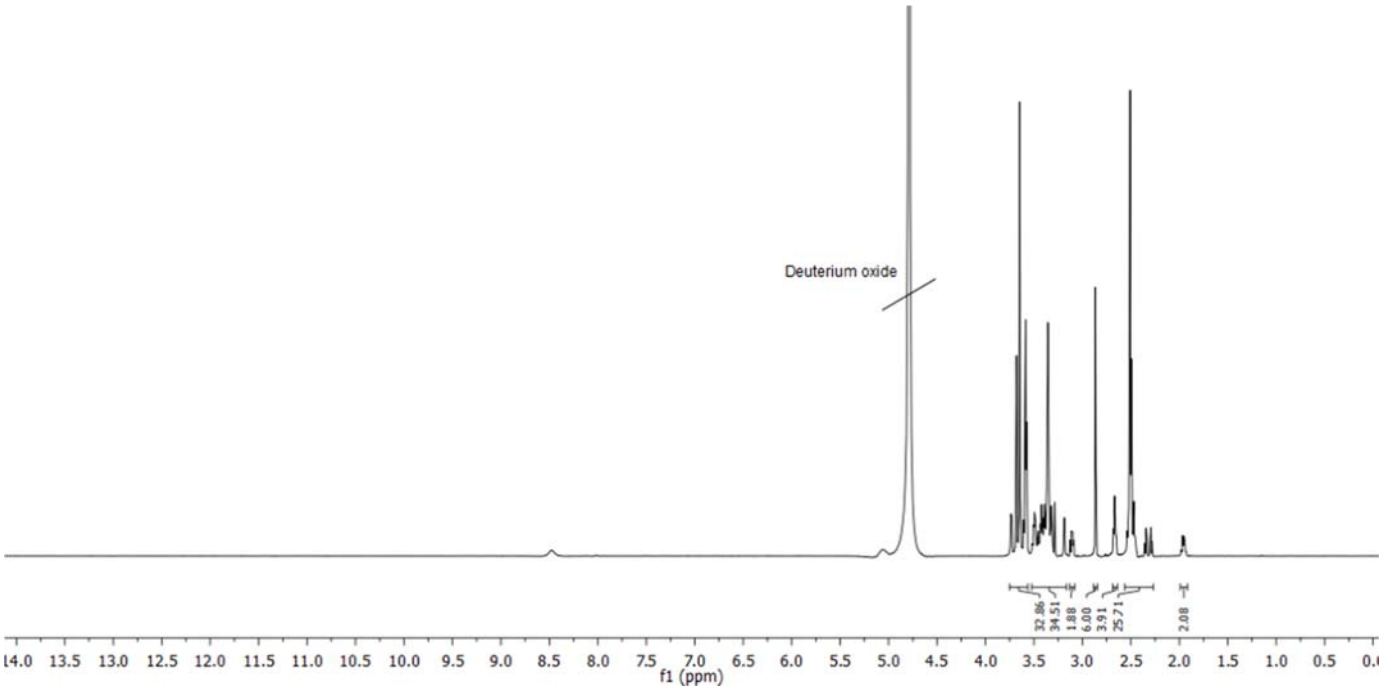

Figure S41. ^{1}H-NMR spectrum of compound **8** (500 MHz, D_2O).

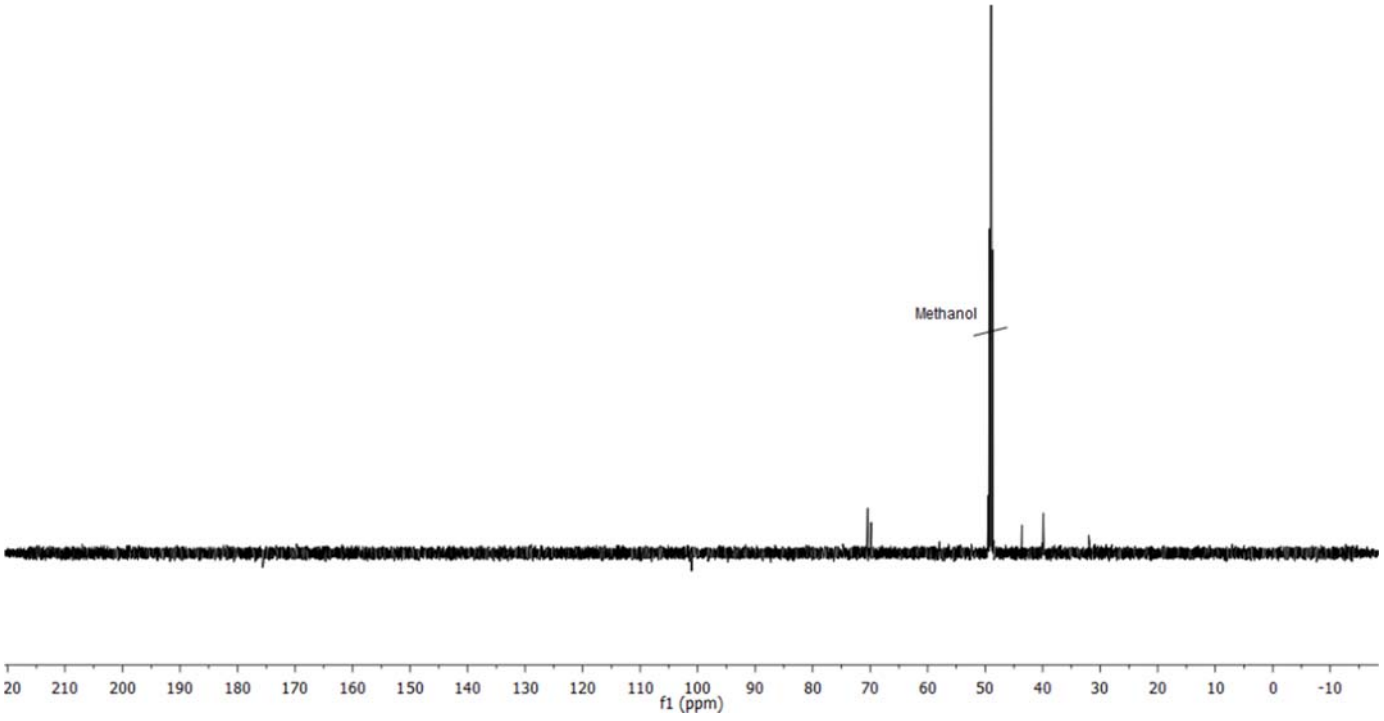

Figure S42. ^{13}C-NMR spectrum of compound **8** (126 MHz, D_2O).

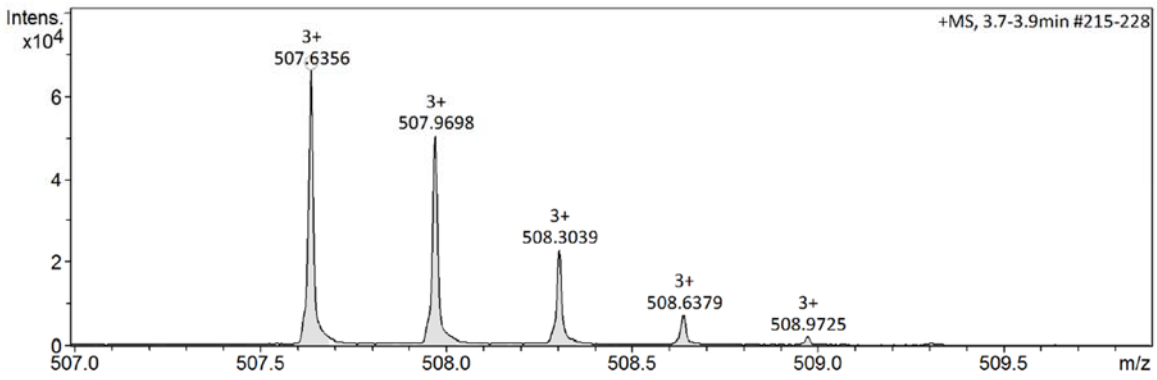

Figure S43. HR-ESI (ESI^+ Q-TOF) of compound **8**.

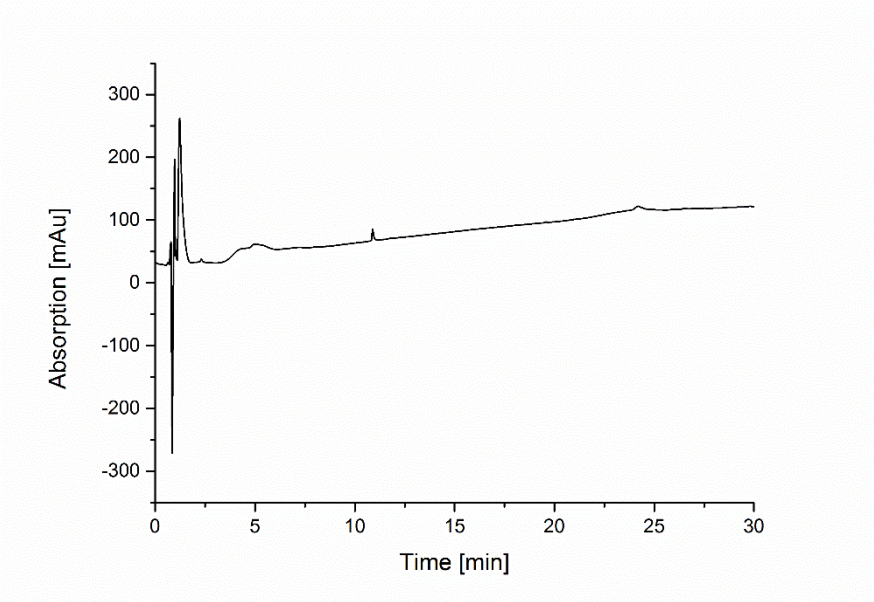

Figure S44. RP-HPLC chromatogram of compound **8** (gradient from 0% to 50% eluent B over 30 min at 25°C).

(**9**) *protected*

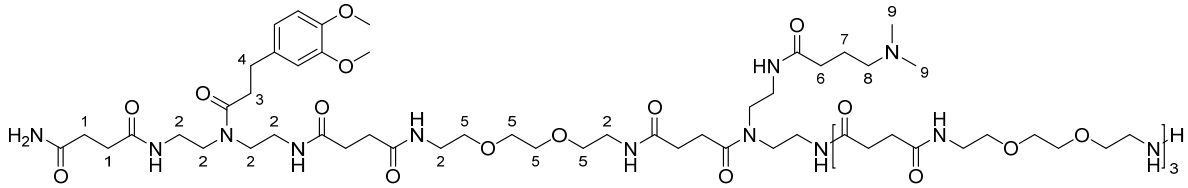

Compound **9** protected was obtained with a yield of 67% after cleavage from solid support and lyophilization.

^{1}H-NMR (500 MHz, D_2O) δ [ppm]: 8.62 (s, NH), 7.05 (d, J = 8.2 Hz, 1H, $H_{Aromatic}$), 7.02 (d, J = 1.9 Hz, 1H, $H_{Aromatic}$), 6.92 (dd, J = 8.2, 1.9 Hz, 1H, $H_{Aromatic}$), 3.91 (s, 3H, OCH_3), 3.89 (s, 3H, OCH_3), 3.85-3.64 (m, 32H, H-5), 3.60-3.26 (m, 32H, H-2), 3.19 (m, 2H, H-8), 2.95 (m, 8H, 4-H, 9-H), 2.75 (m, 4H, 6-H, 3-H), 2.62-2.35 (m, 24H, 1-H), 2.04 (m, 2H, 7-H).

^{13}C-NMR (126 MHz, D_2O) δ [ppm]: 177.88, 176.29, 175.39, 175.36, 175.28, 175.21, 175.16, 175.01, 171.29, 148.70, 147.28, 134.64, 121.50, 112.99, 112.71, 70.12, 69.98, 69.38, 66.91, 57.52, 56.39, 56.32, 47.66, 45.43, 43.24, 39.67, 39.43, 37.92, 37.60, 37.51, 34.68, 32.63, 32.52, 31.60, 31.47, 31.38, 31.20, 30.78, 30.65, 28.58, 20.60, 20.55.

HR-ESI-MS: calculated mass for $C_{73}H_{131}N_{16}O_{24}$ $[M+3H]^{3+}$ 538.6502, found 538.6503.

RP-HPLC (gradient from 0% to 50% eluent B over 30 min at 25°C): t_r=10.6 min, purity 89%.

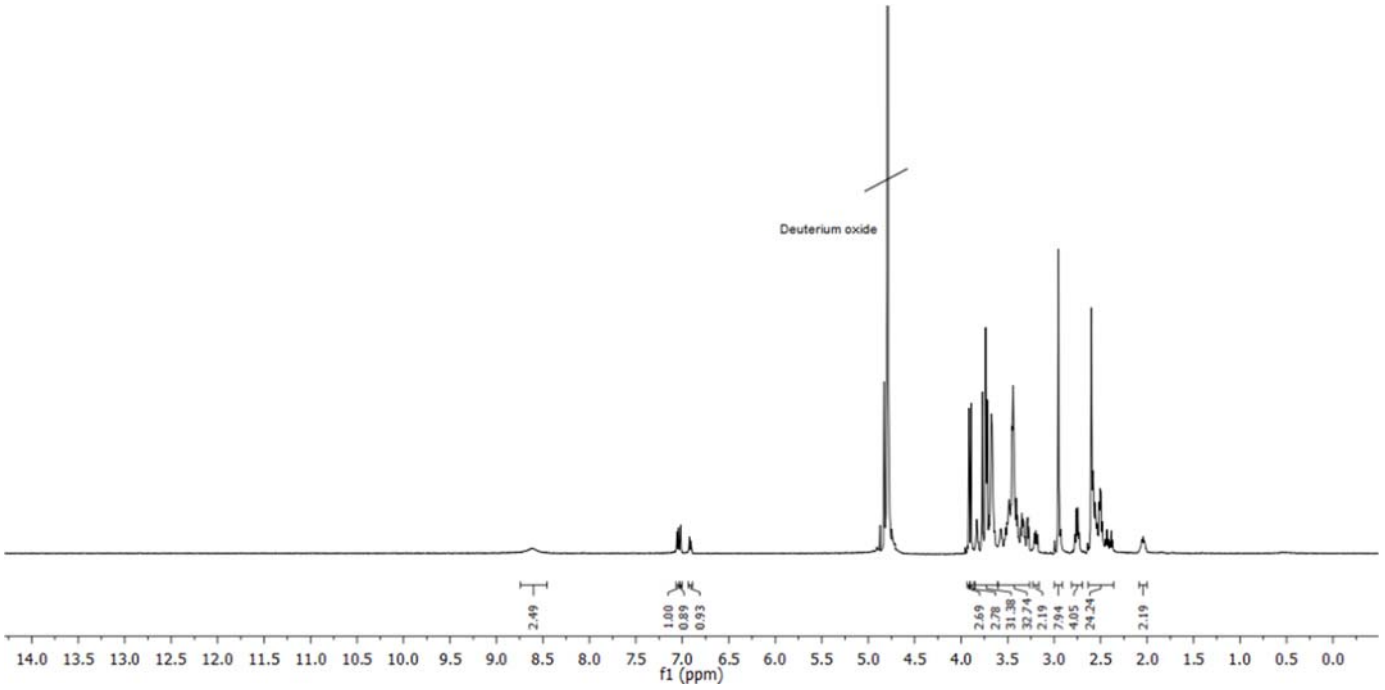

Figure S45. ^{1}H-NMR spectrum of compound **9** protected (500 MHz, D_2O).

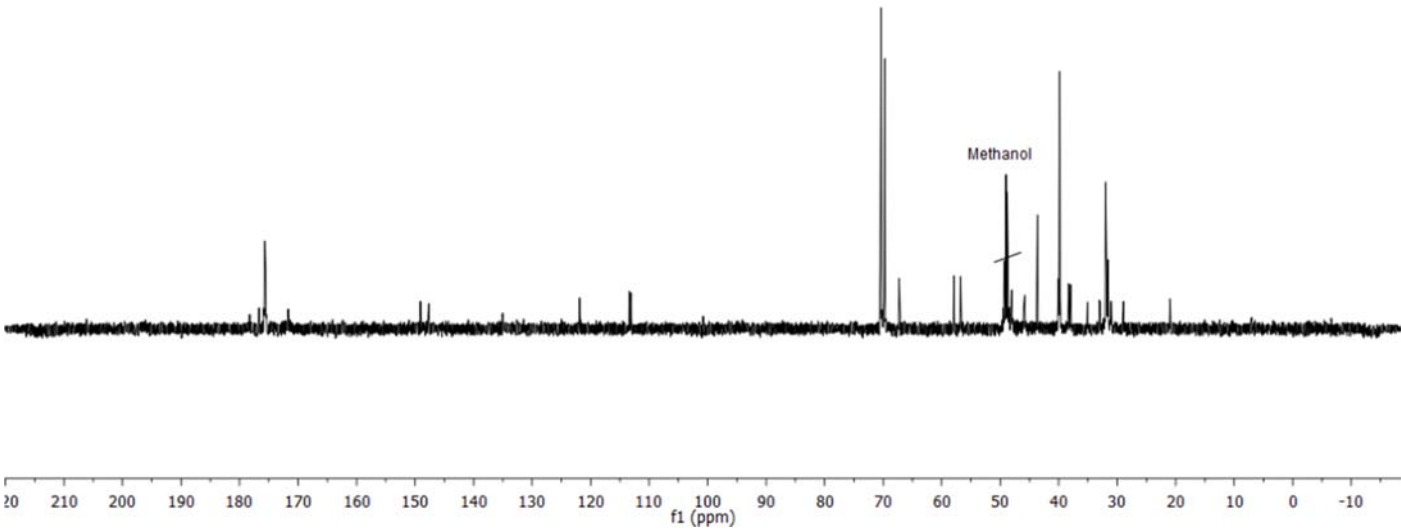

Figure S46. ^{13}C-NMR spectrum of compound **9** protected (126 MHz, D_2O).

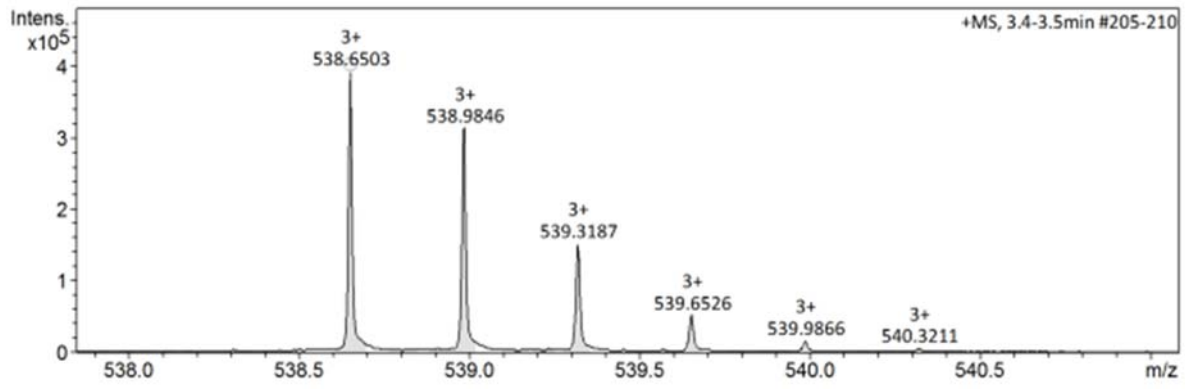

Figure S47. HR-ESI (ESI$^+$ Q-TOF) of compound **9** protected.

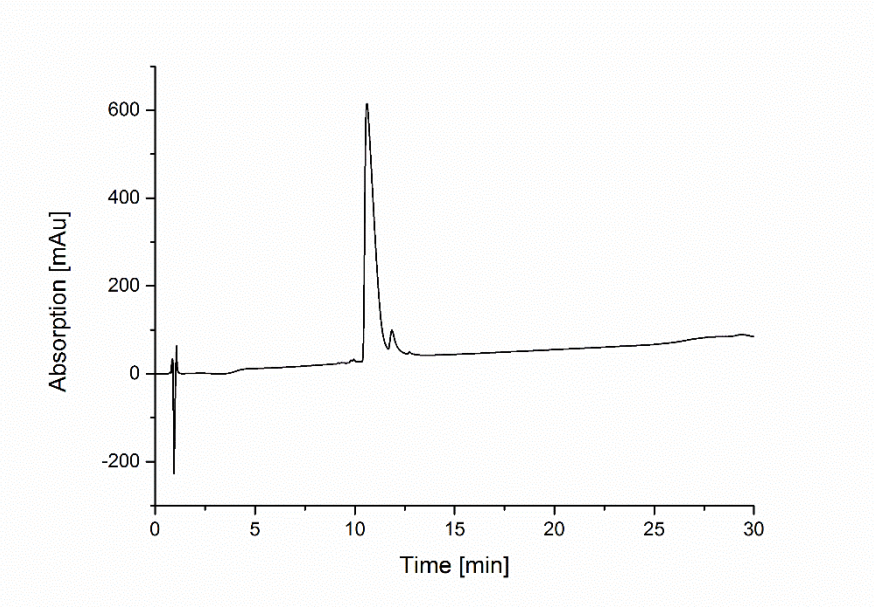

Figure S48. RP-HPLC chromatogram of compound **9** protected (gradient from 0% to 50% eluent B over 30 min at 25°C).

(**9**)

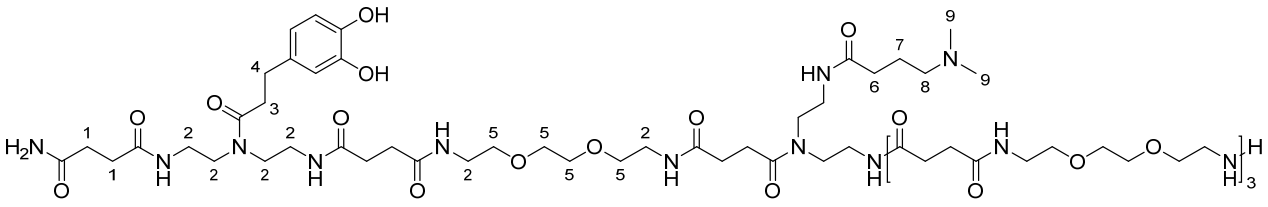

9

Compound **9** was obtained with a yield of 27% after deprotection, purification by preparative RP-HPLC and lyophilization.

^{1}H-NMR (600 MHz, D_2O) δ [ppm]: 8.44 (s, NH), 6.82 (d, J = 8.0 Hz, 1H, $H_{Aromatic}$), 6.76 (s, 1H, $H_{Aromatic}$), 6.67 (d, J = 8.0 HZ, 1H, $H_{Aromatic}$), 3.76-3.55 (m, 32H, H-5), 3.51-3.18 (m, 32H, H-2), 3.11 (t,

J = 8.1Hz, 2H, H-8), 2.87 (s, 6H, H-9), 2.77 (t, J = 7.2 Hz, 2H, H-4), 2.65 (m, 4H, H-3, H-6), 2.55-2.28 (m, 24H, H-1), 1.97 (m, 2H, H-7).

^{13}C-NMR (126 MHz, D_2O) δ [ppm]: 175.76, 175.71, 175.64, 175.54, 171.78, 121.52, 117.10, 70.53, 70.39, 69.79, 67.32, 57.93, 46.02, 45.84, 40.08, 39.86, 39.80, 38.02, 37.94, 37.91, 35.20, 33.04, 32.92, 31.99, 31.95, 31.92, 31.86, 31.78, 31.63, 31.40, 31.08, 29.02, 28.97.

HR-ESI-MS: calculated mass for $C_{71}H_{127}N_{16}O_{24}$ $[M+3H]^{3+}$ 529.3064, found 529.3056.

RP-HPLC (gradient from 0% to 50% eluent B over 30 min at 25°C): t_r=6.3 min, purity 97%.

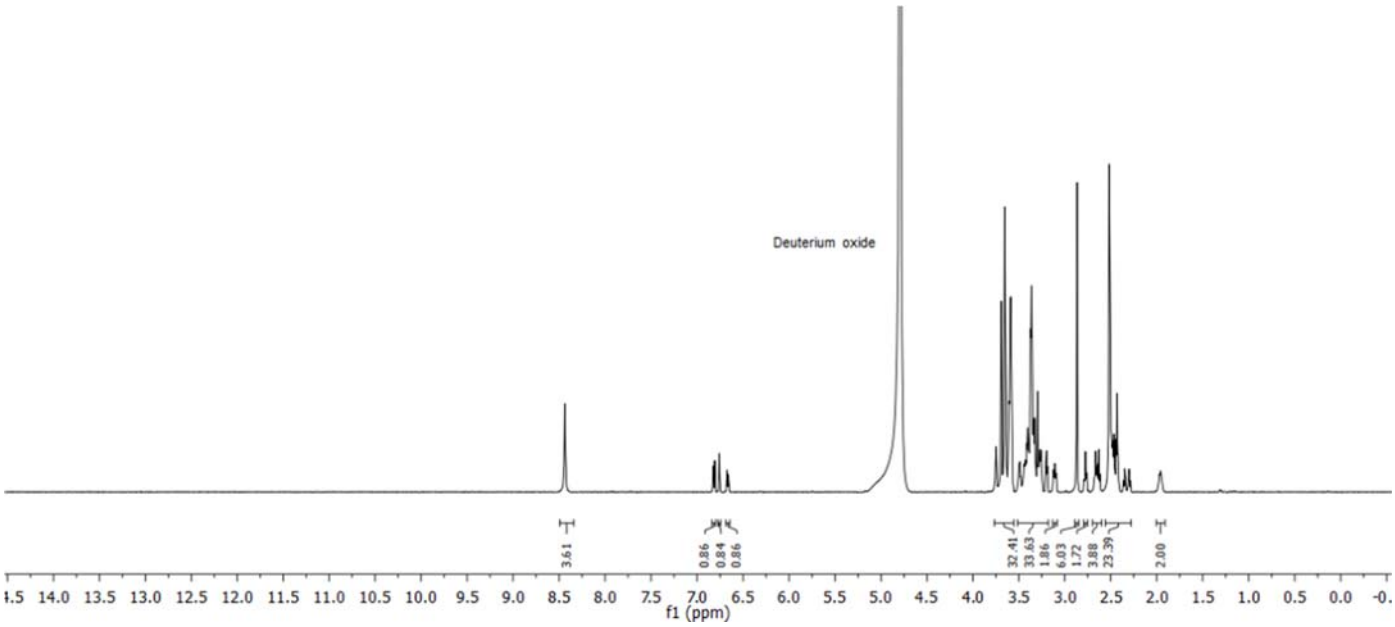

Figure S49. ^{1}H-NMR spectrum of compound **9** (500 MHz, D_2O).

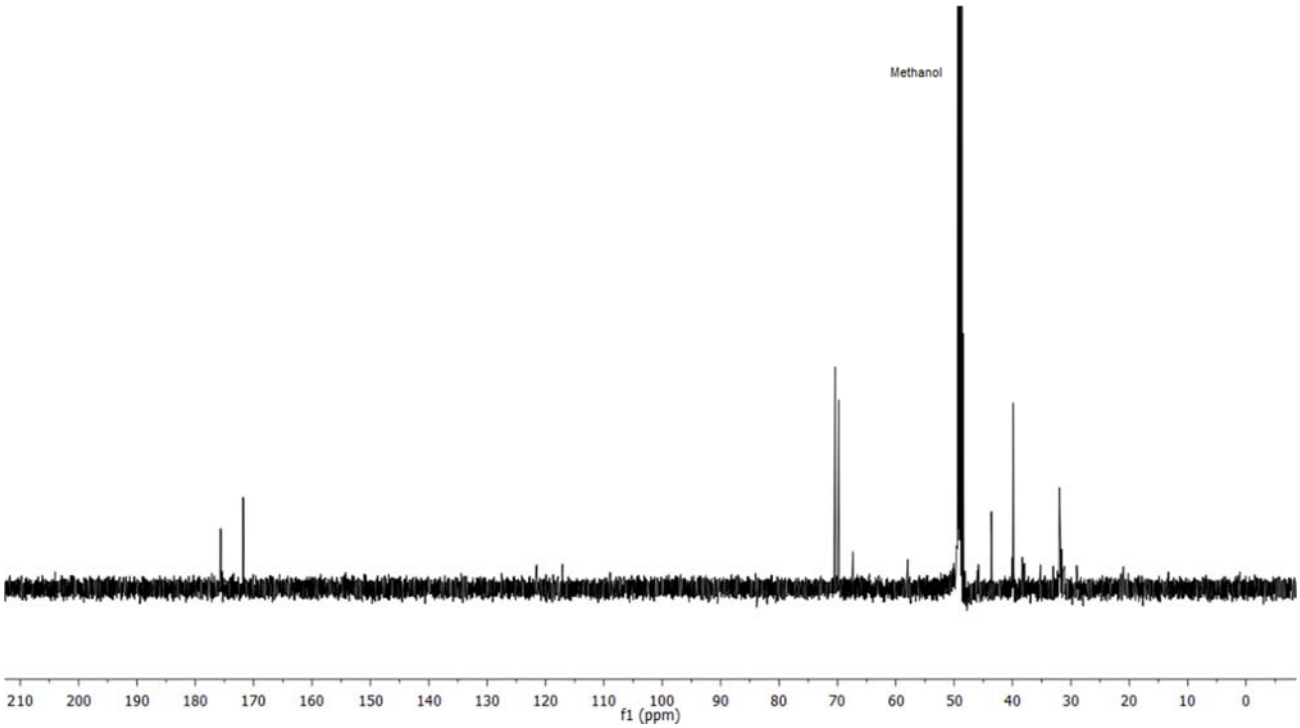

Figure S50. ^{13}C-NMR spectrum of compound **9** (126 MHz, D_2O).

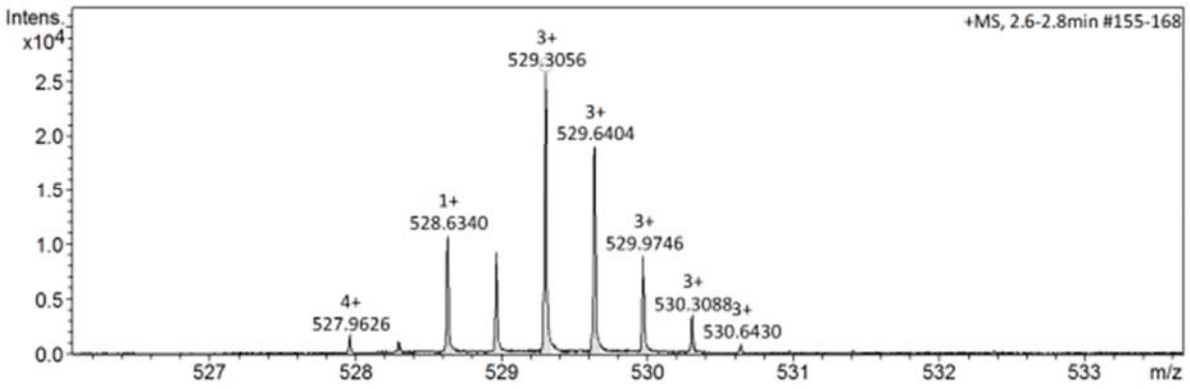

Figure S51. HR-ESI (ESI$^+$ Q-TOF) of compound **9**.

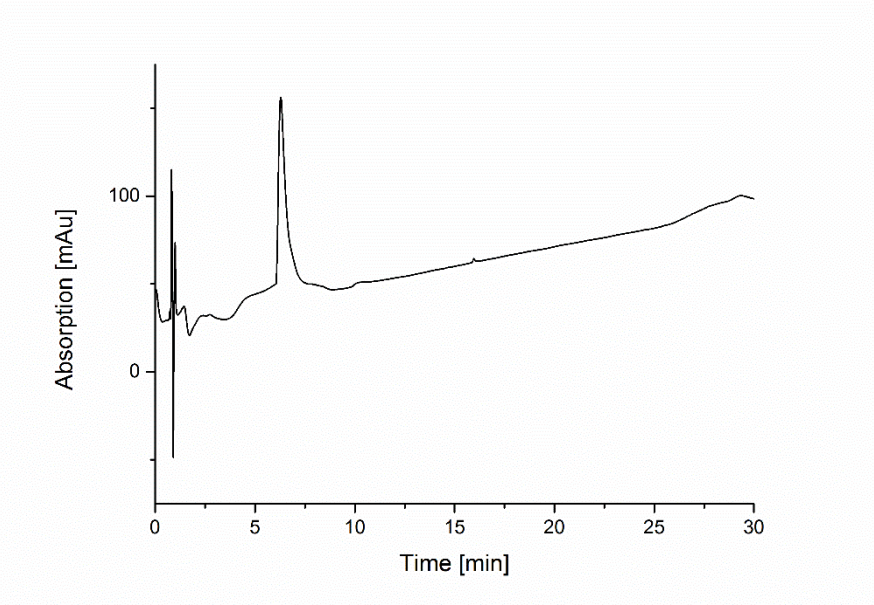

Figure S52. RP-HPLC chromatogram of compound **9** (gradient from 0% to 50% eluent B over 30 min at 25°C).

(**10**) *protected*

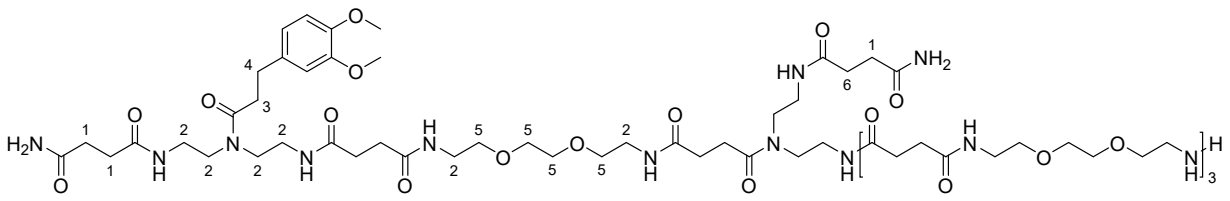

10

Compound **10** protected was obtained with a yield of 61% after cleavage from solid support and lyophilization.

^{1}H-NMR (500 MHz, D_2O) δ [ppm]: 8.45 (s, NH), 7.04 (d, J = 8.2 Hz, 1H, $H_{Aromatic}$), 7.01 (m, 1H, $H_{Aromatic}$), 6.91 (m, 1H, $H_{Aromatic}$), 3.91 (s, 3H, OCH_3), 3.89 (s, 3H, OCH_3), 3.84-3.62 (m, 32H, H-5), 3.58-3.25 (m, 32H, H-2), 2.94 (t, J = 7.2 Hz, 2H, H-4), 2.74 (m, 4H, H-3, H-6), 2.64-2.43 (m, 26H, H-1).

^{13}C-NMR (126 MHz, D_2O) δ [ppm]: 178.00, 177.88, 176.30, 175.43, 175.36, 175.29, 175.25, 175.21, 175.17, 175.03, 148.69, 147.27, 134.63, 121.49, 112.97, 112.69, 70.12, 69.97, 69.40, 69.37, 66.91, 56.38, 56.31, 47.73, 45.75, 45.43, 39.67, 39.46, 39.39, 37.92, 37.59, 37.52, 34.73, 34.68, 31.60, 31.53, 31.50, 31.47, 31.43, 31.39, 31.34, 31.30, 31.24, 31.19, 30.82, 30.78, 30.73, 30.65, 28.60.

HR-ESI-MS: calculated mass for $C_{71}H_{125}N_{16}O_{25}$ $[M+3H]^{3+}$ 533.9662, found 533.9661.

RP-HPLC (gradient from 0% to 50% eluent B over 30 min at 25°C): t_r=11.8 min, purity 98%.

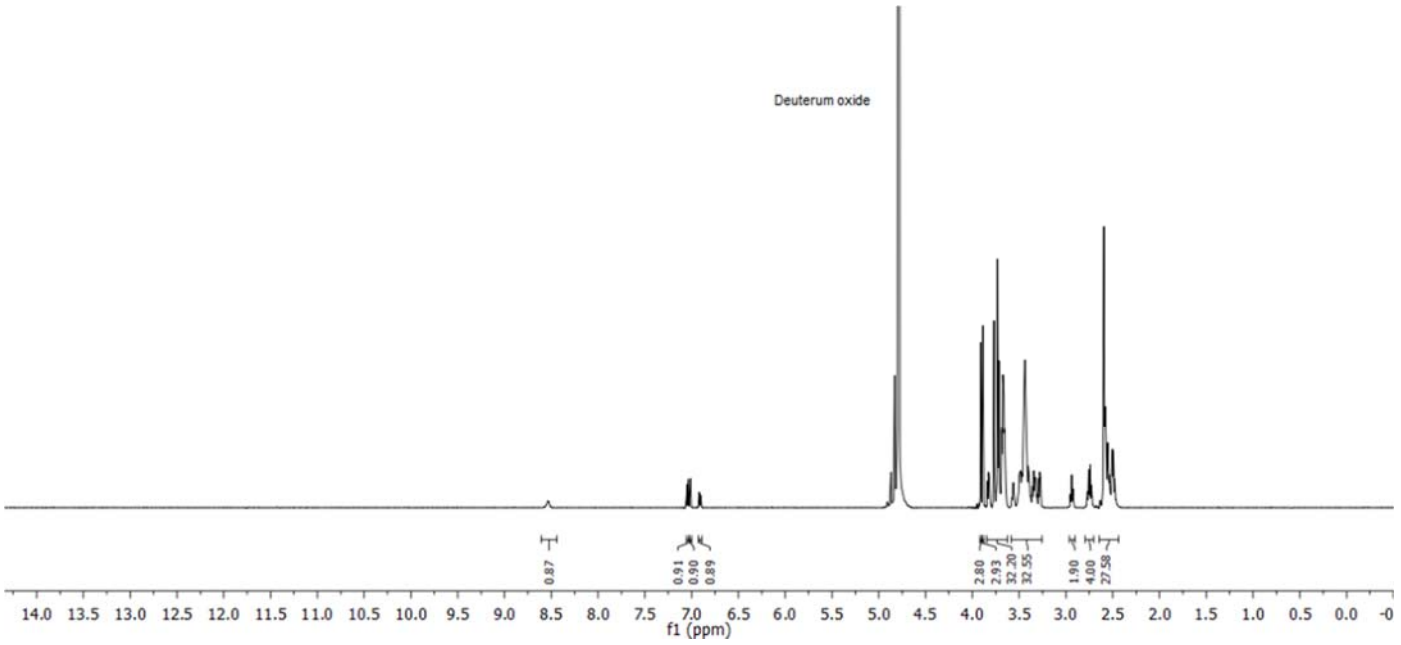

Figure S53. ^{1}H-NMR spectrum of compound **10** protected (500 MHz, D_2O).

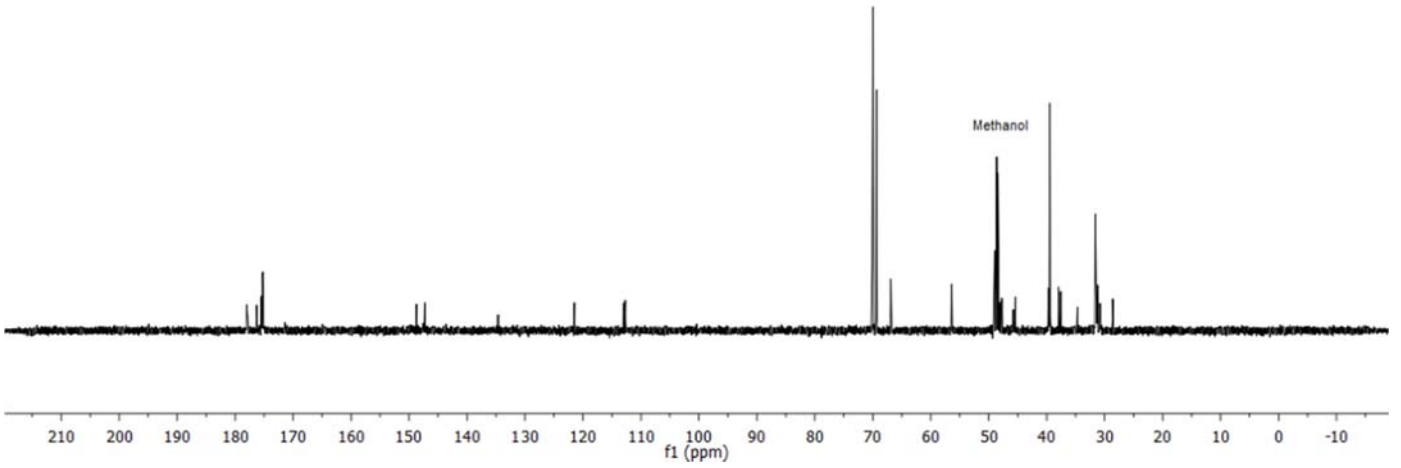

Figure S54. ^{13}C-NMR spectrum of compound **10** protected (126 MHz, D_2O).

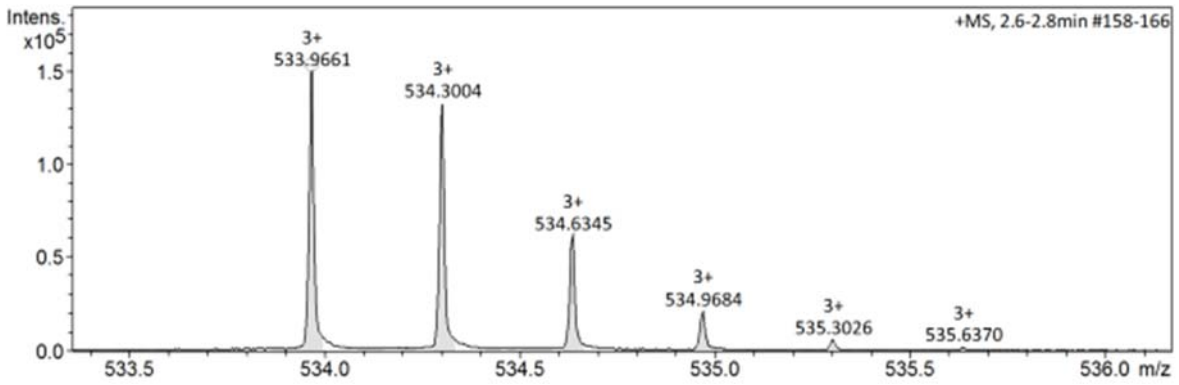

Figure S55. HR-ESI (ESI$^+$ Q-TOF) of compound **10** protected.

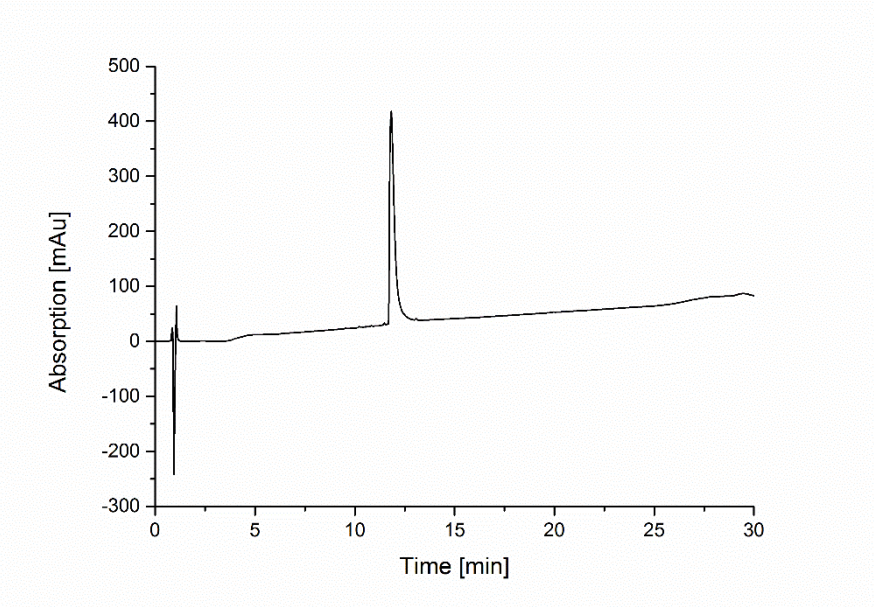

Figure S56. RP-HPLC chromatogram of compound **10** protected (gradient from 0% to 50% eluent B over 30 min at 25°C).

(**10**)

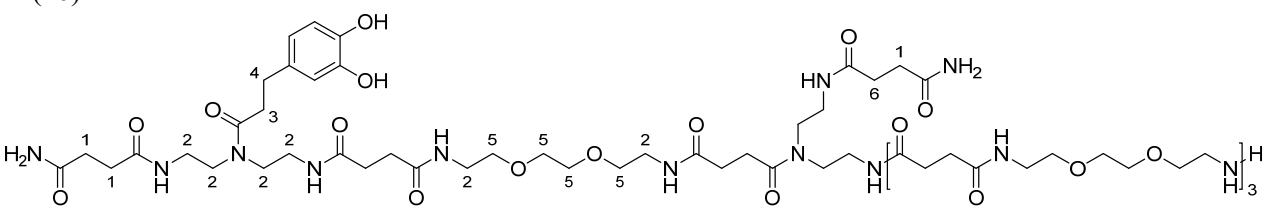

10

Compound **10** was obtained with a yield of 19% after deprotection, purification by preparative RP-HPLC and lyophilization.

^{1}H-NMR (500 MHz, D_2O) δ [ppm]: 8.5 (s, NH), 6.88 (d, J = 8.1 Hz, 1H, $H_{Aromatic}$), 7.82 (d, J = 2.0 Hz, 1H, $H_{Aromatic}$), 6.73 (d, J = 8.1 Hz, 2.0 Hz, 1H, $H_{Aromatic}$), 3.82-3.59 (m, 32H, H-5), 3.57-3.25 (m, 32H, H-2), 2.83 (t, J = 7.1 Hz, 2H, H-4), 2.70 (m, 4H, H-3, H-6), 2.62-2.45 (m, 26H, H-1).

^{13}C-NMR (126 MHz, D_2O) δ [ppm]: 178.01, 177.97, 176.35, 176.33, 175.41, 175.36, 175.32, 175.24, 175.21, 175.15, 144.46, 142.84, 134.05, 121.12, 116.73, 116.68, 70.10, 69.96, 69.38, 69.35, 66.88, 47.70, 45.39, 39.64, 39.43, 39.37, 37.91, 37.88, 37.58, 37.50, 34.76, 34.75, 31.61, 31.57, 31.53, 31.50, 31.45, 31.38, 31.28, 31.22, 30.93, 30.80, 30.75, 30.71, 30.66, 28.58.

HR-ESI-MS: calculated mass for $C_{69}H_{121}N_{16}O_{25}$ $[M+3H]^{3+}$ 524.6224, found 524.6222.

RP-HPLC (gradient from 0% to 50% eluent B over 30 min at 25°C): t_r=9.8 min, purity 89%.

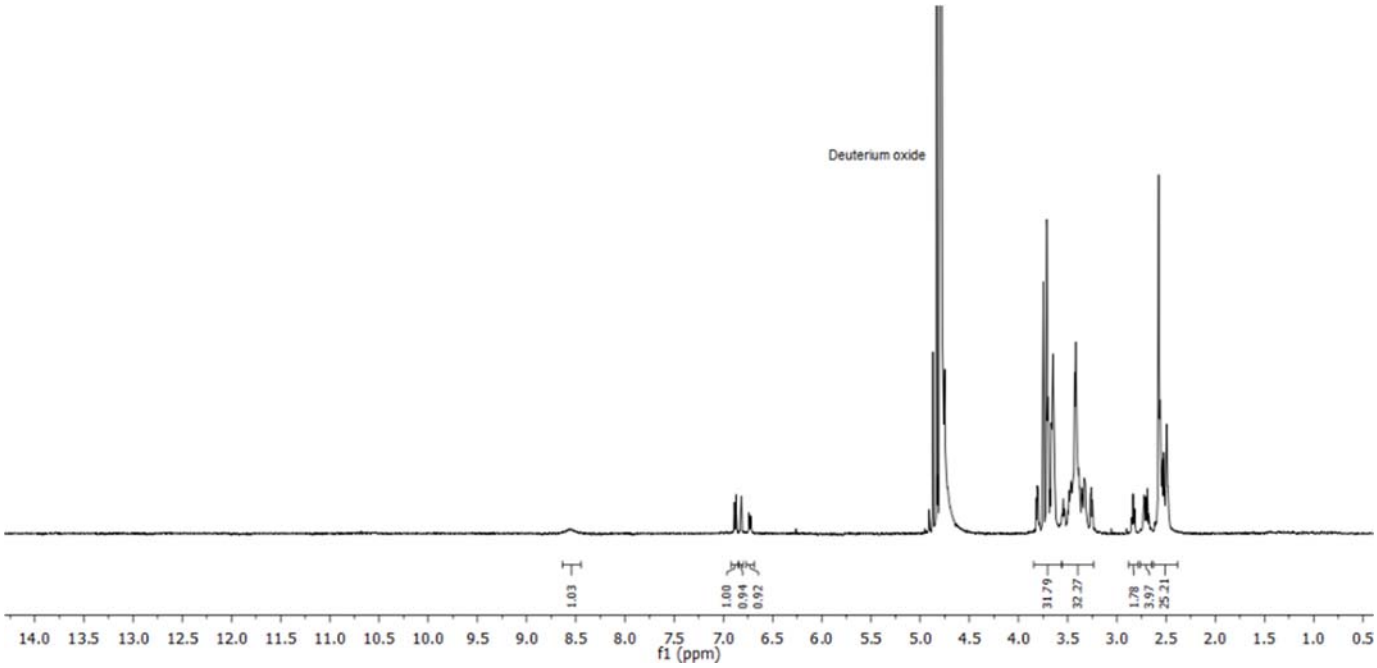

Figure S57. ^{1}H-NMR spectrum of compound **10** (500 MHz, D_2O).

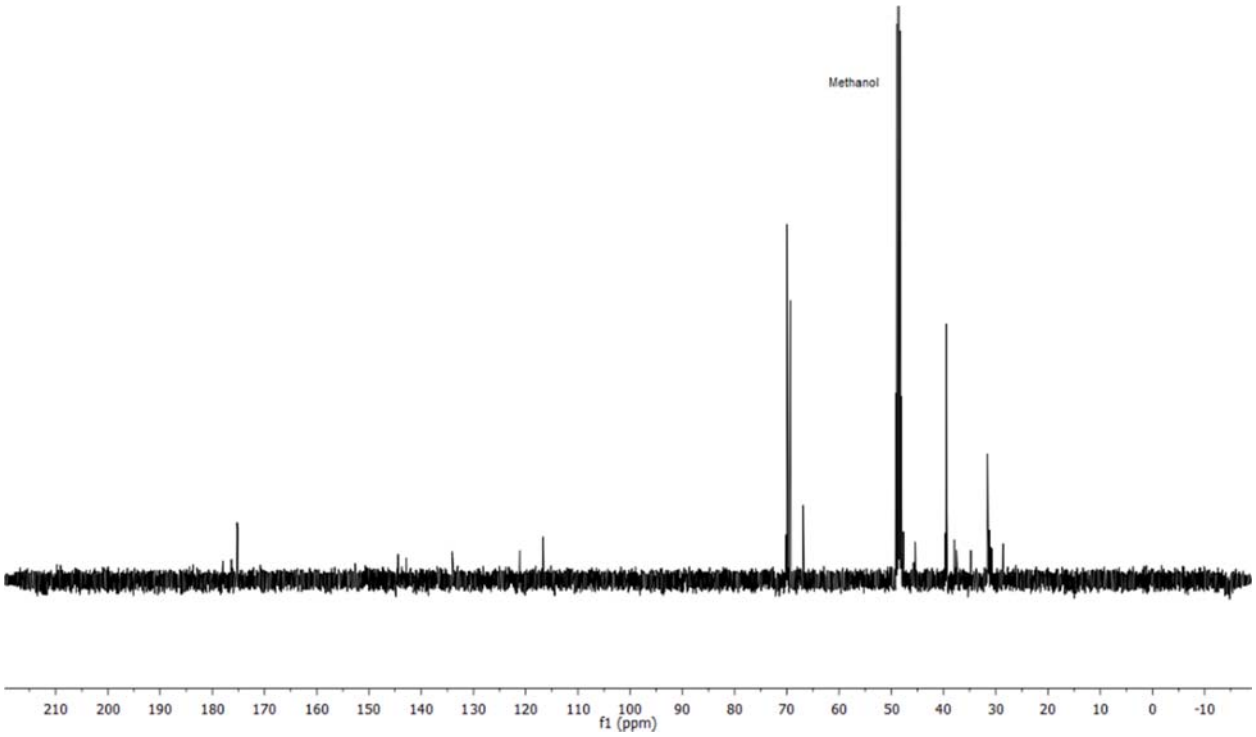

Figure S58. ^{13}C-NMR spectrum of compound **10** (126 MHz, D_2O).

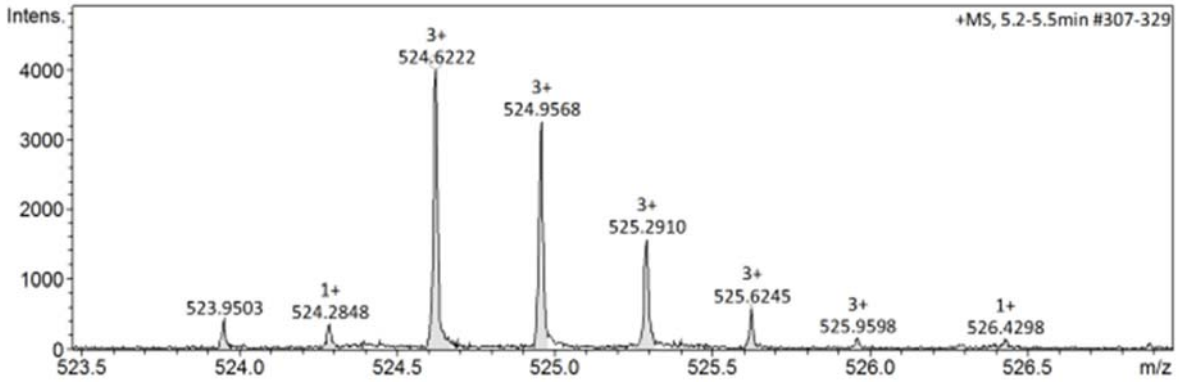

Figure S59. Figure 59: HR-ESI (ESI$^+$ Q-TOF) of compound **10**.

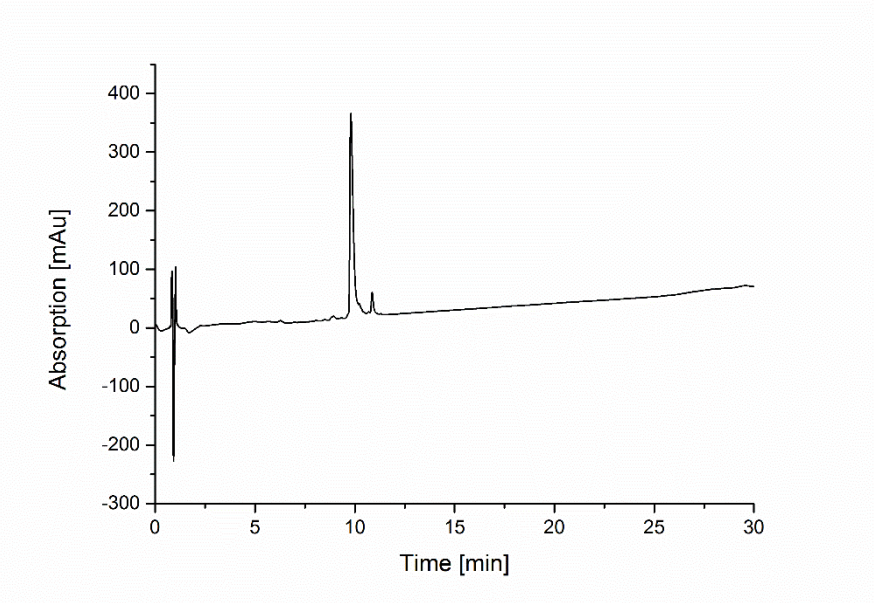

Figure S60. RP-HPLC chromatogram of compound **10** (gradient from 0% to 50% eluent B over 30 min at 25°C).

(**11**) *protected*

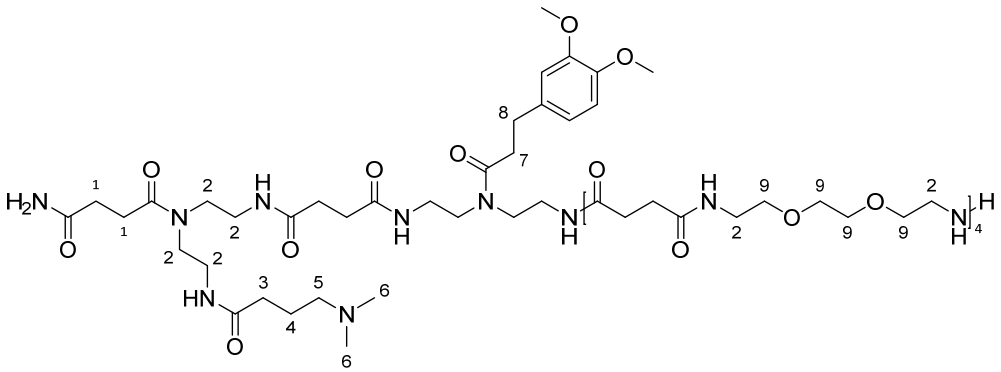

Compound **11** protected was obtained with a yield of 72% after cleavage from solid support and lyophilization

^{1}H-NMR (500 MHz, D_2O) δ [ppm]: 8.50 (s, NH), 7.04 (d, J = 8.2 Hz, 1H, $H_{Aromatic}$), 7.01 (d, J = 2.0 Hz, 1H, $H_{Aromatic}$), 6.91 (dd, J = 8.2, 2.0 Hz, 1H, $H_{Aromatic}$), 3.91 (s, 3H, OCH_3), 3.89 (s, 3H, OCH_3), 3.75-3.52 (m, 32H, H-9), 3.49-3.18 (m, 32H, H-2), 3.10 (m, 2H, H-5), 2.86 (m, 8H, 6-H, 8-H), 2.65 (m, 4H, 3-H, 7-H), 2.55-2.27 (m, 24H, 1-H), 1.94 (m, 2H, 4-H).

^{13}C-NMR (126 MHz, D_2O) δ [ppm]: 178.62, 176.66, 175.74, 175.68, 175.66, 175.63, 175.59, 175.56, 175.5, 175.39, 171.46, 149.09, 147.67, 135.01, 121.83, 113.33, 113.07, 70.51, 70.36, 69.75, 67.29, 57.91, 56.77, 56.69, 43.62, 40.05, 39.81, 38.19, 37.95, 37.87, 35.14, 33.01, 32.88, 31.99, 31.95, 31.92, 31.84, 31.77, 31.72, 31.56, 30.93, 28.92, 28.82, 20.94.

HR-ESI-MS: calculated mass for $C_{73}H_{131}N_{16}O_{24}$ $[M+3H]^{3+}$ 538.6502, found 538.6497.

RP-HPLC (gradient from 0% to 50% eluent B over 30 min at 25°C):t_r =11.1 min, purity 92%.

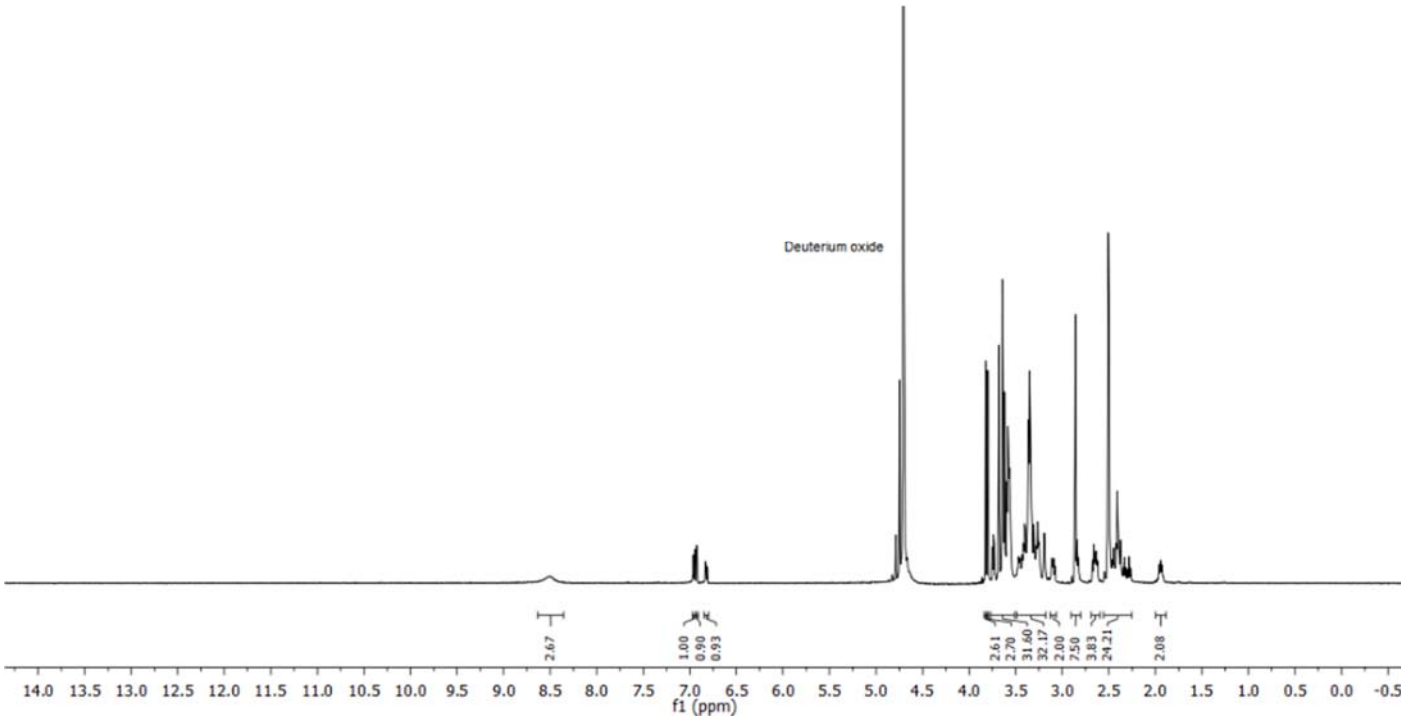

Figure S61. ^{1}H-NMR spectrum of compound **11** protected (500 MHz, D_2O).

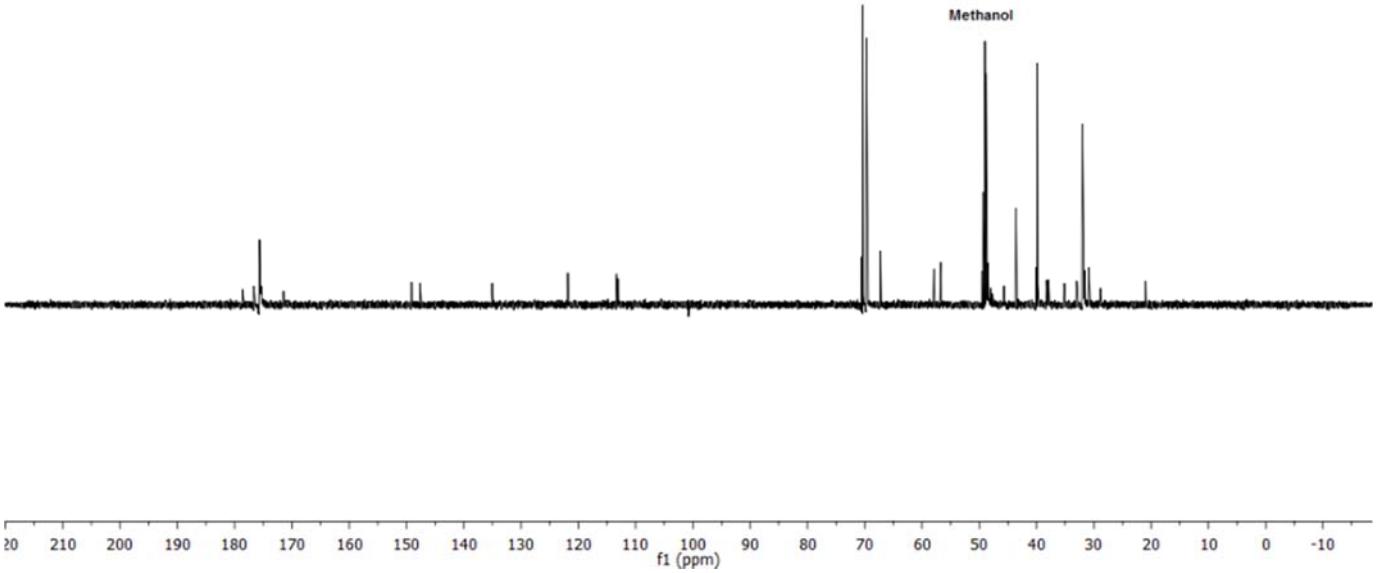

Figure S62. ^{13}C-NMR spectrum of compound **11** protected (126 MHz, D_2O).

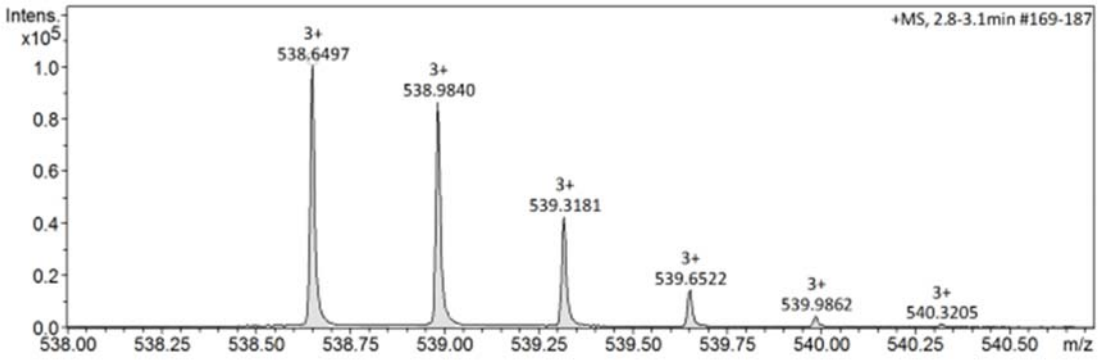

Figure S63. HR-ESI (ESI$^+$ Q-TOF) of compound **11** protected.

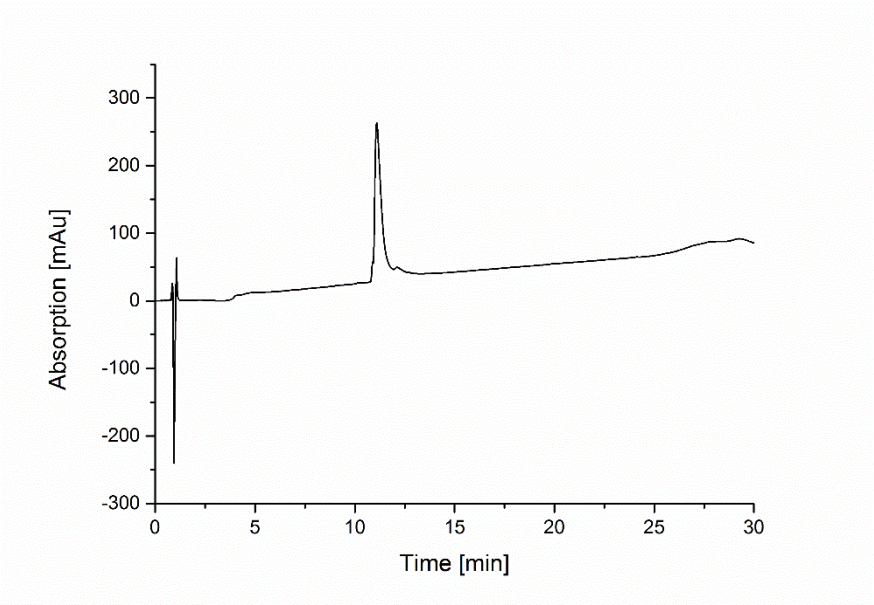

Figure S64. RP-HPLC chromatogram of compound **11** protected (gradient from 0% to 50% eluent B over 30 min at 25°C).

(**11**)

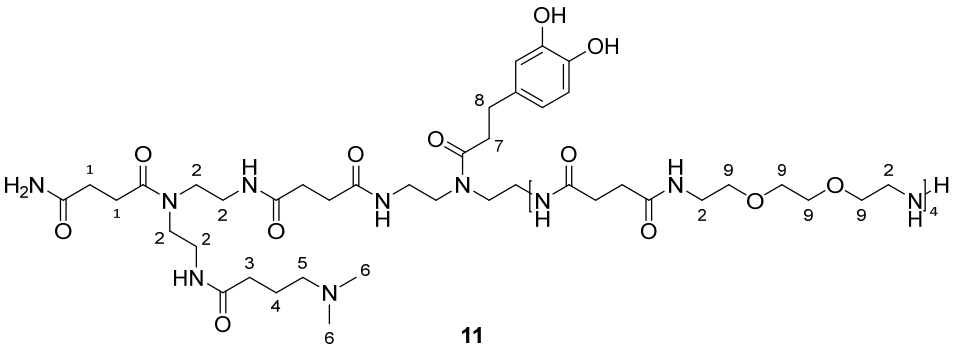

11

Compound **11** was obtained with a yield of 28% after deprotection, purification by preparative RP-HPLC and lyophilization.

^{1}H-NMR (500 MHz, D_2O) δ [ppm]: 8.43 (s, NH), 6.85 (m, 1H, $H_{Aromatic}$), 6.79 (m, 1H, $H_{Aromatic}$), 6.70 (m, 1H, $H_{Aromatic}$), 3.82-3.60 (m, 32H, H-9), 3.59-3.20 (m, 32H, H-2), 3.15 (m, 2H, H-5), 2.91 (s, 6H, H-6), 2.80 (m, 2H, H-8), 2.69 (m, 4H, H-3, H-7), 2.64-2.30 (m, 24H, H-1), 2.01 (m, 2H, 4-H).

^{13}C-NMR (126 MHz, D_2O) δ [ppm]: 178.60, 176.69, 175.73, 175.68, 175.60, 175.54, 175.49, 175.43, 175.39, 175.38, 175.36, 171.57, 144.94, 143.32, 134.42, 121.48, 117.11, 117.06, 70.53, 70.39, 69.78, 67.30, 57.93, 43.62, 40.09, 39.86, 39.79, 38.26, 37.99, 37.90, 35.24, 33.01, 32.89, 31.99, 31.95, 31.91, 31.85, 31.80, 31.75, 31.70, 31.38, 30.94, 28.93, 28.83.

HR-ESI-MS: calculated mass for $C_{71}H_{127}N_{16}O_{24}$ $[M+3H]^{3+}$ 529.3064, found 529.3056.

RP-HPLC (gradient from 0% to 50% eluent B over 30 min at 25°C): t_r=9.5 min, purity 90%.

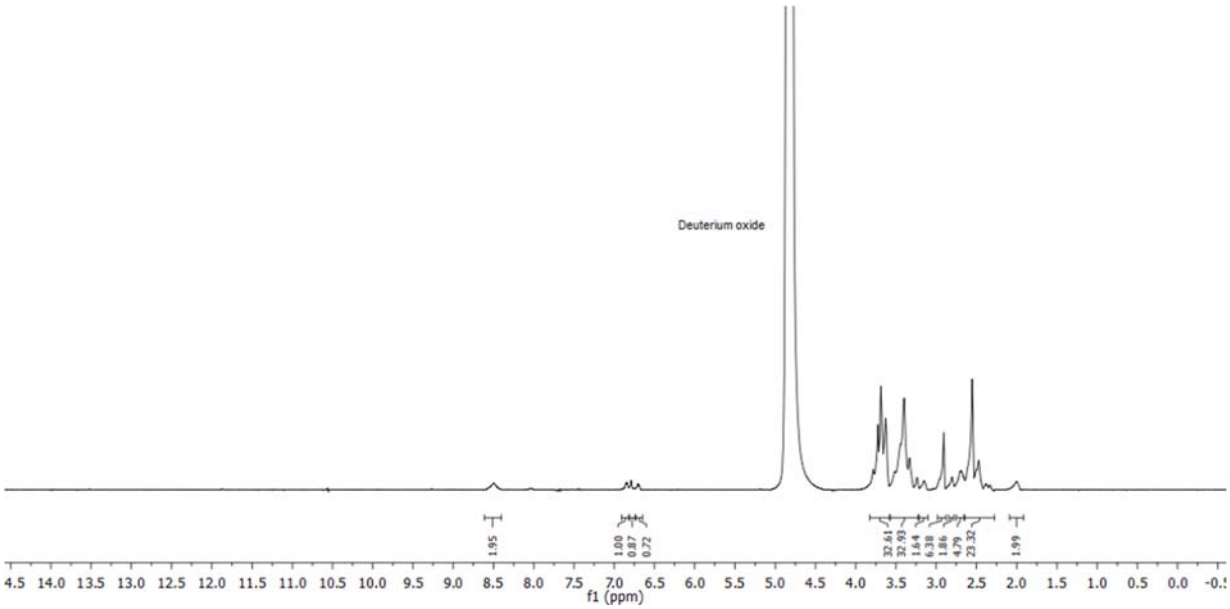

Figure S65. ^{1}H-NMR spectrum of compound **11** (500 MHz, D_2O).

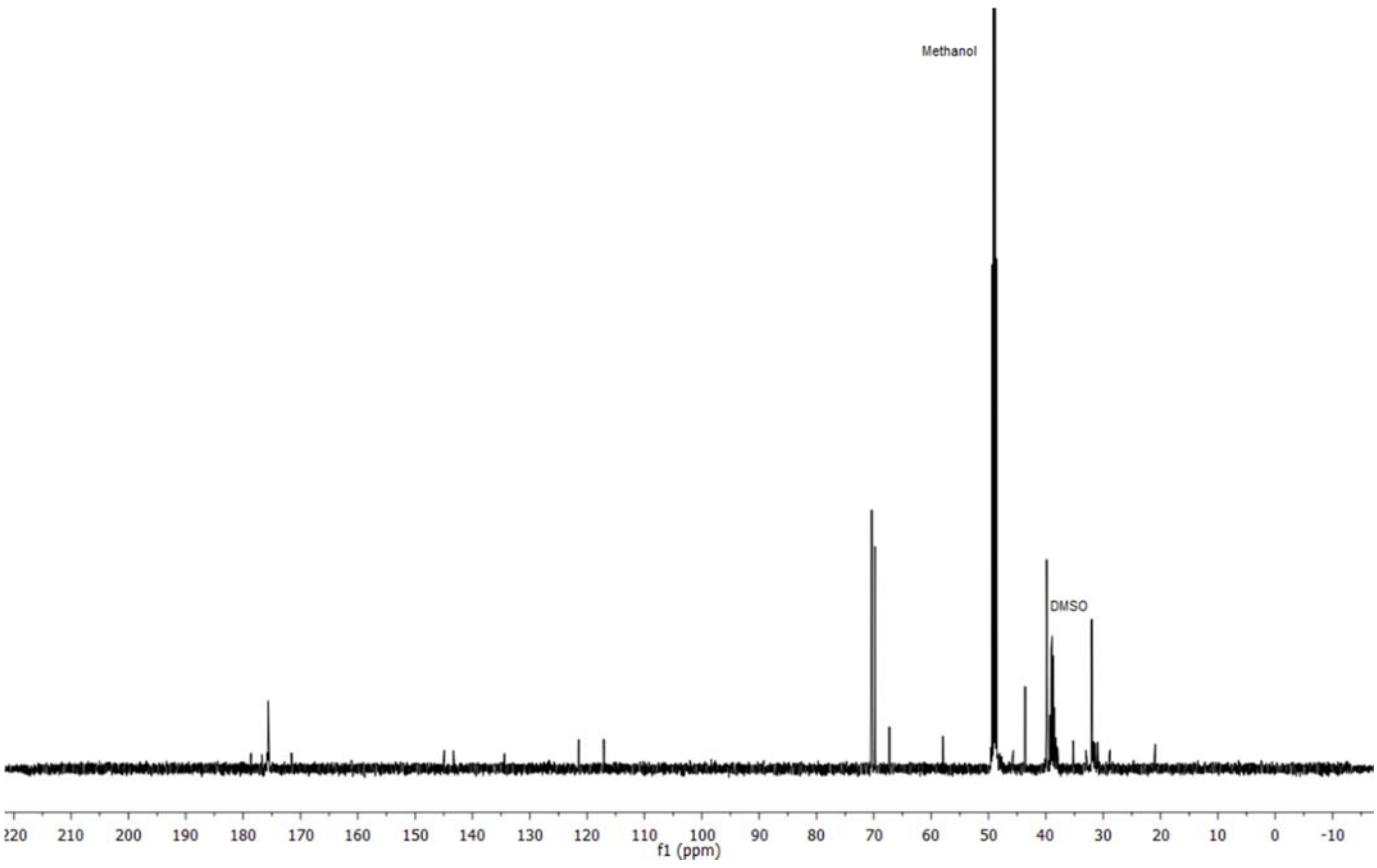

Figure S66. ^{13}C-NMR spectrum of compound **11** (126 MHz, D_2O).

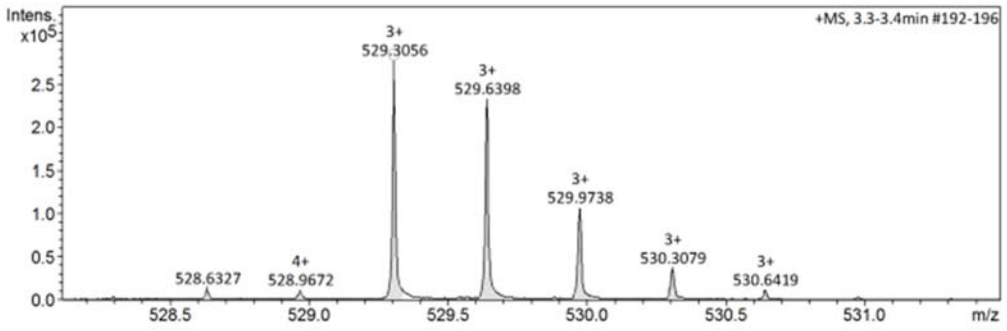

Figure S67. HR-ESI (ESI$^+$ Q-TOF) of compound **11**.

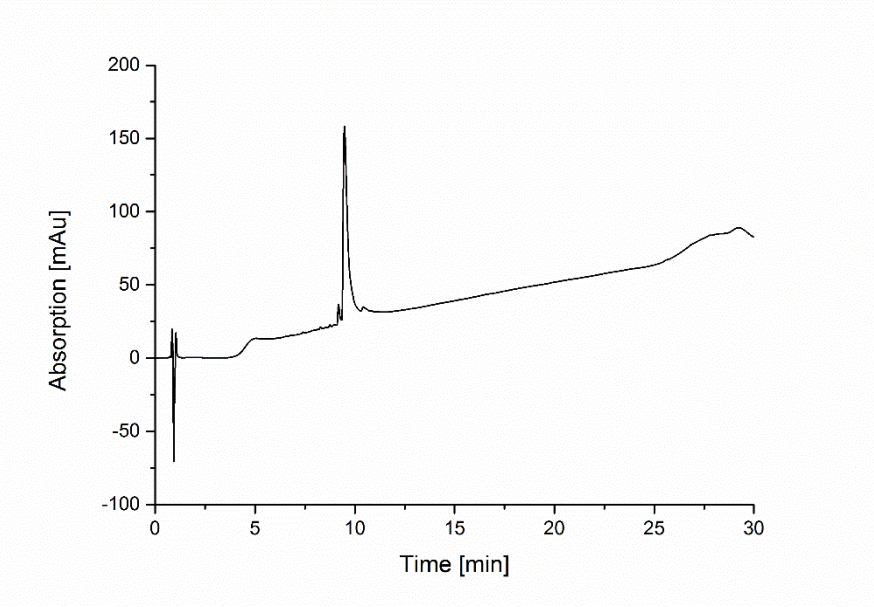

Figure S68. RP-HPLC chromatogram of compound **11** (gradient from 0% to 50% eluent B over 30 min at 25°C)

S5 Determination of SCP Functionalization Degrees

Oligomer Functionalization of PEG-CA-SCPs

For the functionalization of PEG-CA-SCPs with oligomers 1 mL of SCP dispersion is washed with 2-(*N*-morpholino)ethansulfonic acid (MES) buffer with a concentration of 0.1 mol L^{-1} with pH 5 via centrifugation (13500 rpm, 5 min). Afterwards, 200 µL of MES buffer is added to the particles. Additionally, 500 µL of Oligomer in MES buffer is added. The amount of Oligomer was equal to a 10 fold excess in comparison to carboxylic acid groups on the particles (see Table S1). To start the reaction 100 µL of a solution of 1-Ethyl-3-(3-dimethylaminopropyl)carbodiimide hydrochloride (EDC) with concentration 100 mg mL^{-1} in ultrapure water is added. The reaction solution is shaken for 2 h before the reaction solution was removed via centrifugation (13500 rpm, 5 min) and replaced with a fresh reaction solution. After an additional reaction time of 2 h the supernatant is removed and the particle

are washed with ultrapure water via centrifugation (13500 rpm, 5 min). The functionalization degree was determined via microscope based TBO titration.

Table S1: Overview over molecular weight and amount of the oligomers that were used per reaction step for PEG-CA-SCP functionalization and the functionalization degree of the particles determined via microscope based TBO titration.

Oligomer	MW [g/mol]	Amount of oligomer per reaction step [mg]	Functionalization degree [%]
1N3N (4)	1650	3.0	88
1C3C (3)	1636	2.9	98
1D3D (5)	1622	2.9	84
1D3C (6)	1584	2.8	86
1N2C (11)	1584	2.8	87
1C3N (10)	1584	2.8	98
1D3C (7)	1570	2.8	98
1C3D (9)	1570	2.8	98
1N3D (8)	1636	2.9	98

Crotonic Acid Titration via UV-VIS Spectroscopy

The determination of carboxylic acid groups on the PEG-CA particles was done in triplicates. 1 mL of SCP dispersion was dried after exchanging the water with ethanol via centrifugation (13500 rpm, 5 min) to determine the amount of particles. To the dried particles 1 mL of TBO (toluidine blue O) solution with a concentration of 0.3125 mmol L^{-1} with a pH of 10-11 was added wrapped in aluminum foil and shaken overnight. After that the solution was centrifuged (13500 rpm, 5 min) and 0.3 mL were taken and diluted to 2 mL with sodium hydroxide solution with pH 10-11. The same procedure was done with a blank where no particles were added in the beginning. The absorption of this solution was measured via UV-VIS spectroscopy and the absorption at 633 nm was used to calculate the functionalization degree using the following equation:

$$D_{CGF} = N_R(1 - A_S/A_E)/W_{Dry}$$

Where D_{CGF} is the carboxylic acid functionalization degree, A_S and A_R are the UV-VIS absorbances of sample and reference, W_{Dry} is the dry weight of 1.0 mL SCPs, N_R is the amount of TBO in the reference in units of µmol.

Determination of oligomer functionalization degree via microscope based TBO titration

For the determination of functionalization degree of oligomer functionalized SCPs 100 µL of SCP solution was washed via centrifugation (13500 rpm, 5 min) with sodium hydroxide solution pH 10-11. After removing the supernatant 125 µL of TBO solution with 0.3125 mmol L^{-1} were added, wrapped in aluminum foil and shaken overnight. Next, the TBO solution was removed and the particles were washed three times with 1 mL of sodium hydroxide solution with pH 10-11 and afterwards dissolved

in 125 µL. The same procedure was done for PEG-CA particles and non-functionalized PEG particles. Next, for all particle solutions the grey value was determined for 20 particles per batch to calculate the functionalization degree as following:

$$D_{OGF} = (1 - (G_N - G_{SCP})/\Delta G_B) * 100$$

Where D_{OGF} is the oligomer functionalization degree, ΔG_B is the difference of grey values between non-functionalized and carboxylic acid functionalized SCPs ($\Delta G_B > 0$), G_N is the average grey value of non-functionalized SCPs and G_{SCP} is the average grey value of oligomer functionalized SCPs.

S6 Determination of the SCPs elastic modulus

Force-indentation measurement with a NanoWizard 2 AFM provided the elastic modulus of the SCPs. A silica bead with a raduis of 2.3 µm was glued with an epoxy glue onto a tipless, non-coated cantilever (spring constant 0.32 N/m; NanoAndMore GmbH). Several force curves were recorded from different particles and analyzed with the novel contact model developed by Glaubitz et al.[5]. The model considers deformation of the object at two sites: the indentation site of the AFM probe and at the contact with the solid support. The respective deformation (δ) –force (F) dependence reads:

$$\delta(F) = \left(\frac{3F}{4E}\cdot\frac{1-\upsilon^2}{R_{AFM}^{\frac{1}{2}}}\right)^{\frac{2}{3}} + \left[\frac{3(1-\upsilon^2)\left(F + 6W\pi R_{SCP} + \sqrt{12W\pi R_{SCP}F_c(6W\pi R_{SCP})^2}\right)}{4E\cdot R_{SCP}^{\frac{1}{2}}}\right]^{\frac{2}{3}} - \left[\frac{9W\pi(1-\upsilon^2)}{E}\right]^{\frac{2}{3}}\cdot R_{SCP}^{\frac{1}{3}}$$

where E is the elastic modulus of the indented SCP, R_{SCP} its radius, υ the Poisson ratio of the SCP, W the SCP adhesion energy with the support surface and R_{AFM} the radius of the indenter. The Poisson ration was assumed to be 0.5 (volume conservation upon indentation). E and W were free fit parameters. The elastic moduli of FN SCPs were on the order of 72 kPa and their surface energy varied only marginally between 20 and 30 µJ/m^2 for the different fits.

For all SCPs except for the diamine oligomer (**4**) carrying SCPs the elastic moduli were similar, around 71.9 ± 10.5 kPa. The elastic modulus for the diamine oligomer (**4**) functionalized SCPs was 103 ± 14.4 kPa. The increase in elastic modulus for the diamine carrying SCP is probably the to an extended conformation of the of the oligomer stiffening the PEG network. But overall, the rather low variations of the elastic moduli for the different SCPs are expected due to the low density of oligomers in the SCP. About 13.5-14.2 wt% of the SCPs material are oligomers. Due to the high SCP swelling degree the oligomer concentration within the SCP network is 11 mmol l^{-1}.

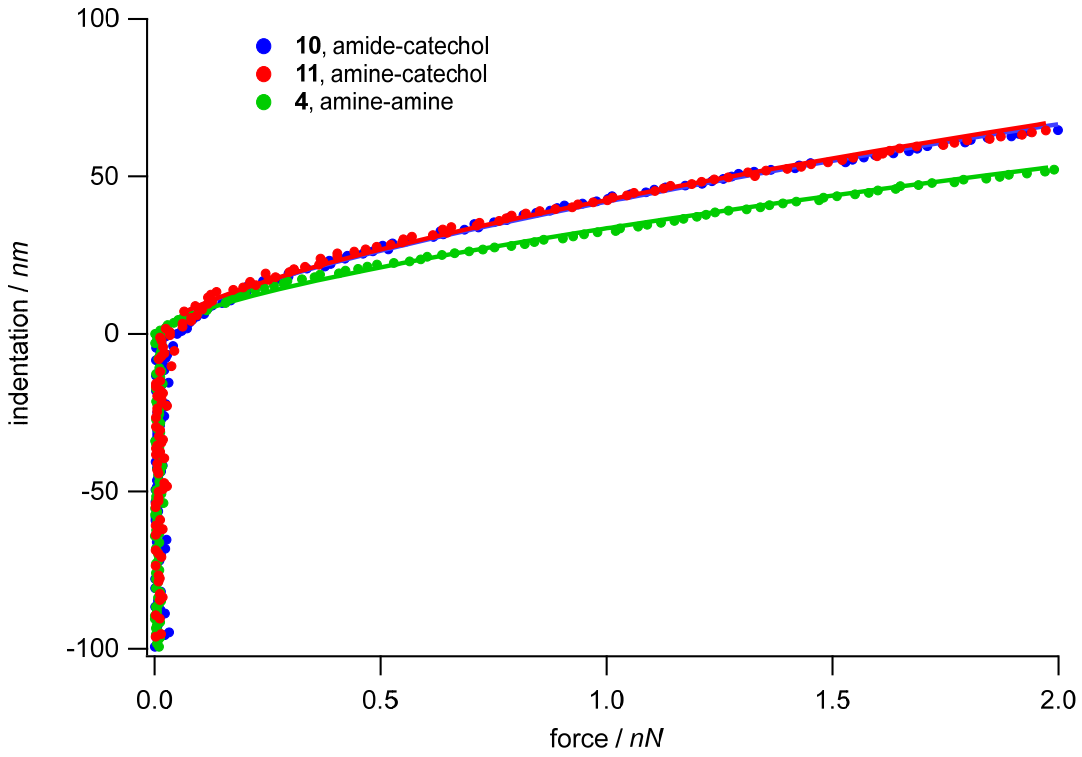

Figure S69. Typical AFM indentation-force curves for the analysis with the contact model developed by Glaubitz et al.[5] The solid lines are fits to the data.

S7 Reflection Interference Contrast Microscopy (RICM) measurements Setup

RICM on an inverted microscope (Olympus IX73) was used to obtain the contact area between the microparticles and a hard glass surface. For illumination a monochromatic (530 nm) collimated LED (Thorlabs, Germany, M530L2-C1) was used. An UPlanFL N 60x/0.90 dry objective (Olympus Corporation, Japan), additional polarizers and a quarter waveplate (Thorlabs, germany) to avoid internal reflections and a monochrome CMOS camera (DMK 33UX174, The Imaging Source Europe GmbH, Germany) were used to image the RICM patterns.

Determination of the Contact Radius

RICM was used to measure the contact radius formed by the SCPs resting on the polymer surface (Figure S2). Polarized light waves reflected from the upper glass surface (I_1) and the surface of the bead (I_2) interact to create an interference image. The intensity at a given position in the image depends on the separation $h(x)$ between the two surfaces: $I(x) = I_1 + I_2 + 2\cdot\mathrm{sqrt}(I_1 \cdot I_2)\cos[2k\cdot h(x) + \pi]$, where $k = 2\pi n/\lambda$, and n and λ are the index of refraction of water and the wavelength of the monochromatic light, respectively. In order to detect the interference pattern, stray light was reduced by an 'antiflex' technique. This is accomplished by crossed polarizer and analyzer filter with a $\lambda/4$-plate placed between the objective lens and the analyzer.[6]

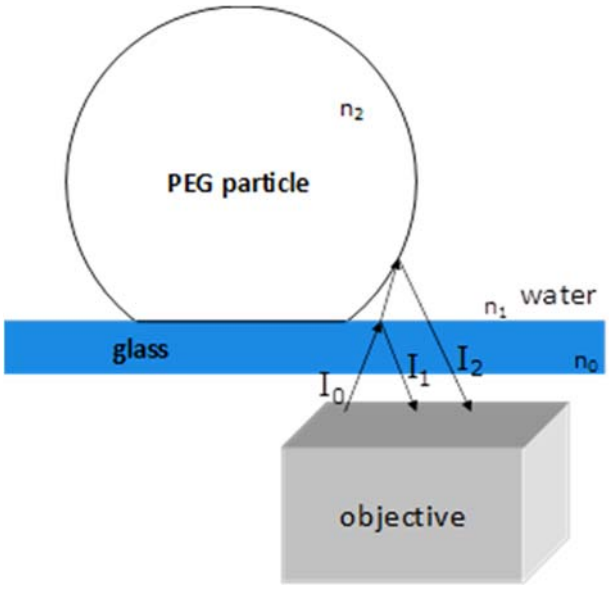

Figure S70. Schematic drawing of the RICM principle.

Correction Factors

For analysis of the RICM patterns correction factors must be determined for finite aperture and geometry effects. To obtain the correction factors, we imaged hard, non-deformable glass beads on a glass surface in RICM mode with a known size and curvature. We recorded 5 glass beads with a diameter in the range of 20-40 µm (polysciences) and extracted the intensity profile. Using the profiles, we reconstructed the shape of the beads and compared it to the known spherical shapes of the glass beads (glass bead radius *R* measured by light microscope), and determined the correction factors, see Pussak et al.[7]

Contact radius determination

To determine the contact radius *a* of the SCP on the polymer surface we reconstructed the height profile of the particles from the RICM images (see Figure S3). This was done by determining the lateral $x(i)$ positions of the i-th minima and maxima by a self-written IgorPro procedure (Wavemetrics, USA). Next, the vertical position $y(i)$ of the maxima and minima were determined by

$$y(i) = \frac{i\lambda}{4n} + c_i ,$$

where n is the refractive index and λ the wavelength. The height profile was then reconstructed by plotting $y(i)$ vs $x(i)$ and fitting the data by a circle equation representing the assumed shape of the SCP:

$$y(x) = y_0 + \sqrt{R^2 - x^2} .$$

where R is the independently measured SCP radius and y_0 the vertical shift of the SCP center due to flattening of the SCP upon adhesion. The fit with y_0 as the only free fit parameter intersects with the x-axis and gives the contact radius a.

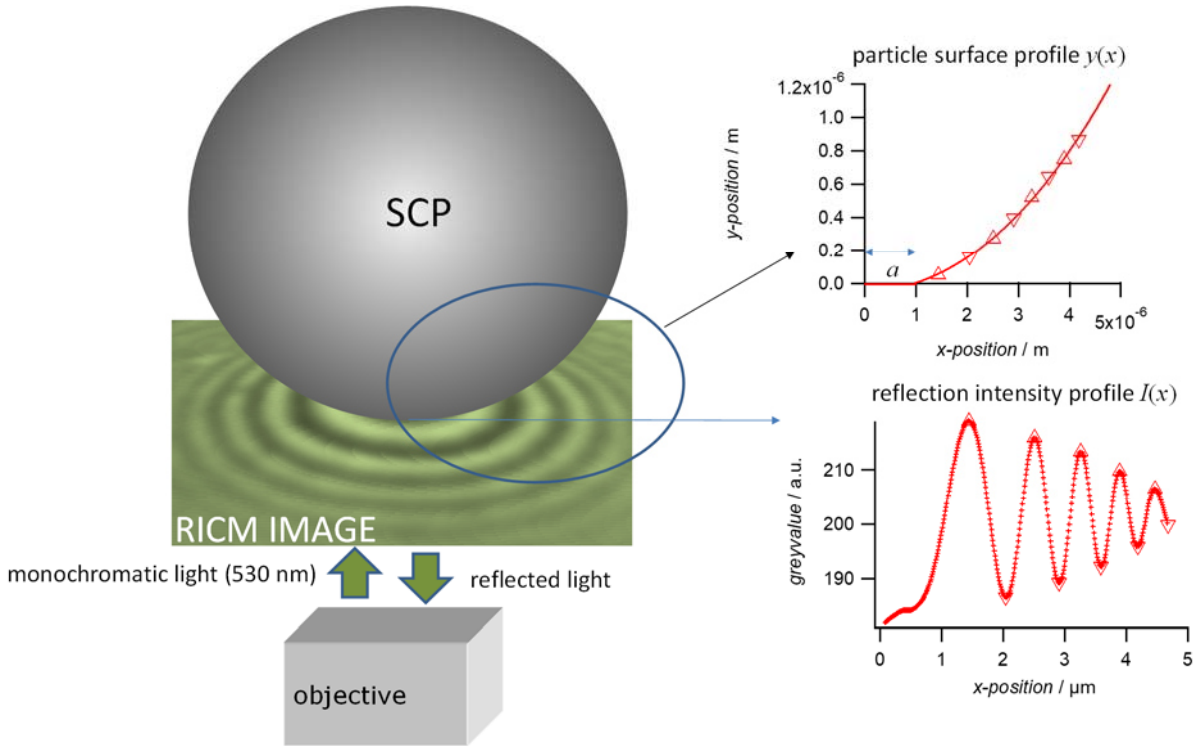

Figure S71. Left: schematic representation of the measurement setup. Bottom right: actual intensity profile of an adherent SCP showing 5 minima and 5 maxima. Top right: reconstructed surface profile of the SCP and the contact radius a at the intersection of the profile at $y = 0$.

S8 Stability of the catechol group

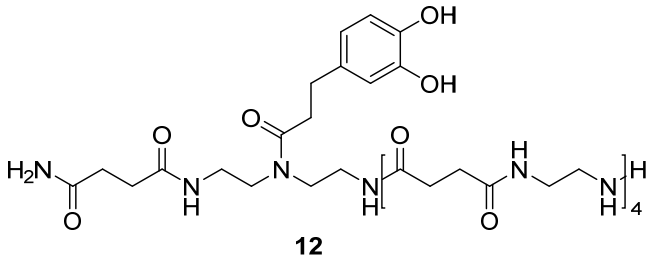

12

Compound **12** was used as a model for the investigation of the catechol stability. For this 1 mg was dissolved in 500 µl water and the mixture was measured via RP-HPLC directly after dissolving and after 12 days.

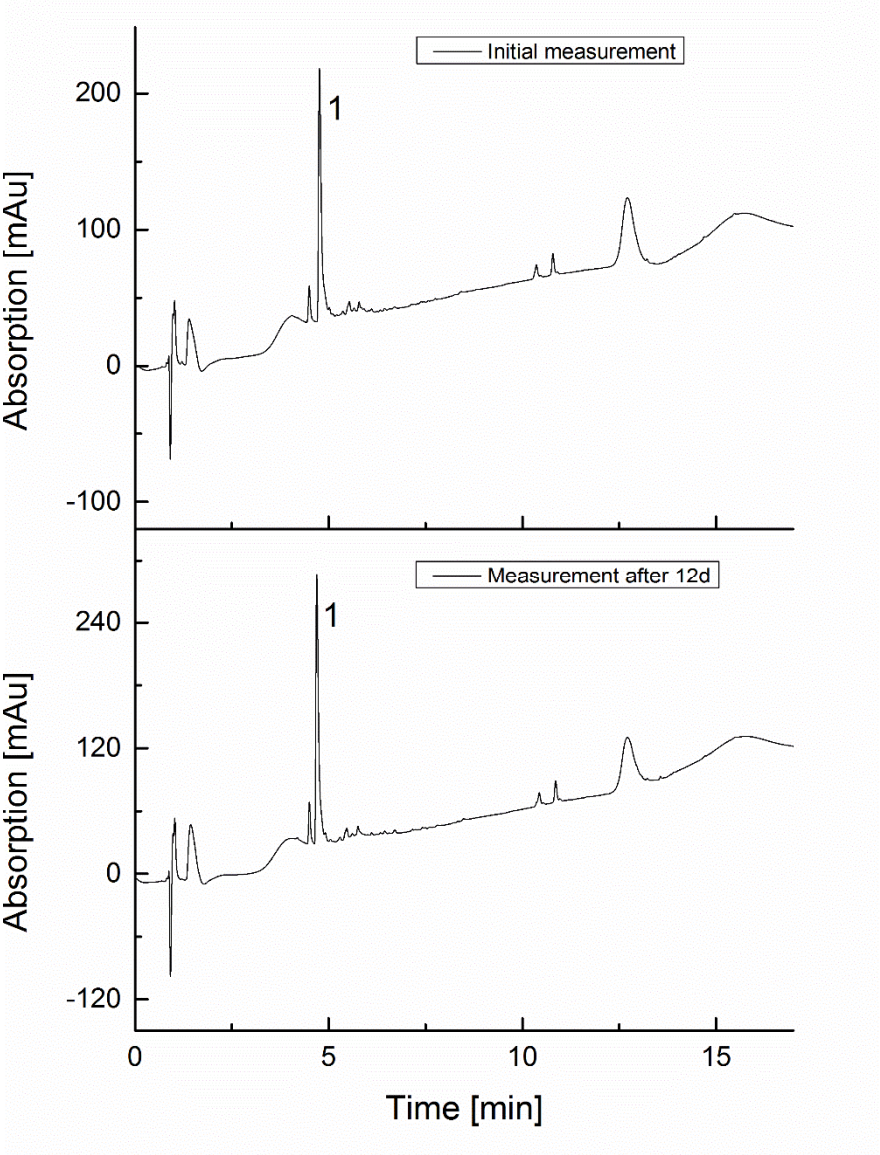

Figure S72. RP-HPLC of compound **12** directly after dissolving and after 12 days. Peak 1 shows compound **12**.

S9 Non-normalized and oligomer concentration normalized adhesion energy values

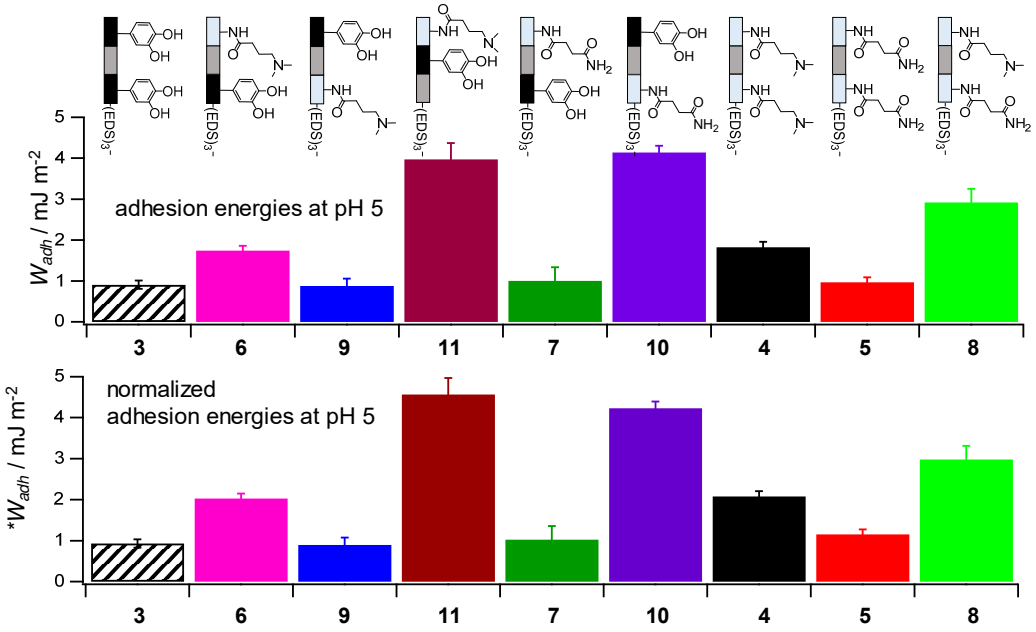

Figure S73. Comparison between non-normalized and normalized adhesion values. Top: non-normalized adhesion values (W_{adh}). Bottom: oligomer concentration normalized adhesion energy values (W_{adh}).

Supporting References

[1] C. Gerke, M. F. Ebbesen, D. Jansen, S. Boden, T. Freichel, L. Hartmann, *Biomacromolecules* **2017**, *18*, 787-796.

[2] D. Pussak, M. Behra, S. Schmidt, L. Hartmann, *Soft Matter* **2012**, *8*, 1664-1672.

[3] S. Schmidt, H. Wang, D. Pussak, S. Mosca, L. Hartmann, *Beilstein Journal of Organic Chemistry* **2015**, *11*, 720-729.

[4] D. Ponader, F. Wojcik, F. Beceren-Braun, J. Dernedde, L. Hartmann, *Biomacromolecules* **2012**, *13*, 1845-1852.

[5] M. Glaubitz, N. Medvedev, D. Pussak, L. Hartmann, s. schmidt, C. A. Helm, M. Delcea, *Soft Matter* **2014**.

[6] L. Limozin, K. Sengupta, *ChemPhysChem* **2009**, *10*, 2752-2768.

[7] D. Pussak, D. Ponader, S. Mosca, S. V. Ruiz, L. Hartmann, S. Schmidt, *Angewandte Chemie International Edition* **2013**, *52*, 6084-6087.

3.3 Catechol-functionalized sequence-defined glycomacromolecules as covalent inhibitors of bacterial adhesion

Authors: **L.Fischer**, R.C. Steffens, T.J. Paul, L. Hartmann

Journal: Polymer Chemistry

DOI: 10.1039/D0PY00975j

Impact Factor: 5.342 (2019)

Own contributions:

Collaborative project development and collaborative design of final structures and assays. Practical guidance and supervision for the synthesis of all building blocks and final structures as well as turbidity, precipitation, MALDI-TOF and SDS-Page assays. Collaborative analysis of ^{1}H-NMR, ^{13}C-NMR, and HR-ESI and RP-HPLC experiments. Development, optimization and performance of the bacterial adhesion-inhibition assay as well as visualization and interpretation of the results. Collaborative visualization and interpretation of the turbidity, precipitation, MALDI-TOF and SDS-Page experiments. Collaborative writing of the manuscript.

Polymer Chemistry

ROYAL SOCIETY OF CHEMISTRY

PAPER

View Article Online
View Journal

Cite this: DOI: 10.1039/d0py00975j

Catechol-functionalized sequence-defined glycomacromolecules as covalent inhibitors of bacterial adhesion†

Lukas Fischer, Ricarda C. Steffens, Tanja J. Paul and Laura Hartmann *

Received 7th July 2020,
Accepted 19th August 2020

DOI: 10.1039/d0py00975j

rsc.li/polymers

Herein, we present the synthesis of catechol functionalized sequence-defined glycomacromolecules that can covalently block the binding site of lectins and bacterial adhesins. These structures produced on a solid phase support combine two important features: the multivalent presentation of carbohydrates for specificity, and catechols as anchors to go from highly reversible interactions to covalent attachment and more efficient inhibition. In our study we demonstrate this on the lectin Concanavalin A (ConA) by showing an increase in clustering for catechol ligands and on the effective inhibition of bacterial adhesion of *E. coli* on mannan surfaces by our catechol functionalized glycomacromolecules. Furthermore, covalent attachment is studied *via* MALDI-TOF measurements and SDS-PAGE analysis. Importantly, by replacing binding sugars with non-binding sugars, no inhibitory effects or covalent attachment were observed.

Introduction

Carbohydrate binding proteins such as lectins play key roles in numerous biological pathways. They are part of cell–cell communication, immune processes, tumorigenesis and pathogen infection.[1–5] For example, galectin-3 mediates the adhesion of cancer cells towards the extracellular membrane, an important step in the formation of tumour metastases.[6] Another example is the adhesin FimH from *E. coli* which binds to the glycocalyx of host cells and promotes biofilm formation.[7,8] Blocking these interactions between the carbohydrate and protein can stop or slow the pathogenic process and is therefore a promising therapeutic route *e.g.* as antiviral or antibacterial treatments.[9] However, single carbohydrates are weak binders and multivalent interactions are required to achieve strong and potentially selective binding.[10,11] Such multivalency can be achieved by the presentation of multiple carbohydrate ligands on a synthetic scaffold, a process that has been shown to provide access to high affinity binders and efficient inhibitors *e.g.* against *E. coli* or influenza.[12,13] It is important to keep in mind though that the carbohydrate–lectin interactions are still highly reversible usually resulting in only temporary inhibition, followed by disassociation from the target receptor and subsequent renal clearance.[14] Ligands with the potential to covalently couple to a protein have the ability to overcome this challenge. For example, Wagner *et al.* recently introduced an epoxide functionalized D-galactose derivative to mark biofilm formation for *P. aeruginosa*, a multiple drug resistant bacteria that is cause for a high amount of hospital infections.[15] The galactose derivative binds to the lectin LecA *via* the carbohydrate recognition domain (CRD) but then covalently attaches to the protein *via* a reactive epoxide group. This process was also shown to be specific as it depends on a cysteine found in the CRD, which however limits this approach to LecA. Next generation covalent ligands as therapeutic inhibitors could address this issue by fulfilling the following requirements: limited reactivity during distribution in order to avoid side-effects, selective covalent binding to the target protein after accumulation to achieve high levels of inhibition and a platform that can be adjusted to different targets *e.g.* different pathogens. As a first proof-of-concept study, here we introduce sequence-defined glycomacromolecules in combination with a catechol moiety and evaluate their potential as carbohydrate-based non-reversible inhibitors of bacterial adhesion. The goal of this study is to provide first insights into using catechols in covalent ligand design.

Catechol groups oxidize to benzoquinone under basic to neutral conditions and afterwards are capable of reacting in a Michael addition-like reaction. This process allows them to covalently bind to proteins *via* surface exposed nucleophiles.[16] One advantage of this process is that the oxidation rate depends on pH and chemical environment, for example dopa-

Institut für Organische und Makromolekulare Chemie, Heinrich-Heine-Universität Düsseldorf, Universitätsstr. 1, 40225 Düsseldorf, Germany.
E-mail: Laura.Hartmann@hhu.de

†Electronic supplementary information (ESI) available. See DOI: 10.1039/d0py00975j

mine prodrugs reach plasma half-lives of several hours with intact catechol moiety.[17,18] This makes catechols promising covalent linker candidates as they could combine plasma stability for distribution with sufficient reactivity after accumulation. However, this advantage can also be a limitation if the catechol is slow to react.

Previously, we have introduced a class of precision glycomacromolecules as sequence-defined glycooligo(amidoamines). These compounds are accessible through the stepwise addition of building blocks on solid support, which allows for the control of the number, position and type of carbohydrates attached to the macromolecular scaffold, and gives access to tailor-made multivalent glycomacromolecules for targeting different proteins such as bacterial adhesins,[19] viral capsid proteins[20] and galectins.[21]

In this work, we introduce for the first time catechol groups to our precision glycomacromolecules to combine both the high affinity and selective binding of the glycomacromolecule with covalent inhibition. We envision that catechols can interact with the targeted protein only after binding through the carbohydrate-functionalized part of the scaffold. Over time the catechol moiety oxidizes to its benzoquichone derivative and can attach covalently *e.g.* to available surface lysines or cysteines (Fig. 1).

Results and discussion

Synthesis of catechol-functionalized precision glycomacromolecules

Six different glycomacromolecules were synthesized presenting either three mannose (Man) or three galactose (Gal) residues and either zero, one or two catechol moieties positioned at the chain ends (Fig. 2). The synthesis of the glycofunctionalized scaffolds followed prior published protocols. In short, as previously introduced, tailor-made building blocks equipped with both an acid and an Fmoc-protected amine functionality, were assembled stepwise on solid support using standard Fmoc-peptide coupling chemistry.[22] Site-specific introduction of alkyne side chains was achieved by using TDS (triple bond diethylenetriamine succinic acid) building blocks. Carbohydrate moieties were then coupled *via* Cu-mediated alkyne–azide-conjugation (CuAAC) using azidoethanol-functionalized Man and Gal derivatives. Catechol groups (Cat) were introduced *via* free primary amine groups and amide coupling using acetonide protected hydrocaffeic acid which was synthesized according to Wei *et al.*[23] For the Cat containing glycomacromolecules **2**, **3**, **5** and **6**, the N-terminal amine was used for functionalization after final Fmoc-deprotection. Additionally, for glycomacromolecules **3** and **6** with two catechol units, Boc-protected lysine was used during assembly on solid support to introduce a second primary amine after on-resin deprotection with HCl in dioxane. As last step, carbohydrate moieties were deprotected using sodium methanolate in methanol and the final glycomacromolecules were cleaved off the resin with trifluoroacetic acid, at the same time resulting in catechol deprotection.

All structures were obtained with a relative purity of >90% after cleavage as determined by RP-HPLC and further characterized by ^{1}H-NMR, ^{13}C-NMR and HRMS (see ESI† for analytical data). Compounds were used in analytical and bioassays without further purification.

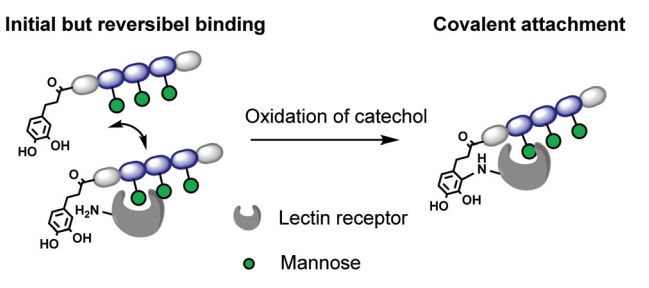

Fig. 1 Model for irreversible inhibition by catechol-functionalized glycomacromolecules through specific binding *via* the carbohydrate ligands followed by irreversible attachment through the catechol group.

Catechol-functionalized precision glycomacromolecules binding to model lectin Concanavalin A (ConA)

To investigate the influence of the Cat moieties on the binding behaviour of glycomacromolecules towards lectins, binding to ConA was first studied *via* turbidity and precipitation assays. ConA is a Man-binding lectin extracted from the jack-bean and is widely used as a model system for sugar–lectin interactions. Forming a tetramer at pH greater than 7, it is capable of cross-linking multivalent glycomimetics, undergoing clustering and resulting in observable precipitation.[24] This precipitation can be quantified *via* UV/Vis spectroscopy to measure the affinity of carbohydrates towards ConA. For the turbidity assay, a protocol adapted from Kiessling *et al.* was used[25,26] to determine the reciprocal half-maximal turbidity ($1/c_{1/2T\max}$) as a value relative to the affinity towards ConA. Additional information was gathered by using a quantitative precipitation assay to derive the amount of ConA precipitated per glycomacromolecule (see ESI†).[27]

The turbidity assay (Fig. 3, dark blue) clearly shows an increase in clustering of ConA in presence of a Cat moiety, with a five-fold increase for glycomacromolecule **2** with one Cat and a three-fold increase for glycomacromolecule **3** with two Cat in comparison to glycomacromolecule **1** having no Cat. Importantly, negative controls presenting Gal instead of Man but also including one or two Cat groups (**5**, **6**) showed no turbidity and thus no binding to ConA (see ESI†). The catechol increases the clustering of the glycomacromolecule but only in combination with the binding carbohydrates, suggesting that Cat can only interact with ConA after the initial binding of the Man moieties. Thus, the overall specificity is retained. When looking at the quantitative precipitation assay (Fig. 3, light blue), more ConA per ligand is precipitated for the structure with two Cat (**3**), with 1.9 ConA bound per ligand *vs.* 0.7 ConA per ligand for structure **2**. Both show a significant increase in comparison to **1** with 0.1 ConA per glycomacromolecule. Again, negative controls with Gal (**4**, **5**, **6**) showed no binding

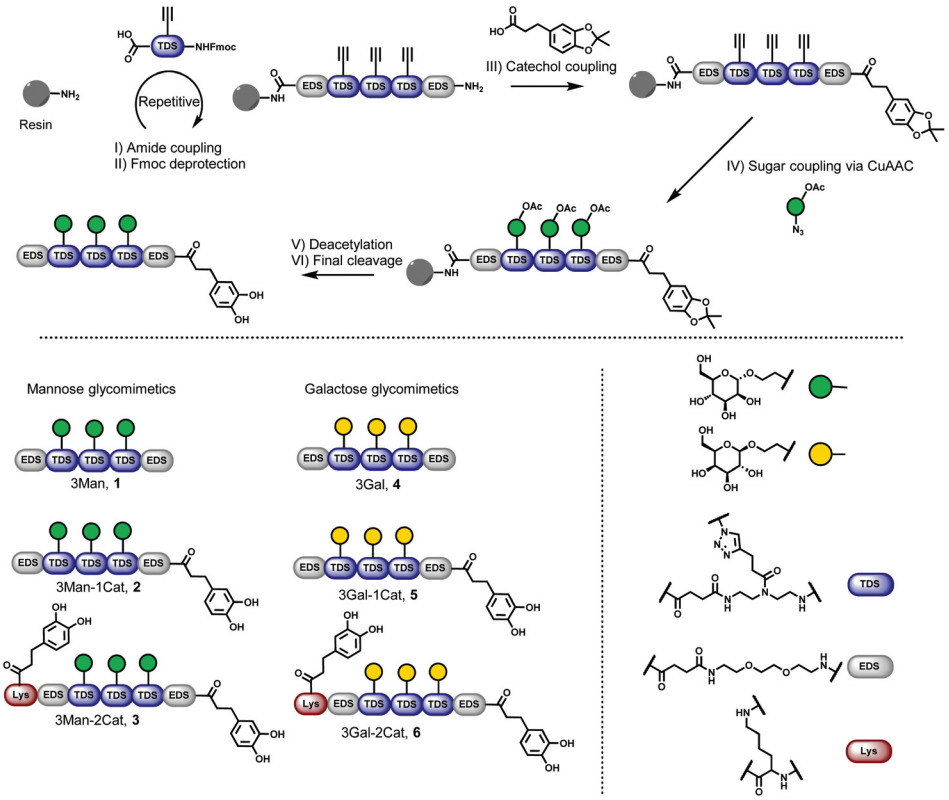

Fig. 2 Solid phase synthesis of catechol containing glycomacromolecules (**1–6**).

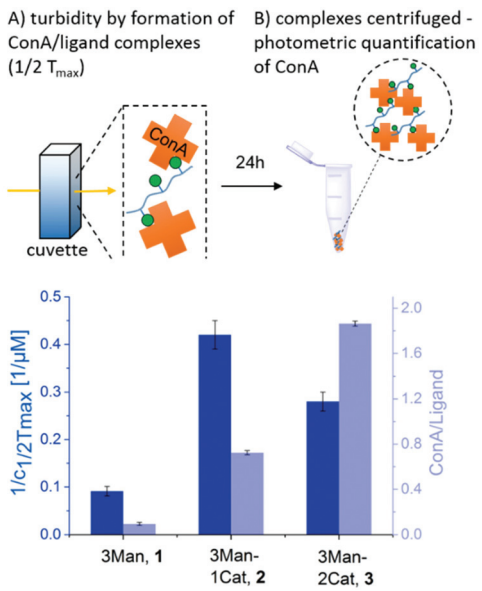

Fig. 3 Results of the turbidity assay (dark blue) and quantitative precipitation assay (light blue) (schematic presentation of the assays are not to scale). Notably, none of the Gal-functionalized glycomacromolecules, with or without catechol, showed any binding in these assays (see ESI, Fig. S29†).

to ConA. There is an important difference between the two assays: in the turbidity assay, glycomacromolecule and ConA were incubated for 20 min before measurement, while for the precipitation assay glycomacromolecule and receptor were incubated for 24 h. This indicates that a second step of binding occurs – the bond formation *via* the catechol group, which probably takes time due to the oxidation and thus a fully non-reversible ligand-complex formation is only observed in the precipitation assay.

Together, both assays show a clear increase in binding towards ConA upon the introduction of catechol groups. Binding of the ligands remains specific as the negative controls presenting a non-binding carbohydrate motif did not show any interaction. We have also seen that the second step, the covalent attachment, seems to be slower than the carbohydrate-mediated first step of the complex formation.

Bacterial adhesion-inhibition studies applying catechol-functionalized precision glycomacromolecules

To further show the applicability of catechol-functionalized precision glycomacromolecules as inhibitors in biological systems and to study the time-dependence of ligand binding, bacterial adhesion-inhibition studies were performed (Fig. 4). Here we used type 1-fimbriated *E. coli* binding to a mannan coated surfaces as model system. Adhesion of *E. coli* onto the mannan surface is promoted by mannose specific FimH receptors and can be reversed by addition of FimH binding molecules such as α-methyl D-mannopyranoside (MeMan).[28] The assay was performed with GFP-tagged *E. coli* and adhesion was inhibited with increasing concentrations of glycomacromole-

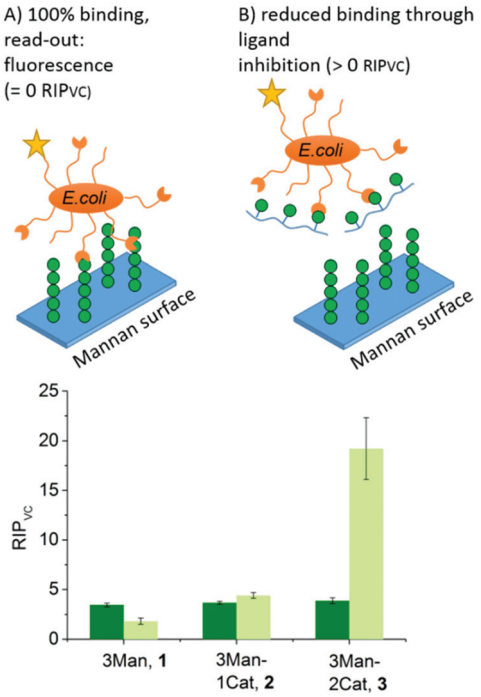

Fig. 4 Results of the *E. coli* adhesion-inhibition assay after 1 h (green) and 24 h (light green) incubation (schematic presentation of the assays are not to scale). Notably, none of the Gal-functionalized glycomacromolecules, with or without catechol, showed any inhibition in these assays (see ESI, Fig. S39–S41†).

cules giving half-maximum inhibitory concentration (IC_{50}) values by detecting the fluorescence signal.[19] Using MeMan as standard inhibitor, the IC_{50} value can be converted to the valency corrected relative inhibitory potential (RIP_{VC}) by referencing the IC_{50} values and number of Man per glycomacromolecule to MeMan allowing for comparison of values across different experiments.

Fig. 4 shows the RIP_{VC} values of glycomacromolecules **1–3** after 1 h (green) and 24 h (light green) incubation with *E. coli*. After 1 h, all Man-containing glycomacromolecules showed similar inhibition potentials, which is about 3.5 more effective per sugar in comparison to MeMan. These values are in the same range as for similar trivalent glycomacromolecules without Cat units as previously studied by our group in bacterial adhesion-inhibition studies.[19] Interestingly, incubating the structures with *E. coli* for 24 h significantly increases the efficacy of glycomacromolecule **3** by a factor of four while glycomacromolecules **1** and **2** remain at a similar inhibitory potential. This clear effect in longer incubation times for glycomacromolecule **3** again indicates the slow oxidation of the catechols and covalent binding over time. It also seems that binding with two Cat moieties leads to a more efficient blocking of the binding site than just one Cat. A possible explanation could be that if the glycomacromolecule is only attached *via* one chain end, the carbohydrate-containing scaffold can still unbind and release a free binding site, while a glycomacromolecule with Cat groups at both chain ends acts as a staple completely blocking the binding site.

Studying covalent attachment of catechol-functionalized precision glycomacromolecules

While the previous studies showed an effect of the introduction of Cat moieties on enhanced binding to ConA/FimH, we sought further support for a covalent attachment by examining glycomacromolecule-ConA complexes with MALDI-TOF. Equimolar amounts of ConA and glycomacromolecules were incubated for 24 h and then analysed by MALDI-TOF mass spectrometry.

Fig. 5 shows the MALDI-TOF measurement for ConA alone and in presence of glycomacromolecules **2** (Man and Cat) and **6** (Gal and Cat). The main mass peak for ConA was found to be 25.6 kDa, which represents the mass of monomeric ConA as the tetramer is divided into its subunits during measurement.[29] In presence of glycomacromolecules **2**, additional mass peaks were found at 27.8 kDa, 30.0 kDa and 32.2 kDa. The mass difference between these peaks is 2.2 kDa, which corresponds to the mass of the glycomacromolecule and thus shows covalent attachment of the ligand to ConA. The MALDI-TOF samples were further investigated by polyacrylamide gel electrophoresis under denaturating conditions (SDS-PAGE) to show spots corresponding to the mass of ConA and glycomacromolecules. Indeed, here we also observed additional spots with higher molecular weight for structure **2** and **3**, pointing towards the covalent attachment to the protein (see ESI†).

Surprisingly, MS data shows that multiple glycomacromolecules bound to one protein, here a maximum of three ligands per protein were detected. This indeed supports our hypothesis, that for glycomacromolecules with just one Cat, the carbohydrate-containing scaffold can still diffuse out of the binding site, which enables the binding of a second glycomacromolecule and successive coupling to the protein. This could then take place repeatedly until the binding site is too sterically hindered by previously attached glycomacromole-

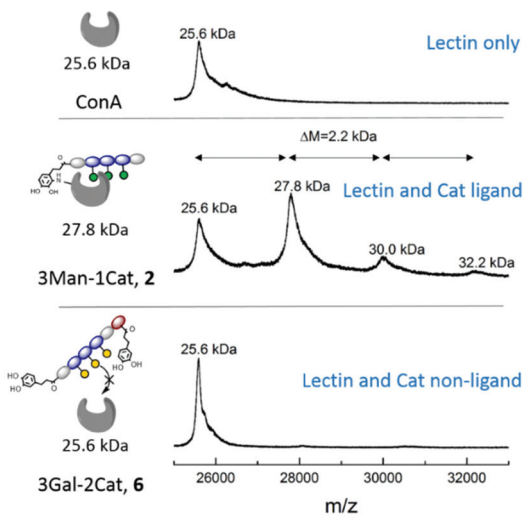

Fig. 5 MALDI-TOF MS measurement after 24 h incubation of glycomacromolecules with ConA.

cules to allow for another structure to bind. Similar behaviour was observed for ligand **3** presenting two catechol units but only with up to two bound oligomers per protein (see ESI†) indicating that two catechols more effectively anchor around the binding site which is also in agreement with the quantitative precipitation study. Importantly, no covalent attachment to the protein was observed for glycomacromolecule **1** presenting Man but no Cat and for Gal glycomacromolecules **5** and **6** with Cat (see ESI†).

Overall, these findings support our model of binding for Cat-functionalized glycomacromolecules where the Cat unit can only interact with ConA after initial binding mediated by the carbohydrate-containing scaffold and it is the interplay of both binding units that enables effective inhibition.

Conclusions

In summary, this study demonstrates the synthesis of Cat-functionalized glycomacromolecules and their potential to covalently inhibit lectin receptors. By investigating the clustering of ConA we could show that the introduction of a Cat moiety increases the apparent binding affinity of glycomacromolecules. The interaction between Cat and receptor seems to occur after initial binding of the carbohydrate-containing scaffold and only if the carbohydrate moiety binds to the targeted receptor. The effect of Cat increases over time, likely due to slow oxidation and covalent bonding. Strong evidence for covalent binding was found in an MALDI-TOF MS assay and confirmed *via* SDS-PAGE. Finally, we show the possible application of these glycomacromolecules to inhibit bacterial adhesion of *E. coli* to mannan coated surfaces. In order to evaluate whether these systems can also be applied to more complex biological settings and might have a long-term perspective for clinical use, future studies will have to further explore the combination of precision glycomacromolecules and Cat moieties and their inhibition potential.

Experimental

General procedure for solid phase synthesis

All glycomacromolecules were synthesized on solid support according to literature using the building blocks EDS (ethylene glycol diamine succinic acid), TDS and Fmoc-Lys(Boc).[26] Tentagel® S RAM was used as a resin, and the structures were synthesized by repetitive Fmoc cleavage and amide coupling. For Fmoc cleavage, the resin was treated with 20% piperidine in DMF for 30 min. For the amide coupling, the resin was treated with a solution of 5 eq. building block, 5 eq. PyBOP and 10 eq. DIPEA in DMF for 1 h. After assembly of the full sequence the lysine was deprotected on solid support using 4 M HCl in dioxane for 30 min. The catechol moiety was introduced at the terminal amine or deprotected lysine or both. For this the resin was treated with 5 eq. 3-(2,2-dimethylbenzo[*d*][1,3]dioxol-5-yl)propionic acid, 5 eq. PyBOP and 10 eq. DIPEA in DMF for 1 h. For oligomers without catechol the terminal amine was capped with acetic anhydride for 5 min. After assembly of the scaffold and either catechol coupling or end capping, sugars were introduced *via* an established CuAAC protocol.[26] Afterwards the sugars were deprotected on solid support using 0.1 M sodium methoxide in methanol. For final cleavage the resin was treated with 95% TFA, 2.5% TIPS and 2.5% DCM for 1 h. The glycomacromolecules were precipitated in diethyl ether and freeze dried.

Concentration dependent turbidity assay

A solution of 5 μM ConA in LBB buffer (10 mM HEPES, 50 mM NaCl, 1 mM $MnCl_2$, 1 mM $CaCl_2$, pH 7.4) was prepared. The transmission of 1 ml of this solution was measured as 100% transmission baseline. Afterwards glycomacromolecules were stepwise titrated to the ConA solution and after 20 min incubation the transmission was measured. Every structure was measured three times.

Quantitative precipitation assay

A solution of 15 μM ConA in LBB buffer (10 mM HEPES, 50 mM NaCl, 1 mM $MnCl_2$, 1 mM $CaCl_2$, pH 7.4) was prepared and the concentration was measured at 280 nm. Afterwards aliquots of this solution were mixed with different concentrations of glycomacromolecules, incubated for 24 h and centrifuged for 5 min at 4400 rpm. The precipitate was resuspended in LBB buffer with 50 mM α-methyl D-mannoside and the ConA concentration was determined at 280 nm. To calculate the amount of ConA precipitated per ligand the linear slope between 1 and 5 μM ligand was used.

MALDI-TOF measurement

For the determination of a covalent bond between ConA and ligand, equimolar amounts of ConA (8 μM) and glycomacromolecule (8 μM) were incubated in LBB buffer (10 mM HEPES, 50 mM NaCl, 1 mM $MnCl_2$, 1 mM $CaCl_2$, pH 7.4) for 24 h. Afterwards the samples were filtrated and measured *via* MALDI-TOF in linear mode.

Bacterial adhesion-inhibition assay

The *E. coli* strain PKL1162 was cultured from a stock in LB media (ampicillin 100 mg ml^{-1} and chloramphenicol 50 mg ml^{-1}) at 37 °C overnight. The bacterial cells were centrifuged and washed twice and suspended in PBS buffer to a cell concentration of OD_{600} = 0.4. The adhesion-inhibition assay was conducted as described prior in this working group.[19] Black 96-well microtiter plates (Nunc, MaxiScorp) were treated with mannan (1.2 mg ml^{-1} in carbonate buffer pH 9.6) for 12 h at 37 °C until full evaporation of water. The plates were washed three times with PBST buffer (PBS buffer + 0.05% v/v Tween®20) and blocked with PVA (1% in PBS) for 2 h. Afterwards the plates were washed with PBST twice and PBS once. For the measurement a serial dilution of glycomacromolecules on the mannan-coated microtiter plates was performed (50 μl). The bacterial suspension was added (50 μl) and the plates were incubated for either 1 h or 24 h at 37 °C. After incu-

bation the microtiter plates were washed three times with PBS and refilled with PBS (100 μl) to measure the fluorescence intensity (excitation 485 nm, emission 535 nm).

Conflicts of interest

There are no conflicts to declare.

Acknowledgements

We thank Dr Monir Tabatabai and Jun.-Prof. Dr Stephan Schmidt for their helpful discussions and the Heinrich Heine University (HHU) for its support.

References

1 P. R. Crocker and T. Feizi, *Curr. Opin. Struct. Biol.*, 1996, **6**, 679–691.
2 A. Varki, *Glycobiology*, 1993, **3**, 97–130.
3 S. D. Rosen, *Semin. Immunol.*, 1993, **5**, 237–247.
4 H. Ghazarian, B. Idoni and S. B. Oppenheimer, *Acta Histochem.*, 2011, **113**, 236–247.
5 N. Sharon and H. Lis, *Glycobiology*, 2004, **14**, 53R–62R.
6 Y. Takenaka, T. Fukumori and A. Raz, *Glycoconjugate J.*, 2002, **19**, 543–549.
7 S. L. Chen, C. S. Hung, J. S. Pinkner, J. N. Walker, C. K. Cusumano, Z. Li, J. Bouckaert, J. I. Gordon and S. J. Hultgren, *Proc. Natl. Acad. Sci. U. S. A.*, 2009, **106**, 22439–22444.
8 H. Koo, R. N. Allan, R. P. Howlin, P. Stoodley and L. Hall-Stoodley, *Nat. Rev. Microbiol.*, 2017, **15**, 740.
9 A. Bernardi, J. Jiménez-Barbero, A. Casnati, C. De Castro, T. Darbre, F. Fieschi, J. Finne, H. Funken, K.-E. Jaeger and M. Lahmann, *Chem. Soc. Rev.*, 2013, **42**, 4709–4727.
10 S. Cecioni, A. Imberty and S. Vidal, *Chem. Rev.*, 2015, **115**, 525–561.
11 T. K. Dam, R. Roy, S. K. Das, S. Oscarson and C. F. Brewer, *J. Biol. Chem.*, 2000, **275**, 14223–14230.
12 M. Hartmann and T. K. Lindhorst, *Eur. J. Org. Chem.*, 2011, **2011**, 3583–3609.
13 X.-L. Sun, *Curr. Med. Chem.*, 2007, **14**, 2304–2313.
14 B. Ernst and J. L. Magnani, *Nat. Rev. Drug Discovery*, 2009, **8**, 661–677.
15 S. Wagner, D. Hauck, M. Hoffmann, R. Sommer, I. Joachim, R. Müller, A. Imberty, A. Varrot and A. Titz, *Angew. Chem., Int. Ed.*, 2017, **56**, 16559–16564.
16 S. Ito, T. Kato and K. Fujita, *Biochem. Pharmacol.*, 1988, **37**, 1707–1710.
17 L. Giannola, V. De Caro, G. Giandalia, M. Siragusa and L. Lamartina, *Die Pharmazie – Int. J. Pharm. Sci.*, 2008, **63**, 704–710.
18 M. Carafa, C. Marianecci, L. D. Marzio, V. D. Caro, G. Giandalia, L. I. Giannola and E. Santucci, *J. Liposome Res.*, 2010, **20**, 250–257.
19 S. Boden, F. Reise, J. Kania, T. K. Lindhorst and L. Hartmann, *Macromol. Biosci.*, 2019, **19**, e1800425.
20 M. Baier, N. H. Rustmeier, J. Harr, N. Cyrus, G. J. Reiss, A. Grafmüller, B. S. Blaum, T. Stehle and L. Hartmann, *Macromol. Biosci.*, 2019, **19**, 1800426.
21 T. Freichel, D. Laaf, M. Hoffmann, P. B. Konietzny, V. Heine, R. Wawrzinek, C. Rademacher, N. L. Snyder, L. Elling and L. Hartmann, *RSC Adv.*, 2019, **9**, 23484–23497.
22 D. Ponader, F. Wojcik, F. Beceren-Braun, J. Dernedde and L. Hartmann, *Biomacromolecules*, 2012, **13**, 1845–1852.
23 Q. Wei, K. Achazi, H. Liebe, A. Schulz, P. L. M. Noeske, I. Grunwald and R. Haag, *Angew. Chem., Int. Ed.*, 2014, **53**, 11650–11655.
24 V. Wittmann, *Curr. Opin. Chem. Biol.*, 2013, **17**, 982–989.
25 J. E. Gestwicki, C. W. Cairo, L. E. Strong, K. A. Oetjen and L. L. Kiessling, *J. Am. Chem. Soc.*, 2002, **124**, 14922–14933.
26 C. Gerke, M. F. Ebbesen, D. Jansen, S. Boden, T. Freichel and L. Hartmann, *Biomacromolecules*, 2017, **18**, 787–796.
27 Y. Gou, J. Geng, S. J. Richards, J. Burns, C. Remzi Becer and D. Haddleton, *J. Polym. Sci., Part A: Polym. Chem.*, 2013, **51**, 2588–2597.
28 T. K. Lindhorst, S. Oscarson and J. Bouckaert, *Glycoscience and Microbial Adhesion*, Springer, 2009.
29 K. Sparbier, T. Wenzel and M. Kostrzewa, *J. Chromatogr. B: Anal. Technol. Biomed. Life Sci.*, 2006, **840**, 29–36.

Supporting Information

Catechol-functionalized sequence-defined glycomacromolecules as covalent inhibitors of bacterial adhesion

Lukas Fischer,[a] Ricarda Steffens [a], Tanja J. Paul,[a] Laura Hartmann [a*]

[a] *Institut für Organische und Makromolekulare Chemie, Heinrich-Heine-Universität Düsseldorf, Universitätsstr. 1, 40225 Düsseldorf, Germany*

Materials

2-Bromoethanol (Carbolution), 2-chloroethanol (Sigma Aldrich), 3-(3,4-dihydroxyphenyl)propionic acid (abcr), acetic anhydride (VWR Chemicals), aceton (Carl Roth), acetonitrile (Sigma Aldrich), succinic anhydride (99%, Acros), boron trifluoride diethyl etherate (98%, Alfa Aesar), calcium chloride (Panreac AppliChem), chloroform-d (Deutero), citric acid (Fisher Chemical), Concanavalin A type IV (Sigma Aldrich), deuterium oxide (Deutero), 1,8-diazabiscyclo[5.4.0]undec-7-ene (Fluorochem), dichloromethane (VWR Prolabo), diethylenetriamine (Carl Roth), diethyl ether (VWR Prolabo), dimethylsulfoxide-d_6 (Deutero), 1,4-Dioxane (Fisher Chemical), D(+)-mannose (99%, Acros), acetic acid (VWR Chemicals), ethanol (Carl Roth), ethyl acetate (VWR-Prolabo), ethylenediamine (Sigma Aldrich), galactose pentaacetate (Fluorochem), 2-(4-(2-hydroxyethyl)-1-piperazinyl)-ethanesulfonic acid (Fisher Scientific), potassium carbonate (Fisher Scientific), copper sulfate (Acros), magnesium sulfate (Fisher Chemical), manganese chloride (Sigma Aldrich), methanol (VWR Prolabo), methanol-d_4 (Deutero), *N,N*-dimethylformamide (VWR Prolabo), sodium ascorbate (Panreac AppliChem), sodium azide (Panreac AppliChem), sodium chloride (98%, Sigma Aldrich), sodium diethyldithiocarbamate (Alfa Aesar), sodium dodecyl sulfate (Carl Roth), sodium bicarbonate (VWR-Chemicals), sodium methoxide (Sigma Aldrich), hexane (VWR Prolabo), oxalyl chloride (Alfa Aesar), 4-pentynoic acid (Sigma Aldrich), phosphorus trichloride (Sigma Aldrich), piperidine (Acros), *p*-toluenesulfonic acid (Sigma Aldrich), (benzotriazol-1-yloxy)-tripyrrolidin-phosphonium hexafluorophosphate (PyBOP) (Carbolution), hydrochloric acid (37%, VWR Chemicals), sulphuric acid (Sigma Aldrich), Tentagel® S RAM (Rapp Polymere), tetrahydrofuran (Sigma Aldrich), trichloroacetonitrile (Fluorochem), triethylamine (Acros Organics), triethylsilane (TCI Chemicals), trifluororacetic acid (Acros), trifluoroacetate (Acros Organics) triisopropylsilane (Sigma Aldrich), trimethylsilyl azide (Sigma Aldrich), trityl chloride (Acros Organics), vanillin (Caelo), tin(IV) chloride (Fisher Scientific).

Instrumentation

Nuclear Magnetic Resonance Spectroscopy (NMR)

^{1}H-NMR and ^{13}C NMR were recorded on a Bruker Avance III 300, a Bruker Avance DRX-500 or a Bruker Avance III 600. Chemical shifts were reported as delta (δ) in parts per million (ppm) and coupling constants as *J* in Hertz (Hz). Multiplicities are stated as following: s = singlet, d = doublet, t = triplet, q = quartet, m = multiplet.

High Resolution-Mass Spectrometry (HR-MS)

HR-MS measurements were conducted on a Bruker UHR-QTOF maxis 4G with a direct inlet via syringe pump, an ESI source and a quadrupole Time of Flight (QTOF) analyzer. Samples were dissolved in water with a concentration of 1 mg/ml.

Matrix-assisted Laser Desorption Ionisation-Time of Flight (MALDI-TOF)-Mass Spectrometry

MALDI-TOF measurements were conducted on a Ultraflex I from Bruker Daltonics. The samples were measured in linear mode with cyano-4-hydroxycinnamic acid (HCCA) as matrix in a ratio of 1:2. As a solvent acetonitrile with 0.1% TFA was used.

Reversed Phase-High Pressure Liquid Chromatography (RP-HPLC)

RP-HPLC was performed with an Agilent 1260 Infinity instrument coupled to a variable wavelength detector (VWD) set to 214 nm. As a column a Poroshell 120 EC-C18 1.8 µM (3.0x50 mm, 2.5 µM) reversed phase column was used. The mobile phase A consisted of 95/5 H_2O/MeCN with 0.1% formic acid and mobile phase B consisted of 95/5 MeCN/H_2O with 0.1% formic acid. The flowrate for all measurements was 0.4 ml/min.

UV/Vis-Spectroscopy

The UV/Vis measurements were done on a „Specord 210 Plus“ from Analytik Jena AG. For the measurement a quartz cuvette from Hellma Analytics with a thickness of 1 cm and a volume of 1 ml was used.

Freeze Dryer

Lyophilization of the final structures was conducted on an Alpha 1-4 LD plus instrument from Martin Christ Freeze Dryers GmbH. The lyophilisation was done at a pressure of 0.1 mbar.

Building Block Synthesis and Analytics

1-(2-azidoethyl)-2,3,4,6-tetra-O-acetyl-α-D-mannose

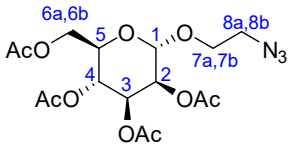

The synthesis was done following literature.[1]

Yield: 19.48 g (46.60 mmol, 77%).

^{1}H-NMR (300 MHz, $CDCl_3$): δ (ppm) 5.35 (dd, J_{HH} = 10.0 Hz, 3.2 Hz, 1H, H3), 5.32-5.24 (m, 2H, H2, H4), 4.86 (d, J_{HH} = 1.7 Hz, 1H, H1), 4.28 (dd, J_{HH} = 12.3, 5.3 Hz, 1H, H5), 4.11 (dd, J_{HH} = 12.2 Hz, 2.5 Hz, 1H, H6a), 4.03 (ddd, J_{HH} = 9.5 Hz, 5.3 Hz, 2.4 Hz, 1H, H6b), 3.86 (ddd, J_{HH} = 10.6 Hz, 6.6 Hz, 4.0 Hz, 1H, H7a), 3.66 (ddd, J_{HH} = 10.6 Hz, 5.8 Hz, 3.7 Hz, 1H, H7b), 3.54-3.40 (m, 2H, H8a, H8b), 2.15 (s, 3H, C(O)CH_3), 2.09 (s, 3H, C(O)CH_3), 2.04 (s, 3H, C(O)CH_3), 1.98 (s, 3H, C(O)CH_3).

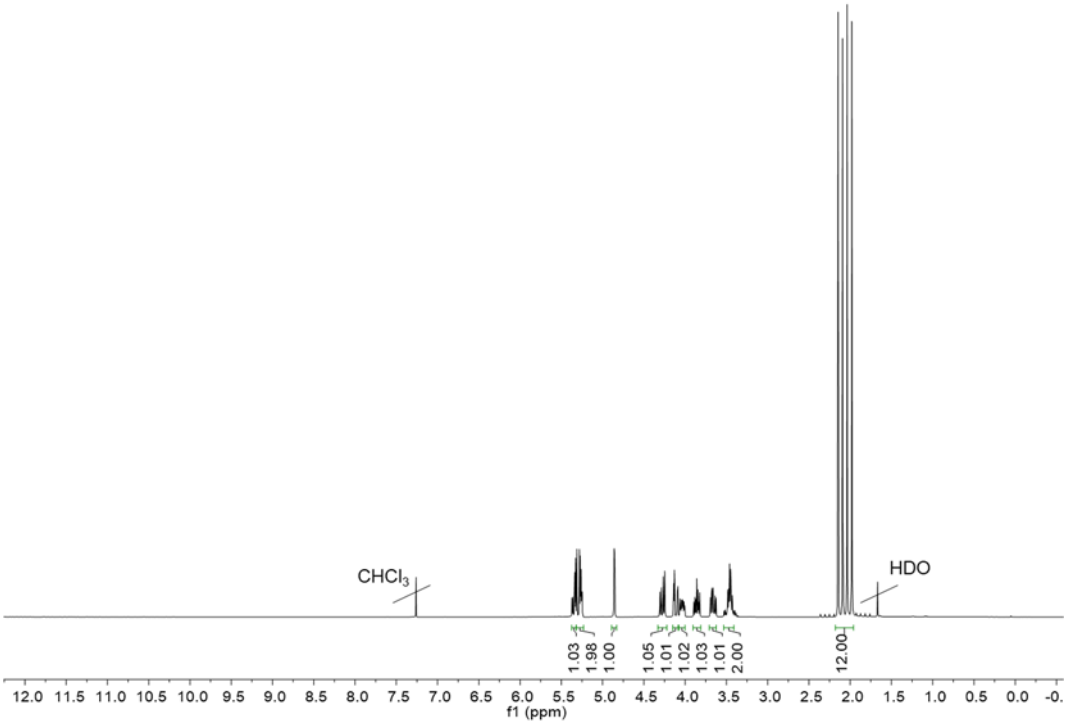

Figure S1: ^{1}H-NMR (300 MHz, $CDCl_3$) of *1-(2-azidoethyl)-2,3,4,6-tetra-O-acetyl-α-D-mannose.*

1-(2-azidoethyl)-2,3,4,6-tetra-O-acetyl-β-galactose

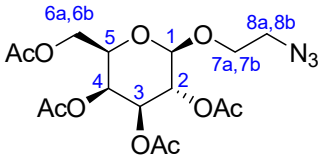

The synthesis was done following literature.[2]

Yield: 2.20 g (5.28 mmol, 72%).

^{1}H-NMR (300 MHz, $CDCl_3$): δ (ppm) 5.36 (dd, J_{HH} = 3.4 Hz, 1.2 Hz, 1H, H3), 5.20 (dd, J_{HH} =10.5 Hz, 7.9 Hz, 1H, H2), 4.99 (dd, J_{HH} = 10.5 Hz, 3.4 Hz, 1H, H4), 4.53 (d, J_{HH} = 7.9 Hz, 1H, H1), 4.17-3,97 (m, 3H, H5, H6a, H6b), 3.90 (td, J_{HH} = 6.6 Hz, 1.2 Hz, 1H, H7a), 3.66 (ddd, J_{HH} = 10.6 Hz, 8.4 Hz, 3.4 Hz, 1H, H7b), 3.47 (ddd, J_{HH} = 13.3 Hz, 8.4 Hz, 3.5 Hz, 1H, H8a), 3.27 (ddd, J_{HH} = 13.4 Hz, 4.8 Hz, 3.4 Hz, 1H, H8b), 2.12 (s, 3H, C(O)CH_3), 2.03 (s, 3H, C(O)CH_3), 2.01 (s, 3H, C(O)CH_3), 1.95 (s, 3H, C(O)CH_3).

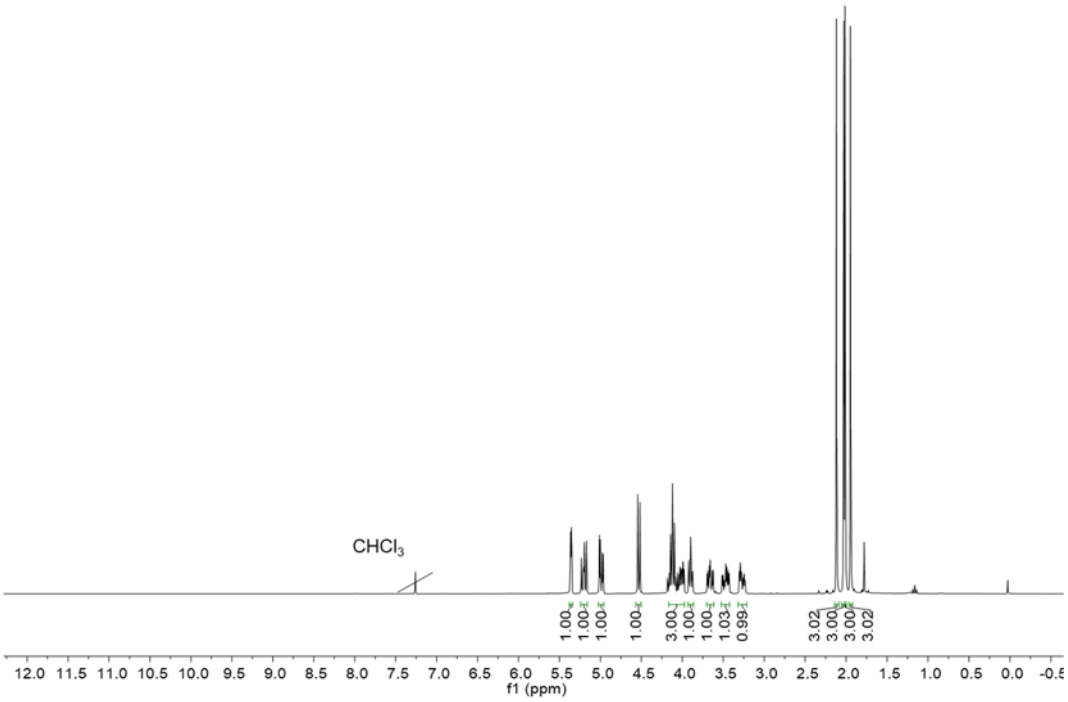

Figure S2: ^{1}H-NMR (300 MHz, $CDCl_3$) of *1-(2-azidoethyl)-2,3,4,6-tetra-O-acetyl-β-galactose.*

3-(2,2-dimethylbenzo[d][1,3]dioxol-5-yl)propionic acid

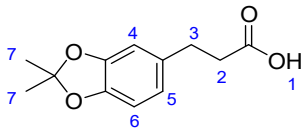

The synthesis was done following literature.[3]

Yield: 10.68 g (51.45 mmol, 57%).

^{1}H-NMR (300 MHz, DMSO-d_6) δ (ppm) 6.73-6.70 (m, 3H, H4, H5, H6), 2.74 (t, J_{HH} = 7.5 Hz, 2H, H3), 2.50 (t, J_{HH} = 7.5 Hz, 2H, H2), 1.60 (s, 6H, H7).

RP-HPLC (Eluent B from 0% to 100% in 17 min): t_r = 9.95 min, relative purity 99%.

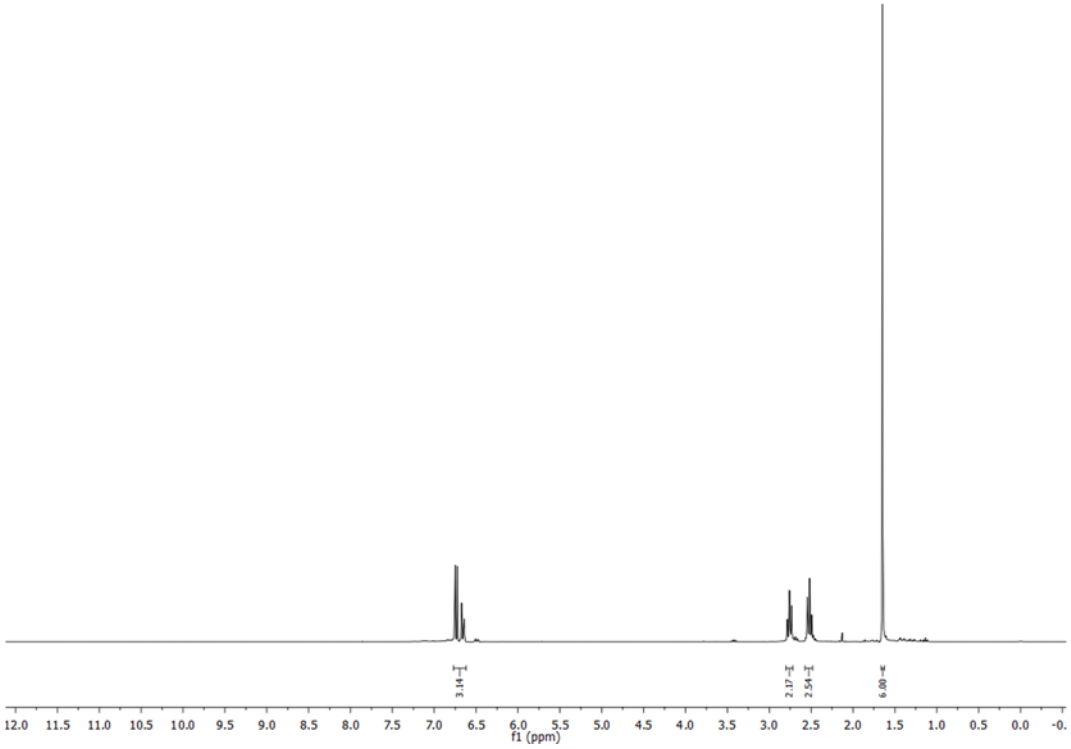

Figure S3: ^{1}H-NMR (300 MHz, DMSO-d_6) of *3-(2,2-dimethylbenzo[d][1,3]dioxol-5-yl)propionic acid*.

1-(9H-fluoren-9-yl)-3,11-dioxo-7-(pent-4-ynoyl)-2-oxa-4,7,10-triazatetradecan-14-oic acid (TDS)

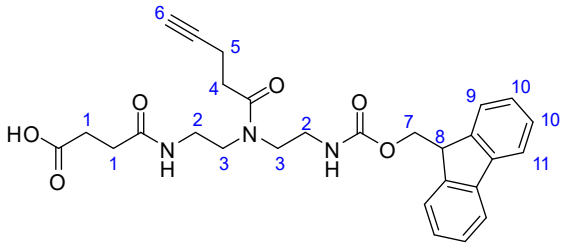

The synthesis was done following literature.[4]

Yield: 12.46 g (24.7 mmol, 38%).

^{1}H-NMR (300 MHz, DMSO-d_6): δ (ppm) 8.03 (t, J_{HH} = 6.2 Hz, 1H, NH), 7.88 (d, J_{HH} = 7.5 Hz, 2H, H11), 7.67 (dd, J_{HH} = 7.5 Hz, 3.0 Hz, 2H, H9), 7.47-7.38 (m, 4H, H10, NH), 7.36-7.30 (m, 4H, H10), 4.30 (dd, J_{HH} = 17.0 Hz, 6.9 Hz, 2H, H7), 4.20 (t, J_{HH} = 6.9 Hz, 1H, H8), 3.33-3.23 (m, 4H, H2), 3.18-3.03 (m, 4H, H3), 2.73 (t, J_{HH} = 2.8 Hz, 1H, H6), 2.41-2.24 (m, 6H, H4, H1).

RP-HPLC (Eluent B from 0% to 100% in 30 min): t_r = 10.28 min, relative purity 99%.

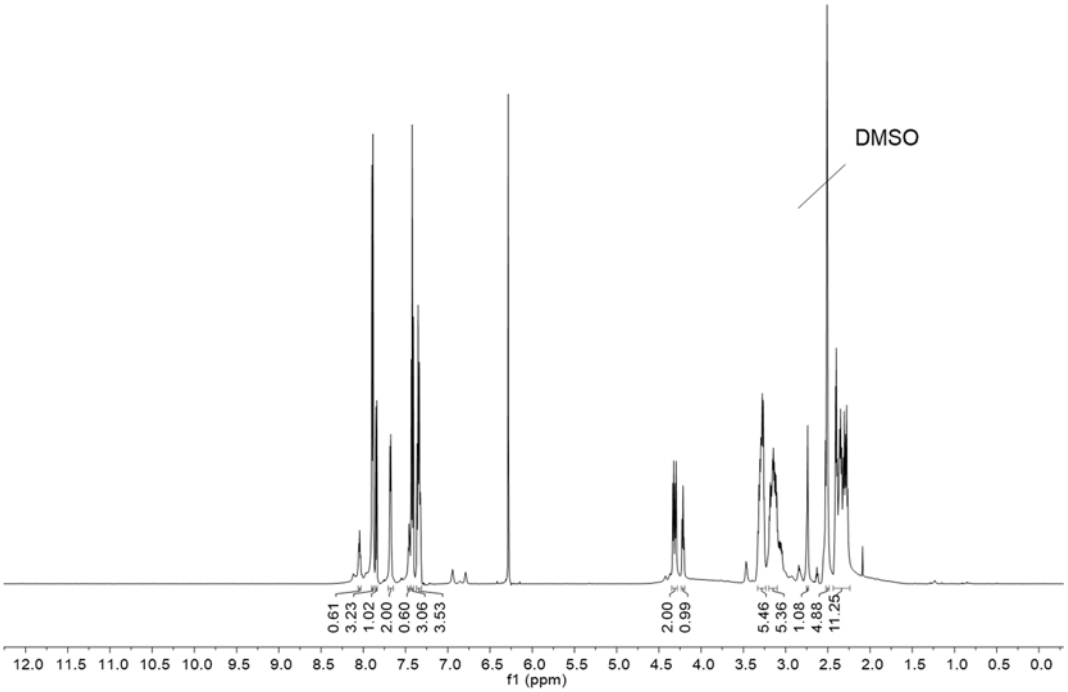

Figure S4: ^{1}H-NMR (300 MHz, DMSO-d_6) of *1-(9H-fluoren-9-yl)-3,11-dioxo-7-(pent-4-ynoyl)-2-oxa-4,7,10-triazatetradecan-14-oic acid (TDS).*

Solid Phase Synthesis and Analytics

All glycomacromolecules were synthesized on solid support according to literature using the building blocks EDS, TDS and Fmoc-Lys(Boc).[5] For functionalization the lysine was deprotected on solid support using 4 M HCl in dioxane for 30 min. The catechol moiety was introduced at the terminal amine or deprotected lysine or both. For this the resin was treated with 5 eq. 3-(2,2-dimethylbenzo[d][1,3]dioxol-5-yl)propionic acid, 5eq. PyBOP and 10 eq. DIPEA in DMF for 1 h. For glycomacromolecules without catechol the terminal amine was capped with acetic anhydride for 5 min. After assembly of the scaffold and either catechol coupling or end capping, sugars were introduced via an established CuAAC protocol.[5] Afterwards the sugars were deprotected on solid support using 0.1 M sodium methoxide in methanol. For final cleavage the resin was treated with 95% TFA, 2.5% TIPS and 2.5% DCM for 1h. The glycomacromolecules were precipitated in diethyl ether and freeze dried. For all structures Tentagel® S RAM as a resin was used.

3Man (**1**)

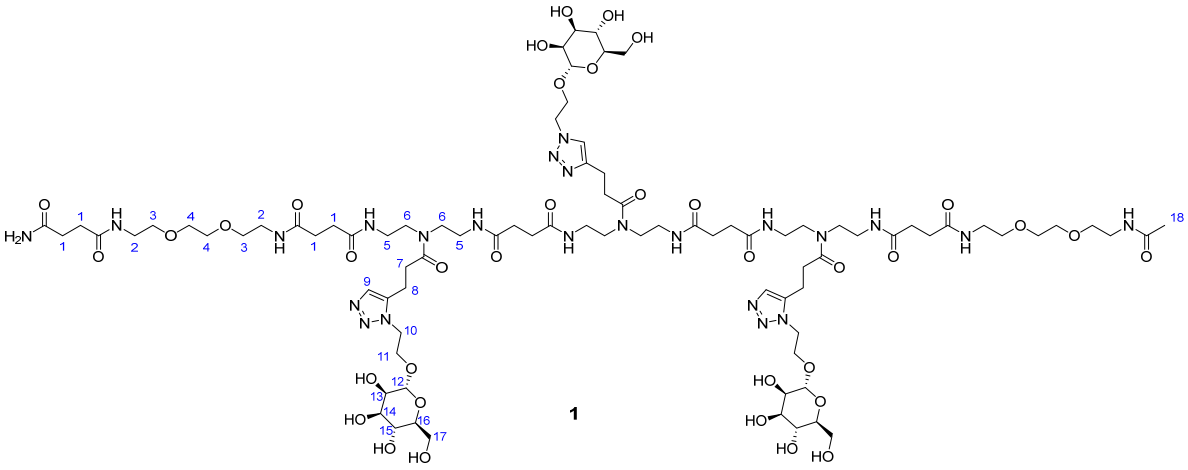

1

Yield: 233 mg (75%).

^{1}H-NMR (600 MHz, D_2O) δ (ppm) 7.97-7.95 (m, 3H, H9), 4.67-4.64 (m, 6H, H10), 4.11-4.08 (m, 3H, H11), 3.94 -3.88 (m, 3H, H11), 3.85-3.82 (m, 3H, H13), 3.74-3.72 (m, 3H, H14), 3.67-3.56 (m, 25H, H3, H4, H15, H17), 3.47-3.33 (m, 32H, H2, H5, H6), 3.08-3.04 (m, 3H, H16), 3.02-2.98 (m, 6H, H7), 2.81-2.77 (m, 6H, H8), 2.56-2.40 (m, 20H, H1), 1.97 (s, 3H, H18).

^{13}C-NMR (150 MHz, D_2O) δ (ppm) 178.59, 175.91, 175.81, 175.76, 175.73, 175.65, 175.62, 175.57, 175.54, 175.41, 175.15, 163.98, 163.75, 163.51, 147.07, 147.07, 125.60, 125.58, 125.55, 118.24, 116.31, 100.50, 73.83, 71.43, 70.87, 70.56, 70.41, 70.39, 69.82, 69.80, 69.75, 67.36, 66.24, 61.68, 51.52, 51.50, 48.08, 48.06, 46.08, 46.06, 46.04, 39.94, 39.88, 38.28, 37.85, 32.71, 31.98, 31.89, 31.85, 31.80, 31.76, 31.72, 31.58, 31.32, 22.77, 21.22.

HR-ESI-MS: calculated mass for $C_{85}H_{143}N_{23}O_{36}$ $[M+3H]^{3+}$: 688.3428, found 688.3427.

RP-HPLC (Eluent B from 0% to 100% in 30 min): t_r = 8.41 min, relative purity 94%.

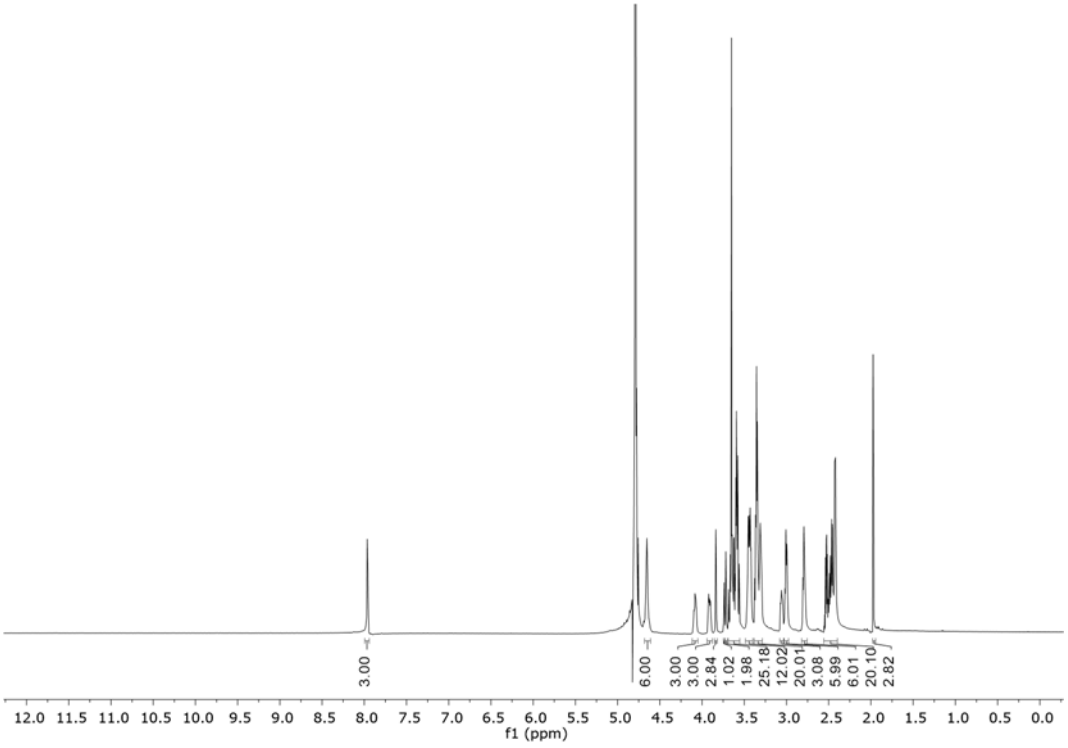

Figure S5: ^{1}H-NMR (600 MHz in D_2O) of 3Man (**1**).

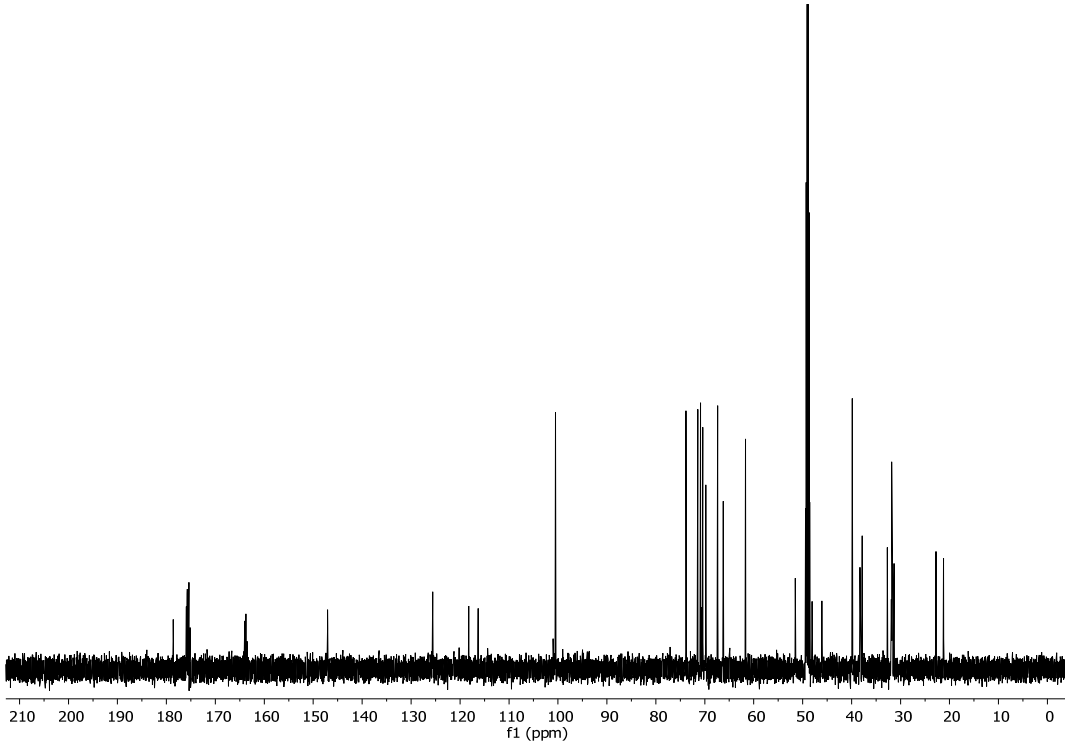

Figure S6: ^{13}C-NMR (150 MHz in D_2O) of 3Man (**1**).

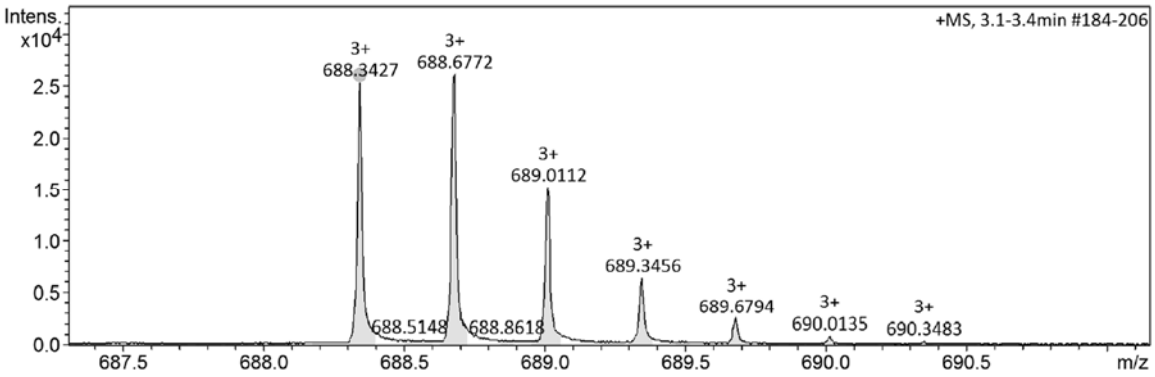

Figure S7: HR-ESI (ESI$^+$ Q-TOF) of 3Man (**1**).

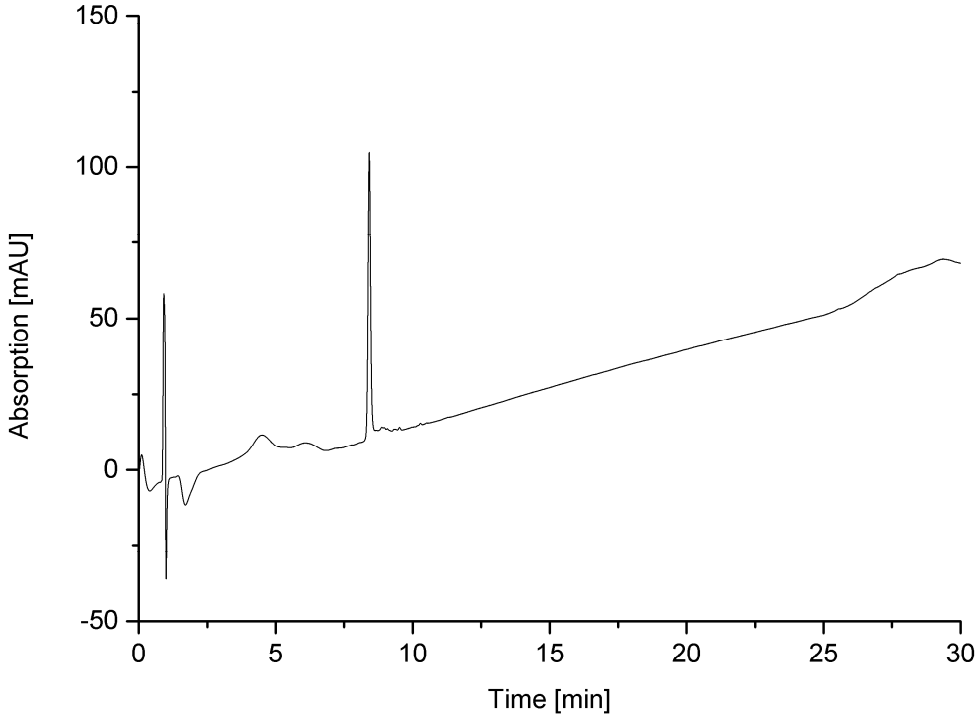

Figure S8: RP-HPLC chromatogram of 3Man (**1**) (gradient from 0% to 50% eluent B over 30 min at 25°C).

3Man-1Cat (**2**)

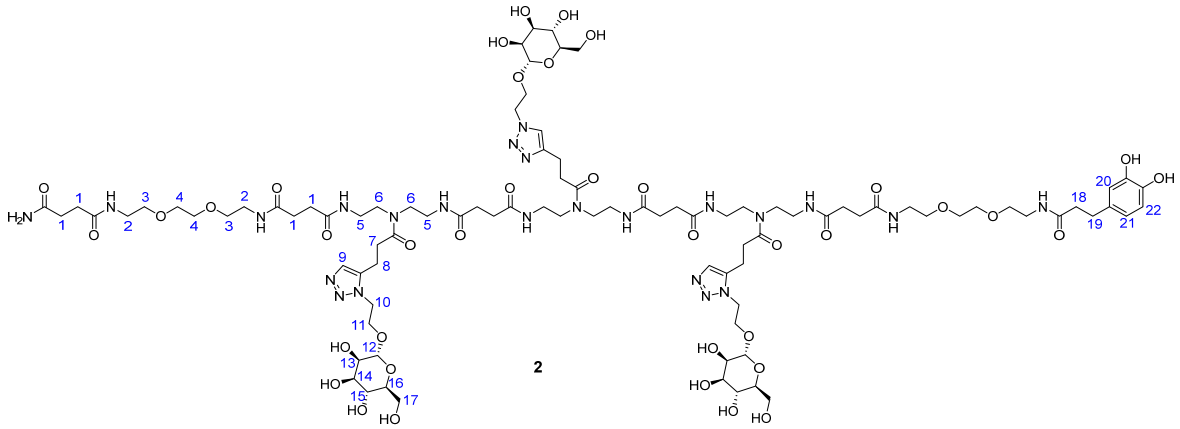

Yield: 315 mg (96%).

^{1}H-NMR (600 MHz, D_2O) δ (ppm) 8.01-7.95 (m, 3H, H9), 6.85 (d, J_{HH} = 8.0 Hz, 1H, H20), 6.78 (d, J_{HH} = 1.9 Hz, 1H, H22), 6.69 (dd, J_{HH} = 8.2 Hz, 2.1 Hz, 1H, H21), 4.71-4.67 (m, 6H, H10), 4.17-4.10 (m, 3H, H11), 4.00-3.93 (m, 3H, H11), 3.91-3.88 (m, 3H, H13), 3.82-3.78 (m, 3H, H14), 3.75-3.60 (m, 25H, H3,

H4, H15, H17), 3.56-3.34 (m, 32H, H2, H5, H6), 3.32 (t, J_{HH} = 5.3 Hz, 2H, H18), 3.15-3.10 (m, 3H, H16), 3.08-3.02 (m, 6H, H7), 2.88-2.80 (m, 8H, H8, H19), 2.61-2.46 (m, 20H, H1).

^{13}C-NMR (150 MHz, D_2O) δ (ppm) 176.61, 175.73, 175.71, 175.64, 175.62, 175.57, 175.55, 175.47, 175.42, 147.17, 144.78, 143.19, 125.37, 125.32, 121.52, 118.42, 117.06, 117.03, 116.10, 100.48, 73.79, 71.43, 70.85, 70.40, 70.36, 69.90, 69.76, 69.71, 67.37, 66.24, 61.66, 51.35, 48.09, 48.06, 46.10, 46.06, 39.85, 38.50, 38.30, 37.86, 32.70, 31.98, 31.88, 31.86, 31.81, 31.74, 31.61, 31.56, 31.32, 21.27.

HR-ESI-MS: calculated mass for $C_{92}H_{149}N_{23}O_{38}$ $[M+3H]^{3+}$: 729.0217, found 729.0213.

RP-HPLC (Eluent B from 0% to 100% in 30 min): t_r = 10.17 min, relative purity 98%.

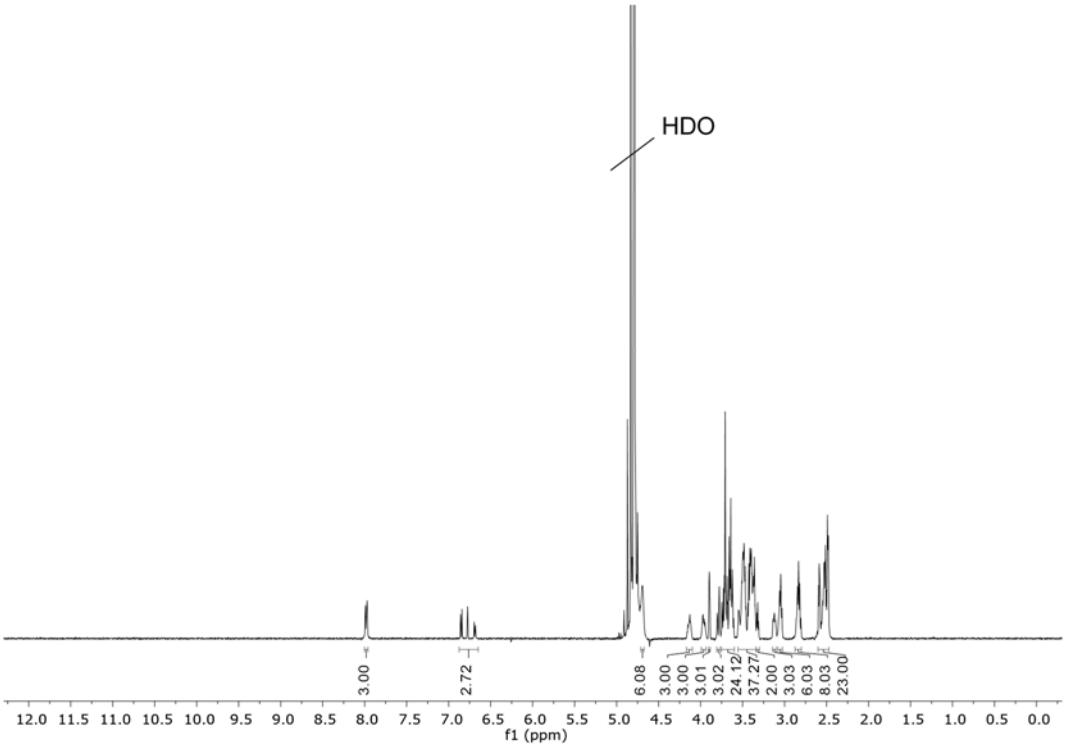

Figure S9: ^{1}H-NMR (600 MHz in D_2O) of 3Man-1Cat (**2**).

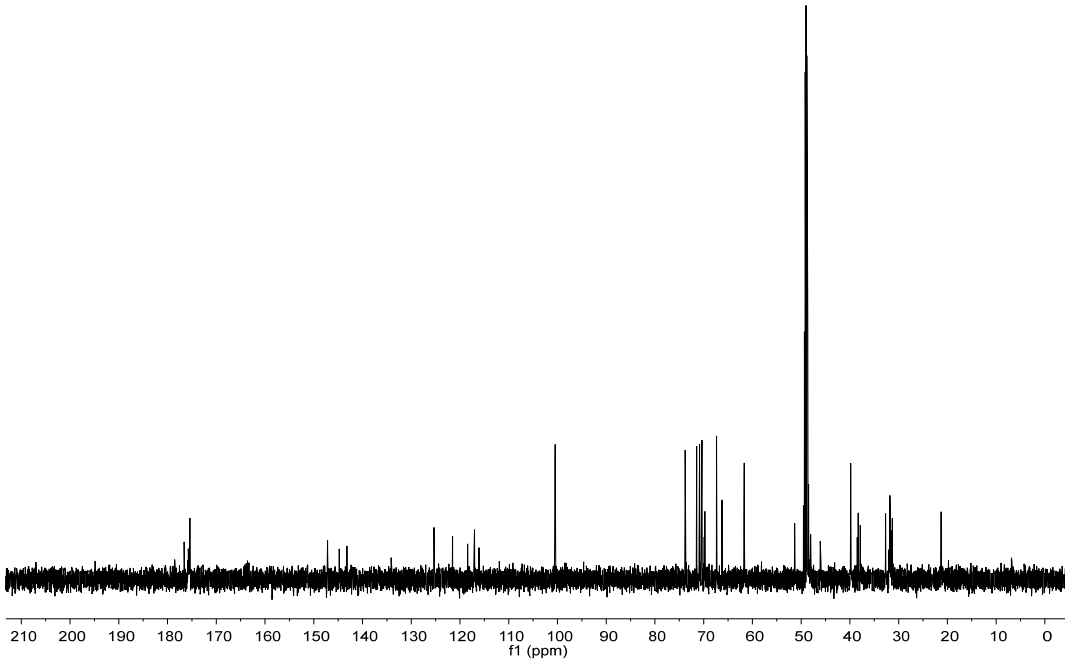

Figure S10: ^{13}C-NMR (150 MHz in D_2O) of 3Man-1Cat (**2**).

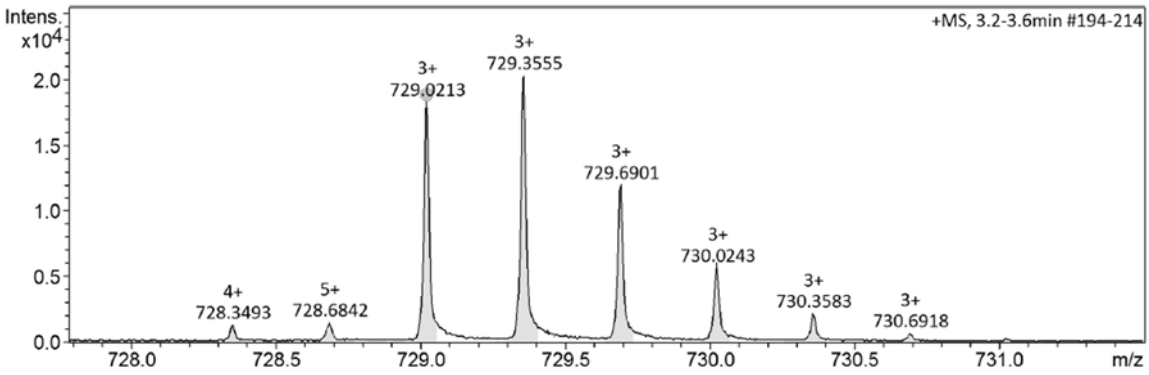

Figure S11: HR-ESI (ESI$^+$ Q-TOF) of 3Man-1Cat (**2**).

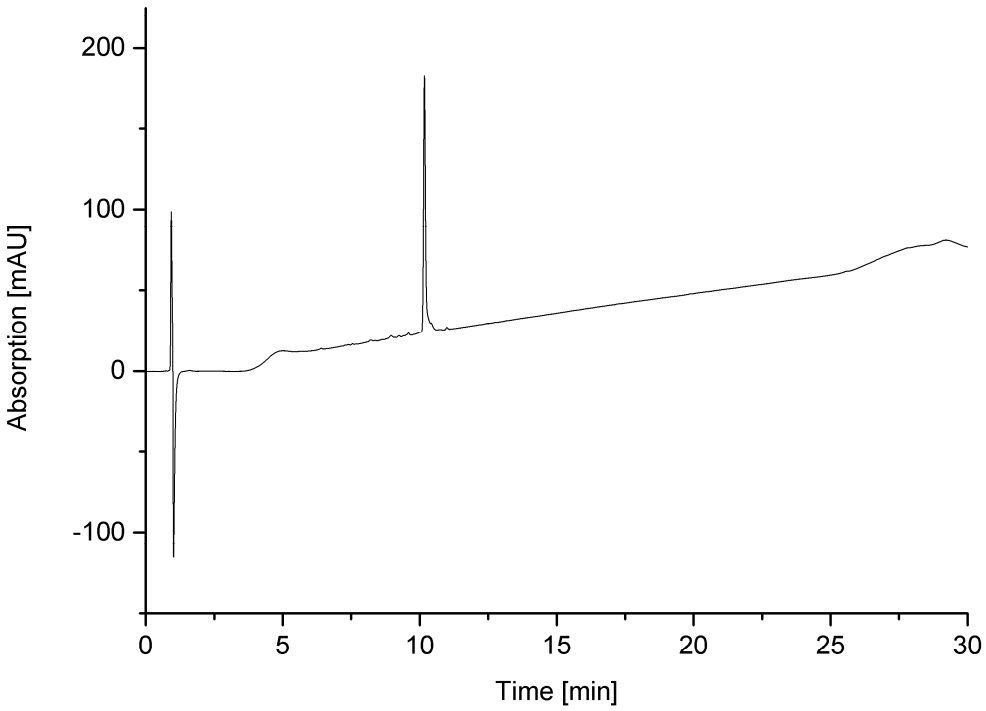

Figure S12: RP-HPLC chromatogram of 3Man-1Cat (**2**) (gradient from 0% to 50% eluent B over 30 min at 25°C).

3Man-2Cat (**3**)

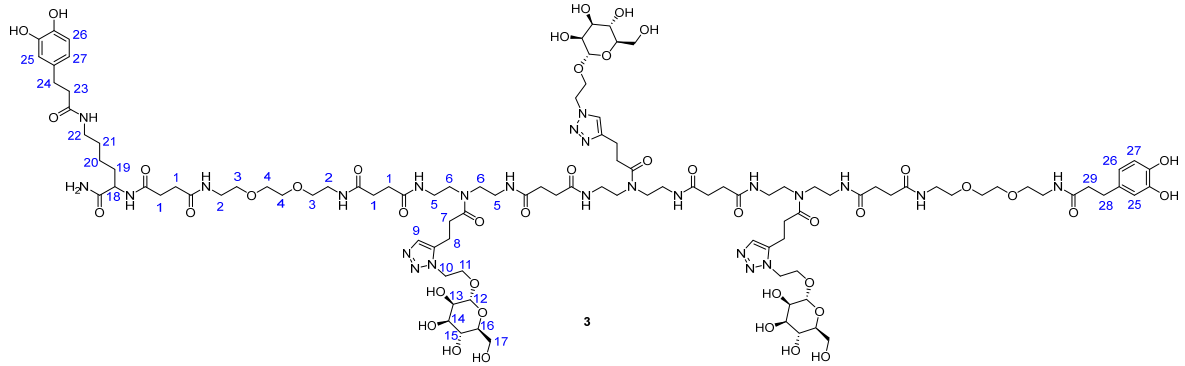

Yield: 214 mg (58%).

^{1}H-NMR (600 MHz, D_2O) δ (ppm) 7.94-7.89 (m, 3H, H9), 6.81 (dd, J_{HH} = 8.1 Hz, 4.5 Hz, 2H, H25), 6.74 (s, 2H, H26), 6.68-6.63 (m, 2H, H27), 4.66-4.63 (m, 6H, H10), 4.16 (dd, J_{HH} = 9.3 Hz, 5.0 Hz, 1H, H18), 4.12-4.06 (m, 3H, H11), 3.95-3.89 (m, 3H, H11), 3.87-3.84 (m, 3H, H13), 3.78-3.73 (m, 3H, H14), 3.72-3.56 (m, 25H, H3, H4, H15, H17), 3.54-3.28 (m, 44H, H2, H5, H6, H29), 3.12-3.05 (m, 5H, H16, H23),

3.03-2.98 (m, 6H, H7), 2.83-2.76 (m, 10H, H8, H28), 2.61-2.55 (m, 4H, H22, H24), 2.52-2.42 (m, 20H, H1), 1.76-1.68 (m, 1H, H19), 1.65-1.57 (m, 1H, H19), 1.35-1.28 (m, 2H, H21), 1.21-1.08 (m, 2H, H20).

^{13}C-NMR (150 MHz, D_2O) δ (ppm) 175.72, 175.58, 175.43, 175.42, 147.38, 144.86, 143.27, 125.17, 125.14, 125.13, 121.56, 121.48, 118.48, 117.18, 117.11, 117.10, 117.07, 117.05, 117.00, 116.16, 100.54, 73.84, 71.50, 70.93, 70.57, 70.41, 69.94, 69.80, 67.42, 66.30, 61.72, 51.21, 48.06, 46.13, 39.90, 39.86, 39.67, 38.65, 38.34, 37.90, 32.79, 31.91, 31.89, 31.80, 31.76, 31.73, 31.66, 31.64, 31.59, 31.55, 31.55, 23.29, 21.41.

HR-ESI-MS: calculated mass for $C_{107}H_{169}N_{25}O_{42}$ $[M+3H]^{3+}$: 826.7370, found 826.7370.

RP-HPLC (Eluent B from 0% to 100% in 30 min): t_r = 11.70 min, relative purity 90%.

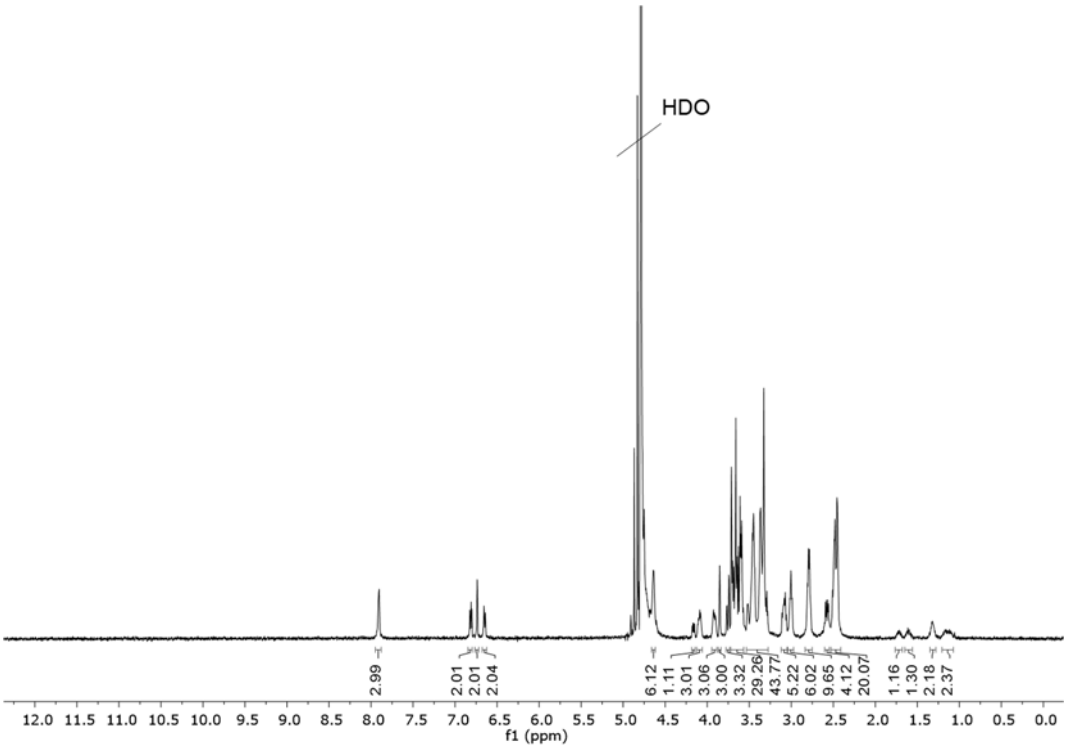

Figure S13: ^{1}H-NMR (600 MHz in D_2O) of 3Man-2Cat (**3**).

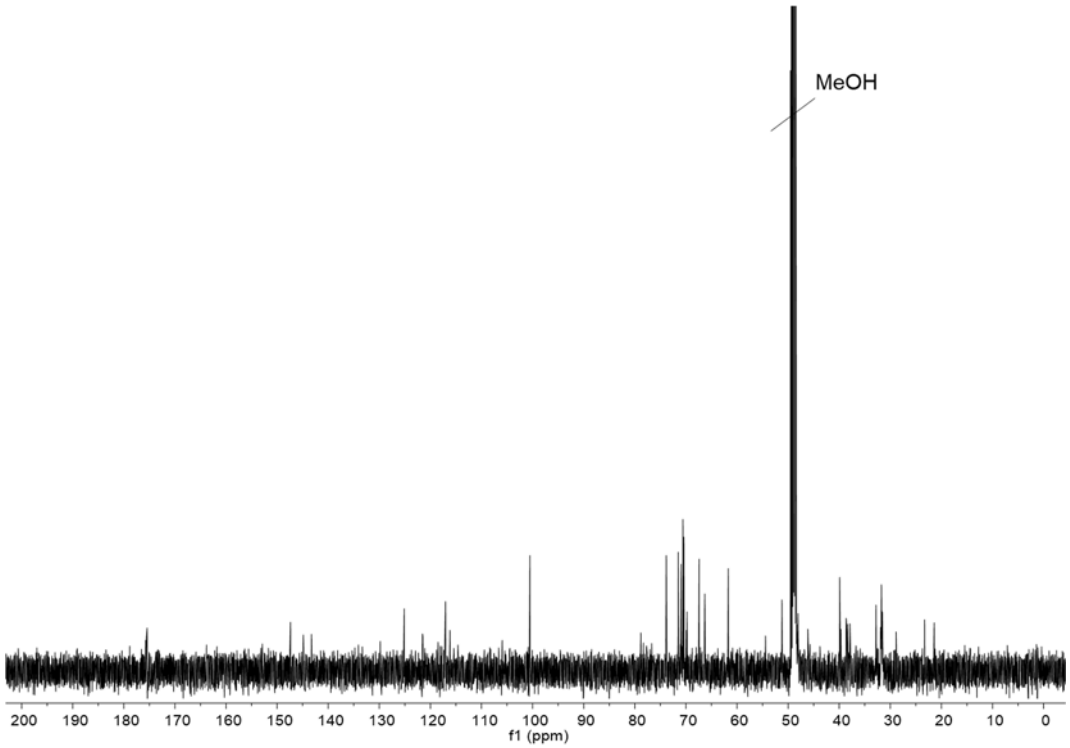

Figure S14: ^{13}C-NMR (150 MHz in D_2O) of 3Man-2Cat (**3**).

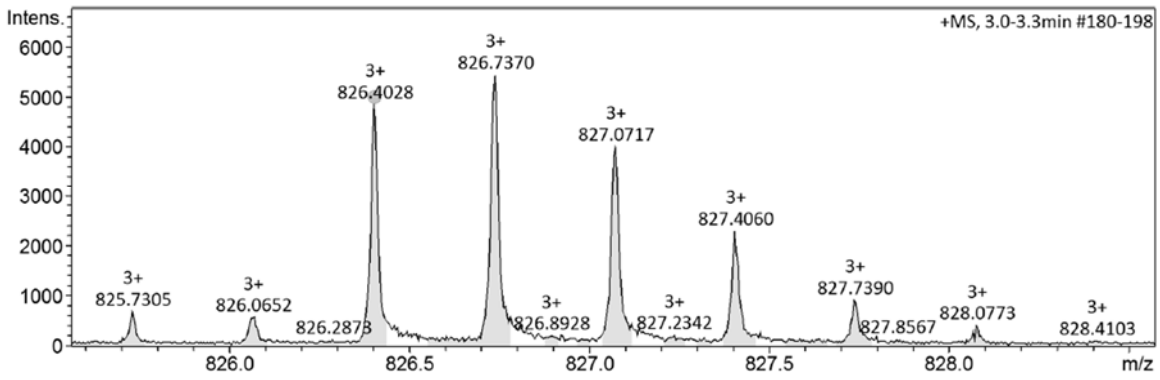

Figure S15: HR-ESI (ESI$^+$ Q-TOF) of 3Man-2Cat (**3**).

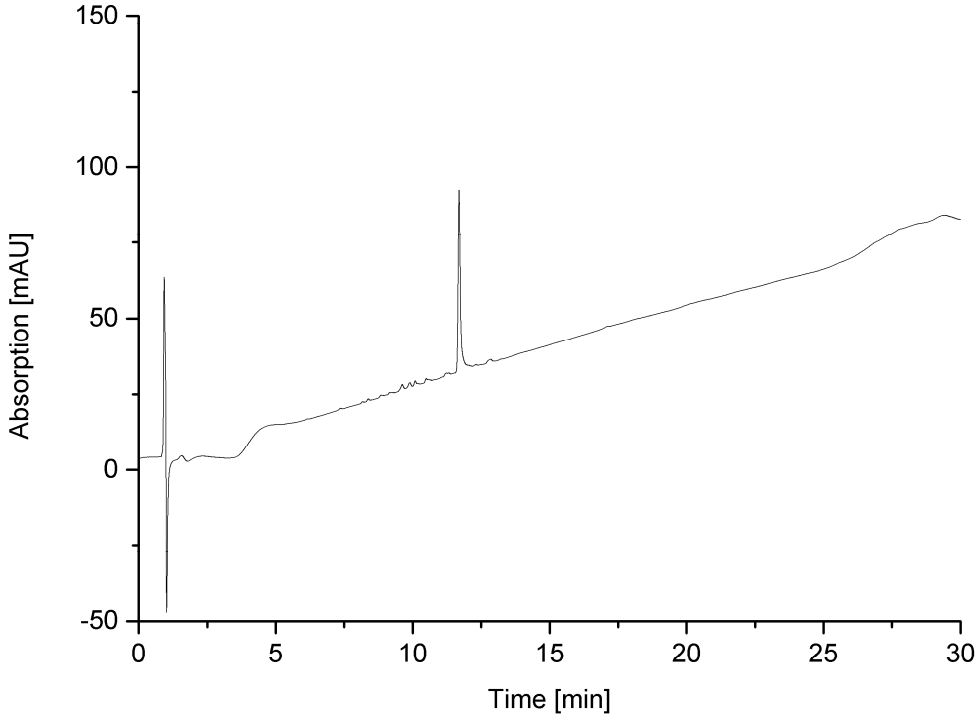

Figure S16: RP-HPLC chromatogram of 3Man-2Cat (**3**) (gradient from 0% to 50% eluent B over 30 min at 25°C).

3Gal (**4**)

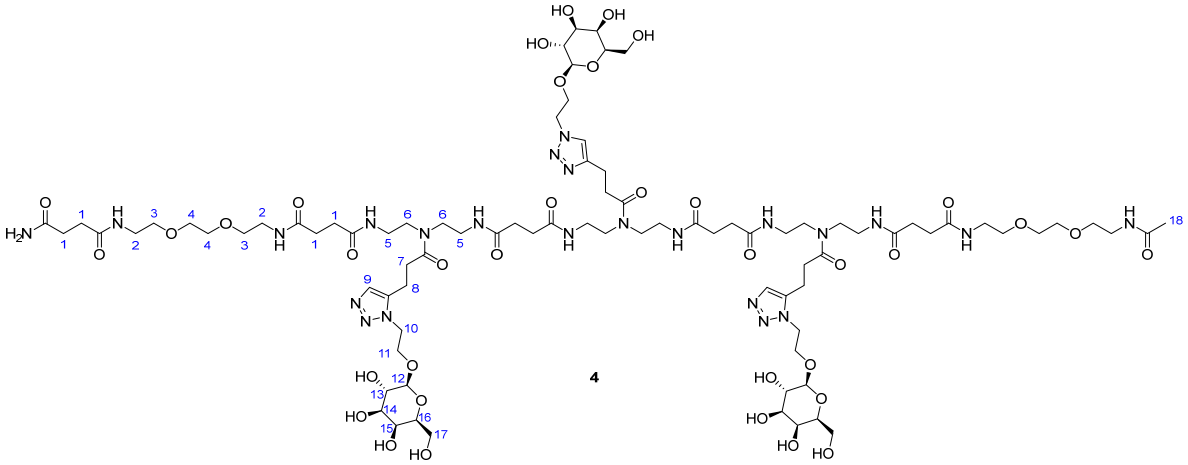

Yield: 131 mg (85%).

^{1}H-NMR (600 MHz, D_2O): δ (ppm) 8.13-8.09 (m, 3H, H9), 4.76-4.74 (m, 6H, H10), 4.41 (d, J_{HH} = 7.9 Hz, 3H, H12), 4.37-4.31 (m, 3H, H11), 4.18-4.12 (m, 3H, H11), 3.94 (d, J_{HH} = 3.5 Hz, 3H, H13), 3.79-3.61 (m,

28H, H3, H4, H14, H15, H17), 3.54-3.33 (m, 32H, H2, H5, H6, H16), 3.11-3.06 (m, 6H, H7), 2.89-2,82 (m, 6H, H8), 2.59-2.44 (m, 20H, H1), 2.02 (s, 3H, H18).

^{13}C-NMR (150 MHz, D_2O): δ (ppm) 178.21, 178.14, 175.48, 175.37, 175.30, 175.28, 175.20, 175.17, 175.12, 175.09, 174.82, 174.70, 163.43, 163.15, 145.92, 145.90, 125.82, 125.79, 125.75, 117.97, 115.65, 103.52, 75.66, 73.18, 71.11, 70.08, 69.92, 69.33, 69.27, 69.08, 68.18, 66.43, 61.45, 51.77, 51.75, 51.73, 51.70, 47.62, 47.60, 45.66, 45.64, 45.61, 39.48, 39.42, 37.85, 37.41, 32.06, 31.55, 31.43, 31.38, 31.32, 31.29, 31.29, 31.14, 30.89, 22.33, 20.56, 20.52.

HR-ESI-MS: calculated mass for $C_{85}H_{143}N_{23}O_{36}$ $[M+3H]^{3+}$: 688.3428, found 688.3432.

RP-HPLC (Eluent B from 0% to 100% in 30 min): t_r = 8.47 min, relative purity 94%.

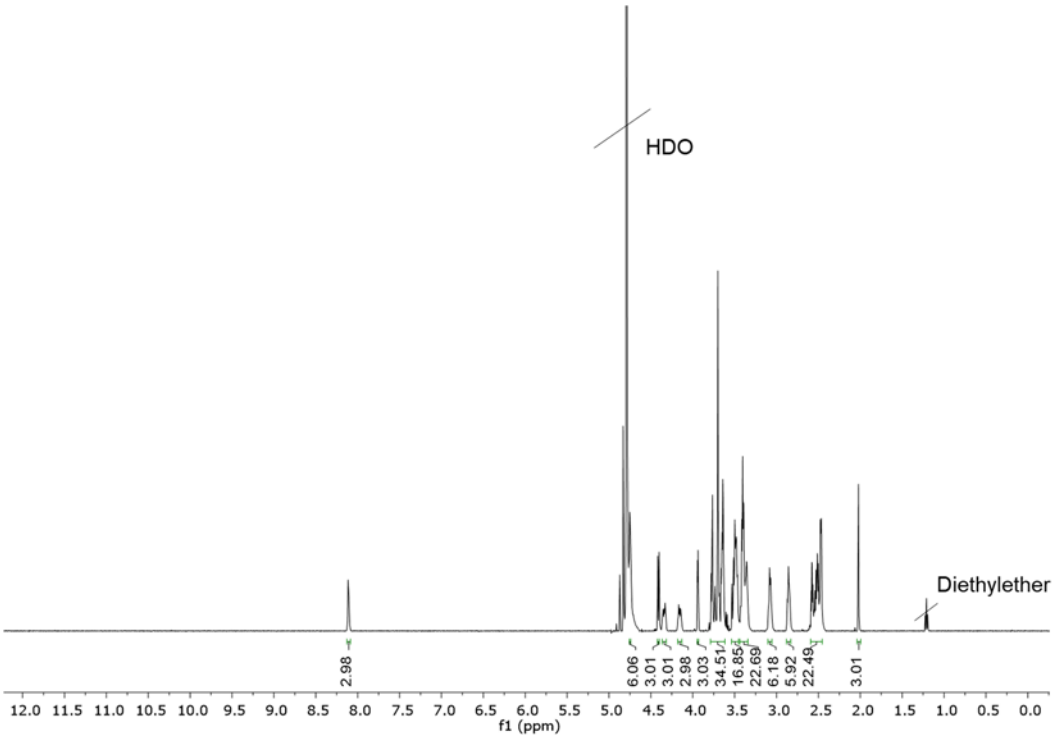

Figure S17: ^{1}H-NMR (600 MHz in D_2O) of 3Gal (**4**).

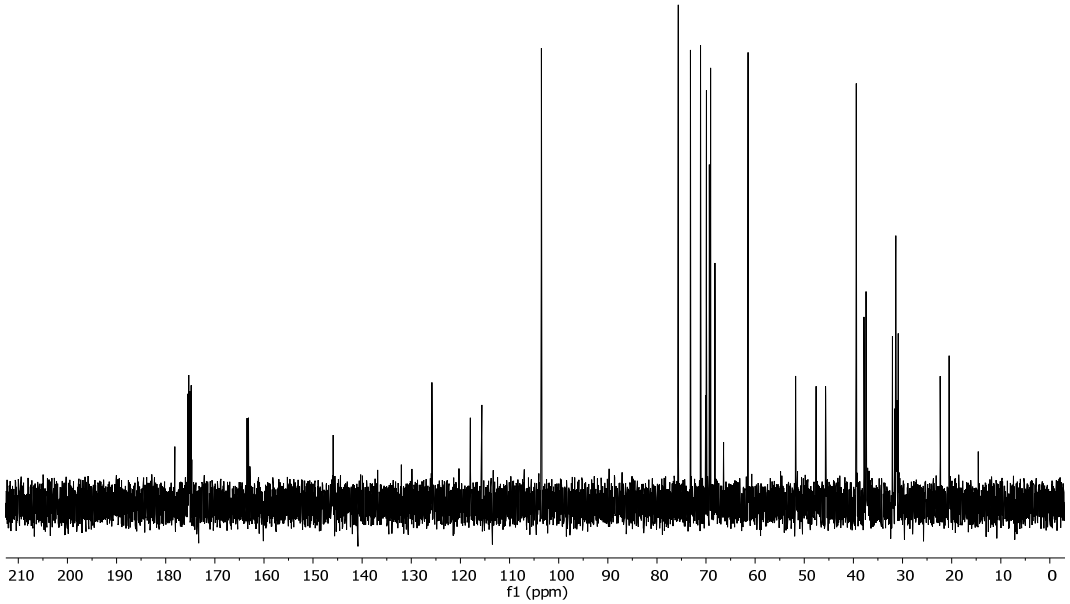

Figure S18: ^{13}C-NMR (150 MHz in D_2O) of 3Gal (**4**).

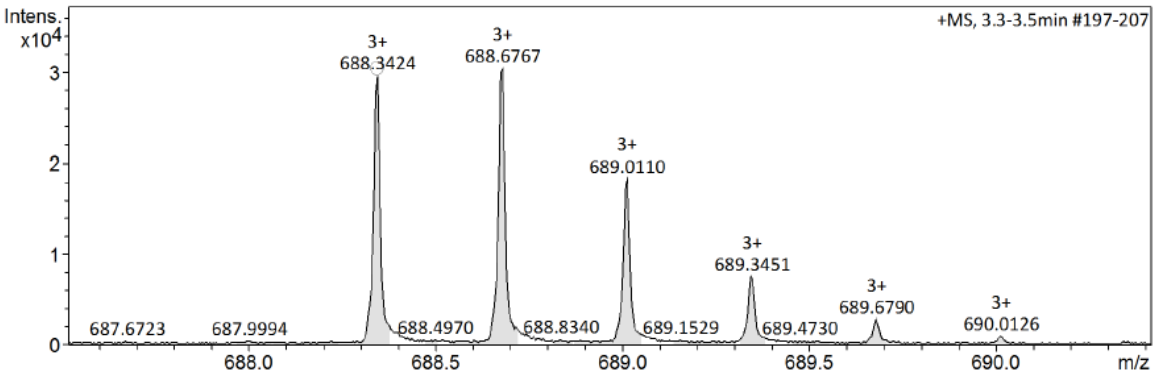

Figure S19: HR-ESI (ESI$^+$ Q-TOF) of 3Gal (**4**).

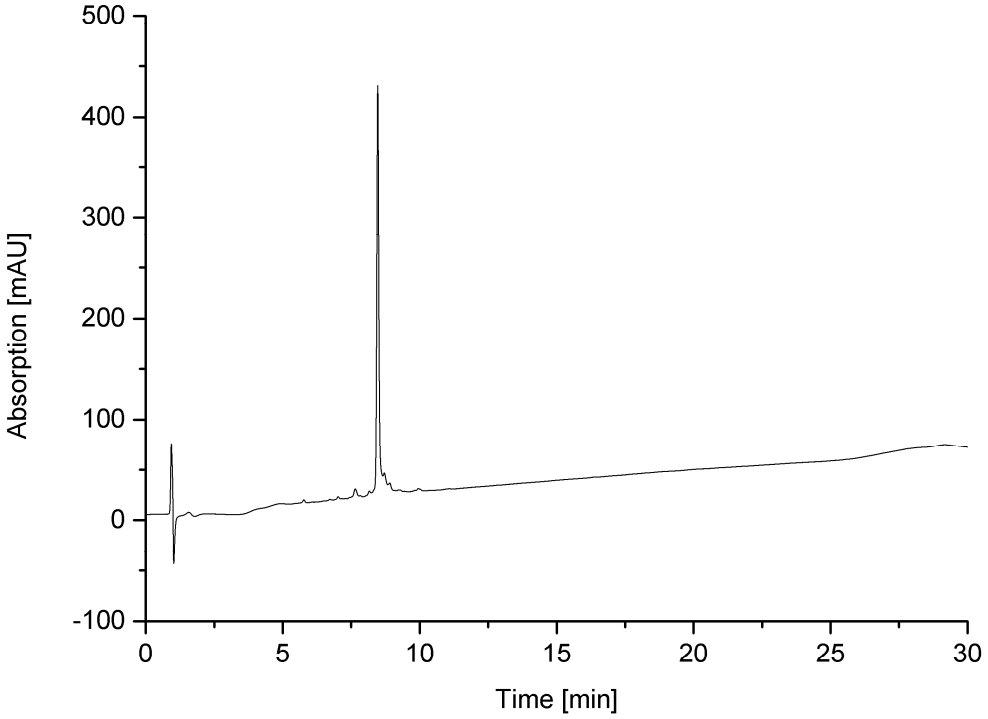

Figure S20: RP-HPLC chromatogram of 3Gal (**4**) (gradient from 0% to 50% eluent B over 30 min at 25°C).

3Gal-1Cat (**5**)

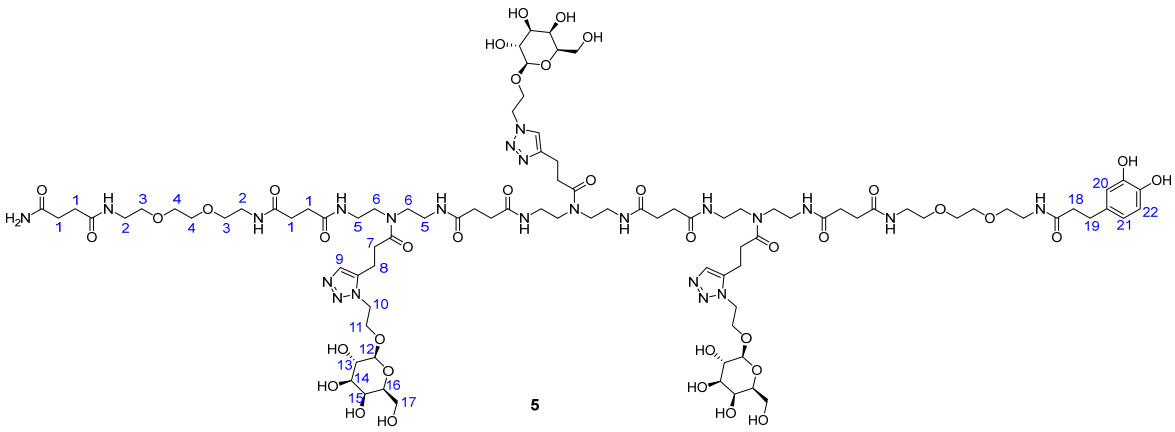

Yield: 138 mg (85%).

^{1}H-NMR (600 MHz, D_2O) δ (ppm) 8.03-7.96 (m, 3H, H9), 6.77 (d, J_{HH} = 8.1 Hz, 1H, H20), 6.70 (d, J_{HH} = 2.1 Hz, 1H, H22), 6.61 (dd, J_{HH} = 8.1 Hz, 2.1 Hz, 1H, H21), 4.67-4.63 (m, 6H, H10), 4.36-4.31 (m, 3H, H12), 4.29-4.23 (m, 3H, H11), 4.10-4.03 (m, 3H, H11), 3.87 (d, J_{HH} = 3.4 Hz, 3H, H13), 3.74-3.53 (m, 28H,

H3, H4, H14, H15, H17), 3.49-3.23 (m, 44H, H2, H5, H6, H18), 3.02-2.95 (m, 6H, H7), 2.81-2.71 (m, 8H, H8, H19), 2.53-2.37 (m, 20H, H1).

^{13}C-NMR (150MHz, D_2O) δ (ppm) 175.67, 175.65, 175.54, 175.48, 175.44, 146.81, 146.78, 144.87, 125.78, 125.76, 125.73, 121.51, 104.01, 76.09, 73.66, 71.59, 70.41, 70.39, 69.94, 69.92, 69.79, 69.78, 69.73, 69.56, 69.54, 68.73, 61.89, 51.83, 51.82, 39.89, 39.86, 38.52, 38.31, 37.91, 37.88, 32.65, 31.91, 31.90, 31.88, 31.82, 31.78, 31.75, 31.59, 31.57, 31.33, 21.27, 21.23, 21.22.

HR-ESI-MS: calculated mass for $C_{92}H_{149}N_{23}O_{38}$ $[M+3H]^{3+}$: 729.0217, found 729.0205.

RP-HPLC (Eluent B from 0% to 100% in 30 min): t_r = 9.78 min, relative purity 99%.

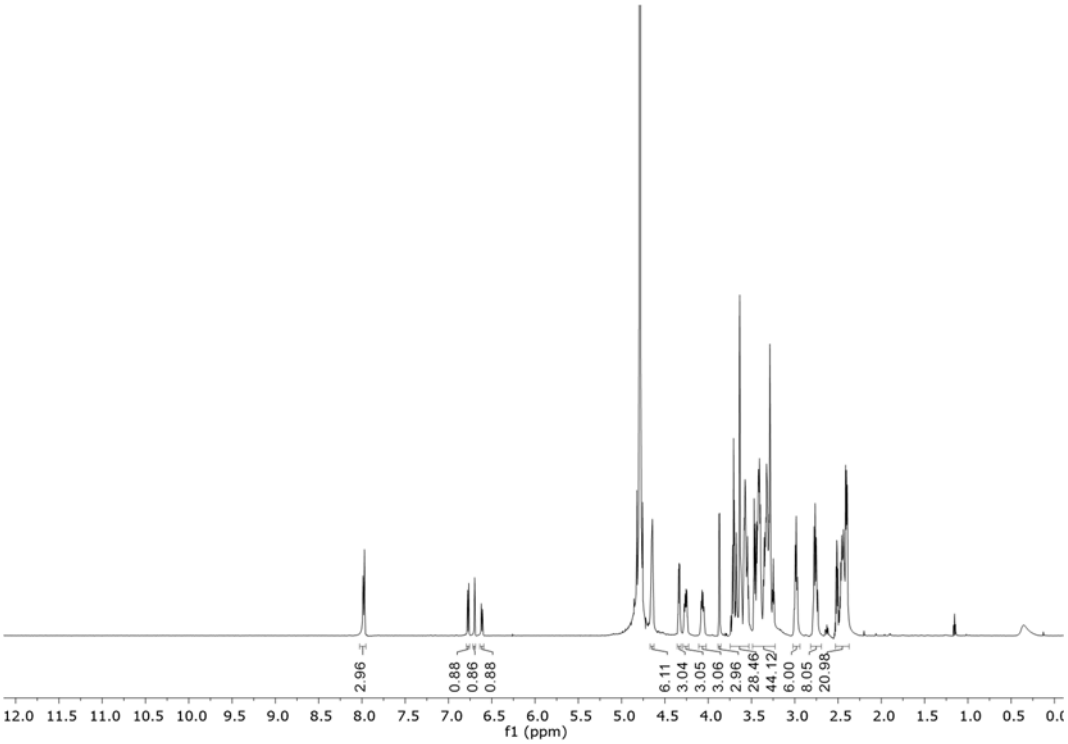

Figure S21: ^{1}H-NMR (600 MHz in D_2O) of 3Gal-1Cat (**5**).

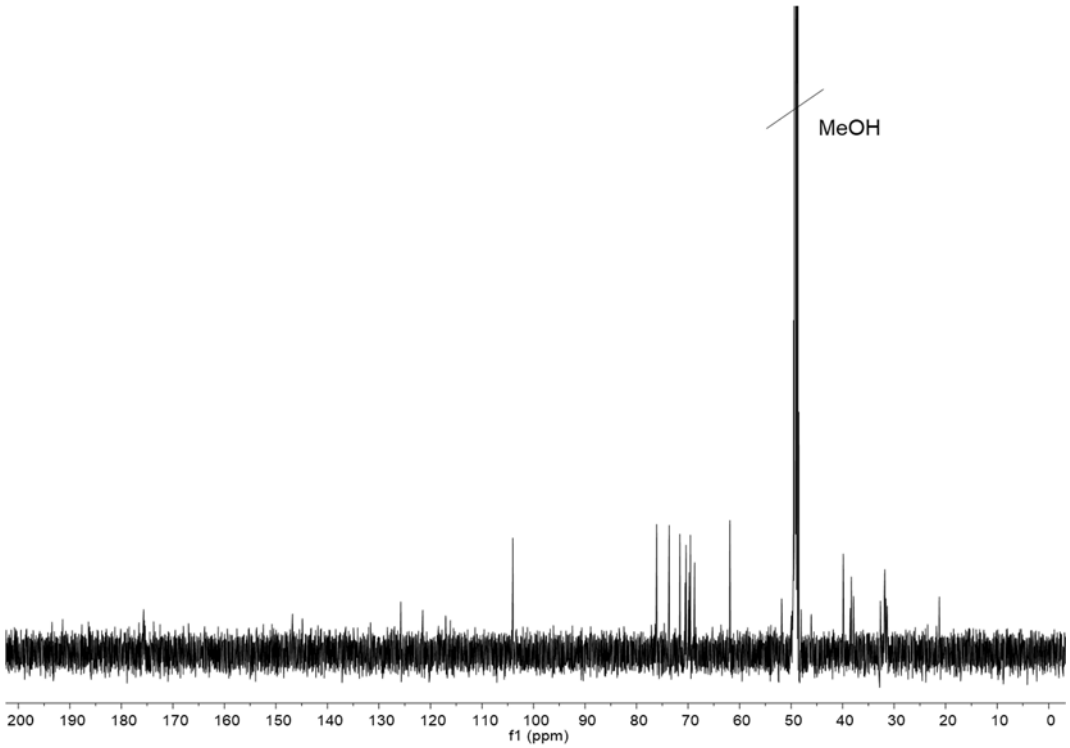

Figure S22: ^{13}C-NMR (150 MHz in D_2O) of 3Gal-1Cat (**5**).

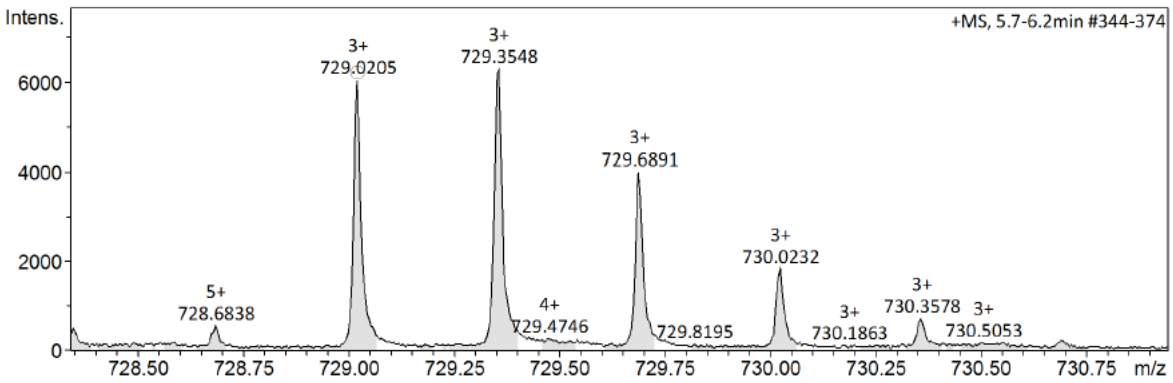

Figure S23: HR-ESI (ESI$^+$ Q-TOF) of 3Gal-1Cat (**5**).

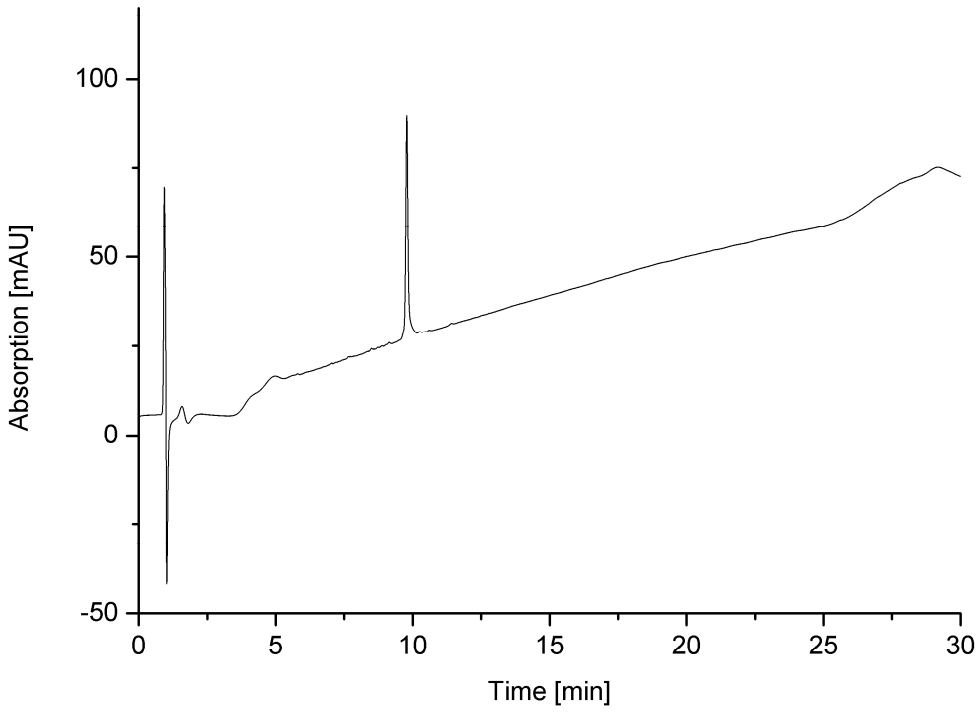

Figure S24: RP-HPLC chromatogram of 3Gal-1Cat (**5**) (gradient from 0% to 50% eluent B over 30 min at 25°C).

3Gal-2Cat (**6**)

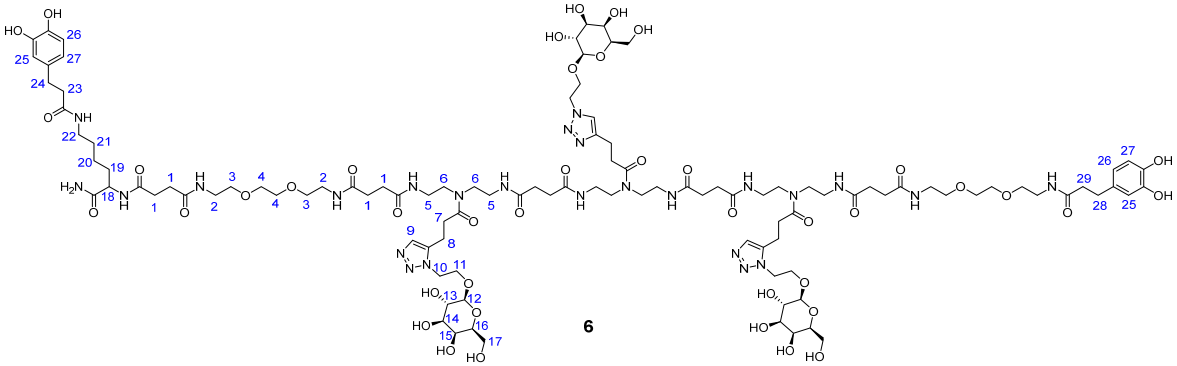

Yield: 91 mg (49%),

^{1}H-NMR (600 MHz, D_2O): δ (ppm) 7.97-7.92 (m, 3H, H9), 6.81 (dd, J_{HH} = 8.1 Hz, 5.9 Hz, 2H, H25), 6.73 (d, J_{HH} = 1.9 Hz, 2H, H27), 6.64 (dt, J_{HH} = 8.1 Hz, 2.2 Hz, 2H, H26), 4.67-4.63 (m, 6H, H10), 4.38-4.34 (m, 3H, H12), 4.30-4.25 (m, 3H, H11), 4.14 (dd, J_{HH} = 9.4 Hz, 5.0 Hz, 1H, H18), 4.11-4.06 (m, 3H, H11), 3.90 (d, J_{HH} = 3.4 Hz, 3H, H13), 3.77-3.56 (m, 28H, H3, H4, H14, H15, H17), 3.51-3.25 (m, 34H, H2, H5, H6,

H29), 3.08-2.95 (m, 9H, H23, H7), 2.80-2.74 (m, 10H, H8, H28, H24), 2.61-2.53 (m, 6H, H16, H22), 2.51-2.39 (m, 20H, H1), 1.73-1.67 (m, 1H, H19), 1.62-1.56 (m, 1H, H19), 1.33-1.03 (m, 4H, H20, H21).

^{13}C-NMR (150 MHz, D_2O) δ (ppm) 175.40, 175.23, 175.21, 175.18, 175.15, 175.04, 175.02, 175.01, 146.44, 146.41, 146.38, 144.32, 125.23, 125.21, 125.16, 125.13, 116.70, 116.68, 116.65, 116.63, 116.60, 116.56, 115.66, 103.53, 75.63, 73.17, 71.11, 70.08, 69.92, 69.31, 69.06, 68.32, 61.43, 51.28, 47.63, 47.60, 45.62, 39.40, 38.16, 38.06, 37.85, 37.42, 32.22, 32.21, 32.20, 31.44, 31.43, 31.36, 31.33, 31.28, 31.24, 31.19, 31.14, 31.13, 31.02, 28.34, 22.76, 20.82.

HR-ESI-MS: calculated mass for $C_{107}H_{169}N_{25}O_{42}$ $[M+3H]^{3+}$: 826.7370, found 826.7371.

RP-HPLC (Eluent B from 0% to 100% in 30 min): t_r = 11.38 min, relative purity 96%.

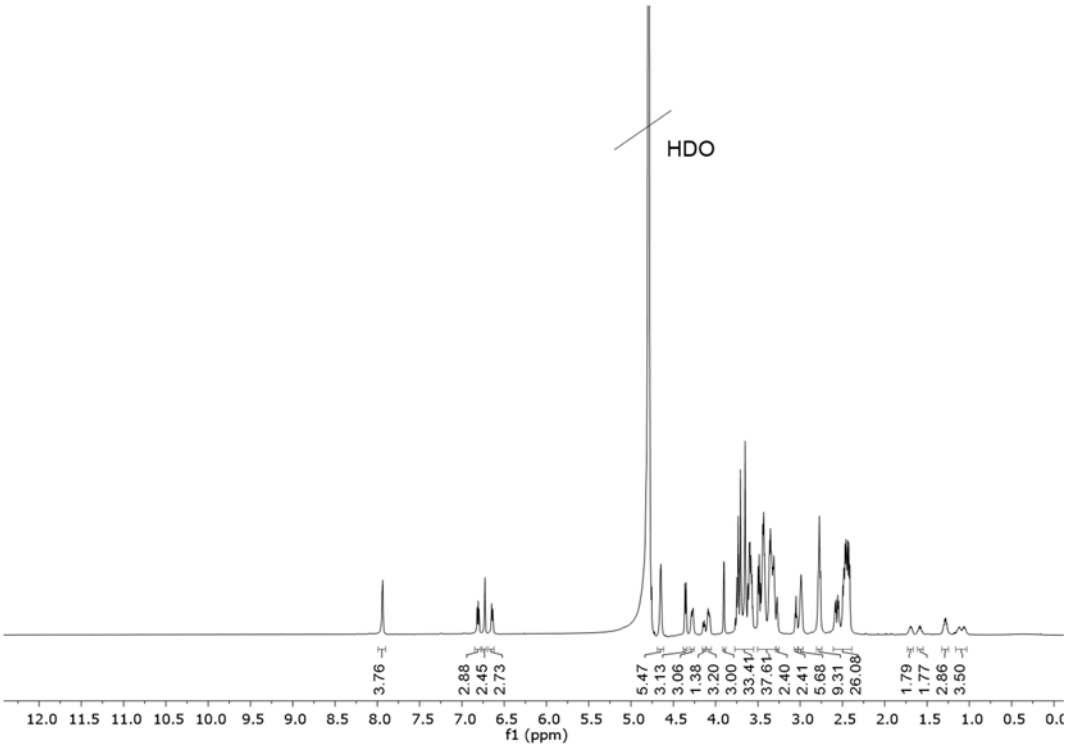

Figure S25: ^{1}H-NMR (600 MHz in D_2O) of 3Gal-2Cat (**6**).

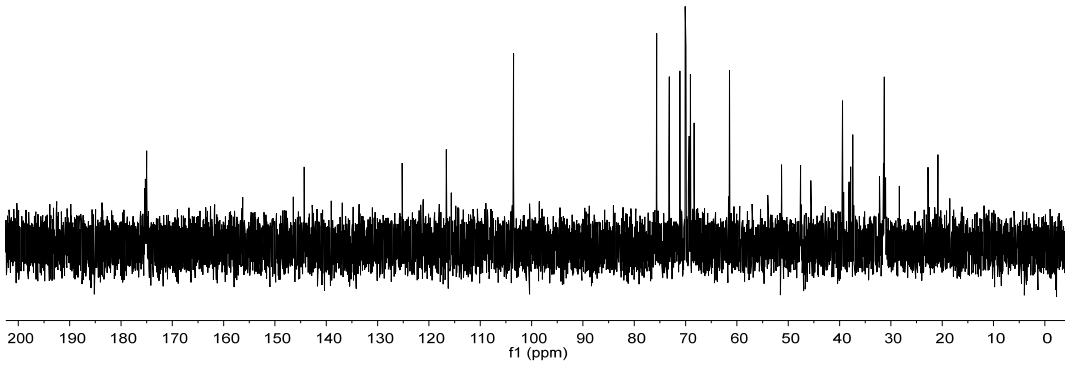

Figure S26: ^{13}C-NMR (150 MHz in D_2O) of 3Gal-2Cat (**6**).

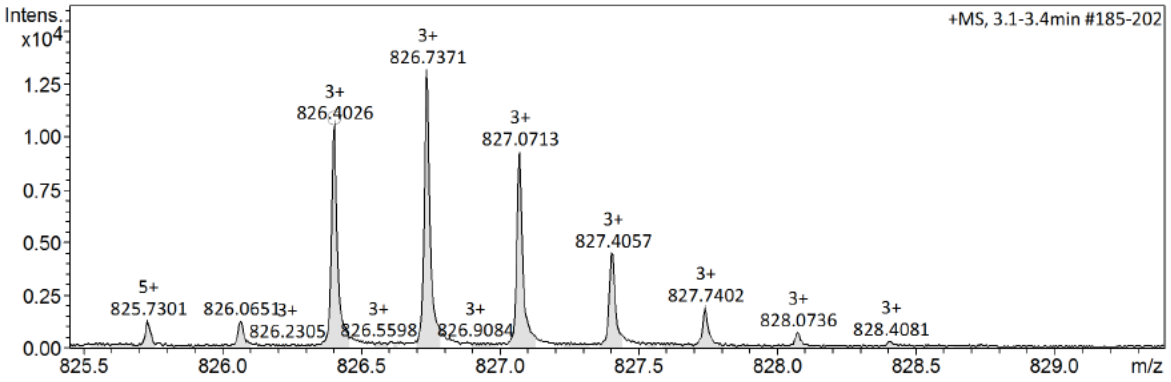

Figure S27: HR-ESI (ESI$^+$ Q-TOF) of 3Gal-2Cat (**6**).

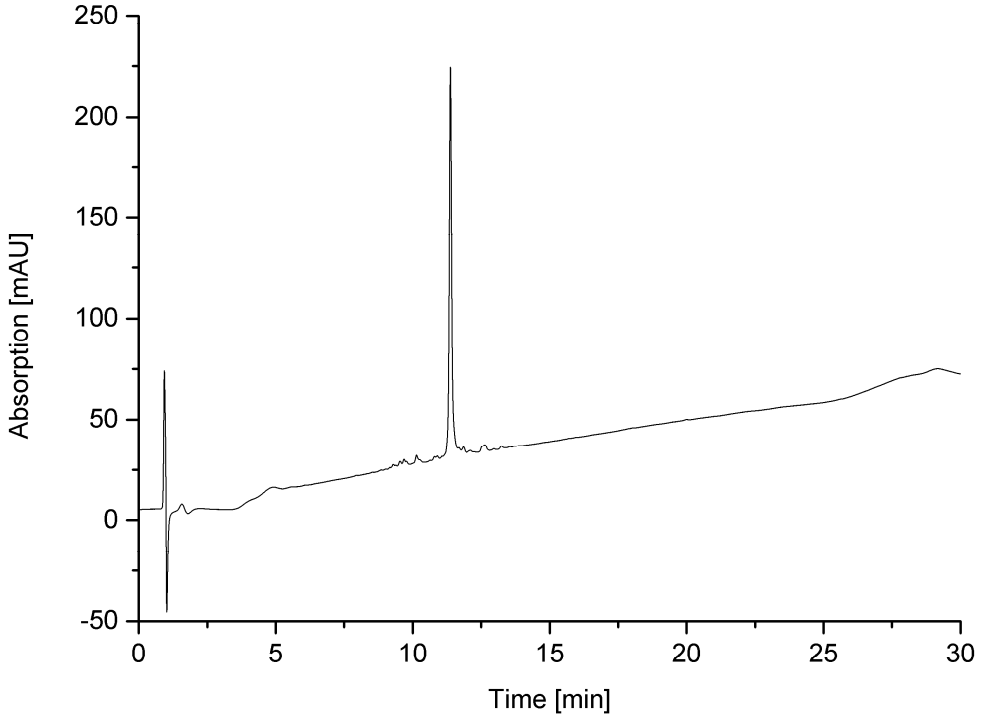

Figure S28: RP-HPLC chromatogram of 3Gal-2Cat (**6**) (gradient from 0% to 50% eluent B over 30 min at 25°C).

Concentration Dependent Turbidity Assay

A solution of 5 µM ConA in LBB buffer (10 mM HEPES, 50 mM NaCl, 1 mM $MnCl_2$, 1 mM $CaCl_2$, pH 7.4) was prepared. The transmission of 1 ml of this solution was measured as 100% transmission baseline. Afterwards glycomacromolecules were stepwise titrated to the ConA solution and after 20 min incubation the transmission was measured. Every glycomacromolecule was measured three times.

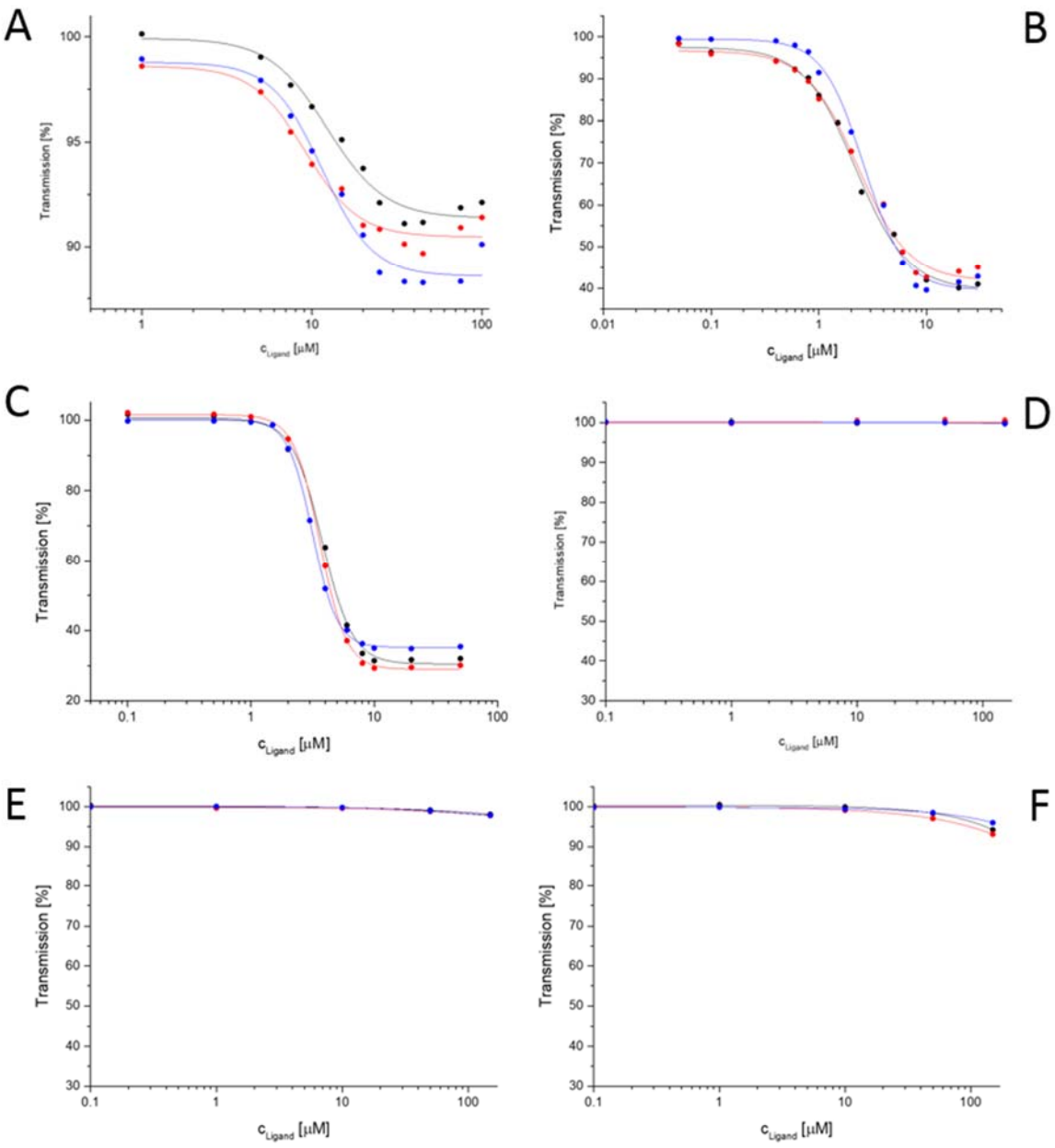

Figure S29: Transmission values obtained in the concentration dependent turbidity assay for different concentrations of glycomacromolecules. A) 3Man (**1**), B) 3Man-1Cat (**2**), C) 3Man-2Cat (**3**), D) 3Gal (**4**), E) 3Gal-1Cat (**5**), F) 3Gal-2Cat (**6**)

Table S1: Results from the concentration dependent turbidity assay.

Ligand	$1/2T_{max}$ [%]	$c_{1/2Tmax}$ [µM]	$1/c_{1/2Tmax}$ [1/µM]
3Man (**1**)	94.62±0.81	11.01±1.34	0.091±0.01
3Man-1Cat (**2**)	69.08±0.40	2.37±0.17	0.42±0.03
3Man-2Cat (**3**)	66.10±1.09	3.53±0.27	0.28±0.02

Quantitative Precipitation Assay

A solution of 15 µM ConA in LBB buffer (10 mM HEPES, 50 mM NaCl, 1 mM $MnCl_2$, 1 mM $CaCl_2$, pH 7.4) was prepared and the concentration was measured at 280 nm. Afterwards aliquots of this solution were mixed with different concentrations of glycomacromolecules, incubated for 24 h and centrifuged for 5 min at 4400 rpm. The precipitate was resuspended in LBB buffer with 50 mM α-methyl D-mannoside and the ConA concentration was determined at 280 nm. To calculate the amount of ConA precipitated per glycomacromolecule the linear slope between 1 and 5 µM ligand was used.

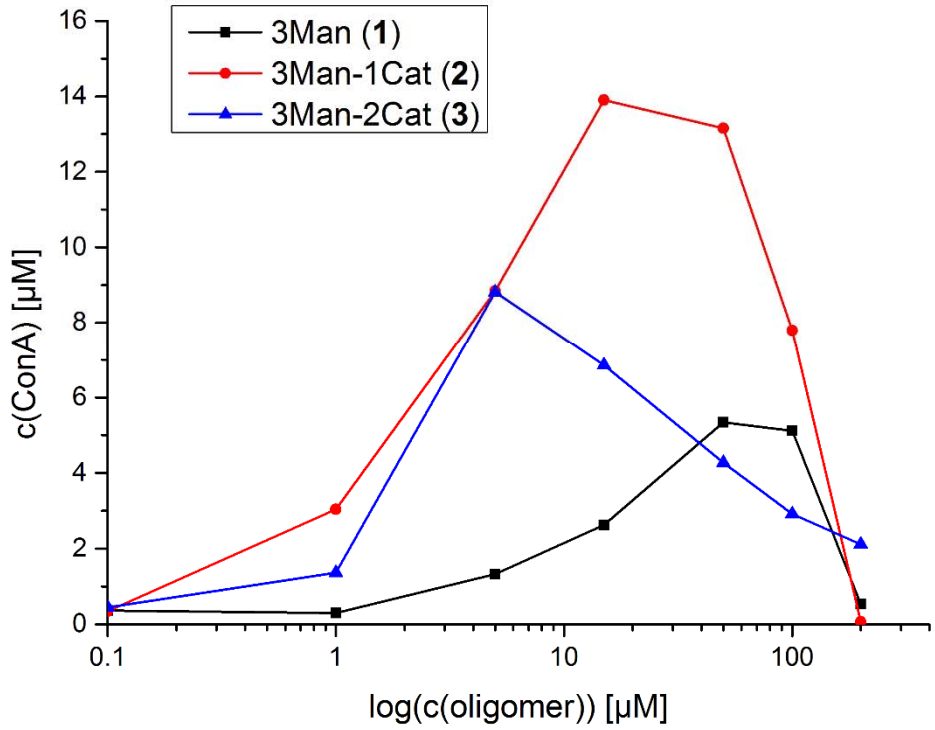

Figure S30: Amount of ConA precipitated per glycomacromolecule in the quantitative precipitation assay.

Table S2: Results from the quantitative precipitation assay.

Ligand	ConA/Ligand
3Man (**1**)	0.10±0.01
3Man-1Cat (**2**)	0.72±0.02
3Man-2Cat (**3**)	1.86±0.02

Covalent Binding Assay (MALDI-TOF)

For the determination of a covalent bond between ConA and ligand, equimolar amounts of ConA (8 µM) and ligand (8 µM) were incubated in LBB buffer (10 mM HEPES, 50 mM NaCl, 1 mM $MnCl_2$, 1 mM $CaCl_2$, pH 7.4) for 24 h. Afterwards the samples were filtrated and measured via MALDI-TOF in linear mode.

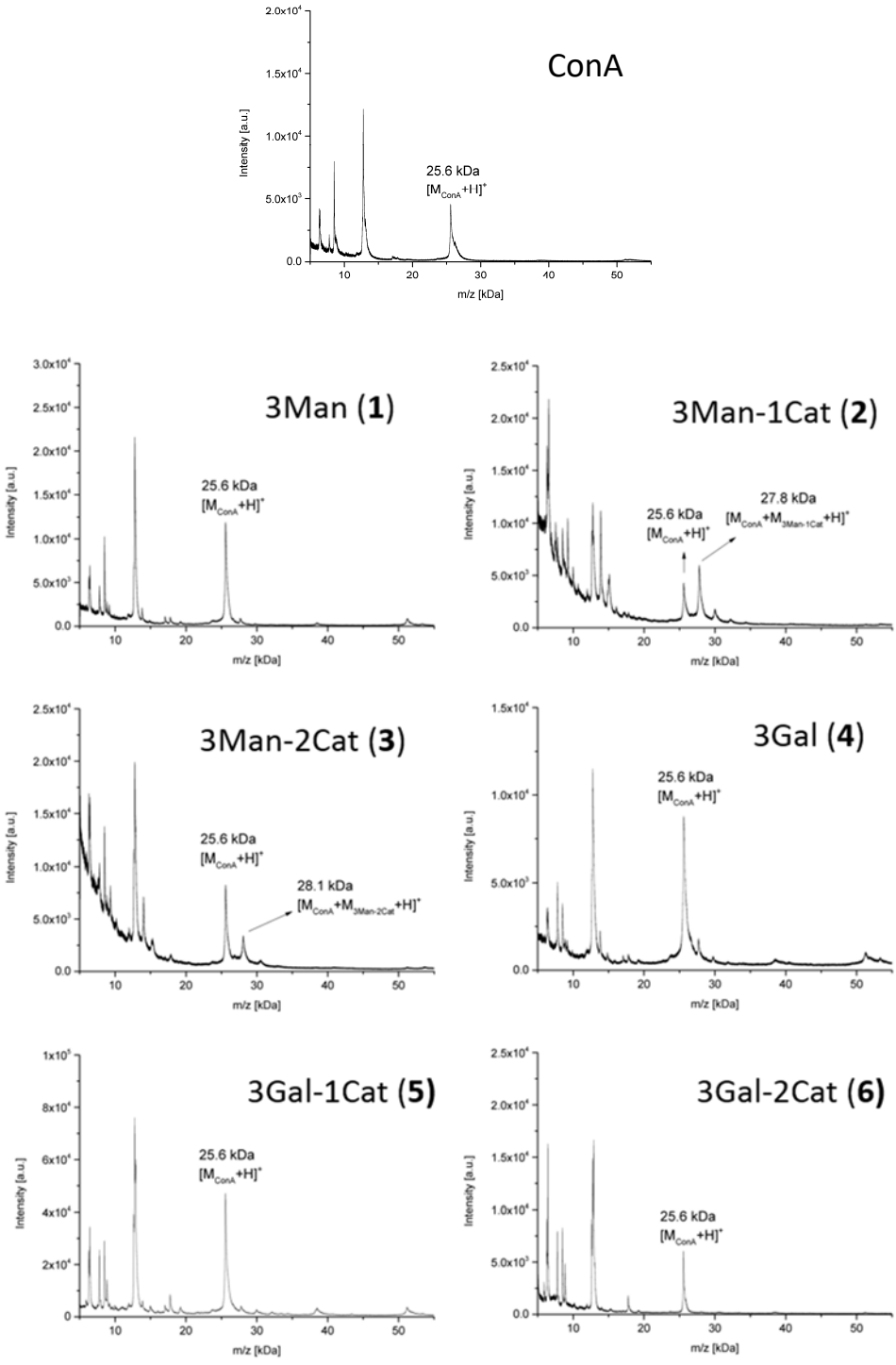

Figure S31: Results from the covalent binding assay via MALDI-TOF for structures **1**-**6**.

Covalent Binding Assay (SDS-PAGE)

Equimolar amounts of ConA (8 µM) and ligand (8 µM) were incubated in LBB buffer (10 mM HEPES, 50 mM NaCl, 1 mM $MnCl_2$, 1 mM $CaCl_2$, pH 7.4) for 24 h. Afterwards the samples were treated with sample buffer (40% glycerol, 4 mg/ml SDS, 0.02% bromophenol blue) and injected into a 15% polyacrylamide gel. The seperation was done over 2 h by 120 V (0.2 A, 300 W) and samples were stained with Coomassie®. As standard Page-Ruler® Prestained Protein Ladder (P/N) 26616 was used.

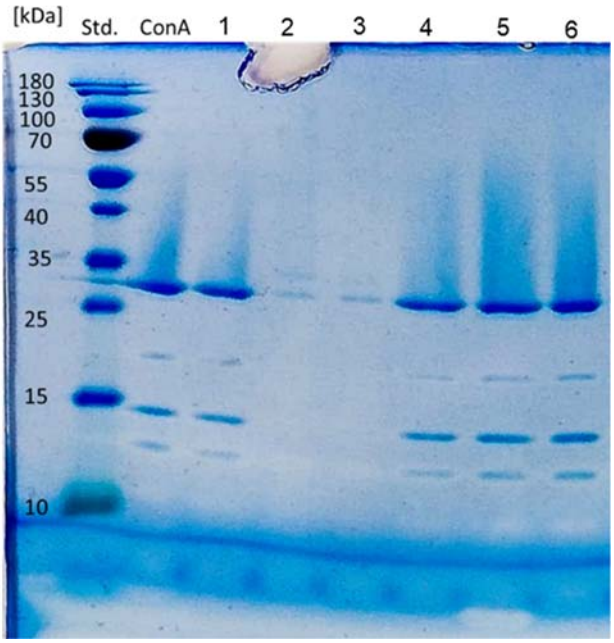

Figure S32: SDS-PAGE of ConA and oligomers **1**-**6**.

Bacterial Adhesion-Inhibition Assay

The *E.coli* strain PKL1162 was cultured from a stock in LB media (ampicillin 100 mg/ml and chloramphenicol 50 mg/ml) at 37°C overnight. The bacterial cells were centrifuged and washed twice and suspended in PBS buffer to a cell concentration of OD_{600} = 0.4. The adhesion-inhibition assay was conducted as described prior in this working group.[6] Black 96-well microtiter plates (Nunc, MaxiScorp) were treated with mannan (1.2 mg/ml in carbonate buffer pH 9.6) for 12 h at 37°C until full evaporation of water. The plates were washed three times with PBST buffer (PBS buffer + 0.05% v/v Tween®20) and blocked with PVA (1% in PBS) for 2 h. Afterwards the plates were washed with PBST twice and PBS once. For the measurement a serial dilution of glycomacromolecules on the mannan-coated microtiter plates was performed (50 µl). The bacterial suspension was added (50 µl) and the plates were incubated for either 1 h or 24 h at 37°C. After incubation the microtiter plates were washed three times with PBS and refilled with PBS (100 µl) to measure the fluorescence intensity (excitation 485 nm, emission 535 nm).

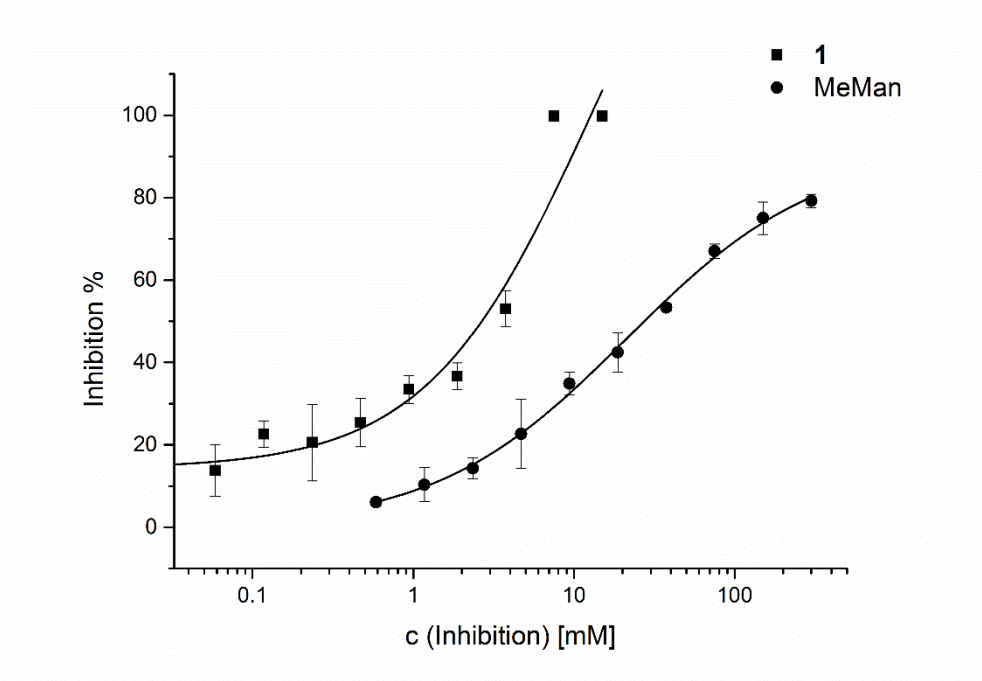

Figure S33: Inhibition curves of structure **1** and MeMan obtained in the bacterial adhesion-inhibtion assay after 1 h incubation.

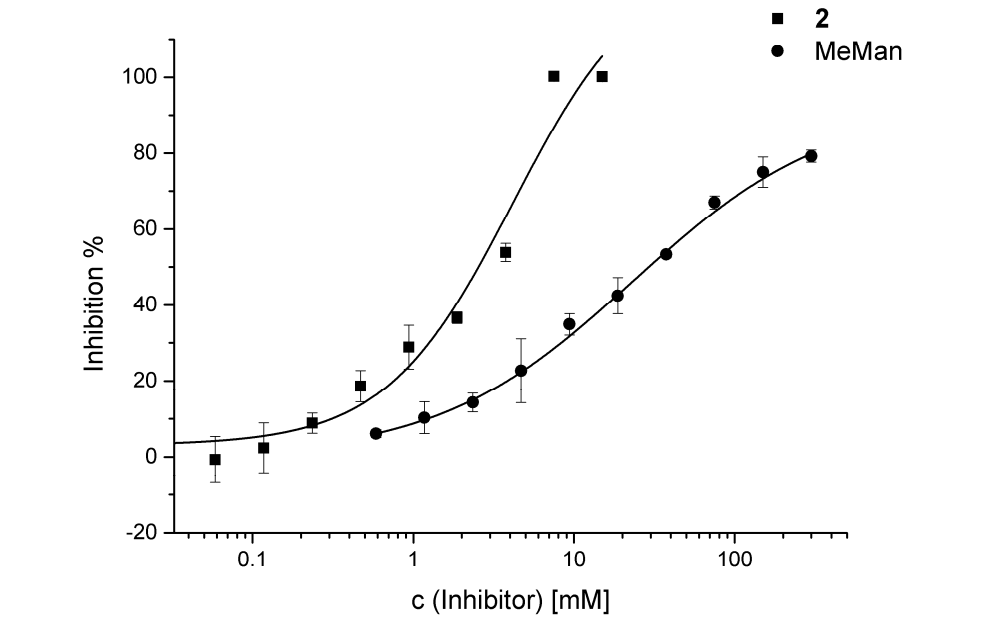

Figure S34: Inhibition curves of structure **2** and MeMan obtained in the bacterial adhesion-inhibition assay after 1 h incubation.

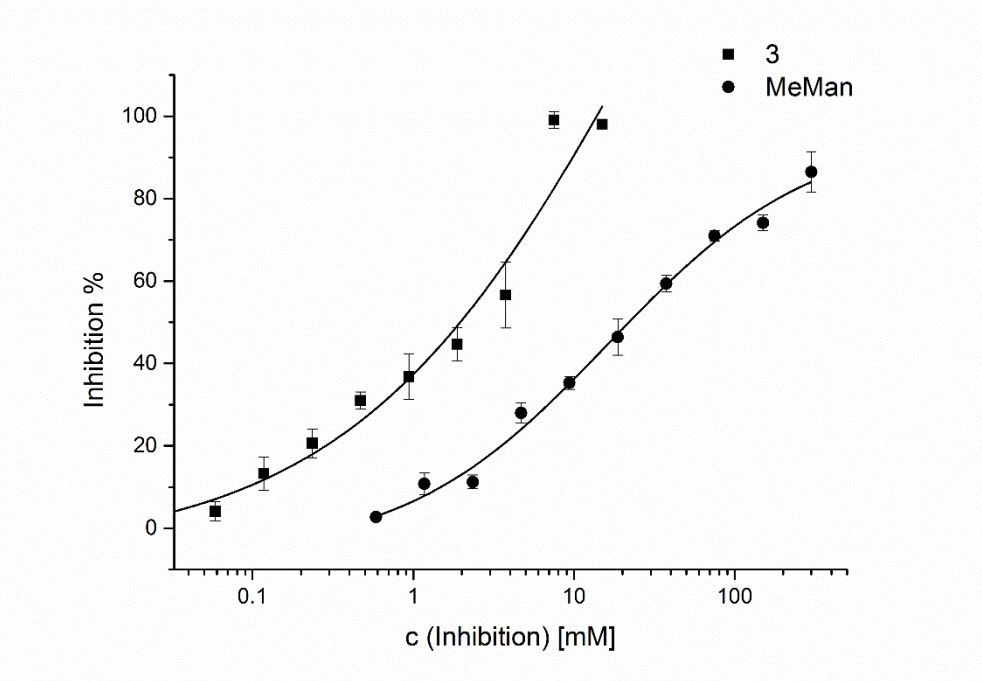

Figure S35: Inhibition curves of structure **3** and MeMan obtained in the bacterial adhesion-inhibition assay after 1 h incubation.

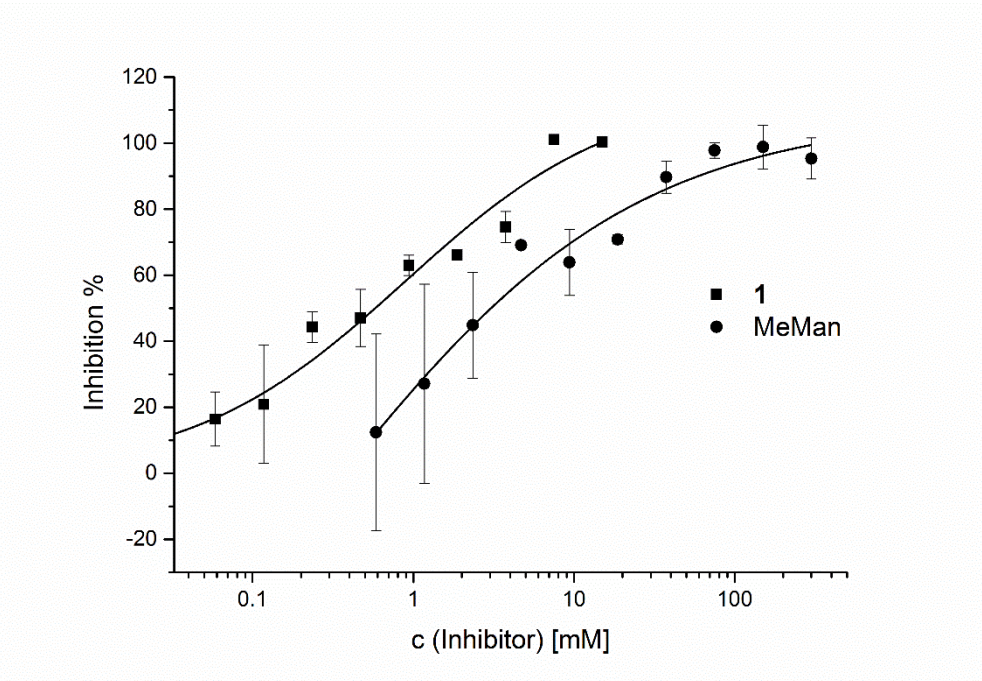

Figure S36: Inhibition curves of structure **1** and MeMan obtained in the bacterial adhesion-inhibition assay after 24 h incubation.

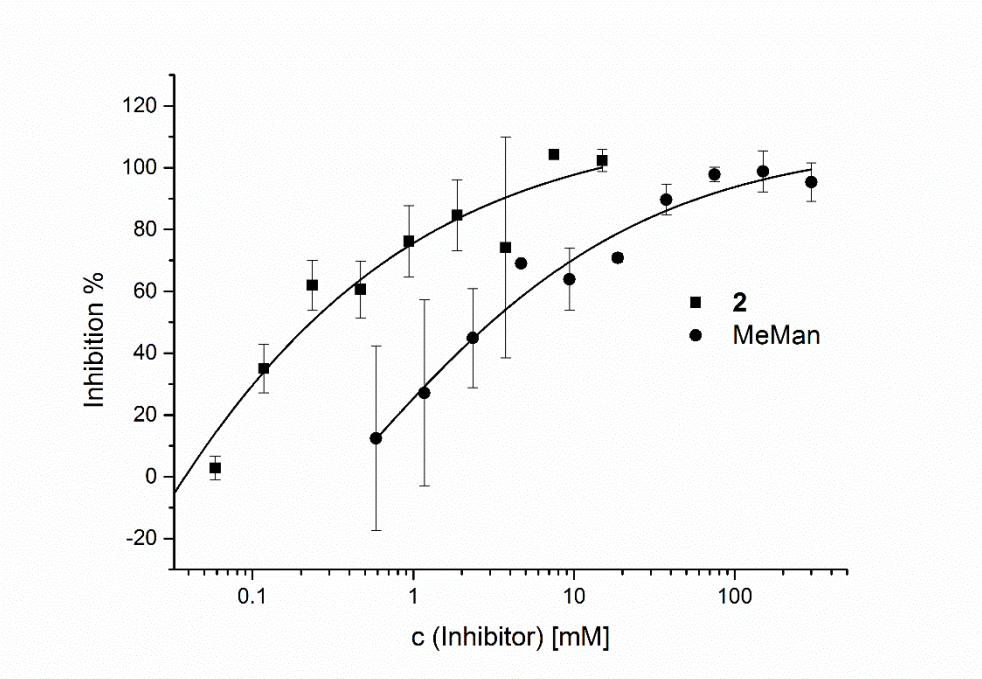

Figure S37: Inhibition curves of structure **2** and MeMan obtained in the bacterial adhesion-inhibition assay after 24 h incubation.

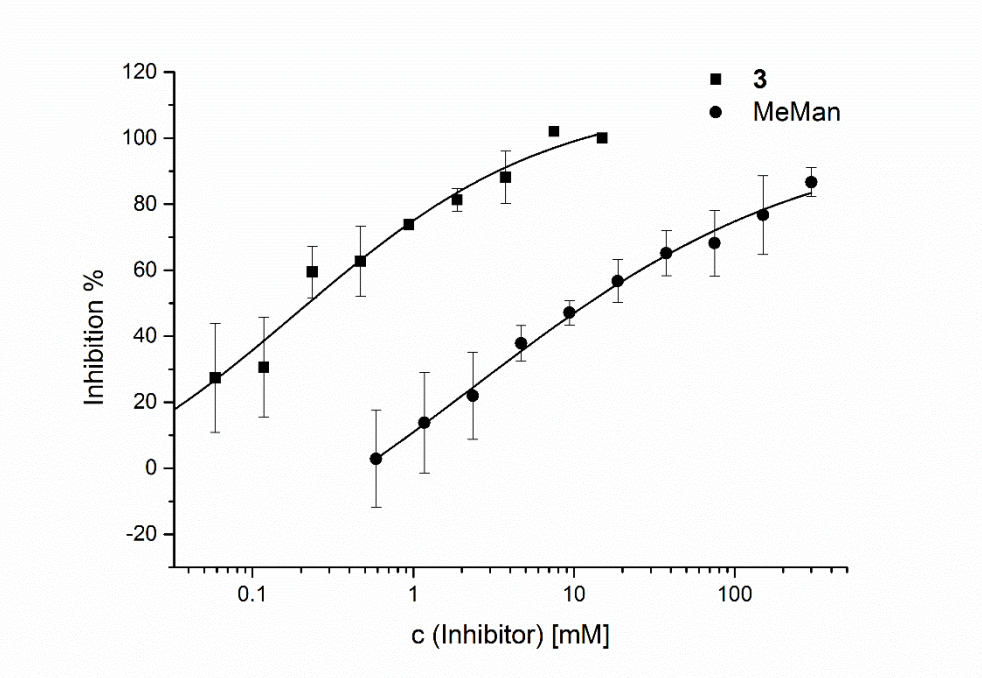

Figure S38: Inhibition curves of structure **3** and MeMan obtained in the bacterial adhesion-inhibition assay after 24 h incubation.

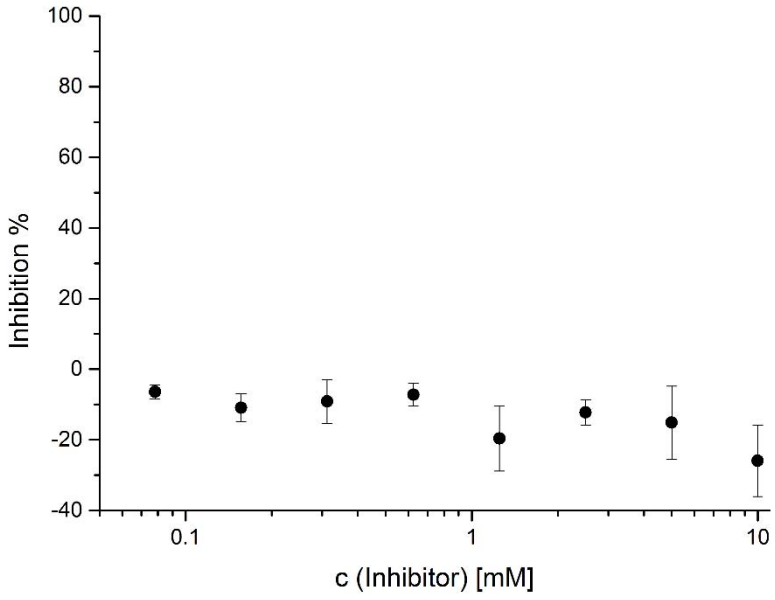

Figure S39: Inhibition curve of structure **4** obtained in the bacterial adhesion-inhibition assay after 1 h incubation.

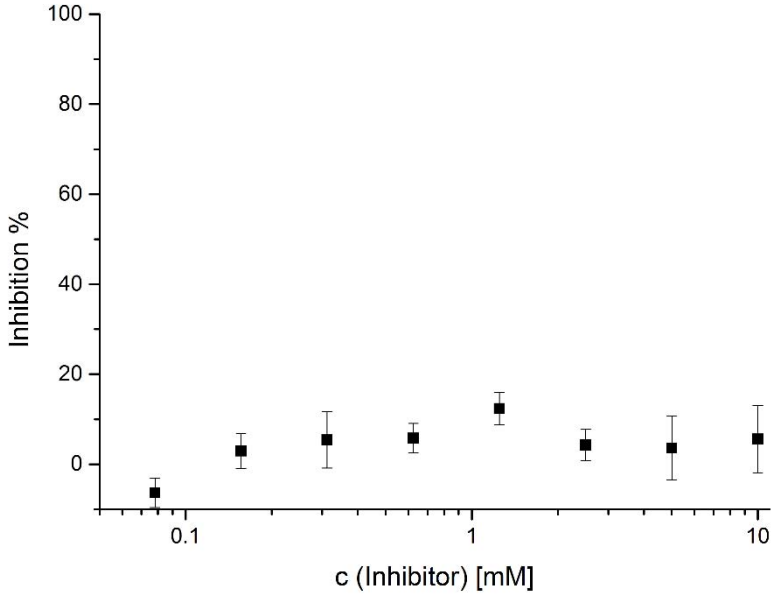

Figure S40: Inhibition curve of structure **5** obtained in the bacterial adhesion-inhibition assay after 1 h incubation.

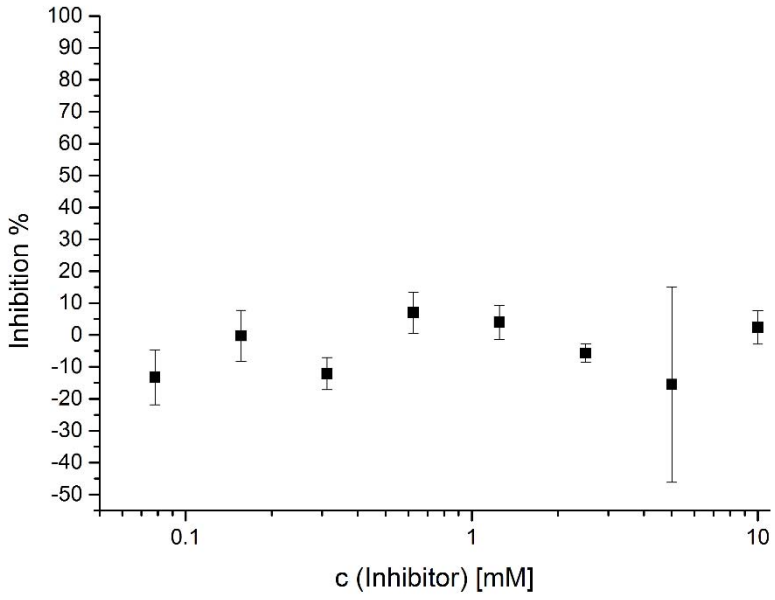

Figure S41: Inhibition curve of structure **6** obtained in the bacterial adhesion-inhibition assay after 1 h incubation.

(1) Hayes, W.; Osborn, H. M.; Osborne, S. D.; Rastall, R. A.; Romagnoli, B. *Tetrahedron* **2003**, *59*, 7983.

(2) Wu, L.; Sampson, N. S. *ACS Chemical Biology* **2014**, *9*, 468.

(3) Wei, Q.; Achazi, K.; Liebe, H.; Schulz, A.; Noeske, P. L. M.; Grunwald, I.; Haag, R. *Angewandte Chemie International Edition* **2014**, *53*, 11650.

(4) Ponader, D.; Wojcik, F.; Beceren-Braun, F.; Dernedde, J.; Hartmann, L. *Biomacromolecules* **2012**, *13*, 1845.

(5) Gerke, C.; Ebbesen, M. F.; Jansen, D.; Boden, S.; Freichel, T.; Hartmann, L. *Biomacromolecules* **2017**, *18*, 787.

(6) Boden, S.; Reise, F.; Kania, J.; Lindhorst, T. K.; Hartmann, L. *Macromolecular Bioscience* **2019**, *19*, e1800425.

4. Conclusion and Outlook

The aim of this thesis was to establish a way to present catechol groups in sequence-defined oligo(amidoamine)s for the synthesis of biomimetic structures and to investigate their interaction based on catechol presentation and sequence. One application was to mimic Mfp like structures by presenting catechol, tertiary amine and primary amide residues in defined macromolecules synthesized with solid phase synthesis. Through the sequence-defined nature of these structures, the underlying mechanisms of the catechol driven adhesion were supposed to be investigated. In a subsequent project, the idea was to use the properties of catechols to synthesize improved and covalent lectin inhibiting glycomimetics and to characterize the interaction for different catechol presentation in binding assays and with live bacteria.

For this, in the first part of this thesis, the synthesis towards sequence-defined structures presenting catechols was developed as well as methods for combination with tertiary amines and primary amides created. This was done using the so called SPPoS, which is based on the Fmoc strategy of peptide synthesis and was developed by the working group of Prof. Hartmann and coworkers.[121] This synthesis towards oligo(amidoamine)s uses building blocks with a free acid and Fmoc protected amine to step wise assemble monodisperse structures on solid support. There are spacer building blocks, responsible for the majority of the backbone composition and important for physicochemical properties, and functional building blocks that present different moieties as side chains.[129,131-133] There was already a diverse library of functional building blocks developed over the years, using an established protocol which starts from diethylenetriamine and utilizes two temporary protection groups to give the final building after seven steps. Additionally, with this protocol, a rearrangement can occur, resulting in lengthy optimization for every new structure.[138] Based on this established protocol, a new building block synthesis was developed that only uses one temporary protection group by introducing Fmoc and the side chain moiety selectively in a one-pot approach, reducing the overall steps from seven to four. Furthermore, the yield is increased to over 50% and no rearrangement can occur with this approach, making this newly development synthesis a more accessible, faster and material saving way towards functional building blocks for SPPoS.

Using the shortened protocol, two new building blocks were synthesized, CDS with a methyl ether protected catechol side chain, and TrDS with a trityl protected primary amine. The first building block was used to develop the synthesis of catechol presenting oligo(amidoamine)s. Using CDS in combination with the spacer building block EDS, the successful assembly of a multivalent and sequence-defined system on solid support was shown. To access the final oligomer with free catechols, a deprotection protocol was developed. Since the backbone presents aliphatic ether groups, and the protection group is a methyl ether, a selective way towards catechol deprotection needed to be found. Different Lewis acids were tested, but were either non-selective or not reactive enough. The successful selective catechol deprotection was achieved using a system of trifluoromethanesulfonic acid with thioanisol, establishing the complete synthesis towards catechol presenting structures. The second building block, TrDS, was used to functionalize an assembled scaffold with either a tertiary amine or primary amide via amide formation. For this, a deprotection method was utilized that selectively cleaves the trityl group of TrDS on solid support while retaining stability of the acid labile rink amide linker. In combination, both building blocks can be used to synthesize structures presenting catechols, tertiary amines and primary amides in free combination and with control over sequence and spacing.

Prominently displayed in mussel foot proteins are catechol groups and cationic residues, which were already in depth investigated and were shown to be key to the wet adhesion.[40] Although also frequently found in Mfps, the presentation of primary amide residues in Mfps was so far neglected as a contributor to adhesion. Furthermore, proteins are defined and monodisperse structures but the influence of presentation and sequence of functional groups in mussel inspired, adhesive structures was yet not investigated. To shine a light on both aspects, in the second part of the thesis the newly established protocols were used to synthesize a library of mussel foot protein mimicking oligomers. This library is comprised of different divalent structures intended for adhesion measurements. The oligomers presenting two of the same functionality (catechol, tertiary amine or primary amide) were synthesized to establish a baseline regarding the adhesive potential of the different moieties. Every functionality was also combined with each other, to investigate possible synergistic effects between groups presented in mussel foot proteins. Finally, the position of catechol and tertiary amine and catechol and primary amide were swapped, to change order of surface

contact, and the distance between catechol and tertiary amine was shortened in one structure, to further investigate the influence of presentation. The adhesion of all structures was measured by Alexander Strzelczyk against glass surface in presence of 0.1M sodium chloride and for different pH values, namely 3, 5, 7 and 8. As assay, the so called SCP-RICM was used for which soft PEG microgels were functionalized with the oligomers via amide formation between the terminal primary amine of the oligomers and free acids presented on the PEG particles. Using this method, the presented oligo(amidoamine)s are oriented and order of surface contact is determined by oligomer sequence. In this adhesion measurement, all structures showed a sharp decline in adhesion for pH 7 and 8, probably due to a deprotonation of the glass surface and loss of H-bonds as surface interaction. The baseline oligomers only presenting one kind of functional group showed that primary amide and tertiary amines achieved higher wet adhesion than catechols, contrary to literature that predominantly names catechols as wet adhesive group.[37]. The combination of functional groups revealed that there is a synergy between catechol and tertiary amine as well as between catechol and primary amide. The combinations of both resulted in higher adhesion values than the sum of its single components. This effect drastically increased for the combination of catechol and tertiary amine with a decrease in distance between the functional groups and also changed the pH dependence, as the adhesion strength was almost constant over the measured pH range. This proves the synergy already described in literature[40], which is attributed to the capability of the tertiary amine to break up the hydration layer on the surface and subsequent binding of the catechol. This effect would also explain the increase of adhesion for a lower distance between both groups, as the catechol has better access to the surface spot where the hydration layer was removed by the tertiary amine. For the combination of catechol and primary amide, a dependence on sequence of presentation was found. For the structure where catechol is presented first and the primary amide second, high adhesion over all pH values was found. Here, probably another effect occurs than for the tertiary amine, as a possible explanation is that the primary amide controls the folding of the structure in solution, making the catechol more accessible towards the surface. This was also the first time that the contribution of primary amides towards wet adhesion as well as its synergy with catechols was shown and explains the high amount of asparagine found in Mfp-3. In conclusion, the sequence-defined presentation of catechols, tertiary amines and primary amides was used to show a significant influence of the presentation pattern of functional

groups, and elucidated the contribution of primary amides towards catechol driven adhesion. To further these insights, it would be interesting to synthesize oligo(amidoamine)s presenting more than two functional groups and to deploy these in additional adhesion assays eg. in quartz crystal microbalance or surface force apparatus measurements to gain additional insights into the underlying mechanisms. An additional step then would be to transfer this knowledge towards classical polymers that are easily up scalable to be used for application.

In the third, and last part, of this thesis, the unique properties of the catechol moiety were used to create improved lectin inhibitors. On the basis of SPPoS, catechol containing glycomimetics were synthesized by Ricarda C. Steffensand collaboratively explored for their potential as lectin inhibitors. For this, a new strategy for introducing catechols was developed, as the used carbohydrates were not stable during deprotection of the methyl ether protected catechol building block CDS. Because of this, dihydrocaffeic acid was acetonide protected and coupled via its free acid to assembled scaffolds either via the terminal primary amine or an incorporated and deprotected lysine. This strategy was combined with the established building block TDS, to introduce the carbohydrates mannose and galactose via CuAAC reaction. With this, a library of six trivalent structures was synthesized, three structures with the binding sugar mannose and three with the negative control galactose. For each carbohydrate a structure without, with one and with two catechols was synthesized. The interaction of these glycomimetics with the mannose binding model lectin ConA were investigated via turbidity and precipitation assays. Both assays are based on the crosslinking of the tetrameric ConA by multivalent ligands resulting in photometric measurable clusters. The turbidity of a solution of ConA with different concentrations of oligomers after 20 minutes incubation was measured. This assay showed more clustering with the introduction of a catechol moiety, showing an increase of affinity through additional interactions with ConA. In comparison, no turbidity was measured for the catechol containing galactose structures, showing that no unspecific interactions between lectin and catechol occur. For the precipitation assay, solutions of ConA with different oligomer concentrations were prepared and incubated for 24 hours. Afterwards, the clusters of ConA and ligand were precipitated, resuspensed with α-MeMan and the concentration of ConA was measured. Again, mannose structures with catechol precipitated more ConA than the structure without. Here, the structure with two catechols showed a higher increase of affinity than in the turbidity assay,

which could be contributed to the longer incubation time, resulting in oxidation over time and subsequent covalent binding of the catechol group. Furthermore, the oligomers were tested as inhibitors for bacterial adhesion. As ligands for the bacterial adhesin FimH, the mannose structures were supposed to block the interaction of bacteria with a mannan grafted surface. This adhesion-inhibition assay was done by incubating live bacteria with different ligand concentrations in a mannan coated titer plate. As inhibitors, all synthesized structures were used as well as α-MeMan as a reference to calculate relative inhibitory potentials (RIP), which enables the comparison of different plates and experiments. The ligands were incubated with *E. coli* for 1 hour at 37°C, and the following measurement revealed no change of RIP with the introduction of catechols. All three structures with mannose achieved relative inhibitory potentials similar to oligomers measured in prior experiments.[133] Increasing the incubation time to 24 hours, a drastic change in inhibitory potential was found. While the structures with no or one catechol remained at the same RIP, the inhibitory potential for the oligomer with two catechols increased by a factor of 4, resulting in an effective bacterial adhesion inhibitor. This shows again, that the interaction of catechol moieties with the target lectin increases over time which could indicate catechol oxidation and covalent binding to the receptor and that the different presentation of catechol units influences the binding strength. This was also proven by measuring MALDI-TOF and SDS-PAGE of a mixture of ConA and ligands after 24 hours incubation. By measuring MALDI-TOF, the covalent binding of catechol containing mannose oligomers was shown via additional mass peaks corresponding to ConA and ligand. Here multiple ligands covalently bound to one subunit of ConA, and, more importantly, no additional mass peaks were found for catechol structures with the non-binding sugar galactose, showing that the selectivity of the carbohydrate moiety is remained and no unspecific binding of catechol occurs. Comparing the amount of ligands covalently bound per ConA subunit, fewer oligomers bound to ConA for the structure with two catechols, one on each end of the structure. Multiple oligomers likely bind to one subunit when the binding mannose diffuses out of the CBD after covalent attachment of one ligand, so additional structures can bind. This means that the oligomer with two catechols more effectively blocs the binding site and shows that the presentation of catechols can control the binding behaviour. This proof of concept could be an interesting approach for the development of glycomimetic therapeutics. For this, next tests stages would include toxicity tests, animal studies and a possible human administration for optimized structures.

Overall, this thesis developed different synthetic routes towards a sequence-defined presentation of catechols in macromolecules and showed the importance of structural control in biomimetic compounds. This lays the foundation for the synthesis of new and optimized wet adhesives with potential applications as medical glues or for surface modifications under aqueous conditions. Especially the use of primary amides as highly adhesive functional group and polymerization methods that allow control over the presentation should become the focus of further developments. Furthermore, the here presented results could potentially yield new glycomimetic therapeutics in the future. As shown in this thesis, glycoligands with specific catechol presentation can act as potent inhibitors, opening the possibility of acquiring irreversibly binding and targetable therapeutic agents.

5. Appendix

5.1 List of Abbreviations

ADS	Azide-Diethylenetriamine-Succinic acid
Alloc	Allyloxycarbonyl
a. u.	Arbitrary unit
BADS	Benzyl azide-Diethylenetriamine-Succinic acid
Boc	*tert*-Butyloxycarbonyl
CBD	Carbohydrate binding domain
CRD	Carbohydrate recognition domain
Con A	Concanavalin A
CuAAC	Copper-catalyzed azide-alkyne cycloaddition
Da	Dalton
DCM	Dichloromethane
DDS	Double bond-Diethylenetriamine-Succinic acid
DIPEA	Diisopropylethylamine
DMF	*N*,*N*-Dimethylformamide
DMSO	Dimethyl sulfoxide
DNA	Deoxyribonucleic acid
e.g.	Exempli gratia
EDC	1-Ethyl-3-(3-dimethylaminopropyl)carbodiimide
EDS	Ethylene glycol-Diamine-Succinic acid
et al.	Et alii
ESI	Electrospray ionization
eq	Equivalent
Fmoc	9-Fluorenylmethoxycarbonyl
Fuc	α-L-Fucose
Gal	D-Galactose
Gal-3	Galectin-3
GalNAc	D-N-acetylgalactosamine
Glc	D-glucose
GlcNAc	*N*-acetylglucosamine
h	Hour
HATU	1-[Bis(dimethylamino)methylene]-1H-1,2,3-triazolo[4,5-b]pyridinium 3-oxide hexafluorophosphate
HEPES	4-(2-Hydroxyethyl)-1-piperazineethanesulfonic acid
HOBt	1-Hydroxybenzotriazole
HR-ESI	High resolution-electrospray ionization
JKR	Johnson−Kendall−Roberts
K_D	Dissociation constant

kDa	Kilo Dalton
LC-MS	Liquid chromatography-mass spectrometry
Man	D-Mannose
MDS	Methyl succinyl-Diethylenetriamine-Succinic acid
min	Minute
m/z	Mass per charge ratio
NMR	Nuclear magnetic resonance
ODS	Octyl-Diamine-Succinic acid
PyBOP	(Benzotriazol-1-yloxy)tripyrrolidinophosphonium hexafluorophosphate
Q-TOF	Quadrupole-time of flight
RICM	Reflection interference contrast microscopy
RIP	Relative inhibitory potential
RP-HPLC	Reverse phase-high pressure liquid chromatography
RT	Room temperature
SCP	Soft colloidal probe
SDS	Short-Diamine-Succinic acid
TDS	Triple bond-Diethylenetriamine-Succinic acid
Trt	Trityl
UV	Ultraviolet
VWD	Variable wavelength detector

5.2 List of Figures

6. Acknowledgments

First of all, I would like to give a special thanks to Prof. Dr. Laura Hartmann for giving me the opportunity to conduct my doctoral thesis in her working group at the Heinrich-Heine-University Düsseldorf. I would also like to thank her for my fruitful project, the helpful discussions and great ideas as well as all her good advice in all the years in the working group. I am happy to say that I could always contact her for inspiration or motivation.

Furthermore, I would like to thank Priv.-Doz. Dr. Klaus Schaper for agreeing to be the second supervisor of this thesis.

I would also like to thank Jun.-Prof. Dr. Stephan Schmidt for all the help during my thesis and especially for the discussions and corrections regarding my publications.

I am also very grateful for the prosperous cooperation with Dr. Wedler and Dr. Kropf, which helped steer this thesis into the direction it took in a lot of presentations and discussions. I also thank Alexander Strzelczyk for the project we did together, all the measurements he did and the input I received from him. Furthermore, I am thankful for the financial support from the Henkel AG & Co. KGaA, which made this thesis possible.

I also want to thank the rest of the institute, especially Dr. Monir Tabatabai for her input and corrections of experimental parts of my publications. A thank you also goes to Stephanie Scheelen and Michaela Kitza for all the help over the years and solving many organisational problems.

I also thank Maria Breuer for measuring NMR and Dr. Peter Tommes and Ralf Bürgel for conducting MALDI-TOF and HR-MS measurements.

A big thank you also goes to the students I supervised, Lara Wedershoven, Ricarda Steffens and Lorand Bonda, whose work contributed a large part to this thesis.

The last, and probably the biggest, thank you goes to the whole working group, which created an environment that made every day enjoyable. I am also grateful for all the people I met and all the friends I made along the way. Every one of you will get a beer at the next RAR. A special shoutout goes to my office partners, Dana Itskalov, Kira Neuhaus and Tanja Freichel, and later also Nina Jahnke and Stephen Hill. I would also like to name Luca and Lorand, but just because our names all start with the same letter.

7. References

(1) Silverman, H. G.; Roberto, F. F. *Marine biotechnology* **2007**, *9*, 661.

(2) Qin, Z.; Buehler, M. J. *Nature communications* **2013**, *4*, 2187.

(3) Brady Jr, R. F. *Progress in organic coatings* **1999**, *35*, 31.

(4) Lee, B. P.; Messersmith, P. B.; Israelachvili, J. N.; Waite, J. H. *Annual review of materials research* **2011**, *41*, 99.

(5) Hagenau, A.; Scheidt, H. A.; Serpell, L.; Huster, D.; Scheibel, T. *Macromolecular bioscience* **2009**, *9*, 162.

(6) Waite, J. H. In *Structure, cellular synthesis and assembly of biopolymers*; Springer: 1992, p 27.

(7) Sun, C.; Lucas, J. M.; Waite, J. H. *Biomacromolecules* **2002**, *3*, 1240.

(8) Zhao, H.; Waite, J. H. *Journal of Biological Chemistry* **2006**, *281*, 26150.

(9) Hwang, D. S.; Zeng, H.; Masic, A.; Harrington, M. J.; Israelachvili, J. N.; Waite, J. H. *Journal of biological chemistry* **2010**, *285*, 25850.

(10) Kord Forooshani, P.; Lee, B. P. *Journal of Polymer Science Part A: Polymer Chemistry* **2017**, *55*, 9.

(11) Danner, E. W.; Kan, Y.; Hammer, M. U.; Israelachvili, J. N.; Waite, J. H. *Biochemistry* **2012**, *51*, 6511.

(12) Wei, W.; Yu, J.; Broomell, C.; Israelachvili, J. N.; Waite, J. H. *Journal of the American Chemical Society* **2013**, *135*, 377.

(13) Lin, Q.; Gourdon, D.; Sun, C.; Holten-Andersen, N.; Anderson, T. H.; Waite, J. H.; Israelachvili, J. N. *Proceedings of the National Academy of Sciences* **2007**, *104*, 3782.

(14) Zhao, H.; Robertson, N. B.; Jewhurst, S. A.; Waite, J. H. *Journal of Biological Chemistry* **2006**, *281*, 11090.

(15) Floriolli, R. Y.; von Langen, J.; Waite, J. H. *Marine Biotechnology* **2000**, *2*, 352.

(16) Papov, V. V.; Diamond, T. V.; Biemann, K.; Waite, J. H. *Journal of Biological Chemistry* **1995**, *270*, 20183.

(17) Lee, B. P.; Messersmith, P. B.; Israelachvili, J. N.; Waite, J. H. *Annual review of materials research* **2011**, *41*, 99.

(18) Hofman, A. H.; van Hees, I. A.; Yang, J.; Kamperman, M. *Advanced materials* **2018**, *30*, e1704640.

(19) Waite, J. H.; Qin, X. *Biochemistry* **2001**, *40*, 2887.

(20) Long, J. R.; Dindot, J. L.; Zebroski, H.; Kiihne, S.; Clark, R. H.; Campbell, A. A.; Stayton, P. S.; Drobny, G. P. *Proceedings of the National Academy of Sciences* **1998**, *95*, 12083.

(21) Yu, J. In *Adhesive interactions of mussel foot proteins*; Springer: 2014, p 31.

(22) Wold, F. *Annual review of biochemistry* **1981**, *50*, 783.

(23) Faure, E.; Falentin-Daudré, C.; Jérôme, C.; Lyskawa, J.; Fournier, D.; Woisel, P.; Detrembleur, C. *Progress in polymer science* **2013**, *38*, 236.

(24) Xu, H.; Nishida, J.; Ma, W.; Wu, H.; Kobayashi, M.; Otsuka, H.; Takahara, A. *ACS Macro Letters* **2012**, *1*, 457.

(25) Postma, A.; Yan, Y.; Wang, Y.; Zelikin, A. N.; Tjipto, E.; Caruso, F. *Chemistry of Materials* **2009**, *21*, 3042.

(26) Monahan, J.; Wilker, J. J. *Langmuir* **2004**, *20*, 3724.

(27) Gantayet, A.; Rees, D. J.; Sone, E. D. *Marine biotechnology* **2014**, *16*, 144.

(28) Lu, Q.; Danner, E.; Waite, J. H.; Israelachvili, J. N.; Zeng, H.; Hwang, D. S. *Journal of The Royal Society Interface* **2013**, *10*, 20120759.

(29) Waite, J. H. *Journal of Experimental Biology* **2017**, *220*, 517.

(30) Hofman, A. H.; van Hees, I. A.; Yang, J.; Kamperman, M. *Advanced materials* **2018**, *30*, 1704640.

(31) Yu, J.; Wei, W.; Menyo, M. S.; Masic, A.; Waite, J. H.; Israelachvili, J. N. *Biomacromolecules* **2013**, *14*, 1072.

(32) Yu, J. In *Adhesive Interactions of Mussel Foot Proteins*; Springer: 2014, p 21.

(33) Yu, J.; Wei, W.; Danner, E.; Ashley, R. K.; Israelachvili, J. N.; Waite, J. H. *Nature chemical biology* **2011**, *7*, 588.

(34) Lee, H.; Dellatore, S. M.; Miller, W. M.; Messersmith, P. B. *science* **2007**, *318*, 426.

(35) North, M. A.; Del Grosso, C. A.; Wilker, J. J. *ACS applied materials & interfaces* **2017**, *9*, 7866.

(36) Li, A.; Mu, Y.; Jiang, W.; Wan, X. *Chemical Communications* **2015**, *51*, 9117.

(37) Saiz-Poseu, J.; Mancebo-Aracil, J.; Nador, F.; Busqué, F.; Ruiz-Molina, D. *Angewandte Chemie International Edition* **2019**, *58*, 696.

(38) Hou, J.; Li, C.; Guan, Y.; Zhang, Y.; Zhu, X. *Polymer Chemistry* **2015**, *6*, 2204.

(39) Narkar, A. R.; Kelley, J. D.; Pinnaratip, R.; Lee, B. P. *Biomacromolecules* **2017**, *19*, 1416.

(40) Maier, G. P.; Rapp, M. V.; Waite, J. H.; Israelachvili, J. N.; Butler, A. *Science* **2015**, *349*, 628.

(41) Wang, B.; Lee, J. S.; Jeon, Y. S.; Kim, J.; Kim, J. H. *Polymer International* **2018**, *67*, 557.

(42) Flammang, P.; Santos, R.; Aldred, N.; Gorb, S. *Biological and biomimetic adhesives: challenges and opportunities*; Royal Society of Chemistry, 2013.

(43) Lee, B. P.; Dalsin, J. L.; Messersmith, P. B. *Biomacromolecules* **2002**, *3*, 1038.

(44) Burke, S. A.; Ritter-Jones, M.; Lee, B. P.; Messersmith, P. B. *Biomedical materials* **2007**, *2*, 203.

(45) Messersmith, P. B.; Dalsin, J. L.; Lee, B. P.; Burke, S. A.; Google Patents: 2014.

(46) Brubaker, C. E.; Kissler, H.; Wang, L.-J.; Kaufman, D. B.; Messersmith, P. B. *Biomaterials* **2010**, *31*, 420.

(47) Ryu, J. H.; Hong, S.; Lee, H. *Acta biomaterialia* **2015**, *27*, 101.

(48) Azad, A. K.; Sermsintham, N.; Chandrkrachang, S.; Stevens, W. F. *Journal of Biomedical Materials Research Part B: Applied Biomaterials: An Official Journal of The Society for Biomaterials, The Japanese Society for Biomaterials, and The Australian Society for Biomaterials and the Korean Society for Biomaterials* **2004**, *69*, 216.

(49) Kim, K.; Ryu, J. H.; Lee, D. Y.; Lee, H. *Biomaterials science* **2013**, *1*, 783.

(50) Kim, K.; Kim, K.; Ryu, J. H.; Lee, H. *Biomaterials* **2015**, *52*, 161.

(51) Ryu, J. H.; Lee, Y.; Kong, W. H.; Kim, T. G.; Park, T. G.; Lee, H. *Biomacromolecules* **2011**, *12*, 2653.

(52) Qiao, H.; Sun, M.; Su, Z.; Xie, Y.; Chen, M.; Zong, L.; Gao, Y.; Li, H.; Qi, J.; Zhao, Q. *Biomaterials* **2014**, *35*, 7157.

(53) Kim, E.; Gordonov, T.; Bentley, W. E.; Payne, G. F. *Analytical chemistry* **2013**, *85*, 2102.

(54) Krogsgaard, M.; Hansen, M. R.; Birkedal, H. *Journal of Materials Chemistry B* **2014**, *2*, 8292.

(55) He, L.; Fullenkamp, D. E.; Rivera, J. G.; Messersmith, P. B. *Chemical Communications* **2011**, *47*, 7497.

(56) Narkar, A. R.; Barker, B.; Clisch, M.; Jiang, J.; Lee, B. P. *Chemistry of Materials* **2016**, *28*, 5432.

(57) Liu, S.; Chen, L.; Tan, L.; Cao, F.; Bai, L.; Wang, Y. *Journal of Materials Chemistry B* **2014**, *2*, 6758.

(58) Dang, Y.; Quan, M.; Xing, C.-M.; Wang, Y.-B.; Gong, Y.-K. *Journal of Materials Chemistry B* **2015**, *3*, 2350.

(59) Pechey, A.; Elwood, C. N.; Wignall, G. R.; Dalsin, J. L.; Lee, B. P.; Vanjecek, M.; Welch, I.; Ko, R.; Razvi, H.; Cadieux, P. A. *The Journal of urology* **2009**, *182*, 1628.

(60) Damodaran, V. B.; Murthy, N. S. *Biomaterials research* **2016**, *20*, 18.

(61) Kobata, A. *Accounts of chemical research* **1993**, *26*, 319.
(62) Smets, L. A.; van Beek, W. P. *Biochimica et Biophysica Acta (BBA)-Reviews on Cancer* **1984**, *738*, 237.
(63) Ernst, B.; Magnani, J. L. *Nature Reviews Drug Discovery* **2009**, *8*, 661.
(64) Tsai, P.-L.; Chen, S.-F. *Mass Spectrometry* **2017**, *6*, S0064.
(65) Werz, D. B.; Ranzinger, R.; Herget, S.; Adibekian, A.; von der Lieth, C.-W.; Seeberger, P. H. *ACS chemical biology* **2007**, *2*, 685.
(66) Lee, R. T.; Lee, Y. C. *Glycoconjugate journal* **2000**, *17*, 543.
(67) Debray, H.; Decout, D.; Strecker, G.; Spik, G.; Montreuil, J. *European Journal of Biochemistry* **1981**, *117*, 41.
(68) Kiessling, L. L.; Gestwicki, J. E.; Strong, L. E. *Angewandte Chemie International Edition* **2006**, *45*, 2348.
(69) Pieters, R. J. *Organic & biomolecular chemistry* **2009**, *7*, 2013.
(70) Jones, M. W.; Otten, L.; Richards, S.-J.; Lowery, R.; Phillips, D. J.; Haddleton, D. M.; Gibson, M. I. *Chemical Science* **2014**, *5*, 1611.
(71) Keller, B. G.; Rademacher, C. *Current Opinion in Structural Biology* **2020**, *62*, 31.
(72) Sumner, J. B.; Howell, S. F. *Journal of Bacteriology* **1936**, *32*, 227.
(73) Cavada, B. S.; Osterne, V. J. S.; Lossio, C. F.; Pinto-Junior, V. R.; Oliveira, M. V.; Silva, M. T. L.; Leal, R. B.; Nascimento, K. S. *International journal of biological macromolecules* **2019**, *134*, 901.
(74) Fujita, T.; Matsushita, M.; Endo, Y. *Immunological reviews* **2004**, *198*, 185.
(75) Medzhitov, R.; Janeway Jr, C. *Immunological reviews* **2000**, *173*, 89.
(76) Turner, M. W. *Molecular immunology* **2003**, *40*, 423.
(77) Matsushita, M.; Fujita, T. *The Journal of experimental medicine* **1992**, *176*, 1497.
(78) Imberty, A.; Varrot, A. *Current opinion in structural biology* **2008**, *18*, 567.
(79) Bishop, J. R.; Gagneux, P. *Glycobiology* **2007**, *17*, 23R.
(80) Rossolini, G.; Mantengoli, E. *Clinical Microbiology and infection* **2005**, *11*, 17.
(81) Karlsson, K.-A. In *The Molecular Immunology of Complex Carbohydrates—2*; Springer: 2001, p 431.
(82) Kirkeby, S.; Wimmerová, M.; Moe, D.; Hansen, A. K. *Microbes and infection* **2007**, *9*, 566.
(83) Glick, J.; Garber, N. *Microbiology* **1983**, *129*, 3085.
(84) Chemani, C.; Imberty, A.; de Bentzmann, S.; Pierre, M.; Wimmerová, M.; Guery, B. P.; Faure, K. *Infection and immunity* **2009**, *77*, 2065.
(85) Pereira, S. G.; Rosa, A. C.; Cardoso, O. *Virulence* **2015**, *6*, 679.
(86) Perret, S.; Sabin, C.; Dumon, C.; Pokorná, M.; Gautier, C.; Galanina, O.; Ilia, S.; Bovin, N.; Nicaise, M.; Desmadril, M. *Biochemical Journal* **2005**, *389*, 325.
(87) Garber, N.; Guempel, U.; Belz, A.; Gilboa-Garber, N.; Doyle, R. J. *Biochimica et Biophysica Acta (BBA)-General Subjects* **1992**, *1116*, 331.
(88) Kadam, R. U.; Bergmann, M.; Hurley, M.; Garg, D.; Cacciarini, M.; Swiderska, M. A.; Nativi, C.; Sattler, M.; Smyth, A. R.; Williams, P. *Angewandte Chemie International Edition* **2011**, *50*, 10631.
(89) Rodrigue, J.; Ganne, G.; Blanchard, B.; Saucier, C.; Giguère, D.; Shiao, T. C.; Varrot, A.; Imberty, A.; Roy, R. *Organic & biomolecular chemistry* **2013**, *11*, 6906.
(90) Sobel, J. *Medical Clinics of North America* **1991**, *75*, 253.
(91) Ofek, I.; Mosek, A.; Sharon, N. *Infection and Immunity* **1981**, *34*, 708.
(92) Pratt, L. A.; Kolter, R. *Molecular microbiology* **1998**, *30*, 285.
(93) Langermann, S.; Palaszynski, S.; Barnhart, M.; Auguste, G.; Pinkner, J. S.; Burlein, J.; Barren, P.; Koenig, S.; Leath, S.; Jones, C. H. *Science* **1997**, *276*, 607.
(94) Kranjčec, B.; Papeš, D.; Altarac, S. *World journal of urology* **2014**, *32*, 79.
(95) Sharon, N. *FEBS letters* **1987**, *217*, 145.

(96) Hartmann, M.; Lindhorst, T. K. *European Journal of Organic Chemistry* **2011**, *2011*, 3583.

(97) Hartmann, M.; Horst, A. K.; Klemm, P.; Lindhorst, T. K. *Chemical communications* **2010**, *46*, 330.

(98) Duffy, M. J. *Clinical chemistry* **2005**, *51*, 494.

(99) Hakomori, S.-i. In *Advances in cancer research*; Elsevier: 1989; Vol. 52, p 257.

(100) Hakomori, S.-i. *Cancer research* **1996**, *56*, 5309.

(101) Mody, R.; Antaram Joshi, S.; Chaney, W. *Journal of pharmacological and Toxicological Methods* **1995**, *33*, 1.

(102) Powlesland, A. S.; Hitchen, P. G.; Parry, S.; Graham, S. A.; Barrio, M. M.; Elola, M. T.; Mordoh, J.; Dell, A.; Drickamer, K.; Taylor, M. E. *Glycobiology* **2009**, *19*, 899.

(103) Büll, C.; Stoel, M. A.; den Brok, M. H.; Adema, G. J. *Cancer research* **2014**, *74*, 3199.

(104) Couldrey, C.; Green, J. E. *Breast Cancer Research* **2000**, *2*, 1.

(105) Wei, M. M.; Wang, Y. S.; Ye, X. S. *Medicinal research reviews* **2018**, *38*, 1003.

(106) Slovin, S.; Ragupathi, G.; Adluri, S.; Ungers, G.; Terry, K.; Kim, S.; Spassova, M.; Bornmann, W.; Fazzari, M.; Dantis, L. *Proceedings of the National Academy of Sciences* **1999**, *96*, 5710.

(107) Goonetilleke, K.; Siriwardena, A. *European Journal of Surgical Oncology (EJSO)* **2007**, *33*, 266.

(108) Plattner, V. E.; Wagner, M.; Ratzinger, G.; Gabor, F.; Wirth, M. *European Journal of Pharmaceutics and Biopharmaceutics* **2008**, *70*, 572.

(109) Bernerd, F.; Sarasin, A.; Magnaldo, T. *Proceedings of the National Academy of Sciences* **1999**, *96*, 11329.

(110) Matarrese, P.; Fusco, O.; Tinari, N.; Natoli, C.; Liu, F. T.; Semeraro, M. L.; Malorni, W.; Iacobelli, S. *International journal of cancer* **2000**, *85*, 545.

(111) Zhang, P.; Shi, B.; Zhou, M.; Jiang, H.; Zhang, H.; Pan, X.; Gao, H.; Sun, H.; Li, Z. *Cell death & disease* **2014**, *5*, e991.

(112) Compagno, D.; Jaworski, F. M.; Gentilini, L.; Contrufo, G.; Pérez, I. G.; Elola, M. T.; Pregi, N.; Rabinovich, G. A.; Laderach, D. J. *Current molecular medicine* **2014**, *14*, 630.

(113) Nabi, I. R.; Shankar, J.; Dennis, J. W. *Journal of cell science* **2015**, *128*, 2213.

(114) Cardoso, A. C. F.; Andrade, L. N. d. S.; Bustos, S. O.; Chammas, R. *Frontiers in oncology* **2016**, *6*, 127.

(115) Tejler, J.; Leffler, H.; Nilsson, U. J. *Bioorganic & medicinal chemistry letters* **2005**, *15*, 2343.

(116) Sörme, P.; Kahl-Knutsson, B.; Huflejt, M.; Nilsson, U. J.; Leffler, H. *Analytical biochemistry* **2004**, *334*, 36.

(117) Böcker, S.; Laaf, D.; Elling, L. *Biomolecules* **2015**, *5*, 1671.

(118) Lu, J.; Fu, C.; Wang, S.; Tao, L.; Yan, L.; Haddleton, D. M.; Chen, G.; Wei, Y. *Macromolecules* **2014**, *47*, 4676.

(119) Merrifield, R. B. *Journal of the American Chemical Society* **1963**, *85*, 2149.

(120) Crowley, J. I.; Rapoport, H. *Accounts of Chemical Research* **1976**, *9*, 135.

(121) Ponader, D.; Wojcik, F.; Beceren-Braun, F.; Dernedde, J.; Hartmann, L. *Biomacromolecules* **2012**, *13*, 1845.

(122) Zalipsky, S.; Chang, J. L.; Albericio, F.; Barany, G. *Reactive Polymers* **1994**, *22*, 243.

(123) Scotchler, J.; Lozier, R.; Robinson, A. B. *The Journal of Organic Chemistry* **1970**, *35*, 3151.

(124) Amblard, M.; Fehrentz, J.-A.; Martinez, J.; Subra, G. *Molecular biotechnology* **2006**, *33*, 239.

(125) Orain, D.; Ellard, J.; Bradley, M. *Journal of combinatorial chemistry* **2002**, *4*, 1.

(126) El-Faham, A.; Albericio, F. *Chemical reviews* **2011**, *111*, 6557.

(127) Hudson, D. *The Journal of Organic Chemistry* **1988**, *53*, 617.

(128) Wojcik, F.; Mosca, S.; Hartmann, L. *The Journal of organic chemistry* **2012**, *77*, 4226.

(129) Freichel, T.; Eierhoff, S.; Snyder, N. L.; Hartmann, L. *The Journal of organic chemistry* **2017**, *82*, 9400.

(130) Shamout, F.; Fischer, L.; Snyder, N. L.; Hartmann, L. *Macromolecular Rapid Communications* **2020**, *41*, 1900473.

(131) Baier, M.; Giesler, M.; Hartmann, L. *Chemistry–A European Journal* **2018**, *24*, 1619.

(132) Ponader, D., 2014.

(133) Boden, S.; Reise, F.; Kania, J.; Lindhorst, T. K.; Hartmann, L. *Macromolecular bioscience* **2019**, *19*, e1800425.

(134) Wuts, P. G.; Greene, T. W. *Greene's protective groups in organic synthesis*; John Wiley & Sons, 2006.

(135) KISO, Y.; UKAWA, K.; NAKAMURA, S.; ITO, K.; AKITA, T. *Chemical and Pharmaceutical Bulletin* **1980**, *28*, 673.

(136) Gerke, C.; Ebbesen, M. F.; Jansen, D.; Boden, S.; Freichel, T.; Hartmann, L. *Biomacromolecules* **2017**, *18*, 787.

(137) Palladino, P.; Stetsenko, D. A. *Organic letters* **2012**, *14*, 6346.

(138) Bücher, K. S.; Konietzny, P. B.; Snyder, N. L.; Hartmann, L. *Chemistry–A European Journal* **2019**, *25*, 3301.